Structure-Property Correlations in Fluoroaryl Functionalized Inorganic-Organic Hybrid Polymers for Telecom Applications

Dissertation zur Erlangung des
naturwissenschaftlichen Doktorgrades
der Bayerischen Julius-Maximilians-Universität Würzburg

vorgelegt von

Frank Kahlenberg

aus Brilon

Würzburg 2004

Eingereicht am:

bei der Fakultät für Chemie und Pharmazie

1. Gutachter:

2. Gutachter:

der Dissertation

1. Prüfer:

2. Prüfer:

3. Prüfer:

des Öffentlichen Promotionskolloquiums

Tag des Öffentlichen Promotionskolloquiums:

Doktorurkunde ausgehändigt am:

TABLE OF CONTENTS

i Index of abbreviations xi

ii Definitions xiii

ii.i Symbolism for highly fluorinated aryl substituents xiii

ii.ii Sample numbering system xiii

ii.iii Silicon species in siloxane oligo-/polymers xiv

1 Introduction 1

2 Theoretical Fundamentals 7

2.1 Refractive index 7

2.2 Optical loss in waveguides 9

2.2.1 Absorption loss 10

2.2.2 Other sources of optical loss 13

2.3 Processing / patterning methods 14

2.4 Polymers for optical waveguides 16

2.4.1 Polyacrylates 21

2.4.2 Epoxy-based materials 23

2.4.3 Benzocyclobutenes 25

2.4.4 Polyimides 27

2.4.5 Polycarbonates 29

2.4.6 Amorphous fluoropolymers 31

2.4.7 Perfluorocyclobutyl (PFCB) aryl ether polymers 31

2.4.8 Polyether ketones (PEK) 33

2.4.9 Fluorinated dendrimers and hyperbranched polymers 34

2.4.10 Miscellaneous fluorinated polymers 35

2.4.11 Polysiloxanes and inorganic-organic hybrid polymers 38

2.5 ORMOCER®s – Fraunhofer's inorganic-organic hybrids 41

2.5.1 ORMOCER®s for microsystems 41

2.5.2 Polycondensation of ORMOCER® precursor silanes 44

2.5.3 Photoinitiators for direct photopatterning of ORMOCER®s 45

2.5.4 b59d – reference ORMOCER® for optical waveguide applications 46

2.5.5 Fluoroaryl modified ORMOCER®s – preliminary results 47

3 Results and Discussion 49

3.1 Precursor silane syntheses 49

3.1.1 Fluoroarylalkoxysilanes 50

3.1.2 Unfluorinated arylalkoxysilanes 51

3.1.3 Methylene spacer silane via Grignard synthesis 52

3.1.4 Ethylene spacer silane by hydrosilation of pentafluorostyrene 54

3.2 Optical properties of precursor silanes 55

3.2.1 Refractive indices 56

3.2.2 Optical losses at telecom wavelengths 1310 nm and 1550 nm 58

3.3 Development of ORMOCER® resins 59

3.3.1 NMR analyses of polycondensation reactions 60

3.3.2 Polycondensation of bis-(pentafluorophenyl)dimethoxysilane (**2**) 61

3.3.3 Polycondensation of pentafluorophenyl(vinyl)dimethoxysilane (**5**) – condensation stoichiometry 62

3.3.4 Polycondensation of pentafluorophenyl(vinyl)dimethoxysilane (**5**) – hydrolysis stoichiometry 69

3.3.5 Polycondensation of pentafluorophenyltrimethoxysilane (**1**) 72

3.3.6 Polycondensation of 4-vinyltetrafluorophenyltrimethoxysilane (**4**) 75

3.3.7 Control experiments – polycondensation reactions of vinyltrimethoxysilane and tetramethoxysilane 78

3.4 Synthesis and characterization of ORMOCER® resins from precursor silane mixtures 80

3.4.1 Preparation of soluble fluoroaryl-functionalized ORMOCER® resins 80

3.4.2 First photopatternable fluoroaryl-functionalized ORMOCER®s 83

3.4.3 Synthesis of photopatternable ORMOCER® resins based on advanced formulations 85

3.4.4 Characterization of selected ORMOCER® resins 88

3.4.5 Interpretation of structural characterization data 90

3.4.6 Refractive indices of ORMOCER® resins 94

3.4.7 NIR absorption of photopatternable ORMOCER® resins 95

3.4.8 Molecular modeling of a fluorinated organosiloxane oligomer 99

3.5 Syntheses of ORMOCER® inorganic-organic hybrid polymers 106

3.5.1 General method for the manufacture of ORMOCER® micropatterns 106

3.5.2 Micropatterns of fluoroaryl functionalized ORMOCER®s 107

3.5.3 Oligosiloxane crosslinking via the styrene-analogous group 109

3.5.4 Structural characterization of ORMOCER® hybrid networks by magic angle spinning (MAS) solid state ^{29}Si-NMR 111

3.5.5 Thermal analysis 113

3.5.6 Optical properties 115

3.5.7 Dielectrical properties 117

3.5.8 Mechanical properties 118

4 Experimental Section 120

4.1 Chemicals 120

4.2 Analytical methods and apparatuses 120

4.2.1 Nuclear magnetic resonance spectroscopy (NMR) in solution 120

4.2.2 Solid state NMR 121

4.2.3 Infrared spectroscopy (FT-IR) 121

4.2.4 Ultraviolet / visible / near-infrared spectroscopy (UV/VIS/NIR) 122

4.2.5 Refractive index measurements 122

4.2.6 Small angle X-ray scattering (SAXS) 122

4.2.7 Thermogravimetry – differential thermal analysis (TG-DTA) 122

4.2.8 Determination of ORMOCER® thin film optical losses 122

4.2.9 Micro indenter measurements 123

4.2.10 Dielectrical testing 123

4.3 Precursor syntheses 124

4.3.1 Concurrent synthesis of pentafluorophenyltrimethoxysilane (**1**) and bis-(pentafluorophenyl)dimethoxysilane (**2**) 124

4.3.2 Synthesis of 1-bromo-2,3,5,6-tetrafluoro-4-vinylbenzene (**3**) 126

4.3.3 Synthesis of 4-vinyltetrafluorophenyltrimethoxysilane (**4**) 127

4.3.4 Synthesis of pentafluorophenyl(vinyl)dimethoxysilane (**5**) 129

4.3.5 Synthesis of pentafluorophenyl(methyl)dimethoxysilane (**6**) 130

4.3.6 Synthesis of phenyl(vinyl)dimethoxysilane (**7**) 131

4.3.7 Concurrent synthesis of phenyl(vinyl)dimethoxysilane (7) and diphenyl(vinyl)methoxysilane (**8**) 133

4.3.8 Reaction of pentafluorobenzyl bromide with magnesium and tetramethoxysilane I (two-step approach) 134

4.3.9 Reaction of pentafluorobenzyl bromide with magnesium and tetramethoxysilane II (one-pot approach) 136

4.3.10 Reaction of pentafluorostyrene with trimethoxysilane under hydrosilylation conditions 137

4.3.11 Synthesis of 2-(pentafluorophenyl)ethyltriethoxysilane (**12**) 139

4.4 Polycondensation reactions 140

4.4.1 Reaction of bis-(pentafluorophenyl)dimethoxysilane (**2**) with dilute hydrochloric acid in acetone 140

4.4.2 Reaction of bis-(pentafluorophenyl)dimethoxysilane (**2**) with dilute sodium hydroxide solution in acetone 141

4.4.3 Reaction of pentafluorophenyl(vinyl)dimethoxysilane (**5**) with dilute hydrochloric acid – condensation stoichiometry 142

4.4.4 Reaction of pentafluorophenyl(vinyl)dimethoxysilane (**5**) with dilute hydrochloric acid – hydrolysis stoichiometry 145

4.4.5 Reaction of pentafluorophenyltrimethoxysilane (**1**) with dilute hydrochloric acid – hydrolysis stoichiometry 147

4.4.6 Reaction of 4-vinyltetrafluorophenyltrimethoxysilane (**4**) with dilute hydrochloric acid – hydrolysis stoichiometry 148

4.4.7 Reaction of vinyltrimethoxysilane with dilute hydrochloric acid – ^{29}Si-NMR study 149

4.4.8 Reaction of tetramethoxysilane with dilute hydrochloric acid – ^{29}Si-NMR study 150

4.4.9 Reaction of pentafluorophenyltrimethoxysilane (**1**) mixed with pentafluorophenyl(vinyl)dimethoxysilane (**5**) with dilute hydrochloric acid in methanol 152

4.4.10 Preparation of ORMOCER® resins **fk13** and **fk14** 153

4.4.11 Preparation of gel **fk15** and ORMOCER® resin **fk16** 155

4.4.12 Preparation of ORMOCER® resins **fk18** and **fk19** 156

4.4.13 Preparation of ORMOCER® resin **fk20** 157

4.4.14 Preparation of ORMOCER® resin **fk34** 158

4.4.15 Preparation of ORMOCER® resins **fk35** and **fk37** 159

4.4.16 Preparation of ORMOCER® resin **fk36** 161

4.4.17 Preparation of ORMOCER® resin **fk38** 162

4.4.18 Preparation of ORMOCER® resin **fk48** 163

4.4.19 Preparation of ORMOCER® resin **fk54** 164

4.5 Syntheses of ORMOCER® inorganic-organic hybrid polymers 166

4.5.1 General method for clean room processing of ORMOCER® resins 166

4.5.2 Preparation of ORMOCER® lacquers 167

4.5.3 Preparation and characterization of ORMOCER® powder samples 169

4.5.4 ORMOCER® thin films and multilayers 171

4.5.5 Capacitors with embedded ORMOCER® fk37 thin films for dielectrical testing 180

5 Summary 181

6 Zusammenfassung – Summary in German 183

7 References 186

8 Danksagung – Acknowledgments 193

9 Lebenslauf – curriculum vitae 194

Appendix 1 Numeration of precursors

Appendix 2 ORMOCER® resins I

Appendix 3 ORMOCER® resins II

i INDEX OF ABBREVIATIONS

2PP	two-photon polymerization
3D	three-dimensional
AMDS	3-(acryloxypropyl)methyldimethoxysilane
aq.	aqueous
Ar	arylic residue (as in: Ar-CH=CH_2)
AWG	arrayed waveguide grating(s)
BCB	benzocyclobutene(s)
bp	boiling point
(br)	broad (peak)
conc.	concentrated
CTE	coefficient of thermal expansion
d	day(s)
DMAc	N,N-dimethylacetamide
eq(s).	equation(s)
equiv.	equivalent(s)
expos.	exposure (UV)
Fig(s).	figure(s)
FT-IR	Fourier transform infrared (spectroscopy)
GLYMO	3-glycidyloxypropyltrimethoxysilane
IOF	Fraunhofer-Institut für Angewandte Optik und Feinmechanik (Fraunhofer Institute for Applied Optics and Precision Engineering), Jena
IC	integrated circuit(s)
IR	infrared
ISC	Fraunhofer-Institut für Silicatforschung, Würzburg
LAN	local area network(s)
(m)	medium (intensity)
MAS	magic angle spinning (solid state NMR)
MCM	multichip module
MEMO	3-methacryloxypropyltrimethoxysilane
MEMS	microelectromechanical system(s)
MIBK	4-methyl-2-pentanone (methyl isobutyl ketone)
mol.%	molar percentage
NIR	near infrared
NLO	non-linear optical/optics
NMR	nuclear magnetic resonance (spectroscopy)

No.	number
PEK	polyether ketone
PFCB	perfluorocyclobutyl/perfluorocyclobutane
PGMEA	propylene glycol monomethyl ether acetate
PMMA	polymethylmethacrylate
POF	polymer/plastic optical fiber
POSS	polyhedral oligosilsesquioxane
postexp.	postexposurebake
^{i}PrOH	2-propanol (isopropanol)
PTFE	polytetrafluoroethylene
PVD	physical vapor deposition
ref.	reference
RIE	reactive ion etching
(s)	strong (intensity)
SAXS	small angle X-ray scattering
SBU	sequential build-up (technology)
soln.	solution
substr.	substrate
Tab(s).	table(s)
TE	transverse electric mode
TEOS	tetraethoxysilane/tetraethyl orthosilicate
THF	tetrahydrofuran
THFA	tetrahydrofurfuryl acrylate
TM	transverse magnetic mode
TMOS	tetramethoxysilane/tetramethyl orthosilicate
TMPTA	tetramethyloylpropane triacrylate
TMS	tetramethylsilane
UV	ultraviolet (radiation)
VCSEL	vertical cavity surface emitting laser
VIS	visible (light)
w	week(s)
(w)	weak (intensity)
WAN	wide area network(s)
WDM(D)	wavelength division (de-)multiplexing
wt.%	weight percent

ii DEFINITIONS

ii.i Symbolism for highly fluorinated aryl substituents

In order to simplify the depiction of chemical structures and to make figures easier to comprehend with the eye, perfluorinated aryl rings are symbolized as exemplified in Fig. i. A capital letter "F" drawn in the center of a phenyl or phenylene ring means that to all arylic carbon atoms, except to those with explicitly marked substituents, fluorine atoms are attached. However, this symbolism only applies to the aryl ring itself and does not affect the depiction of other chemical moieties within the molecule, e.g. vinyl or alkyl groups.

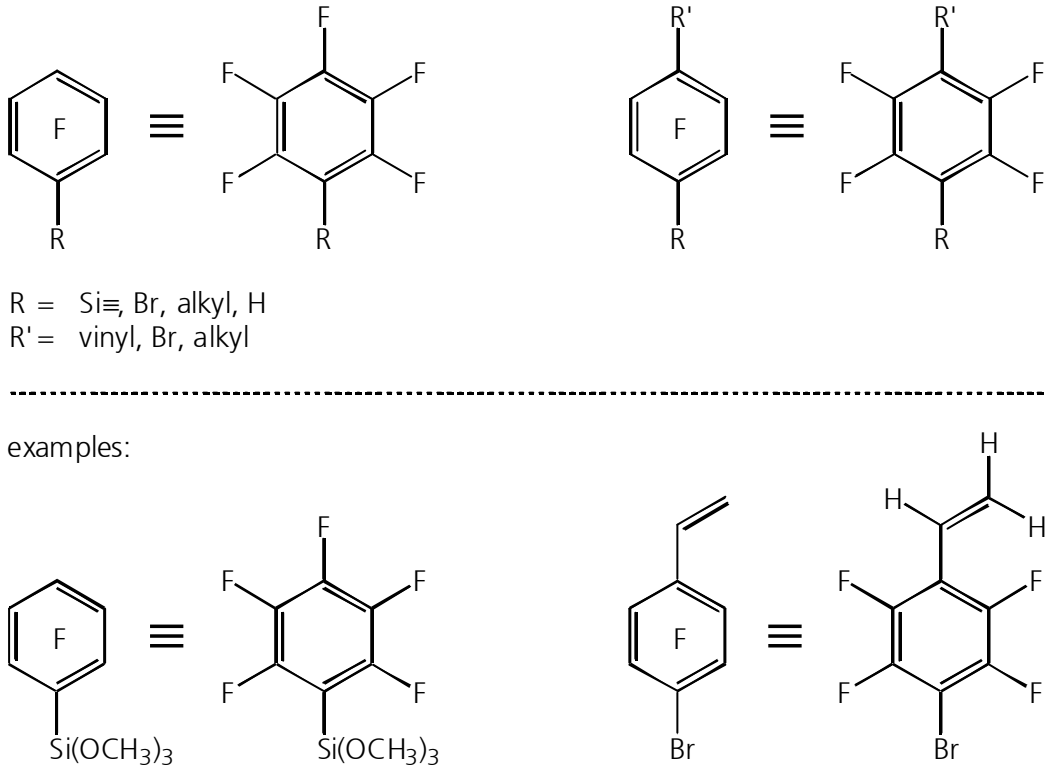

Fig. i: Highly fluorinated aryl rings are symbolized with a capital letter "F" in the center.

ii.ii Sample numbering system

In general, this work employs labels of the kind **fk*ii*** (***ii*** = two-digit number) in order to name ORMOCER®[1] systems (inorganic-organic hybrid polymers, see chapters 1, 2.5) after their chemical compositions. The exact compositions (precursor silane mixtures) as well as the polycondensation conditions utilized in the preparation of the respective resins (water content, catalyst, temperature, reaction time) are described in detail in the experimental part of this work (chapter 4).

A label **fk*ii*** always refers to an ORMOCER® system as a whole, i.e. not only to the respective resin, but also to the lacquers (resin plus diluting solvent plus photo initiator) and completely

cured bulk materials and thin-films. Thus, for clarity reasons, when a specific stage of the ORMOCER® synthesis is meant, this is added explicitly to the label, as in "**fk37** resin". ORMOCER® lacquers and bulk samples as well as film samples are numbered as illustrated in Fig. ii, where an exemplary sample label, "**fk37-4a/1**", is split into its components in order to find out information about the sample's chemical composition and processing conditions.

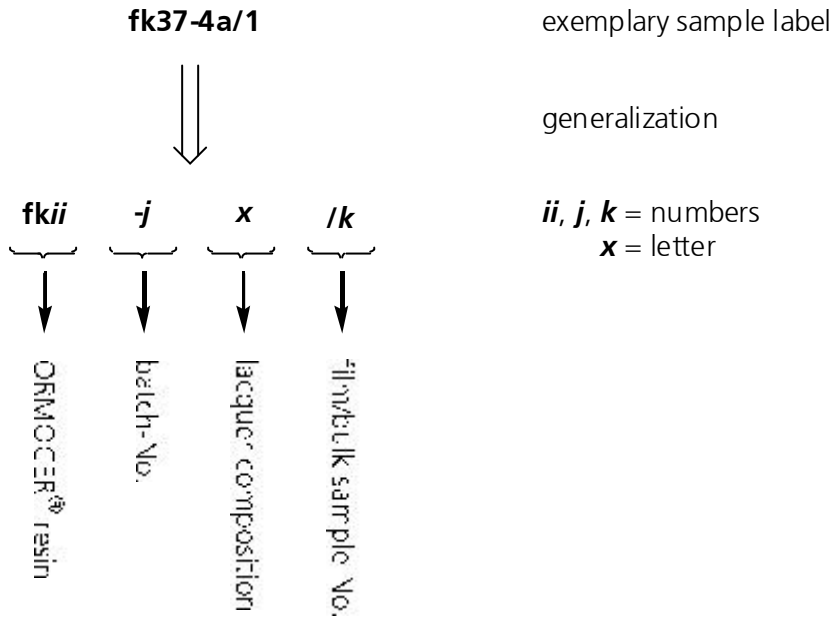

Fig. ii: ORMOCER® sample labeling.

The first label part **fk*ii*** denotes the label of the ORMOCER® resin derived from hydrolysis/polycondensation of a certain mixture of organoalkoxysilanes including final removal of volatiles. The second label part ***-j*** labels the batch number of the respective resin composition, i.e. an ORMOCER® resin numbered **fk37-4** would be the fourth synthesis carried out following the **fk37** recipe. The following letter ***x*** gives information on the composition of the respective **fk*ii-jx*** ORMOCER® lacquer, i.e. an ORMOCER® resin mixed with a diluting solvent and a photo-initiator. The final figure ***/k*** specifies a certain ORMOCER® bulk or thin-film sample.

Only for multilayer samples, i.e. samples consisting of two or three stacked thin films made from different **fk*ii*** ORMOCER® systems, the first label part does not indicate a single resin composition, but denotes a particular combination of ORMOCER® films. Specifically, the multilayers **fk43*/k*** combine thin-films made from compositions **fk34** and **fk38**.

ii.iii Silicon species in siloxane oligo-/polymers

In sol-gel chemistry, an X^n (X = Q,T,D,M; n = 0,1,2,3,4) nomenclature has been widely accepted for the assignment of the numerous different silicon species present in (organo)polysiloxanes[2]. The letter X is connected with the number m of possible condensations,

which a silicon center $R_{4-m}Si(OR')_m$ (R = alkyl,aryl; *m* = 1,2,3,4; R' = alkyl,H,Si) can undergo or has already undergone. Q systems $Si(OR')_4$ are able to condense four times, T systems $RSi(OR')_3$ three times, D systems $R_2Si(OR')_2$ twice, and M systems R_3SiOR' only once, taking into account that the number (4-*m*) of organic substituents R on the silicon atom lowers the number of possible condensation reactions.

The superscript *n* gives the actual degree of condensation, i.e. the number of condensations that a Q, T, D, or M system actually underwent. For example, the symbol Q^4 assigns a fully condensed orthosilicate unit, whereas T^2 symbolizes a silicon atom with one organic substituent and three sites of possible condensation, of which two have formed siloxane bonds and the remaining one is still reactive.

However, so far no standardized nomenclature can be found in literature for the further, more exact specification of X^n species in terms of different stages of hydrolysis. Several methods are in use, one of which had to be chosen after its best suitability for use in this work. The chosen nomenclature adds a second number written below the index *n* in order to specify the number of hydroxyl groups attached to the silicon center[3]. The symbol D_2^0, for example, designates a D^0 system $R_2Si(OH)_2$ with two hydroxyl groups attached. D_0^1 refers to a monocondensed D-silicon with the second hydrolyzable moiety, e.g. an alkoxy group, still attached.

Other nomenclature methods that have been proposed but not chosen for use in this work are variations of the above. One employs explicit notation of hydroxyl and remaining alkoxy groups, also as a second index below *n*[4]. For the same examples as above, the symbol $D^0_{(OH)(OH)}$ is suggested instead of D_2^0, as well as $D^1_{(OMe)}$ (in case of methoxy silanes) instead of D_0^1. This method was rejected because the chosen one offers better generality and more ease of use. Other authors use a symbolism very similar to the chosen one, but with inversed indices[5]. To prevent confusion, this method was also rejected for the presented work.

1 INTRODUCTION

During the last decades, high-volume telecommunications such as trunk (large-distance) and metro lines have been converted from electrical to optical data transfer[6,7]. In optical interconnection, a vast number of laser frequencies can be multiplexed on a single optical waveguide and transmitted simultaneously. Thus, a much higher amount of information can be transmitted. This technological progress is currently being transferred also to a smaller scale, such as high integration density components and computer (optical) backplanes.

Extensive studies are conducted on the development of new materials, which exhibit suitable properties for application in optical telecom and datacom technology. An optical waveguide generally consists of a waveguide core, in which the signal propagates, and a cladding, which surrounds the core and detains the optical signal inside the waveguide core (Fig. 1)[7-9]. The core material has to have a slightly higher index of refraction than the cladding material (index step typically 0.3% – 8%), with the layer boundary forming a mirror for the guided light. Thus, a key property of an optical waveguide material is a defined index of refraction.

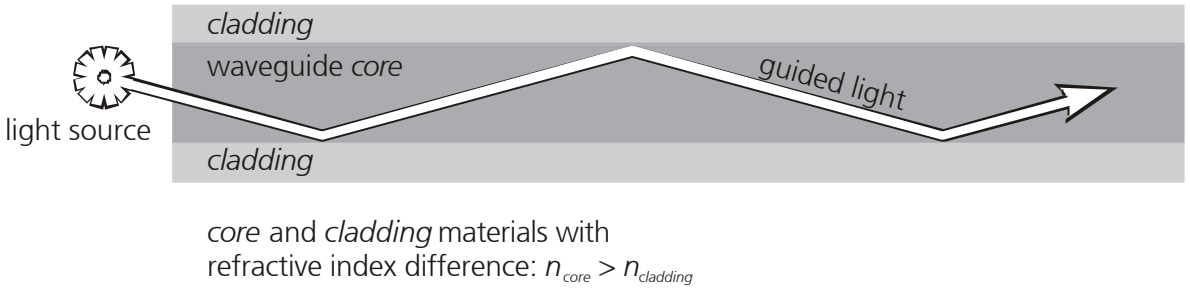

Fig. 1: Longitudinal section of an optical waveguide consisting of a core layer embedded in a cladding of lower refraction. Incoupled light is guided by total reflectance.

A likewise important waveguide specification is optical transparency or the optical loss in certain frequency ranges, which have been established as quasi-standard carrier bands for telecom and datacom. In silica fibers (refractive index around 1.45), which are widely used for long-range optical data transmission, three "wavelength windows" are distinguished: 850 nm (1st window), 1310 nm (2nd window), and 1550 nm (3rd window)[7]. Outside and in between those windows, transmission losses due to scattering and vibrational absorption of the material are predominant. As Rayleigh scattering is inversely proportional to the fourth power of the wavelength, it mainly affects the short-wave bands, making the long-wave bands all the more important. At wavelengths above 1600 nm, however, infrared absorption of the fiber becomes predominant, thus inhibiting further transmission windows. Since suitable light sources and amplifiers for the 2nd and 3rd windows are available, contemporary long-haul and trunk networks

chiefly operate at 1310 nm and 1550 nm, respectively. This in turn leads to the necessity that new materials intended for use in the field also have to be optically transparent in these regions.

Such new materials are needed in particular for the further miniaturization of optical network components. Thus, the benefit of optical data transmission is transferred from wide area networks (WAN) and local area networks (LAN) down to the backplane and board levels (Fig. 2)[6]. Further progression in the field of micro-optoelectronics is intended to lead to the full integration of optical communication backbones into multichip modules (MCM) and chips/integrated circuits (IC). Whereas WAN and LAN technologies rely on glass fibers or plastic optical fibers (POF) on a macroscopic scale, miniaturization increasingly requires new micropatternable materials, from which the optical network components are manufactured.

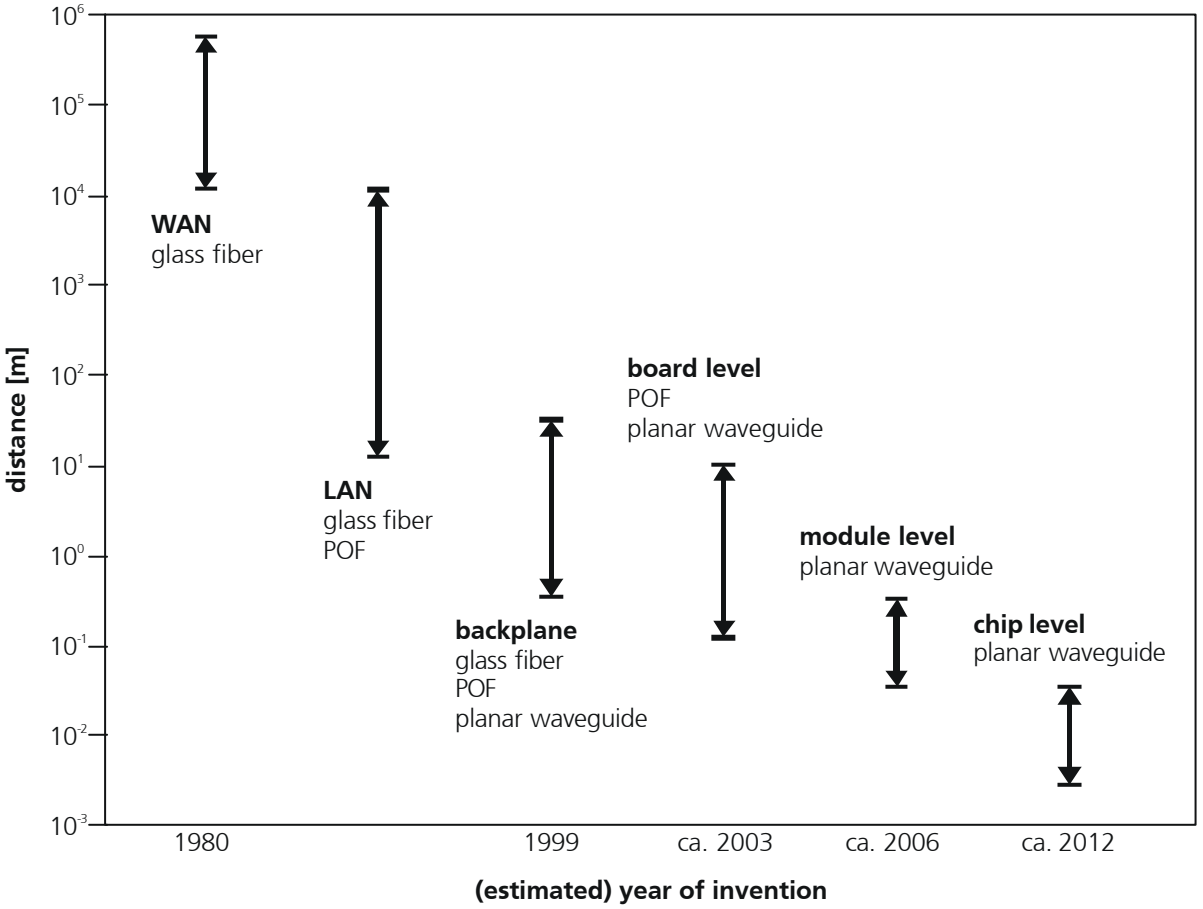

Fig. 2: Miniaturization in the field of optical data transmission[6].

The basic principle underlying all optical broadband parallel telecommunication systems is wavelength division multiplexing (WDM)[7]. WDM multiplexers are optical devices designed to combine discrete narrow bands each corresponding to an individual signal channel to a broad wavelength band that is coupled into the waveguide. Thus, all information is transferred in a parallel way through the same optical fiber. WDM demultiplexing (WDMD) then separates these

broad bands again into the individual channels each bound to a separate destination within the optical network. A key example for a WDM component is the arrayed waveguide grating (AWG), a planar optical filter, which can be employed as multiplexing and demultiplexing device. Together with optical switches, AWG can be combined to optical add-drop multiplexers, which redirect selected signals between different senders and receivers within the network. Beside the mentioned examples, a large variety of other components are involved in optical data transmission[6,7]. All such devices are subject to miniaturization in order to achieve highly integrated, low power consuming systems. In microelectronics, electrical noise is one of the biggest problems. Thus, for high-end computing, certain limitations are met concerning high-speed data transfer between primary processing units that are each situated on separate printed wiring boards. Since electronic backplane technology suffers from signal distortion caused by cross-talk between individual data lines and electromagnetic interference, optical backplanes become increasingly important[10,11]. Such architectures offer higher data rates than electrical connects at lower cost, lower power consumption, and lower spatial demand.

The search for suitable materials meeting the specifications mentioned above is a major task in the progress of optical interconnection technology on the micrometer scale. Numerous polymeric materials for optical waveguide devices have been studied due to their ease in processibility, mechanical flexibility and cost-effective technology[12-15]. Based on low-loss polymer materials, various microoptical waveguide devices have been demonstrated including AWG multi-/demultiplexers[16-20], directional couplers[21], splitters[22], switches[23,24], modulators[25], and tunable filters[26,27]. Together with integrated all-polymer solutions in microelectronics[28], a high degree of plastic incorporation into all kinds of optical, electronic, and combined electro-optical IC is aimed for[29].

Beside a variety of other materials, an overview of which will be given later (chapter 2.4), members of the ORMOCER®[1] material family (inorganic-organic hybrid polymers) have been found outstandingly useful for application in optical interconnection technology[30-35]. These hybrid polymers, which have been developed at the Fraunhofer-Institut für Silicatforschung (ISC) in Würzburg, incorporate a metal oxide (mainly polysiloxane) backbone with organic crosslinking (e.g. acrylate or styryl polymer). ORMOCER®s are synthesized via a two-step process from organoalkoxysilane precursors. First, an applicable resin or lacquer is prepared by inorganic polycondensation of the alkoxysilane moieties. Photochemical or thermal curing as the second stage is accomplished by cross-linking of the organosiloxane oligomers via organically polymerizable units. The chemistry of ORMOCER® processing will be presented in more detail later (chapter 2.5). The resulting materials can have low-loss characteristics, adjustable refractive indices, and show high thermal stability. Additionally, they are easy to apply and to process, allowing cost-effective manufacture of micropatterns. Figure 3 shows several ORMOCER®

microoptical devices exemplarily[36]. Microlens arrays (Fig. 3a) have been manufactured by means of replication and embedded optical waveguide splitters (Fig. 3b) could be produced with photolithography. Figure 3c) demonstrates the three-dimensional (3D) integration of a deflecting prism and polymer fiber holding structures on a silicon wafer. In this case, patterning of the ORMOCER® inorganic-organic hybrid polymer was achieved by a combination of replication (prism) and lithography (fiber holders).

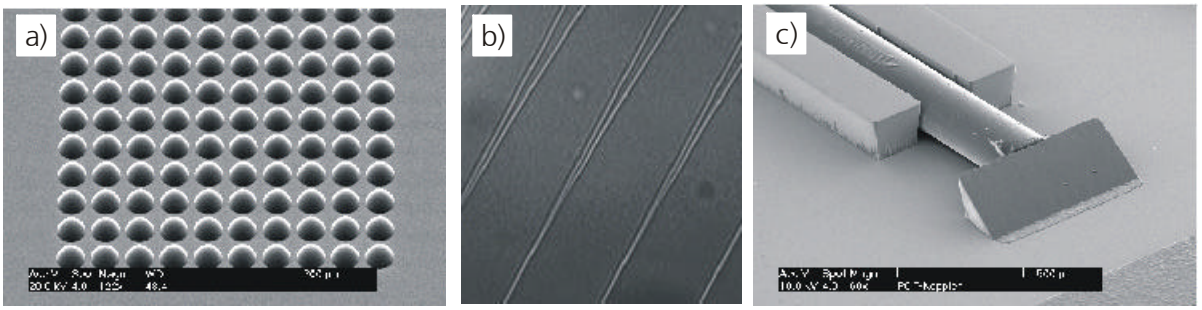

Fig. 3: ORMOCER® microoptical devices[36]: a) 10x10 microlens array; b) optical waveguide splitters (ca. 5 µm in diameter); c) 3D integration of a polymer fiber holding structure (with POF clipped in) and deflecting prism.

Properties of the materials are tailorable according to specific requirements by alteration of their molecular structures. Thus, ORMOCER®s can be optimized for use as optical waveguides in telecom and datacom devices, and as photopatternable dielectric or passivation layers in electrical components, respectively[32]. Furthermore, the possibility to combine the specifications for optical and electrical materials in a single polymer allows for high integration densities in combined opto-electrical devices[37]. The simultaneous use of an ORMOCER® for optical waveguiding and as dielectric layer is presented by a demonstrator device shown in Fig. 4.

Recently, direct 3D writing of ORMOCER® micropatterns via two-photon polymerization (2PP) has been demonstrated[30]. The highly selective process is initiated by focusing pulsed laser light of 780 nm into the liquid resin, giving rise to two-photon absorption and therefore polymerization within a very small volume. Upon movement of the laser focus through the resin, arbitrary 3D micropatterns (Fig. 5) with a resolution of down to 100 nm have been produced. Micro clamps (Fig. 5a) as micromechanical holding devices have been demonstrated as well as an impressive micron-scale adaptation (Fig. 5b) of the famous Hellenistic sculpture "Aphrodite of Melos" (2nd century BC, Musée du Louvre, Paris). Figure 5c) finally points up the excellent resolution of the process exemplified by a pattern resembling a photonic crystal structure.

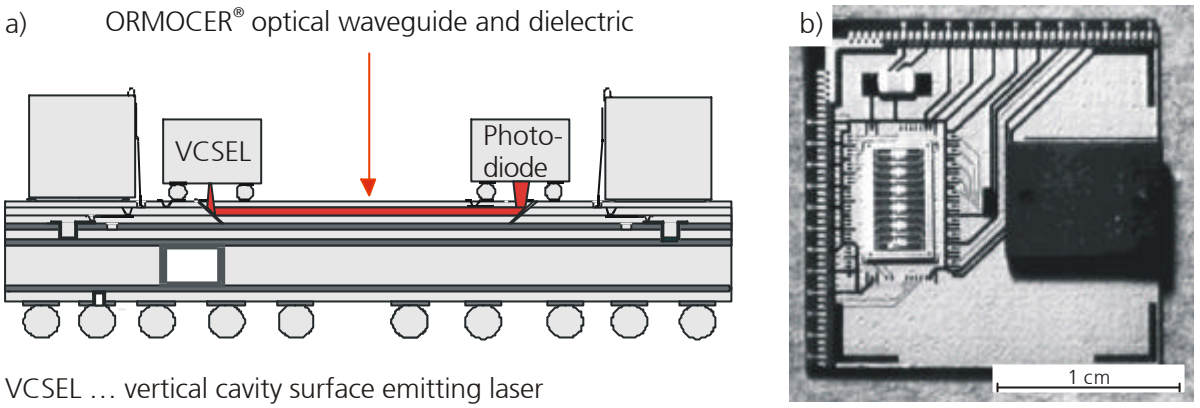

Fig. 4: a) Schematic representation of an opto-electrical MCM demonstrator, in which an ORMOCER® film serves as an optical waveguide and dielectric layer simultaneously[37]. b) Top view photograph of the sender VCSEL array, which is sketched in the left half of a).

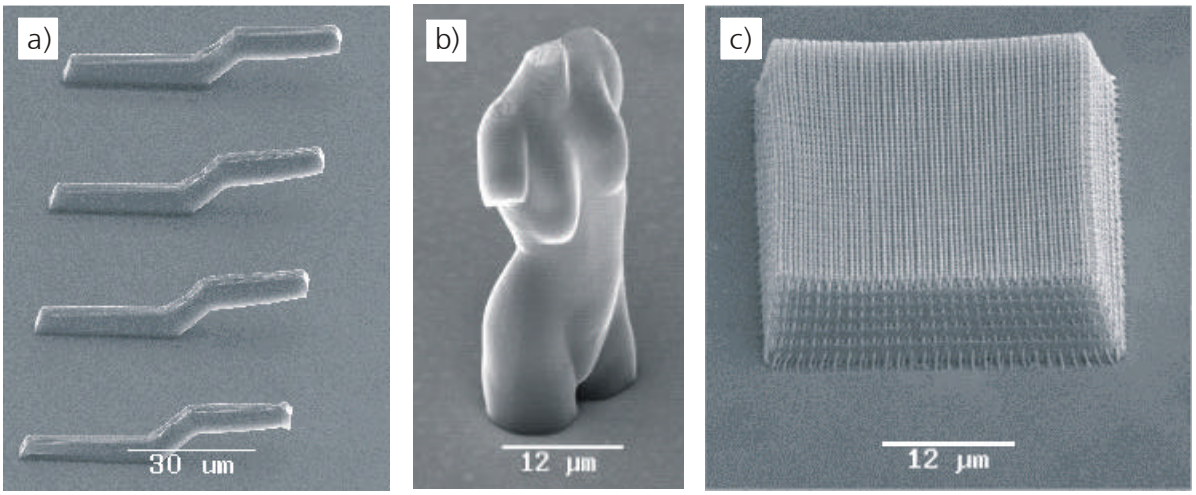

Fig. 5: True 3D lithography of ORMOCER®s via 2PP processing[30]: a) micro clamps; b) „Aphrodite of Melos" on a micrometer-scale; c) photonic crystal-like structure.

Beside an improvement of patterning methods, the advancement of ORMOCER® technology likewise involves intensive research in the field of materials chemistry. By variation of precursor compounds and reaction conditions, materials properties are continuously improved. Particularly for telecom and datacom applications, the reduction of optical transmission losses is a major task. For this purpose, the basic concept is a reduction of hydrocarbon (C-H) and hydroxyl (O-H) bonds within the material, as these are responsible for vibrational absorption in the telecom bands around 1310 nm and 1550 nm[38,39]. With proper reaction control, a low silanol content can be achieved[33,34]. Because of their inorganic backbone, ORMOCER®s also meet the C-H reduction criterion. Further C-H bond reduction in the organic part, however, can be realized generally by complete or partial fluorination of materials[40]. First examples of fluorinated ORMOCER®s have proven to effectively reduce transmission losses[41].

Within the scope of this work, the development and characterization of several new – mainly fluorinated – ORMOCER® materials with improved properties for telecom and datacom applications is presented. Technical fields covered herein are preparative organic and metal-organic chemistry, sol-gel processing, and the fabrication of simple microsystem demonstrators with photolithography under clean room conditions. Starting from the synthesis of precursor silanes, the ORMOCER® preparation proceeds via hydrolysis/condensation processes of the alkoxysilane moieties until the establishment of the inorganic-organic hybrid network by organic crosslinking. The different intermediate stages undergo in-depth structural characterization by various means of material analysis, with special attention to nuclear magnetic resonance spectroscopy (NMR). Molecular modeling tools allow the visualization and interpretation of spectroscopic data, which in turn leads to the deduction of structure-property correlations. Focused on the new materials presented, correlations are deduced with respect to their transmission losses at the telecom wavelengths 1310 nm and 1550 nm as well as their refractive indices.

2 THEORETICAL FUNDAMENTALS

Before directing attention to the discussion of new results within the next capital sections, the present chapter outlines a theoretical background of materials for telecom applications. With refractive index and transmission losses at the telecom wavelengths, the key optical properties relevant for the materials are introduced. Additionally, several micropatterning methods are described, which are employed for the manufacture of microsystems such as microoptical devices. A variety of low-loss materials are reviewed, prior to a description of ORMOCER® hybrid polymers, which is completed by an outline of relevant aspects of sol-gel chemistry and photolithographic patterning.

2.1 Refractive index

The index of refraction n quantifies the proportion to which velocity c_{medium} of light travelling through a medium is slower than the speed c_0 of light travelling through vacuum[9] (eq. 1).

$$c_{medium} = \frac{c_0}{n} \quad \text{(eq. 1)}$$

The refractive index of a material is in close relation to its dielectric constant ($n \approx \sqrt{e}$)[42]. Both properties depend on the polarizability of a substance, i.e. its susceptibility to charge separation when exposed to an electric field. In case of refraction, interaction between the electromagnetic light wave with the polarizable material leads to the above mentioned decrease in light speed. Three phenomena contribute to the polarization of a molecule, orientational, atomic displacement, and electronic increments[43]. Orientational polarization comes into play, if the molecule has a permanent dipole. Upon exposure to an electric field, the molecules undergo orientation so as to point with their partial charges towards the respective electrodes of opposing charge. Atomic polarization means stretching and bending of atomic bonds within the molecule in order to interact with the field. The electronic mode of polarization, finally, originates from redistribution of electronic density within the molecule without affecting its nuclear backbone or directional orientation. It is of particular importance in the presence of π-systems such as conjugated olefins or aromatic systems. The high electronic mobility in such systems allows the quick redistribution of electronic densities within the molecule, which enables easy interaction with external electric fields. Therefore, aromatic systems generally have higher refractive indices than aliphatic ones.

Fluorination, however, affects the dielectric constant/refractive index of a material in several ways simultaneously. From studies on fluorinated and non-fluorinated polyimides[44], it has been suggested that replacement of hydrogen with fluorine always lowers the dielectric constant/refractive index increment due to electronic mode of polarization because of the smaller electronic polarizability of the C-F compared to C-H bonds. Fluorination has no effect on the atomic mode of polarization. Fluorination also results in an increase of free volume due to the greater steric volume of the fluorine relative to the hydrogen atoms. In combination with frequently present mutual repulsion of fluorinated moieties, this accounts for an additional decrease in polarizability by reducing the number of polarizable groups in a volume unit. In case of asymmetric incorporation of fluorine, however, the orientation increment of polarization is increased.

As a compilation of compounds with relevance to this work, Tab. 1 outlines the refractive indices of possible commercially available precursor silanes of ORMOCER®s for telecom applications. Only 4-vinylphenyltrimethoxysilane is unavailable and has been synthesized at ISC. Comparison of analogous compounds illustrates the above mentioned influences of chemical structure on refraction. Since the refraction of a material or compound is additive with respect to molar increments of functional groups or molecular fragments[45,46], Tab. 1 allows a rough index estimation of materials with certain precursor compositions.

Refraction is subject to dispersion, i.e. the refractive index of a material is wavelength dependent[42,43]. Due to its additional temperature dependence, index values are commonly measured with light of 589 nm wavelength (sodium D-line) at 20 °C, which is denoted by the symbol n_D^{20}. In the infrared (IR), near infrared (NIR), and visible (VIS) spectral regions, the index normally decreases with increasing wavelength. This is due to the fact that photons of higher energy (low wavelength / high frequency) can interact more strongly with a medium than photons of lower energy (high wavelength / low frequency)[43]. In the ultraviolet (UV) region and at higher frequencies, however, often deflections from this rule of thumb can be observed in case of a frequency match with an absorption band of the material.

Transparent anisotropic materials are birefringent, i.e. the refractive index depends on the direction, in which light travels through the medium[47]. Birefringence in polymer systems arises from molecular orientation, which can be either natural, such as in semi-crystalline polymers, or artificial, such as mechanically induced stress[45]. A birefringent material has the ability to rotate the plane of polarized light, whereby the birefringence is quantified by the difference between the refractive indices parallel and perpendicular to the plane of orientation. Perpendicular indices of anisotropic waveguide materials are labeled n_{TE} and n_{TM}, whereupon the subscripts denote the transverse electric (TE) and transverse magnetic (TM) modes in the fiber, respectively[22,48,49].

Birefringence is an undesirable effect in materials for optical waveguide applications, because of its contribution to optical loss.

Tab. 1: Refractive indices n_D^{20} of selected organosilanes.

Silane	n_D^{20}
pentafluorophenyltriethoxysilane	1.417[50]
phenyltrimethoxysilane	1.473[51]
phenyltriethoxysilane	1.472[51]
diphenyldimethoxysilane	1.545[51]
diphenyldiethoxysilane	1.527[51]
4-vinylphenyltrimethoxysilane	1.505[52]
phenylmethyldimethoxysilane	1.469[51]
phenylmethyldiethoxysilane	1.469[51]
3-methacryloxypropyltrimethoxysilane (MEMO)	1.431[51]
3-methacryloxypropyltriethoxysilane	1.428[51]
3-glycidyloxypropyltrimethoxysilane (GLYMO)	1.429[51]
tetramethoxysilane (TMOS)	1.369[51]
tetraethoxysilane (TEOS)	1.382[51]
vinyltrimethoxysilane	1.393[51]
methyltrimethoxysilane	1.370[51]
n-propyltrimethoxysilane	1.388[51]
n-propyltriethoxysilane	1.396[51]
(3,3,3-trifluoropropyl)trimethoxysilane	1.355[51]

2.2 Optical loss in waveguides

In general, light propagating in optical waveguides suffers from intensity losses, i.e. the intensity I_{in} of the light coupled into the waveguide is higher than the intensity I_{out} that is received at its end. This phenomenon is known as optical loss, often also referred to as attenuation. The attenuation A given in decibel [dB] is expressed by the Beer-Lambert Law[7,53] (eq. 2). A is proportional to the absorption pathlength l and to the concentration c of the absorbing species, of which the molar (decadic) absorption coefficient α is a characteristic.

$$A = 10 \log_{10} \frac{I_{in}}{I_{out}} = \alpha c l \qquad \text{(eq. 2).}$$

Usually in polymer waveguides, loss values are given in [dB/cm], i.e. the attenuation is normalized to the length. For example, an attenuation of 10 dB/cm means that after traveling 1 cm, the intensity of the incoupled light is reduced to 10% of its original value, after traveling another centimeter, it is reduced to 1%, and so on. As for ORMOCER® optical materials, 0.5 dB/cm is a typical value for attenuation at 1550 nm, which is an excellent figure for a micropatternable polymer[32]. This means that by traveling through an optical waveguide of 1 cm in length, the intensity of a respective signal is reduced to 89% of its original value. In contrast to polymeric materials, however, contemporary high-grade optical silica fibers for long-range telecommunication (WAN) exhibit losses as low as 0.26 dB/km[7]. Optical loss can be caused by a variety of mechanisms such as absorption and scattering losses, which are strongly dependent on the light's wavelength.

2.2.1 Absorption loss

In the telecom wavelengths region 1300 – 1600 nm, absorption losses in optically conductive materials originate from molecular vibrations. Particularly, vibrational overtones of C-H, O-H, and N-H bonds have been identified as highly absorptive in the telecommunication windows[38,39,54,55]. Thus, in order to reduce attenuation, a straightforward approach is to find materials with low contents of the respective functionalities.

Ground state molecular vibrations can be described in a very simplified way with the model of the harmonic oscillator[43]. The fundamental vibrational frequency ν_f of a chemical bond A-B depends on the restoring force K (bond strength) and the reduced mass $\mu_{A\text{-}B}$ (eqs. 3a, 3b).

$$\nu_f = \frac{1}{2\pi}\sqrt{\frac{K}{\mu_{A-B}}} \qquad \text{(eq. 3a)}$$

with

$$\mu_{A\text{-}B} = \frac{m_A m_B}{m_A + m_B} \qquad \text{(eq. 3b).}$$

Thus, upon variation of the reduced mass, e.g. substitution of hydrogen by a heavier atom, vibrational frequencies can easily be manipulated. In case of the C-H bonds, this easily leads to the approach of hydrogen replacement by deuterium. Another possibility is their substitution by halogen atoms. C-F and C-Cl functionalities, for example, are generally easier and cheaper available than deuteration. In addition, they can offer interesting opportunities for the alteration of properties such as refractive index, or hydrophobicity.

The model of the harmonic oscillator is sufficient to explain the dependence of molecular vibrations on atomic masses. However, in real molecular systems, the concept of anharmonicity

has to be considered. The symmetric (harmonic) parabolic curve is replaced by an asymmetric (anharmonic) one in order to explain the dissociation boundary at high atomic distances[43]. Moreover, differences between energy levels E_v corresponding to the different vibrational states v_n become gradually smaller towards higher atomic distances, which is quantified by the anharmonicity constant x_e (eq. 4).

$$E_v = \left(v + \frac{1}{2}\right)h\nu - x_e\left(v + \frac{1}{2}\right)^2 h\nu \qquad \text{(eq. 4)}.$$

Anharmonicity makes possible vibrational transitions with $\Delta v \neq \pm 1$, thus overcoming the strict selection rule of the harmonic model and thus giving rise to the appearance of vibrational overtones. The larger the anharmonicity, the stronger are the spectral overtone bands. The higher the overtone order, however, the lower is the corresponding band strength. The latter decrease in absorption strength is about one order of magnitude between each harmonic order[13].

Several theoretical as well as experimental studies have been conducted on the influence of deuteration, fluorination, and chlorination on molecular vibrations in contrast to C-H bonds. Hydroxyl as well as carbonyl bonds have also been considered. Table 2 outlines important vibrational frequencies (fundamentals ν_f and overtones) in optical polymers determined *via* a theoretical approach[38,39]. This survey clearly shows that in the interesting NIR region, C-H and O-H vibrations contribute to absorption in the 1300 – 1600 nm region with overtones of only low order ($\nu_{2\text{-}3}$), thus leading to high spectral band strengths. In contrast, C-F and C-Cl vibrational overtones in the relevant NIR wavelengths are already of high order ($\nu_{5\text{-}11}$) and thus account only for low spectral band strengths. Further theoretical studies[56] revealed that the C-H bond expresses a higher anharmonicity constant compared to C-F and C-Cl, additionally accounting for higher overtone band strengths.

A recent spectroscopic investigation resulted in C-H and O-H overtone peak assignments for a hybrid inorganic/organic polymer derived from a condensation reaction of MEMO, zirconium(IV)-*n*-propoxide and methacrylic acid (Tab. 3)[57]. The spectral analysis generally corresponds to the theoretical studies mentioned before and in addition to that, renders differences between aliphatic and olefinic C-H bonds more precisely. The results are supported by a thorough investigation on the vibrational spectrum of bisphenol A polycarbonate (Fig. 6), which gave detailed peak assignments of aromatic and aliphatic C-H overtone vibrations (Tab. 4)[58]. Consistently with the noted investigations on the hybrid material, C-H bonds in aromatic/olefinic systems have slightly higher overtone frequencies than in aliphatic ones. During a survey on hydrocarbon gases, finally, it was shown that the fifth C-H overtone band energies

decrease with an increase in bond length[59]. Thus, in the literature, a general progression in C-H vibrational frequencies is found as follows: $\nu_{CH(aromatic)} > \nu_{CH(vinyl)} > \nu_{CH4} > \nu_{CH3} > \nu_{CH2} > \nu_{CH}$.

Tab. 2: Theoretically determined fundamentals ν_f and overtones ν_n of organic bond vibrations in the VIS, NIR and IR[38,39]. Vibrations relevant for transmission losses in optical waveguides are highlighted in terms of color.

vibration	λ (C-H) [nm]	λ (C-D) [nm]	λ (C-F) [nm]	λ (C-Cl) [nm]	λ (C=O) [nm]	λ (O-H) [nm]
ν_f	3390	4484	8000	12987	5417	2818
ν_2	1729	2276	4016	6533	2727	1438
ν_3	1176	1541	2688	4318	1830	979
ν_4	901	1174	2024	3306	1382	750
ν_5	736	954	1626	2661	1113	613
ν_6	627	808	1361	2231	934	523
ν_7	549	706	1171	1924	806	
ν_8		626	1029	1694	710	
ν_9		566	919	1515	635	
ν_{10}			830	1372		
ν_{11}			758	1256		
ν_{12}			698	1158		
ν_{13}			647	1076		
ν_{14}			603	1006		
ν_{15}				945		
ν_{16}				892		
ν_{17}				845		
ν_{18}				803		

Tab. 3: C-H overtone peak assignments for a hybrid inorganic/organic polymer[57].

λ **[nm]**	**assignment**
1750-1680	first overtone, CH [CH_3 or CH_2 (saturated)]
1630	first overtone, CH [HC=CH]
1600-1480	Zr-OH and Si-OH, linked
1480-1300	Zr-OH and Si-OH, free
1420	first overtone, CH [CH_2] + δSiOSi
1380	first overtone, CH [CH_3] + δSiOSi
1200	second overtone, CH [CH_2]
1150	second overtone, CH [CH_3]

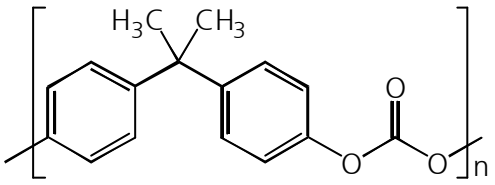

Fig. 6: Bisphenol A polycarbonate[58].

Tab. 4: C-H overtone peak assignments for bisphenol A polycarbonate[58].

$\tilde{\nu}$ **[cm^{-1}]**	≈ λ **[nm]**	**assignment**
5714	1750	first overtone, aliphatic
5952	1680	first overtone, aromatic
8403	1190	second overtone, aliphatic
8772	1140	second overtone, aromatic
10989	910	third overtone, aliphatic
11494	870	third overtone, aromatic

2.2.2 Other sources of optical loss

Rayleigh scattering affects the short-wave telecommunication band at 850 nm, but becomes insignificant at the long-wave bands around 1310 nm and 1550 nm[60]. However, defects of all

kinds in waveguides are responsible for various types of scattering losses. Physical defects such as surface roughness, cracks, voids, and inclusions of impurities such as dust as extrinsic scattering sources have to be avoided[61]. This also applies to intrinsic sources like materials defects such as phase separation or density fluctuations resulting in birefringence. If a material is birefringent, an optical device made from this material will have strong polarization dependence concerning its waveguiding abilities[62]. Therefore, amorphous, isotropic materials are required for application in telecom optics. Highly ordered polymers with a tendency to crystallize such as polytetrafluoroethylene (PTFE) have substantial scattering losses and are bad candidates for optical applications[63,64]. Beside material properties, attenuation can also originate from waveguide design. Waveguide surface roughness[65] as well as alignments and reflections in fiber joints[7] are extrinsic examples of optical loss.

2.3 Processing / patterning methods

A variety of patterning processes are in use for the manufacture of microsystems[66-68]. An easy to use and relatively cheap patterning method is hot embossing of a thermoplast film, which is stamped by a heated embossing tool carrying a negative relief of the desired pattern[69,70]. Upon softening of the polymer by heat followed by cooling, the patterns, e.g. optical waveguide structures, are transferred to the material. A related high-throughput patterning method is imprint lithography[71]. Within this technology, compression molding is used to create a thickness contrast in a resist, followed by reactive ion or wet etching for the completion of patterning. Nanoimprint lithography can produce features in the 25 nm scale and works preferably with thermoplastic polymers, which upon heating soften and thus facilitate the imprint process. High-resolution structure formation of dielectric polymers can be induced electrostatically[72]. For this, a dielectric polymer film is placed between the two electrodes of a capacitor, one of which is topographically structured (<140 nm resolution). Upon application of a strong electric field the pattern is transferred to the polymer.

For polymeric materials other than thermoplasts, other constructive and destructive techniques come into play. Some of these techniques exploit the ability of liquid prepolymer resins to harden upon irradiation. Soft lithography is a replication method making use of transparent molds or stamps to generate patterns from UV-sensitive resins in the micrometer and sub-micrometer scale[73-78]. Casting and curing polydimethylsiloxane against a photolithographically produced relief pattern forms these elastomeric elements for molding and stamping. Irradiation of the prepolymer being in contact with the mold then produces a negative pattern by photopolymerization.

Well established in microsystems technology is photolithographic micropatterning of a UV-sensitive film through a mask[66-68,79-82]. Applied to prepolymer films, which harden upon UV exposure, local polymerization is initiated by irradiation through a transparent glass or quartz-glass mask, which is partially covered with a metal absorber layer pattern. The mask can either be in contact with the resin, or contact-free in close proximity[83]. The prepolymer film is only hardened in the irradiated areas, whereas unexposed areas are subsequently washed away with a developer solvent, thus transferring the patterns from the mask to the polymer film. Proximity-mode UV-photolithography is a preferred method for the manufacture of ORMOCER® micropatterns[32,33,37,84].

A combination of lithography and replication is the UV reaction molding technique, by which microoptical elements (waveguides, prisms, lenses) have been fabricated[36]. In this process, a liquid prepolymer resin is cast onto a UV-transparent replication master, which is in addition partially metallized like a conventional mask for lithography. Upon UV-irradiation, photochemical crosslinking of monomers occurs. Thus, ORMOCER® holding structures for fibers, coupling prisms (see Fig. 3, chapter 1), and multimode waveguide optical interconnects have been produced within one step.

Beside photolithography, laser direct writing is a versatile method for the manufacture of patterns from irradiation-hardenable prepolymer films[85,86]. Instead of limiting the exposed area with a mask, a laser spot is guided over the film, which literally writes the polymerization pattern into the layer. The 2PP process mentioned earlier (chapter 1, cf. Fig. 5) is a highly-developed 3D descendant of the laser direct writing technique with a resolution on the 200 nm scale[30]. Other than in the constructive writing process, lasers can also be used to modify polymer surfaces in a destructive way by means of ablation[87-89]. High-energy UV-laser pulses cause bond breaking in macromolecules resulting in multiple fragmentation products. Thus, micropatterning of structures can either occur by irradiation through a mask or by directing a narrowly focused laser beam in a form of direct writing/ablating technique. Laser ablation is self-developing in the sense that ablated material possesses high kinetic surplus energy and can be extracted by suction.

Particularly in the microelectronics industry, photoresist-based patterning is of great importance[67,68]. A photoresist is a photopatternable material, which serves as a patterning aid for a non-photopatternable thin film. A differentiation is made between negative and positive photoresists. Negative resists form polymer networks upon irradiation, i.e. they reduce their solubility in the developer solvent, so that the consecutive developing step accounts for a removal only of the unexposed areas. Positive photoresists in contrast enhance their solubility, so that the UV-exposed areas are washed away. The actual patterning of the underlying film is then achieved by either wet or dry etching of the partially resist-covered surface. In case of wet-

etching, i.e. the use of etching solutions, the resist must be insoluble, allowing for only the material surface that is not covered with the resist to be removed. In case of dry-etching techniques such as reactive ion etching (RIE), the resist relief is etched simultaneously to the bare film, thus protecting the covered area and transferring the pattern. However, a potential disadvantage of destructive patterning methods such as RIE or laser ablation for the manufacture of waveguide devices is increased scattering loss due to surface roughness[73].

Besides being etching-masks, photoresists are also utilized in lift-off processes as stripping vehicles for insoluble materials[67,68]. For the patterning of a metal layer, e.g., onto a substrate, the latter is first coated with a patterned photoresist film. Then the substrate/resist surface is covered completely with a metal layer, e.g. by a physical vapor deposition (PVD) method such as sputter deposition. Finally, the metal-covered resist layer is developed with a solvent, thus lifting off the metal resting thereon and leaving a micropatterned metal layer, where it had been deposited directly onto the substrate.

2.4 Polymers for optical waveguides

In the following, a compilation of commercial as well as experimental polymeric materials for passive microoptical waveguides is presented as published in the literature. Table 5 gives an overview in table form, in which the materials are ordered by polymer classes. As far as published, the compositions of the materials are roughly given, besides an outline of characteristic properties such as NIR optical loss, refractive index, micropatternability and thermal stability. Subsequently, the materials are reviewed in more detail, particularly in terms of chemical compositions. As this work deals with ORMOCER®s for microoptics, preliminary work published in this field will be presented within a special section afterwards.

Tab. 5: Polymers for optical waveguides, ordered by polymer classes.

Polymer type, brand name (company)	optical loss	refractive index	micropatterning	other properties	refs.
Polyacrylates					
PMMA	0.25 dB/cm (1300 nm) 0.75 – 1 dB/cm (1500 nm)	1.49 (680 nm) 1.48 (1550 nm)	photopatternable		[24,65, 90]
PMMA, ZK50 (Röhm)	1.0 dB/cm (1320 nm)	1.512 (1320 nm)		T_g: 85 – 115 °C, poor viscosity control	[21]
Polyguide™ (DuPont)	0.12 dB/cm (800 nm) 0.2 dB/cm (1300 nm) 0.6 dB/cm (1550 nm)	1.48 – 1.51	photopatternable	layer quality, thickness control	[91]
halogenated polyacrylates (AlliedSignal)	0.3 – 1.2 dB/cm (1550 nm)		photopatternable	thermal stability up to 365 °C, index-tunable	[19,92,93]
Sulfur-containing polyacrylates, Truemode™ (Terahertz Photonics)	0.5 dB/cm (1300 nm) 0.5 dB/cm (1550 nm)	1.45 – 1.58	photopatternable	low birefringence, thermal stability > 250 °C	[94,95]
halogenated polyacrylates	0.2 dB/cm (1300 nm) 0.7 dB/cm (1500 nm)	1.464 – 1.518 (1300 nm), tunable	photopatternable	T_g: 81 – 105 °C	[46,96,97]
partially fluorinated polyacrylates	1 dB/cm (1300 nm) 2 dB/cm (1550 nm)	1.39 – 1.45	RIE		[98]
fluoroether acrylate polymers	0.10 – 0.25 dB/cm (1550 nm)	1.319 – 1.341	photopatternable	thermal stability: 260 °C	[61]
aromatic epoxy-acrylate copolymers	0.5 dB/cm (1310 nm)	1.500 – 1.505 (1310 nm)	RIE	thermal stability: >150 °C	[99]
Epoxy-based materials					
SU-8 polymer family	0.5 dB/cm (1300 nm) 3 dB/cm (1550 nm)	1.596 (633 nm) 1.575 (1550 nm)	photopatternable (cationic initiation)		[100-102]
Benzocyclobutenes (BCB)					
Cyclotene® 3022 (Dow)	0.04 – 0.2 dB/cm (1300 – 1320 nm) <1.5 dB/cm (1550 nm)	1.560 (633 nm) 1.538 (1550 nm)	RIE	thermal stability: 350 °C	[48,103-106]
Cyclotene® 4000 (Dow)	0.81 dB/cm (1300 nm)	1.562 (589 nm)	photopatternable		[107]

Tab. 5: continued (1).

Polymer type, brand name (company)	optical loss	refractive index	micropatterning	other properties	refs.
Polyimides					
partially fluorinated polyimides	0.3 dB/cm (1300 nm, TE) 0.7 dB/cm (1300 nm, TM)		RIE	birefringence, thermal stability: 380 °C, reduced water uptake	[108,109]
methacrylate end-capped imide oligomers			photopatternable		[110]
polyimide-silica hybrids	0.5 – 1.9 dB/cm (1310 nm)	1.50 – 1.66 (1310 nm)	spin-coating / thermal curing		[111]
Polycarbonates					
polycarbonate (Aldrich)	0.8 dB/cm (1310 nm, TE) 1.4 dB/cm (1310 nm, TM)	1.543 – 1.546 (1550 nm)	RIE	birefringence, thermal stability: 90 – 230 °C	[48]
fluorinated polycarbonates	0.10 – 0.15 dB/cm (1565 nm)	1.464 – 1.517 (1565 nm)	RIE	T_g: 165 °C	[112]
Amorphous fluoropolymers					
Teflon™ AF (DuPont)		1.31 – 1.29			[113-115]
Cytop™ (Asahi Glass)		1.356 (633 nm) 1.34 (680 nm)			[90]
PFCB aryl ether polymers					
PFCB family, e.g. XU 35121 (Dow)	0.25 dB/cm (1300 nm) 0.25 dB/cm (1550 nm)	1.443 – 1.508 (1550 nm)	RIE	T_g: 175 – 350 °C	[116,117]
PEK					
unfluorinated PEK	0.7 dB/cm (1550 nm)	1.6112 (1550 nm)	molding	thermal stability: 500 °C	[118]
fluorinated PEK	<0.5 dB/cm (1550 nm)	1.514 – 1.517	RIE	thermal stability: 460 °C (N_2), birefringence	[22,62]
fluoroaryl PEK	0.2 dB/cm (1550 nm)	1,495 – 1.530 (1550 nm)	RIE	thermal stability: 510 °C (N_2), birefringence	[49]

Tab. 5: continued (2).

Polymer type, brand name (company)	optical loss	refractive index	micropatterning	other properties	refs.
Fluorinated dendrimers					
perfluoroaryl dendrimer	<0.5 dB/cm (1550 nm)	1.5 – 1.6 (1550 nm)	spin-coating, thermal curing		[119]
Miscellaneous fluorinated polymers					
fluorinated maleimide polymers	<0.5 dB/cm (1550 nm)	1.433 – 1.493	photopatternable		[120]
fluorinated thioether polymers	approx. 0.5 dB/cm (1550 nm)	1.336 – 1.418			[54]
fluorinated poly(arylene ether sulfide)	0.40 dB/cm (1550 nm)	1.520 – 1.552	RIE	high temperature resistance	[121]
pentafluorostyrene + glycidyl methacrylate	0.39 dB/cm (1320 nm) 0.42 dB/cm (1550 nm)	1.471 – 1.487 (589 nm)	photopatternable (cationic initiation)		[122]
as above + trifluoroethylmethacrylate	<0.8 dB/cm (1550 nm)		RIE		[16]
halogenated polyphosphazenes		1.389 – 1.561		high thermal stability	[123]
Polysiloxanes, inorganic-organic hybrids					
TMOS based sol-gel films		1.420 – 1.456	curing / lithography / wet etching		[124]
deuterated poly(phenylsiloxane)	<0.1 dB/cm (1300 nm) <0.5 dB/cm (1550 nm)	1.537 (1310 nm)	RIE		[125]
cross-linked silicone	0.5 dB/cm (1550 nm)	1.49 (1550 nm)	RIE		[126]
deuterated organopolysiloxanes	0.23 dB/cm (1550 nm)		RIE	T_g: >300 °C	[127]
hybrid acrylate-silica polymers	0.27 dB/cm (810 nm)	1.46 – 1.49 (633 nm)	photopatternable	low shrinkage	[128]

Tab. 5: continued (3).

Polymer type, brand name (company)	optical loss	refractive index	micropatterning	other properties	refs.
Polysiloxanes, inorganic-organic hybrids (continued)					
MEMO + phenyl/methyltriethoxysilane		1.517 / 1.474 (633 nm)	laser direct-writing		[55]
hybrid polymers with TiO_2, ZnO_2, SnO_2 nanoparticles		1.711 – 1.796 (633 nm)			[129]
polymethylsilsesquioxane/titania networks	0.18 – 0.31 dB/cm (1300 nm)	1.394 – 1.561			[130]
epoxy inorganic/organic hybrids	0.5 dB/cm (1300 nm) 0.8 dB/cm (1550 nm)		photopatternable (cationic initiator)		[131]
deuterated epoxy inorganic/organic hybrid polymers	0.1 dB/cm (1300 nm) 0.5 dB/cm (1550 nm)		photopatternable (cationic initiator)		[131]
ZrO_2 containing epoxy inorganic/organic hybrid polymers		1.477 – 1.542 (633 nm)	RIE		[132]

2.4.1 Polyacrylates

The absorption limited loss of polymethylmethacrylate (PMMA, Fig. 7) has been reported approx. 0.25 dB/cm at 1300 nm and approx. 0.75 dB/cm at 1550 nm, respectively[65]. The index of refraction at 1550 nm was 1.48, other authors report an index of 1.49 at 680 nm[90]. According to another source, waveguides directly photo-patterned from commercially available PMMA ZK50 (Röhm) have a refractive index of 1.512 and an attenuation of 1.0 dB/cm at 1320 nm[21]. It is true that the material could be processed even to form three-dimensional patterns, but the major drawback is its poor thermal stability due to its low glass transition temperature T_g of 85 – 115 °C, depending on modification. Another difficulty with PMMA is the control of viscosity, which is crucial when thicker films are needed. PMMA has been utilized for the manufacture of thermo-optic switches, where it has been directly photo-patterned in a thickness of 5 µm onto a SiO_2 layer[24] after mixing with a photoinitiator. Operating at 1550 nm, an attenuation of 1 dB/cm was found.

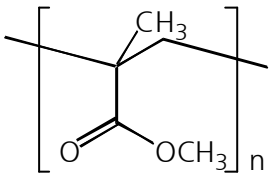

Fig. 7: Polymethylmethacrylate (PMMA).

Polyguide™, a photopatternable acrylate-based polymer developed by DuPont exhibits layer quality and thickness control and possesses tunable refractive indices (1.48 to 1.51)[91]. The non-halogenated material has optical losses of 0.12 dB/cm at 800 nm, 0.2 dB/cm at 1300 nm, and 0.6 dB/cm at 1550 nm, respectively. Thermal stability of up to 85 °C has been found.

A series of photopatternable, index-tunable acrylate polymers with various degrees of halogenation as provided by AlliedSignal Inc. was reported to have absorption losses of 0.3 dB/cm to 1.2 dB/cm at 1550 nm and a thermal stability of up to 365 °C[19,92,93].

Novel Truemode™ acrylate polymers based on a variety of sulfur containing monomers are commercially available from Terahertz Photonics[94,95]. These polymers exhibit tunable refractive indices of 1.45 – 1.58, low waveguide losses of 0.5 dB/cm at 1300 nm and 0.5 dB/cm at 1550 nm as well as low birefringence ($<10^{-4}$) and thermal stability exceeding 250 °C. After admixing a suitable photoinitiator, the prepolymers are reported direct photo-patternable. Figure 8 depicts the acrylate and methacrylate monomers necessary in the production of a polymer with 0.5 dB/cm loss at 1550 nm[95].

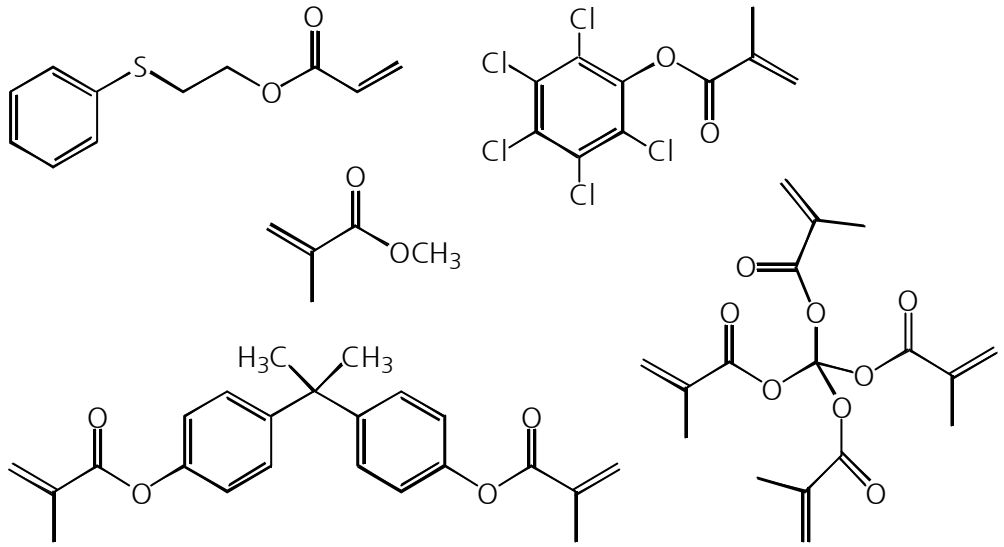

Fig. 8: Multifunctional acrylate and methacrylate monomers for Truemode™ polymer[95].

Halogenated acrylate and methacrylate monomers tetrachloroethylacrylate (Fig. 9a), pentafluorophenylacrylate (Fig. 9b) and pentafluorophenylmethacrylate (Fig. 9c) have been combined in varying compositions and copolymerized photochemically after addition of a photoinitiator[46,96,97]. Lowest absorption values measured at 1300 nm and 1550 nm were 0.2 dB/cm and 0.7 dB/cm, respectively, and the refractive index was tunable in a range of 1.464 and 1.518 (1300 nm). Thermal stability, still, was limited by glass transition temperatures around 81 – 105 °C.

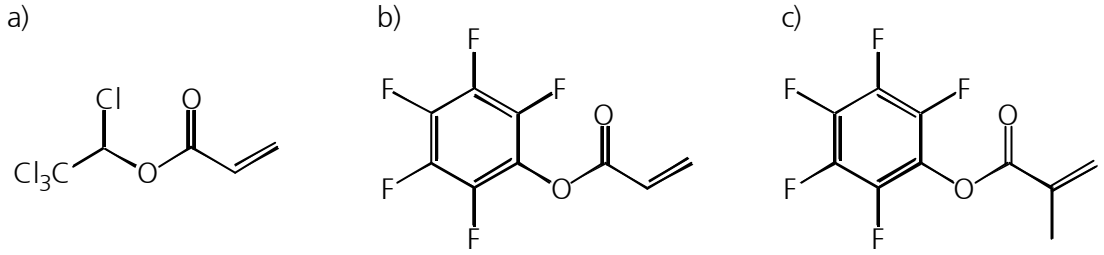

Fig. 9: Halogenated monomers for acrylate-based polymers[46,96,97].

Optical losses of 1 dB/cm at 1300 nm and 2 dB/cm at 1550 nm have been measured on waveguides fabricated from different mixtures of partially fluorinated acrylate monomers (Fig. 10)[98]. Depending on the monomer ratios, the refractive index was tunable within a range of $1.39 < n < 1.45$. Patterning was conducted using spin-coating, lithography of a resist and oxygen plasma reactive ion etching steps followed by resist lift-off, i.e. the material was not directly photopatterned.

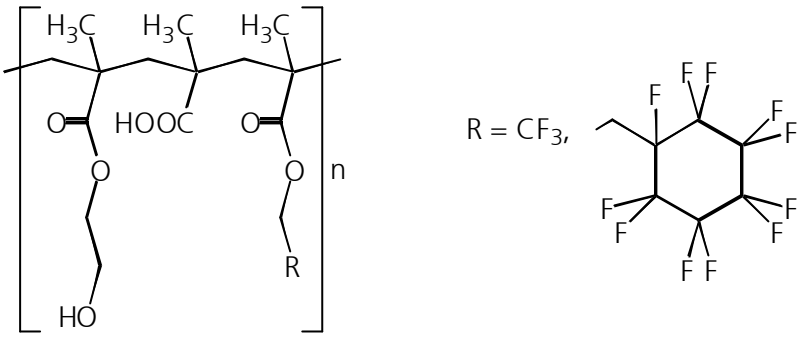

Fig. 10: Partially fluorinated acrylate-based polymer[98].

Very recently, low-loss fluoroether acrylate polymers have been reported, which do not undergo phase separation, offer appropriate viscosity required for spin-coating and for direct UV patterning[61]. The materials express thermal stabilities up to 260 °C. Different formulations from monomers as shown in Fig. 11 have refractive indices of 1.319 – 1.341 and losses of 0.10 – 0.25 dB/cm at 1550 nm. Optical loss values measured on liquid monomer/liquid monomer mixtures did not differ significantly from values measured on the corresponding singlemode waveguides.

Materials made from aromatic acrylated epoxy compounds copolymerized with difunctional acrylates have been reported with optical losses of 0.5 dB/cm and refractive indices of 1.500 to 1.505 at 1310 nm[99]. Embedded waveguides have been prepared by photo-curing and RIE resulting in materials with thermal stability exceeding 150 °C.

2.4.2 Epoxy-based materials

A major role in microsystems technology, particularly for microelectromechanical systems (MEMS), plays the SU-8 family of materials[100]. These epoxy-based polymers (Fig. 12) are direct-UV patternable upon cationic initiation, exhibiting negative-photoresist properties. Refractive indices of 1.596 at 633 nm and 1.575 at 1550 nm, respectively, have been reported[101]. Patterned SU-8 waveguides exhibited optical losses of 0.5 dB/cm at 1300 nm[102]. A high absorption of 3 dB/cm at 1550 nm, however, makes SU-8 a poor candidate for application in the third telecom window.

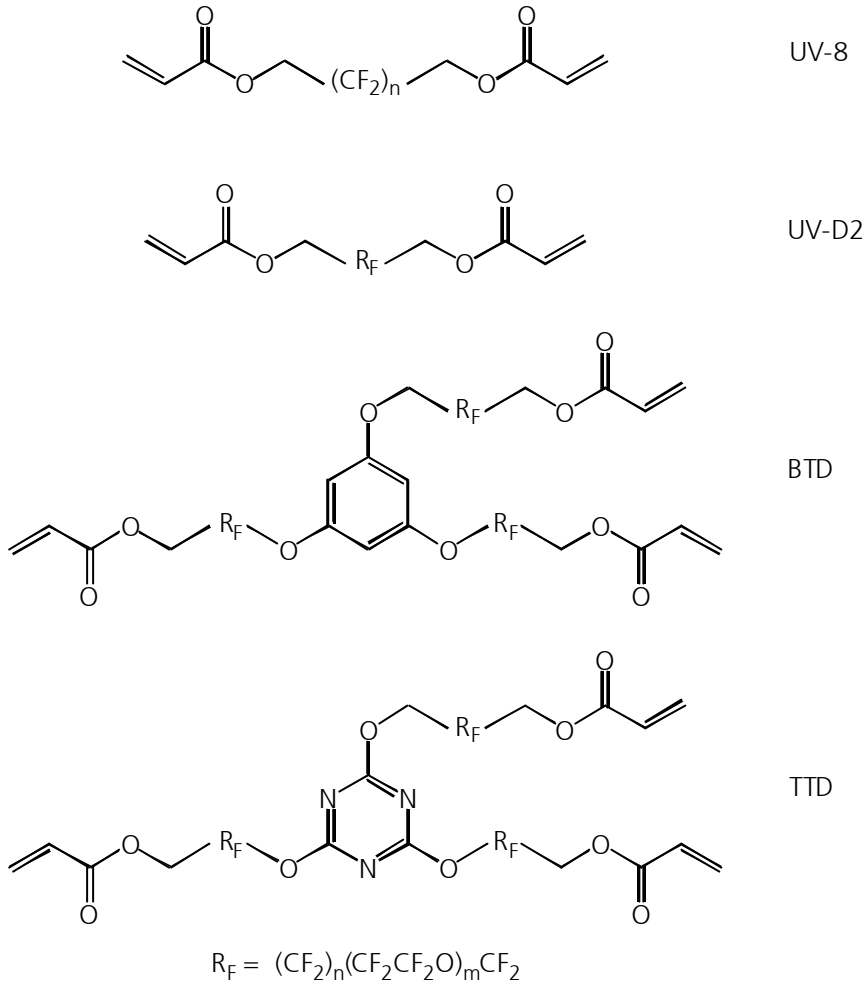

Fig. 11: Fluoroether acrylate monomers[61].

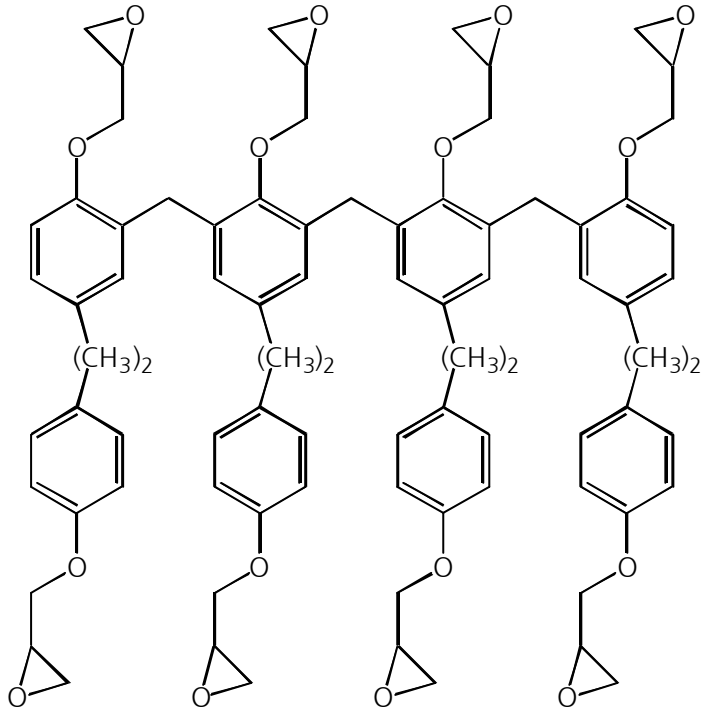

Fig. 12: Major component in SU-8 epoxy prepolymer resin[100].

2.4.3 Benzocyclobutenes (BCB)

Benzocyclobutenes (BCB) are materials developed by Dow Chemical originally designed as thin-film dielectrics. Since low optical loss values as low as 0.04 dB/cm at 1320 nm[103] and less than 1.5 dB/cm at 1550 nm[104] have been reported for the commercially available Cyclotene® 3022, these materials have gained interest for optical applications as well. However, the same material has also been reported with losses of 0.2 dB/cm at 1300 nm[105]. The material has a refractive index of 1.560 at 633 nm[106] and 1.538 at 1550 nm[48], respectively. Cyclotene® 3022 is based on the divinylsiloxane-containing monomer DVS-bis-BCB which is yielded by a Heck-type reaction of brominated BCB with the siloxane compound (Fig. 13)[105].

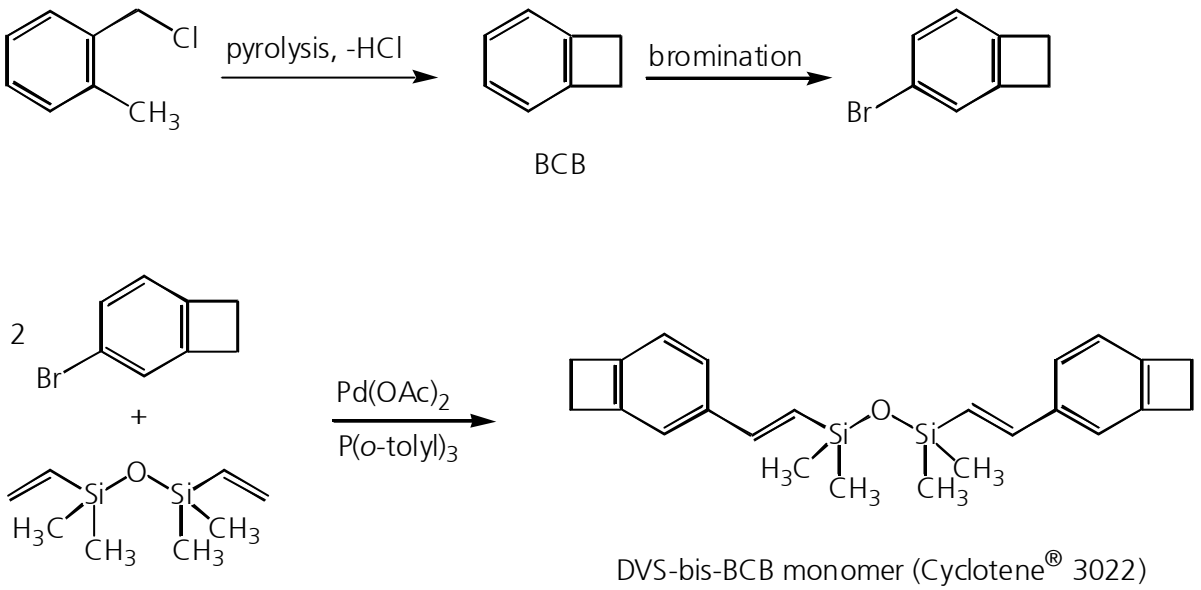

Fig. 13: DVS-bis-BCB monomer synthesis, including the palladium-catalyzed Heck-type reaction step[105].

Cross-linking occurs via thermal opening of the cyclobutene ring with the intermediate formation of an *o*-quinodimethane which readily undergoes Diels-Alder-type [4+2]-cycloaddition with the C=C double bond in the vicinity of the siloxane center. This leads to a rigid network, which exhibits high thermal resistance up to 350 °C (Fig. 14).

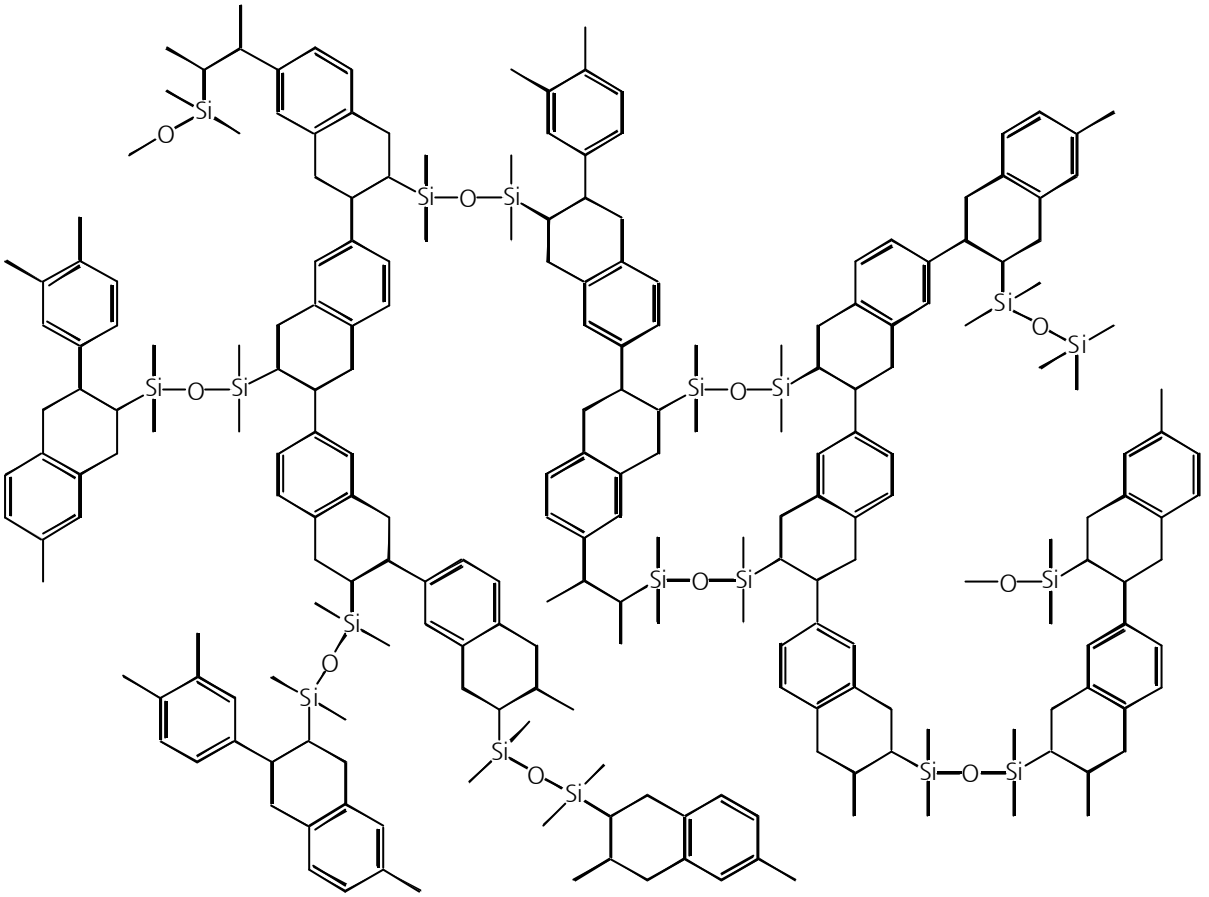

Fig. 14: BCB polymerization and cured Cyclotene® 3022[105].

Applicable resins are formed by allowing polymerization up to a certain point and then stopping the reaction, before the curing is fully completed. After thermal curing of the resin at 205 to 285 °C, photolithography in combination with dry-etching is used for the fabrication of micropatterns. While Cyclotene® 3022 cannot be photopatterned directly, a second set of formulations, the Cyclotene® 4000 series, has been used for direct photo-definition of waveguides. These resins include besides the said monomer the photocrosslinking agent 2,6-bis{(4-azidophenyl)methylene}-4-ethylcyclohexanone (Fig. 15), in low amounts (0.3% to 2.7%)[133].

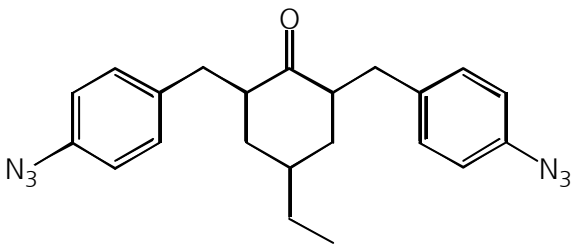

Fig. 15: Crosslinking agent for photoimageable BCB series Cyclotene® 4000[133].

After polymerization, the material has a refractive index of 1.562 at 589 nm[107]. Within a waveguide device fabricated from both formulations with the former as cladding and the latter as the core, an absorption loss of 0.81 dB/cm at 1300 nm was found. The large difference compared to the earlier published value of 0.04 dB/cm is attributed to the added photoactive component.

2.4.4 Polyimides

Non-fluorinated polyimides are well-suited for microelectronics because of their good thermal stability (> 300 °C), dielectric and mechanical properties. Their optical properties, however, make them poor performers as optical waveguiding materials. Polyimides tend to undergo ordering processes, which lead to the formation of scattering centers, thus giving rise to high scattering losses. In addition, formation of water during the imidization process can lead to voids and pinholes that again contribute to high scattering losses.

Partially fluorinated polyimides, examples of which are shown in Fig. 16, on the other hand, exhibit much less of the typical ordering processes[108]. The steric hindrance between the trifluoromethyl groups being attached to the arylic moieties forces the biphenyl units out of plane and thus partly prevent ordering due to chain packing. Thus, these materials can be used as optical waveguiding materials with a high thermal stability and low optical losses. However, aromatic ordering is still not negligible resulting in large birefringence and therefore a high degree of polarization dependent loss. As an example, single-mode waveguides fabricated from fluorinated polyimides 6FDA/TFDB and PMDA/TFDB as shown in Fig. 16 exhibited polarization-dependent losses at 1300 nm of 0.3 dB/cm and 0.7 dB/cm for TE and TM polarizations, respectively[108]. After heating the waveguides at 380 °C for 1 h and after exposure to 85% relative humidity at 85 °C for 200 h, respectively, no changes in optical loss could be detected, thus accounting for high heat and moisture resistance. Reduced water uptake (0.2 – 0.7%) due to fluorination compared to nonfluorinated polyimides (2%) contributes to low loss values at 1300 nm and 1550 nm as the O-H absorption around 1400 nm is decreased[109].

The reported polyimides, however, could not be directly photopatterned but had to be patterned by lithography/RIE. An alternative way of producing waveguide patterns from just one material was demonstrated when the refractive index of a 6FDA/TFDB film was altered locally by electron beam bombardment[134]. The core waveguide structure thus was made without further photolithography/RIE. In order to provide photosensitive polyimides for optical applications, methacrylate end-capped imide oligomers of the kind depicted in Fig. 17 have been prepared[110]. Upon addition of a photoinitiator, the soluble polyimides could be patterned by UV-induced cross-linking.

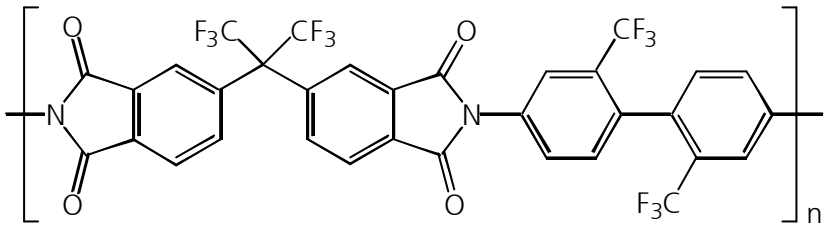

6FDA / TFDB

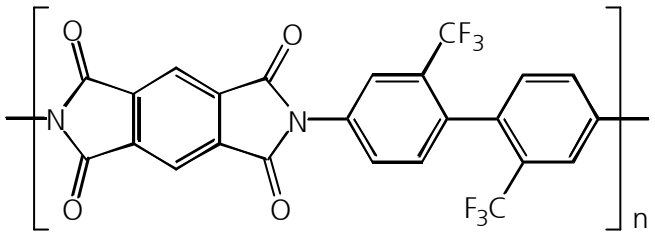

PMDA / TFDB

Fig. 16: Representatives of fluorinated polyimides[108].

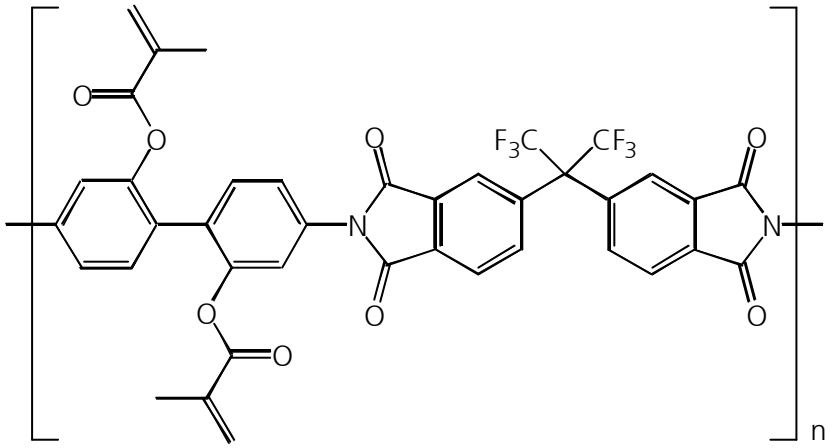

Fig. 17: Photo-patternable fluorinated imide oligomers[110].

A series of polyimide-silica hybrid materials with varying silica content has been reported having optical losses of 0.5 dB/cm to 1.9 dB/cm at 1310 nm, with refractive indices in a range from 1.50 to 1.66[111]. Thin films were prepared by sol-gel reaction combined with spin-coating on an oxidized silicon wafer and multistep curing resulting in high-temperature stable (>300 °C) planar optical waveguides. The pure polyimides have also been processed and their optical properties have been determined. Absorption values of 2.9 dB/cm and 1.7 dB/cm at 1310 nm for formulations PMDA-ODA and 6FDA-ODA, respectively (Fig. 18), indicate that the major source for optical loss are the C-H vibrations which are reduced in the silica-modified hybrid polymers.

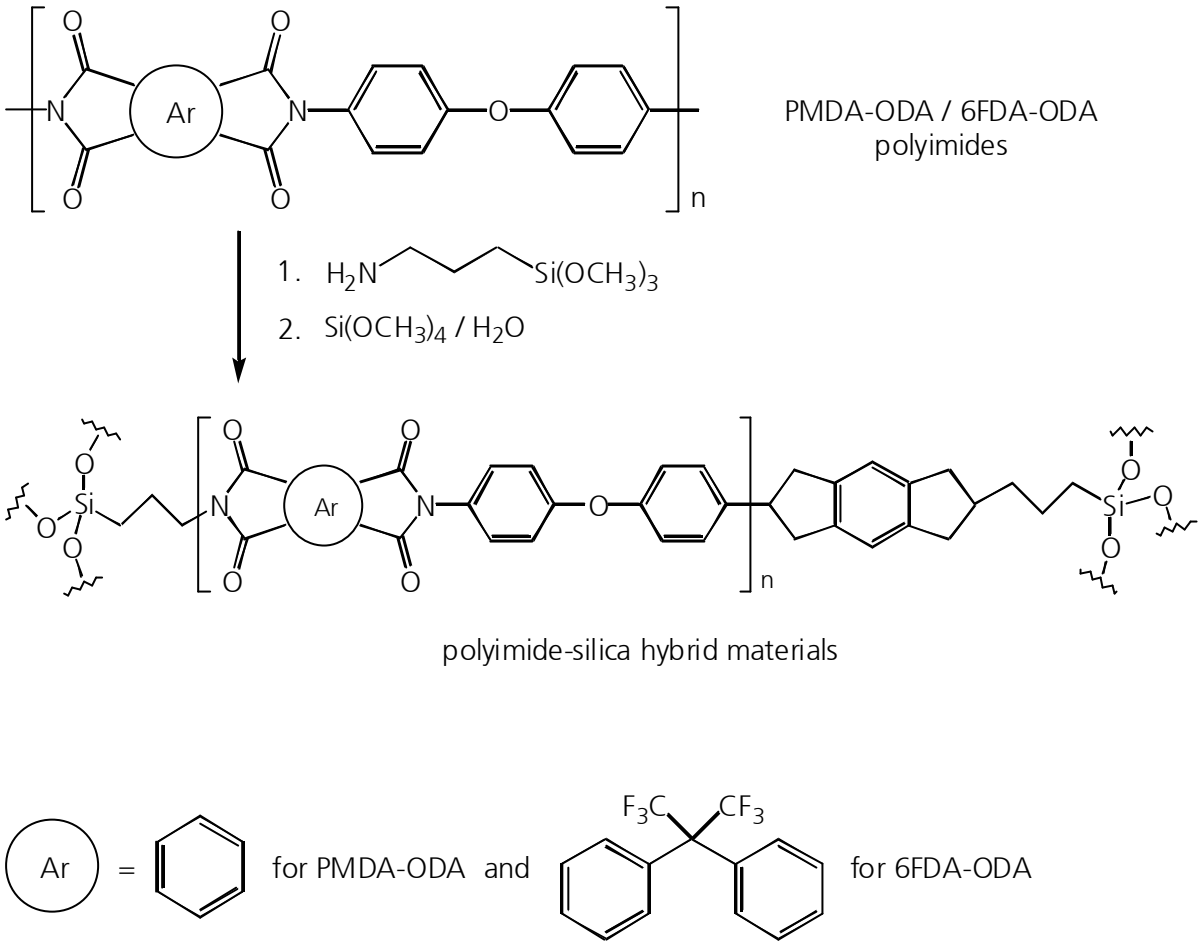

Fig. 18: Polyimides PMDA-ODA and 6FDA-ODA as well as their silica-modified organic-inorganic counterparts[111].

2.4.5 Polycarbonates

Bisphenol A polycarbonate (see Fig. 6), of which films have been prepared by dip-coating of a borosilicate substrate with the polymer solution, has a refractive index of 1.590 in the VIS range[135]. However, the coating technique produced films of a low thickness uniformity, thus resulting in high optical loss. A different polycarbonate commercially available from Aldrich Chemicals (Fig. 19) was patterned by oxygen plasma etching onto a buffer layer of benzocyclobutene Cyclotene® 3022 from Dow Chemicals[48]. The resulting waveguides had refractive indices n_{TE} and n_{TM} of 1.546 and 1.543, respectively, measured at 1550 nm. For 1310 nm, the material exhibited optical losses of 0.8 dB/cm and 1.4 dB/cm for the TE and TM polarizations, respectively. Thermal stability of the material up to 190 °C to 230 °C was reported.

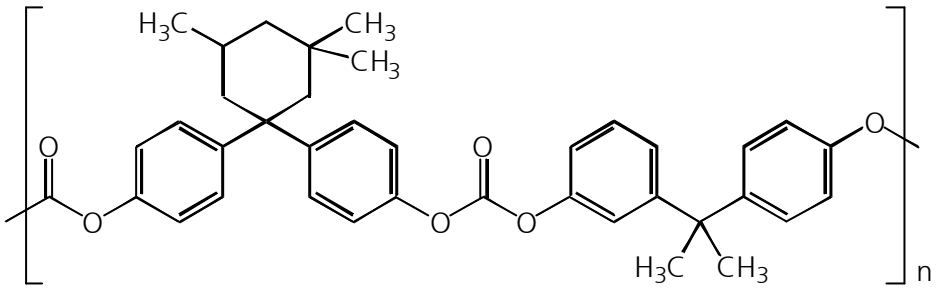

Fig. 19: Polycarbonate poly(bisphenol A carbonate-co-diphenol carbonate)[48].

Low-loss partially fluorinated optical polycarbonates with optical loss values at 1565 nm as low as 0.1 dB/cm to 0.15 dB/cm and refractive indices between 1.464 and 1.517 at same wavelength have been reported elsewhere (Tab. 6 / Fig. 20)[112]. Waveguide patterning has been performed by applying thermal curing prior to oxygen plasma etching resulting in the polymers with glass transition temperatures around 165 °C.

Tab. 6: Fluorinated polycarbonate formulations from monomers A-E [mol.%] (legend given in Fig. 20)[112].

Formulation	A	B	C	D	E	$n_{1565\ nm}$	optical loss$_{1565\ nm}$
I	50	25	25			1.5170	0.10 dB/cm
II	40	25	25	10		1.5111	0.10 dB/cm
III		25	25	50		1.4837	0.12 dB/cm
IV			25	50	25	1.4676	0.15 dB/cm

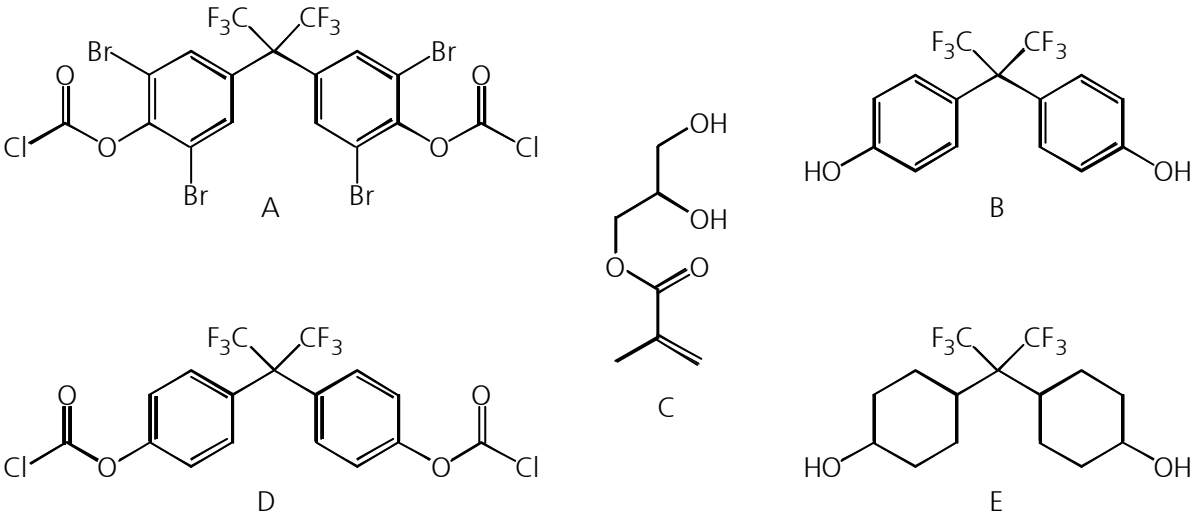

Fig. 20: Legend to Tab. 6: polycarbonate monomers A-E[112].

From formulations III and IV, the influence of phenyl in contrast to cyclohexyl rings on optical properties can clearly be seen. On the one hand, the aromatic component rises the index of refraction, on the other hand its reduced C-H content leads to a lower transmission loss at 1565 nm. From a comparison between compositions I and III, the influence of bromination instead of C-H bonds can be deduced. Again, reduced C-H content leads to lower absorption, and additionally, the incorporation of bromine atoms substantially rises refraction.

2.4.6 Amorphous fluoropolymers

While polytetrafluoroethylene (PTFE) as a highly ordered material gives rise to major scattering losses and is therefore not suitable for use in optical waveguide applications, the copolymer of tetrafluoroethylene with perfluoro-2,2-dimethyl-1,3-dioxole has found its place among the commercially successful optical polymers[113]. Under the brand name Teflon™ AF (amorphous fluoropolymer) it is commercially available from DuPont Fluoroproducts in a variety of different monomer ratios[114] (Fig. 21a). Teflon™ AF 1600 and 2400 have dioxole contents of 65% and 87 – 90%, respectively, and exhibit refractive indices of 1.31 and 1.29[114,115]. These very low index values are not only due to the high degree of fluorination, but can be attributed largely to the very large free volume the polymer morphology offers. The latter also leads to a high gas permeability, which can be exploited in gas sensor applications. The high degree of fluorination, however, makes adhesion to nonfluorinated substrates difficult. The fluorinated polyether Cytop™ (Fig. 21b), commercially available from Asahi Glass Co., has been used as a low-loss cladding for polymer optical waveguides with bisbenzocyclobutane Cyclotene® 3022-32 or PMMA as the core layers[106]. The refractive index of Cytop™ was determined as 1.356 at 633 nm, and 1.34 at 680 nm[90], respectively.

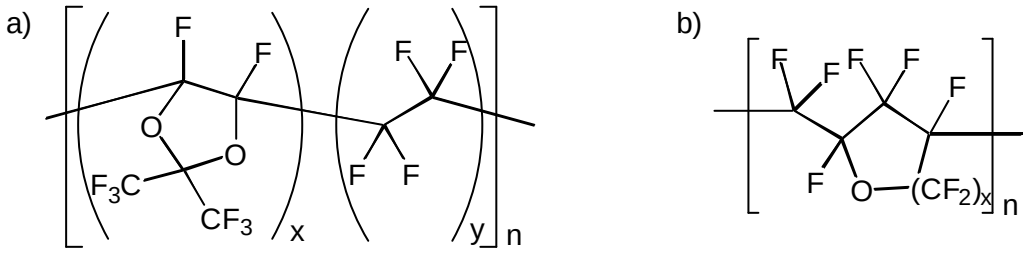

Fig. 21: Commercial fluoropolymers: a) Teflon™ AF (DuPont); b) Cytop™ (Asahi Glass).

2.4.7 Perfluorocyclobutyl (PFCB) aryl ether polymers

Singlemode optical waveguides have been fabricated from a Dow Chemical prepolymer resin, XU 35121[116]. The resulting PFCB aryl ether polymer (Fig. 22) shows high thermal stability and low optical losses of 0.25 dB/cm at both 1300 nm and 1550 nm. Similar loss values as well

as refractive index tunability in a range of 1.443 – 1.508 (1550 nm) are described for a series of PFCB materials copolymerized from monomers with varying arylic functions (Fig 23)[117]. High thermal stabilities as deduced from glass transition temperatures T_g of 175 °C to 350 °C for different formulations were found.

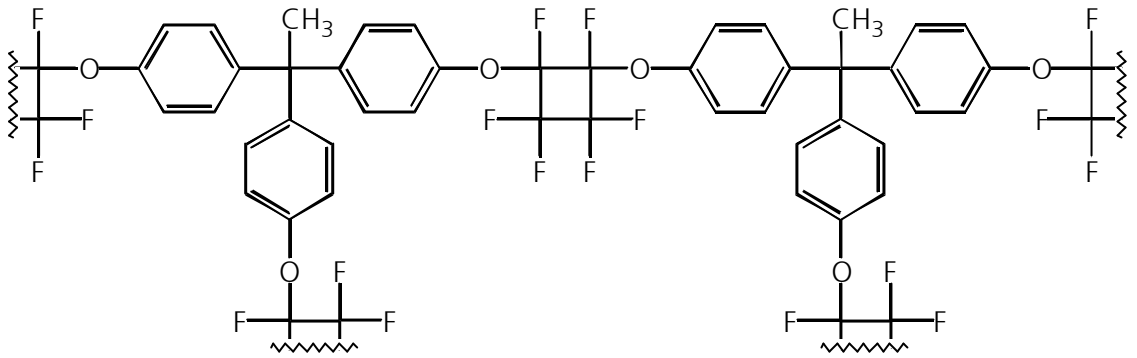

Fig. 22: 1,1,1-Tris(4'-trifluorovinyloxyphenyl)ethane polymer network[116].

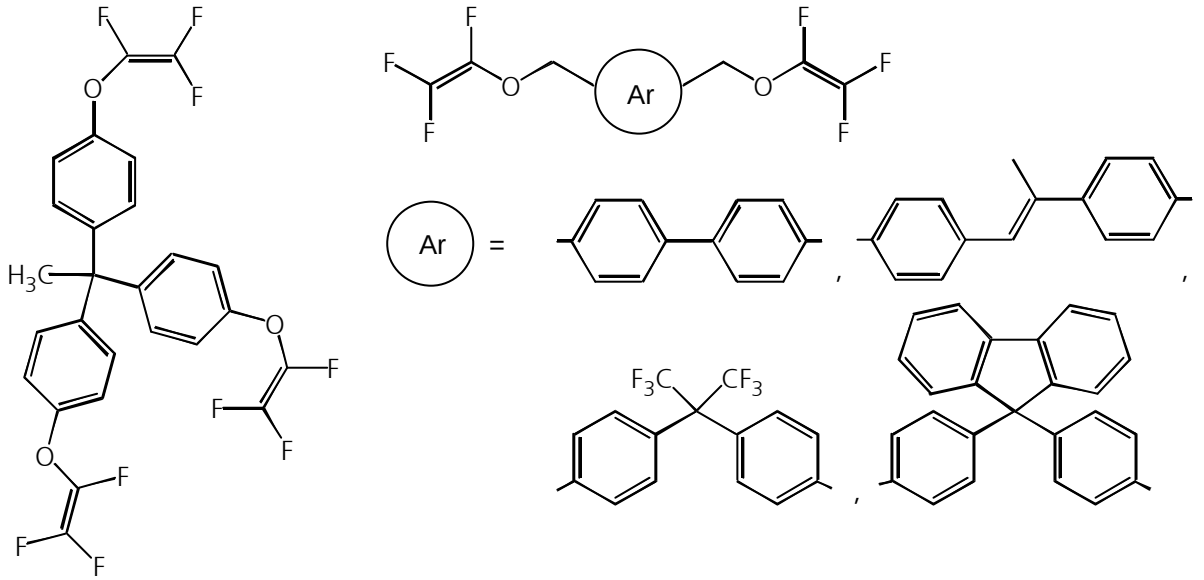

Fig. 23: Trifluorovinyl aryl ether monomers for PFCB copolymers[117].

However, PFCB materials are not photopatternable. In contrast, the fabrication process included patterning (lithography/RIE) of an inverse structure of the desired rib waveguide into the substrate silicon, then thermal growth of silicon oxide as the buffer layer and afterwards spin-coating of the polymer resin into the thus prepared grooves and thermal curing. This multi-step process makes waveguide fabrication from PFCB very expensive and presents a major drawback of this class of materials.

2.4.8 Polyether ketones (PEK)

An unfluorinated polyether ketone (PEK) has been found thermally stable up to 500 °C, having a refractive index of 1.612 and an optical loss of 0.7 dB/cm at 1550 nm[118]. Waveguide patterning was performed indirectly by first patterning the silicon/silicon dioxide substrate and then filling the resulting grooves with the PEK core layer. A fluorinated poly(ether ketone) FPEK-EP (Fig. 24) has been reported as a crosslinkable fluorinated polymer possessing a low optical loss (<0.5 dB/cm at 1550 nm measured on a single-mode waveguide) and a high thermal stability of up to 460 °C under nitrogen atmosphere[62]. The material has been utilized in the fabrication of waveguide splitters and the patterning process included thermal curing at 250 °C and oxygen reactive ion etching[22]. A slight birefringence leads to polarization-dependent refractive index values n_{TE} and n_{TM} of 1.517 and 1.514, respectively.

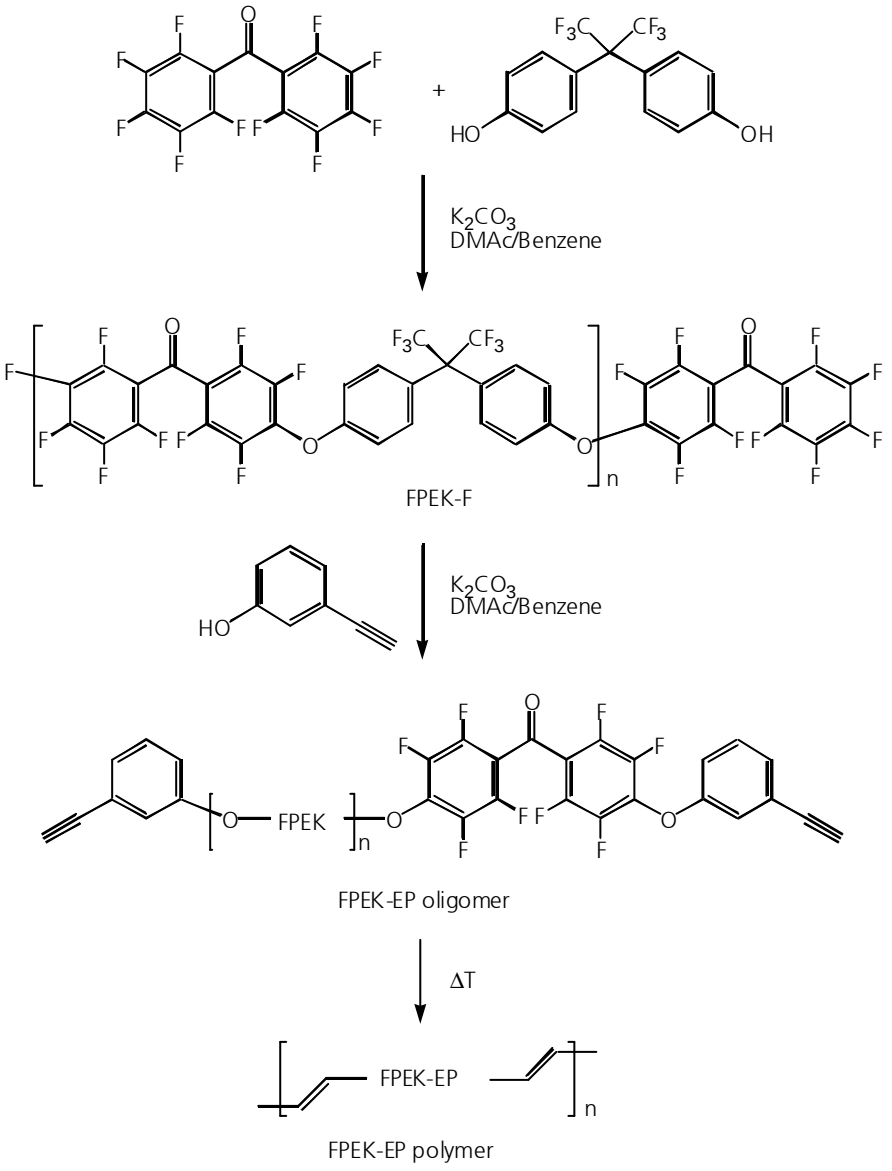

Fig. 24: Synthesis of fluorinated polyether ketone FPEK-EP[62]. DMAc = N,N-dimethylacetamide.

Figure 25 shows a similarly synthesized crosslinkable fluorinated poly(arylene ether) FPAE-Fn-PEP, which, after thermal curing, has been reported to exhibit an optical loss of 0.2 dB/cm at 1550 nm as well as thermal stability as high as 510 °C in a nitrogen atmosphere[49]. Upon adjusting the oligomer molecular weight, the refractive index could be tuned in a range between 1.495 and 1.530 at 1550 nm. The loss measurements were carried out on a single-mode waveguide, which had been patterned by spin-coating on a silicon dioxide cladding, thermal curing at 320 °C, photolithography and oxygen reactive ion etching. However, besides the necessity of high curing temperatures, the material suffered from birefringence ($\Delta n = |n_{TE} - n_{TM}| = 0.007$).

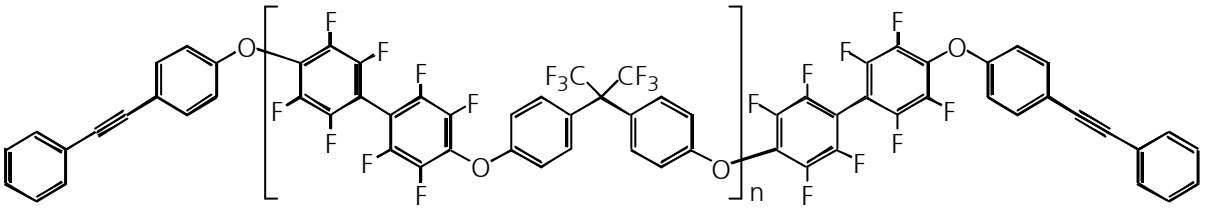

FPAE-Fn-PEP oligomer

Fig. 25: Crosslinkable fluorinated poly(arylene ether) FPAE-Fn-PEP[49].

2.4.9 Fluorinated dendrimers and hyperbranched polymers

Polymers consisting of branched repeat units can either exhibit an irregular architecture to form hyperbranched polymers or can be highly ordered in which case they are referred to as dendrimers[136]. The globular character of dendrimers offers the possibility to encapsulate functionalities that allow emission, light amplification, and light-harvesting applications. With the development of highly fluorinated hyperbranched polymers, low-loss materials for waveguide applications are available, which are particularly interesting as matrices for the incorporation of luminescent lanthanoids such as Er^{3+} or Nd^{3+} for light amplification[119]. Figure 26 outlines a typical hyperbranched fluorinated polymer synthesized from 3,5-bis(pentafluorophenyl)phenol. Termination with styryl functionalities provides crosslinkability. Optically conducting films have been prepared by spin-coating and thermal curing. For 1550 nm, optical losses below 0.5 dB/cm as well as tunable refractive indices in the range of 1.5 to 1.6 have been reported[119]. In case of the hyperbranched polymer prior to the incorporation of cross-linkable styryl groups, the loss at 1550 nm was as low as 0.1 dB/cm due to the absence of C-H[137].

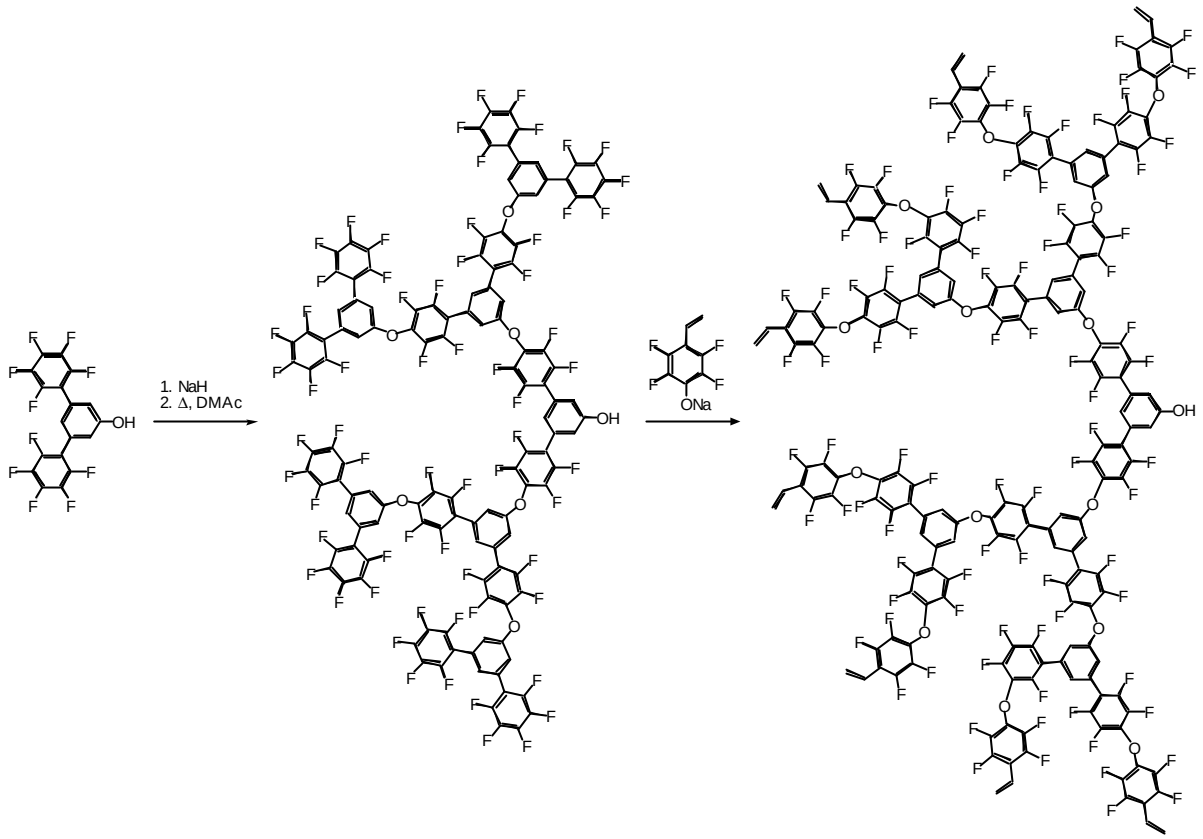

Fig. 26: Synthesis and functionalization of a fluorinated hyperbranched polymer for optical applications[119].

2.4.10 Miscellaneous fluorinated polymers

A group of highly fluorinated polyesters has a reported optical loss of 0.5 dB/cm at 1550 nm and tunable refractive indices between 1.474 and 1.559[138]. From this class of condensation polyesters, polymer optical fibers (POF) have been fabricated as well as planar optical devices, such as embedded waveguides.

Several fluorinated maleimide polymers, which are compatible to all major processing technologies (direct photolithography, hot embossing, micromolding) have refractive indices in a range from 1.433 to 1.493[120]. Optical losses of less than 0.5 dB/cm at 1550 nm have been reported, resulting from low losses of the monomers as outlined in Fig. 27 (at 1550 nm: 0.13 dB/cm for pentafluorophenylmaleimide, and 0.18 dB/cm for heptdecafluorodecyl acrylate).

Polymers generated radically *via* the thiol-ene reaction from an at least difunctional thiol compound and an at least difunctional fluorinated ethylene unsaturated compound have been proposed as optical materials (Fig. 28)[54]. The radical reaction may be initiated thermally or photochemically by decomposition of a suitable photo initiator admixed prior to processing. An important advantage for the choice of thiol compounds as prepolymers is the fact that unreacted S-H moieties do not affect transmission in the NIR in a way the silanol group does.

This is due to the fact that the thiol function has a higher reduced mass than O-H, resulting in different fundamental as well as overtone vibrations. Optical losses of 0.5 dB/cm at 1550 nm are expected from said fluorinated thioether polymers with refractive indices around 1.336 to 1.418.

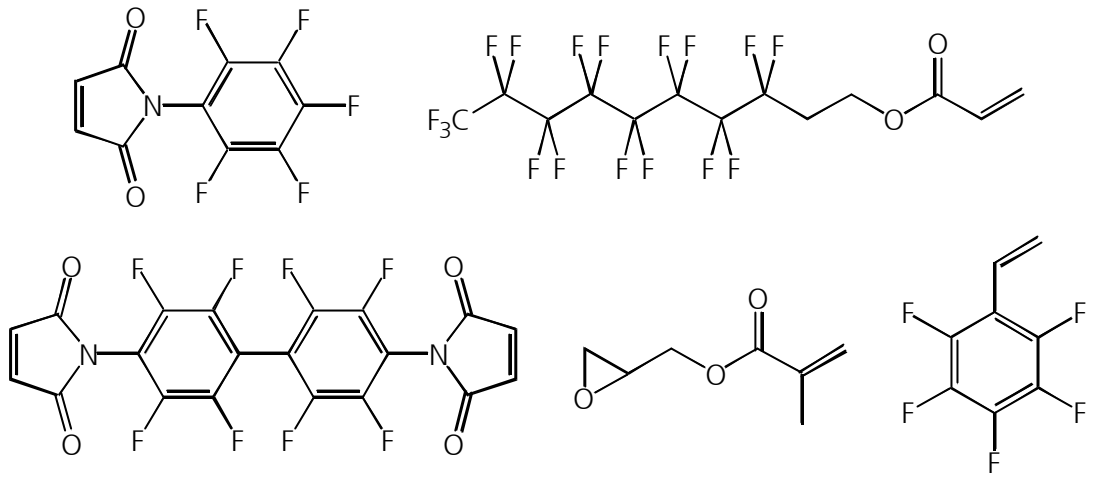

Fig. 27: Exemplary monomers for fluorinated maleimide copolymers[120].

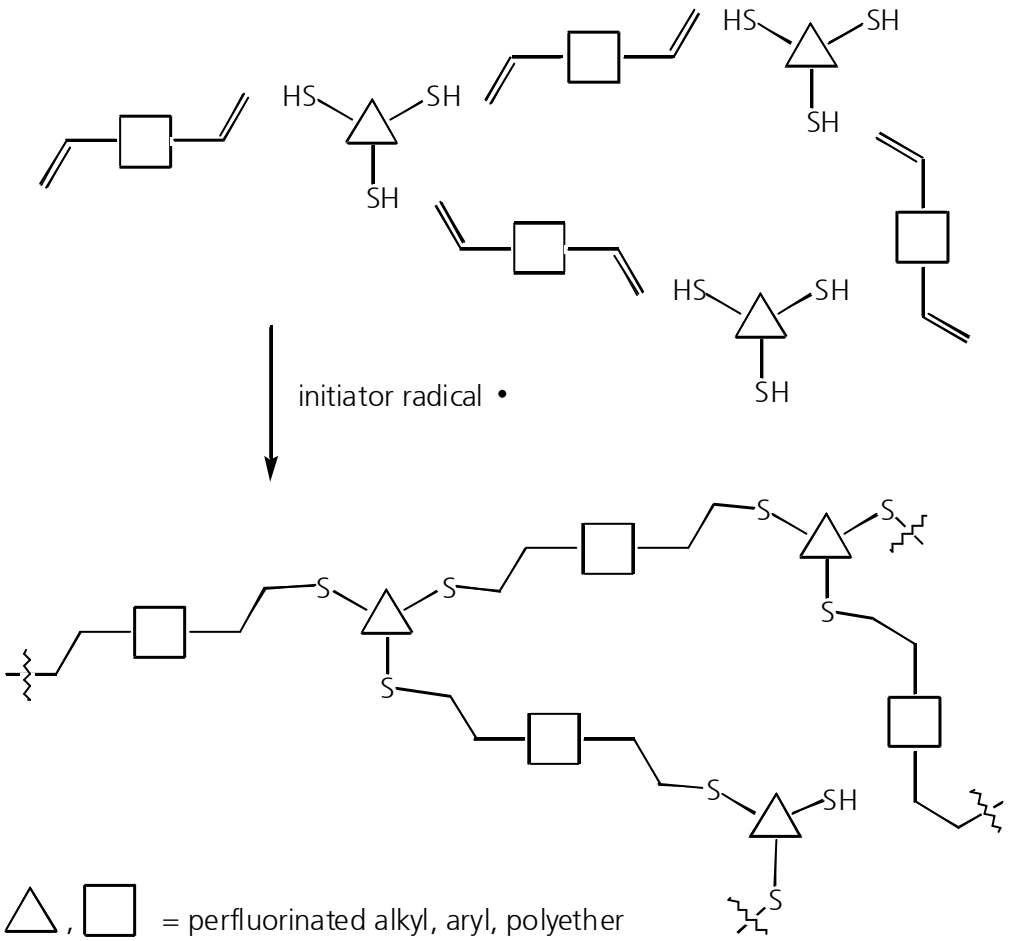

Fig. 28: Fluorinated thioether polymers (schematic representation)[54].

Poly(arylene ether sulfides) have been proposed as high-temperature resistant materials for optical waveguide devices[121]. Polymer films were fabricated by spin-coating and subsequent thermal curing of oligomers of the kind outlined in Fig. 29. The ether sulfide moieties account for a flexible polymer backbone, which gives the materials ease of processibility. Single-mode waveguides could be defined by photo lithography/RIE. Refractive index tunability in the range from 1.520 to 1.552 and optical loss of 0.40 dB/cm at 1550 nm was determined.

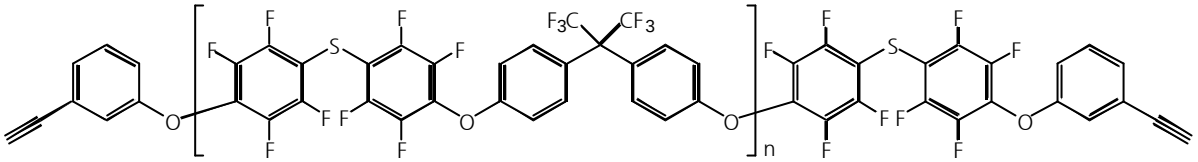

Fig. 29: Fluorinated poly(arylene ether sulfide) oligomers[121].

Single- and multi-mode waveguides fabricated from copolymers of pentafluorostyrene and glycidyl methacrylate had optical losses of 0.39 dB/cm and 0.42 dB/cm at 1320 and 1550 nm, respectively[122]. The refractive index could be tuned in a range from 1.471 to 1.487 at 589 nm, depending on monomer ratio. Patterning was achieved by photo-lithography of the negative resist behaving prepolymers after mixing with a cationic photo initiator. According to another source, copolymers composed of different contents of pentafluorostyrene, trifluoroethylmethacrylate, and glycidylmethacrylate (Fig. 30) were patterned by photolithography/reactive ion etching and manufactured into an 8x8 AWG multiplexer. At 1550 nm, optical losses were below 0.8 dB/cm[16].

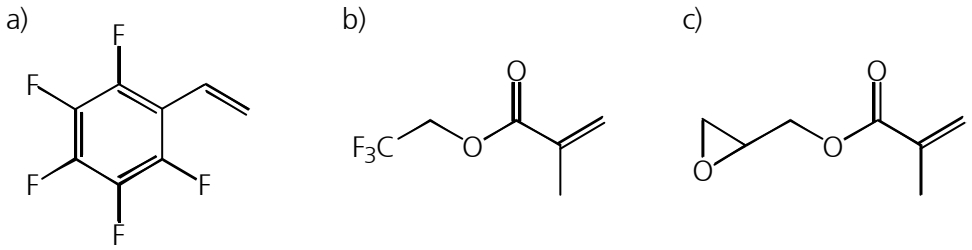

Fig. 30: Pentafluorostyrene (a), trifluoroethylmethacrylate (b), and glycidylmethacrylate (c) as monomers for the composition of partially fluorinated waveguiding polymers[16].

Recently, a series of novel halogenated alkoxy and aryloxy substituted polyphosphazenes has been presented as a new class of refractive index-tunable optical materials with high thermal stability (Fig. 31)[123]. Polyphosphazenes consist of alternating phosphorous and nitrogen atoms with the possibility to attach functional sidegroups to the phosphorous atoms, thus providing a C-H free backbone with tunability of properties. The refractive index could be lowered *via* incorporation of fluorine atoms, whereas chlorination led to higher index-values. Polymers were

synthesized by ring-opening polymerization of cyclotriphosphazenes in coreaction with the desired substituents. The reported refractive indices of these polyphosphazenes thus could be controlled over a range of 1.389 to 1.561.

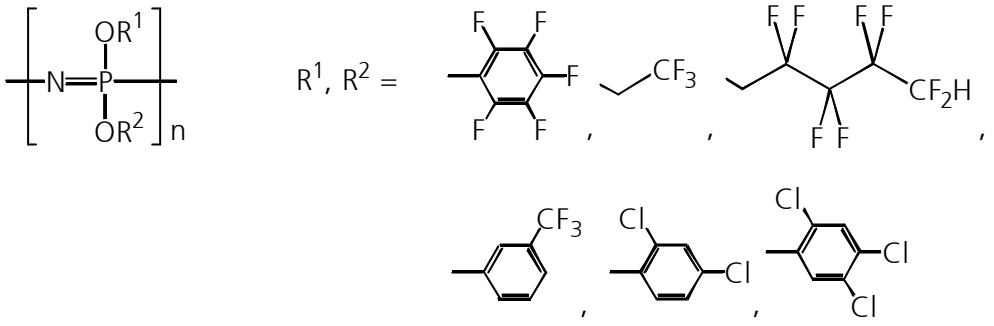

Fig. 31: Halogenated alkoxy and aryloxy substituted polyphosphazenes[123].

2.4.11 Polysiloxanes and inorganic-organic hybrid polymers

Polysiloxanes and hybrid polymers with a siloxane backbone are highly suitable materials for optical applications. The siloxane network not only accounts for mechanical and thermal rigidity, but also reduces the organic C-H concentration resulting in low absorption losses at 1310 nm and 1550 nm due to minimized overtone absorption. However, as (Si-)O-H also effects optical losses, especially around 1550 nm, the build-up of the inorganic network has to be thoroughly controlled in order to minimize residual Si-OH content. In hybrid inorganic-organic materials, the organic moieties account for tunable properties such as refractive index, dielectric and adhesion properties. In case of functionalization with organically polymerizable groups such as acrylic or epoxy, direct photolithographic patterning is possible.

Silica films derived from the sol-gel reaction of TMOS have been patterned by photolithography/wet etching processing[124]. After thermal curing, the film was covered with a photo resist, exposed to UV light, and etched with aqueous hydrofluoric acid. The resulting films exhibited refractive indices in a range from 1.420 to 1.456, varying with thermal curing conditions.

In singlemode channel waveguides made from a deuterated poly(phenylsiloxane), absorption losses of less than 0.1 dB/cm and less than 0.5 dB/cm at 1300 and 1550 nm, respectively, were observed[125]. The process outlined includes hydrolysis and polycondensation of deuterated phenylsilylchloride monomers, spin-coating and lithography/reactive ion etching for the patterning step. The cured polymer possessed a refractive index of 1.537 at 1310 nm.

A cross-linked silicone with a propagation loss of 0.5 dB/cm and a refractive index of 1.49 at 1550 nm and with long-term environmental stability has been reported[126]. RIE needs to be

employed in the fabrication of patterned structures. The chemical composition of the material, however, has not been further specified.

A number of materials were prepared by co-polymerization of pentadeuterophenyltrichlorosilane and methyltrichlorosilane in various monomer ratios (Fig. 32)[127]. The authors state that in the case of methyl groups, deuteration by way of exception leads to a higher absorption at 1550 nm than C-H bonds. From the silicones, single-mode optical waveguides were fabricated by spin-coating, lithography and dry-etching techniques. In case of a formulation containing 95 mol.% deuterated phenylsilane, a propagation loss as low as 0.23 dB/cm at 1550 nm was found. Glass transition temperatures above 300 °C for all different formulations indicated thermal stability.

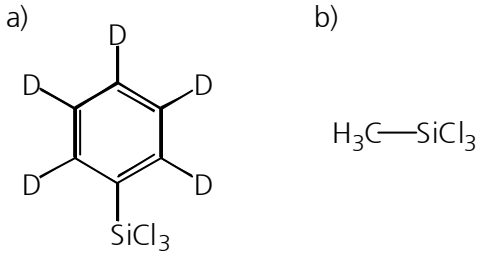

Fig. 32: Pentadeuterophenyltrichlorosilane (a) and methyltrichlorosilane (b) as monomers for an optical silicone[127].

Since the first results in the field of organically modified silica at Fraunhofer-ISC[139], a vast number of studies have been carried out in the topic of hybrid inorganic-organic polymers. The next chapter of this work will be dedicated to the newer developments at ISC. Therefore, comparative examples of hybrid materials for optics will be presented first.

Figure 33 outlines the monomers used for a system of photoimageable, low-shrinkage hybrids of acrylate polymers and silica: TEOS, 3-acryloxypropylmethyldimethoxysilane (AMDS), tetrahydrofurfuryl acrylate (THFA), and trimethylolpropane triacrylate (TMPTA)[128]. The materials derived from hydrolysis/condensation of the alkoxy silanes and subsequent cross-linkage by acrylate polymerization exhibited refractive indices of 1.46 to 1.49 at 633 nm and 0.27 dB/cm loss at 810 nm.

UV-curable low Si-OH waveguide materials have been reported that consist of mixtures of MEMO with phenyltriethoxysilane (core), and with dimethyldimethoxysilane (cladding), respectively[55]. The hydrolysis/condensation was catalyzed by boric acid, which is believed to get built into the siloxane network to some extent as oxidic glass modifier, thus enhancing the backbone's hardness. Waveguides have been produced by spin-coating and laser direct-writing techniques. The refractive indices for core and cladding at 633 nm were 1.517 and 1.474, respectively.

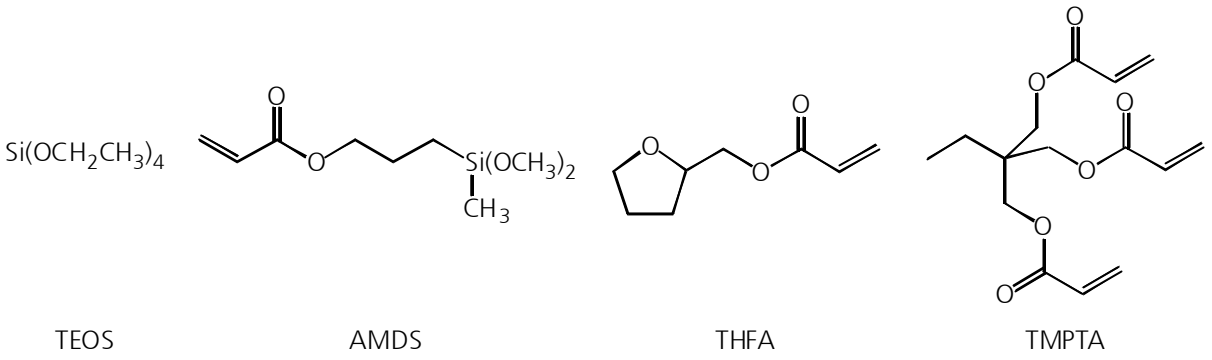

Fig. 33: Monomers for hybrid acrylate-silica polymers according to ref. [128].

UV-curable high refractive index inorganic/organic hybrids incorporate metal oxide nanoparticles of the kinds TiO_2, ZnO_2, and SnO_2 in a size range from 1 nm to 50 nm[129]. Sols of the said particles have been cocondensed with mixtures from bromophenyltrimethoxysilane, MEMO and several sulfur-containing acrylates. The resulting optical films expressed refractive indices from 1.711 to 1.796 at 633 nm, 1.685 to 1.755 at 1300 nm, and 1.678 to 1.753 at 1541 nm, respectively.

Within sol-gel derived polymethylsilsesquioxane/titania networks, the optical properties could be tuned by variation of titania content[130]. Optical films were prepared by thermal curing. By increasing the titania content from 10.6 wt.% to 41.6 wt.%, the refractive index was increased from 1.394 to 1.561, whereas the absorption loss at 1319 nm decreased from 0.31 dB/cm to 0.18 dB/cm due to minimization of C-H bonds.

Buried channel waveguides from photopatternable inorganic/organic hybrid polymers with epoxy cross-linkage have been reported[131]. Among various different formulations, optical loss values of 0.5 dB/cm at 1300 nm and 0.8 dB/cm at 1550 nm, respectively, could be reached from a monomer mixture of phenyltrichlorosilane, methyltrichlorosilane, and GLYMO (Fig. 34). After base-catalyzed hydrolysis/condensation the resulting resin was mixed with a cationic photoinitiator and cured by UV exposure and subsequent heating. Upon replacing phenyltrichlorosilane by pentadeuterophenyltrichlorosilane, the transmission could be improved to 0.1 dB/cm at 1300 nm and 0.5 dB/cm at 1550 nm.

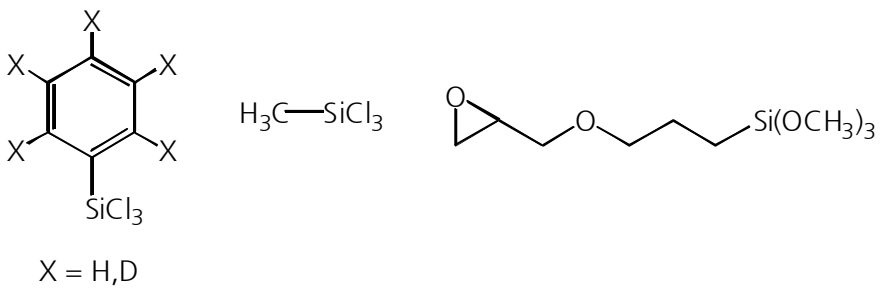

Fig. 34: Silane monomers for hydrolysis/condensation and following photopatterning[131].

Waveguides made from hybrid materials synthesized by hydrolytic cocondensation of zirconium isopropoxide with GLYMO for the core, and of TMOS and GLYMO for the cladding layer, respectively, have been reported[132]. For the application of the films to silicon/silicon dioxide wafers, spin-coating and thermal curing techniques were utilized. Photolithography and RIE were used for patterning. For the core layer with a 60/40 zirconia/GLYMO ratio and the cladding with a 50/50 TMOS/GLYMO ratio, the refractive indices were 1.542 and 1.477 at 633 nm, respectively.

2.5 ORMOCER®s – Fraunhofer's inorganic-organic hybrids

Since their first mention in the 1980's[139], ORMOCER®s have been developed at the Fraunhofer-Institut für Silicatforschung (ISC) in Würzburg for a variety of applications[140]. The different ORMOCER®s all show the basic structural principle of a hybrid polymer network incorporating a metal oxide backbone with organic crosslinking. Upon variation of precursor components and synthesis parameters, the properties of the materials can be tailored to meet specifications as required for their use in manifold fields of application. ORMOCER®s have been published e.g. as protective and functional coating materials for abrasion resistance[141], decoration[142] and barrier tasks[143]. Members of the family are also processed in bulk[144], e.g. as dental filling materials[145].

2.5.1 ORMOCER®s for microsystems

ORMOCER®s have also been developed for application as photopatternable dielectrical and optical thin films in microsystems[32,33,35,37,84], as already mentioned in the introductory part of this work (chapter 1). Other fields of development include solid-state ion conductors for lithium batteries[146] and proton-conductive materials for application in micro-fuel cells[147].

ORMOCER®s for microsystems are synthesized in a two-step polymerization process from organoalkoxysilanes bearing organically polymerizable moieties such as olefinic or epoxy groups. Figures 35 & 36 outline the process considering the GMP2T formulation as exemplary material, the synthesis of which starts with a mixture of MEMO, GLYMO, TEOS and diphenylsilanediol[32]. The composition is particularly suited for dielectric and passivation purposes, but can be seen as an archetype for a series of hybrid materials used in microsystems applications and covers the basic functionalities as well as processing steps. At first, the precursor silane mixture is hydrolyzed and cocondensed upon addition of water and catalyst, resulting in a viscous resin of siloxane oligomers, which in the image are simplified as spherical or elliptical objects (Fig. 35). In some cases, also alumina, zirconia or titania are incorporated into the inorganic network. At this

stage of ORMOCER® synthesis it is important to find condensation conditions that prevent the generation of an insoluble gel, which would be useless for further thin film processing.

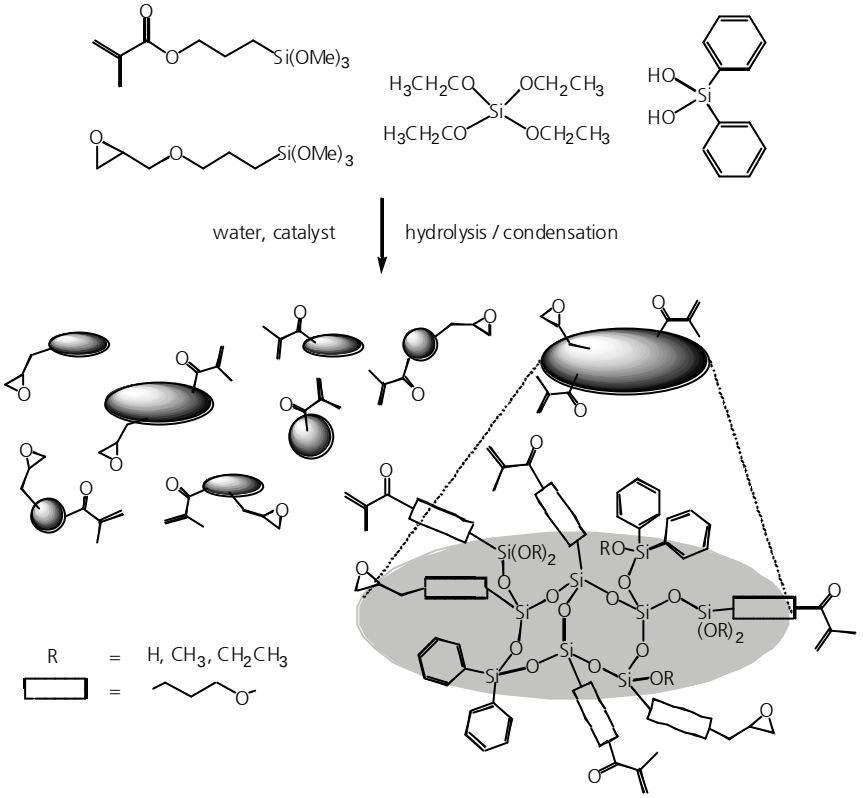

Fig. 35: ORMOCER® GMP2T for microsystems applications (I) – Preparation of the ORMOCER® resin by hydrolysis and condensation of methacryl- and epoxy-functionalized organoalkoxysilanes [32].

After admixture of a photo- and a thermal initiator the condensate resin is ready for application to a substrate, whereby its viscosity can be varied by addition of a diluting solvent according to the required film thickness. Various means of coating techniques such as dip coating, spray coating, backfilling, screen printing, or curtain coating are utilized for film preparation[31]. Particularly for application in microsystems technology, spin coating is commonly used for the fabrication of ORMOCER® thin films.

The curing of films and patterns occurs during a second polymerization step by photochemically and/or thermally initiated crosslinking of the inorganic oligomers via the pendant organically polymerizable groups. Particularly the presence of (meth)acryl or styryl moieties enables direct photolithographic patterning of wet ORMOCER® films due to their negative resist behavior, i.e. they are locally hardened upon irradiation, leaving a rigid, duroplastic inorganic-organic hybrid network. For microsystem applications, the photopatternability offers low-cost processing of functional materials. Competitive patterning technologies that require e.g. reactive ion etching, are much more cost-intensive, because not

only costly equipment is involved but also multiple processing steps. Figure 36 depicts the organic crosslinking of a GMP2T resin, which has been prepared according to Fig. 35. Upon UV-initiated radical polymerization of methacrylic groups in the periphery of siloxane oligomers, the exposed area is hardened so that unexposed condensate can be washed away with a developer solvent. The thus patterned film is completely cured in a final thermal baking step, during which the epoxy-functions are also polymerized.

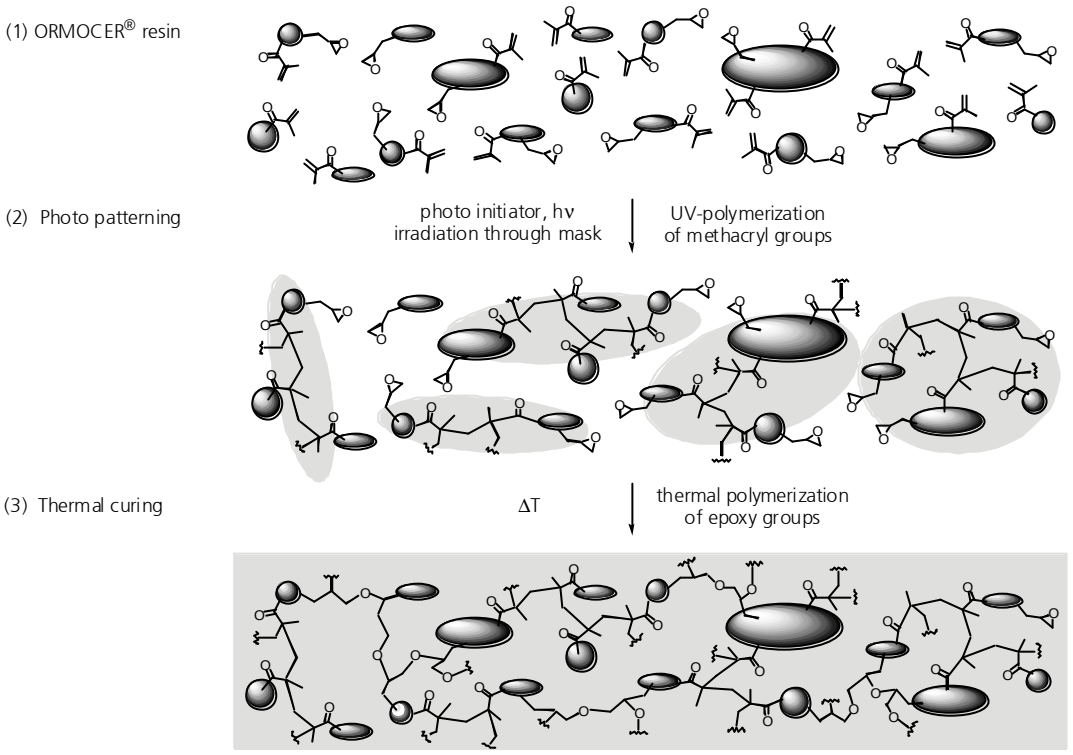

Fig. 36: ORMOCER® GMP2T for microsystems applications (II) – Patterning by photochemical polymerization of methacrylic moieties, development of micro-structures, and subsequent thermal curing of epoxy groups[32].

The chemical structure of the ORMOCER® polymer network, which can be classified as an intermediate between inorganic glass, silicones and organic polymers, accounts for material properties that reflect its hybrid nature. The inorganic oxidic backbone accounts for high thermal and mechanical stability as well as for high optical transparency making the materials suitable for optical applications. The organic functionalization on the other hand can easily be influenced by chemical modification of precursor silanes and allows for the tunability of a multitude of properties such as refractive index, hydrophobic/hydrophilic wetting behavior, or ionic conductivity.

2.5.2 Polycondensation of ORMOCER® precursor silanes

Control of the inorganic polycondensation process is crucial for the predetermination of material properties in the completely cured inorganic/organic hybrid network. The siloxane network formation can be actively influenced by variation of precursor silanes and reaction conditions. Thus, properties such as rigidity/flexibility of the material as well as thermal stability and other characteristics are tailored. Particularly with respect to low optical loss, a major criterion for optical waveguide materials, a low silanol content is fundamental, which can only be achieved by stringent reaction control.

Hydrolysis/polycondensation of organoalkoxysilanes generally follows the principles of sol-gel chemistry[2]. However, it must be emphasized that in the case of ORMOCER® resins/lacquers for microsystems technology, the condensation must not proceed to gelation, but the formation of soluble resins is decisive in order to provide further processibility. Figure 37a depicts the hydrolysis of a methoxy silane schematically. Usually, the reaction is carried out under addition of a suitable catalyst[148]. This may be an acid such as hydrochloric acid, a base such as sodium hydroxide, or a fluoride salt such as ammonium fluoride. During hydrolysis often already the condensation of hydrolyzed species commences. This happens either under release of alcohol (alcoxolation) upon reaction of a silanol group with an alkoxysilane (Fig. 37b) or under release of water (oxolation) in case of the condensation of two silanol groups (Fig. 37c)[2]. The predominant process is primarily determined by the amount of water added to the silane. In case of condensation stoichiometry, i.e. addition of 0.5 mol water per mol hydrolyzable groups, the condensation reaction is forced to proceed via alcoxolation. Upon addition of an at least stoichiometric amount of water for hydrolysis, i.e. not less than one mol water per mol hydrolyzable groups, oxolation becomes favored.

The chosen catalyst likewise has a strong effect on the network formation process. In general, acidic catalysis activates those alkoxy and silanol groups, which are located in a terminal position within an intermediate oligomer. Thus, the formation of chain-like siloxane oligomers is preferred. In the case of base catalysis, reactive groups that are attached to already higher condensed silicon centers are activated, which favors the formation of dense three-dimensional networks. Additionally, the growing oligomers bear an increasingly negative charge due to the deprotonation of silanol groups. Thus, Coulomb repulsion accounts for an Ostwald ripening process and therefore particles up to a size of several hundred nanometers can be formed. The dependence of polycondensation processes on multiple parameters offers a multitude of possibilities to manipulate the network formation.

a) hydrolysis

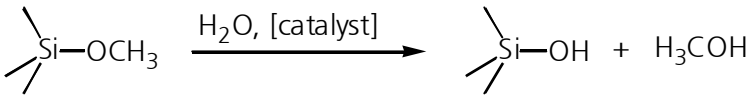

b) condensation (alcoxolation)

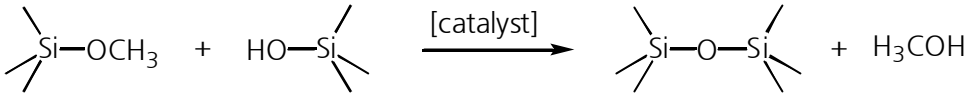

c) condensation (oxolation)

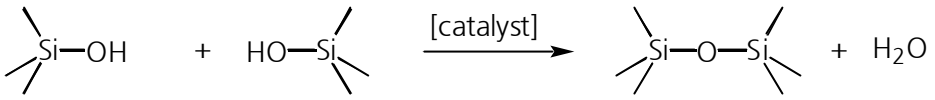

Fig. 37: Hydrolysis of a methoxysilane (a) and condensation under alcoxolation (b) and oxolation (c) conditions[2].

2.5.3 Photoinitiators for direct photopatterning of ORMOCER®s

For the photopatterning of ORMOCER® resins, the resin is mixed with a suitable photoinitiator, which starts the local polymerization of pendant acrylic or styrylic bonds upon irradiation. A large variety of photostarters for UV curing of polymer resins is available for the initiation of radical and ionic polymerization reactions[149,150]. Figure 38 depicts the initial Norrish type I photo-cleavage of photoinitiator 2-methyl-[1-(4-(methylthio)phenyl]-2-morpholinopropan-1-one[149,150] (Irgacure® 907), which is a typical radical initiator used for ORMOCER® patterning. This initiator of the α-aminoacetophenone class has been designed for the photocuring of acrylate and vinyl monomers[151].

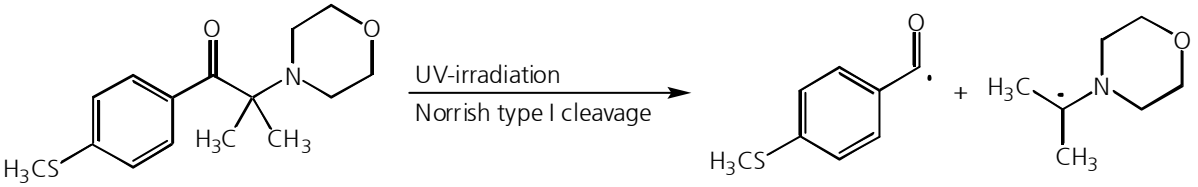

Irgacure® 907

benzoyl and 2-morpholinopropyl initiator radicals

Fig. 38: Photo-induced Norrish type I cleavage of photo initiator Irgacure® 907[149,150].

The photo-cleavage of initiator ethyl-2,4,6-trimethylbenzoylphenylphosphinate (Lucirin® TPO-L, formerly Lucirin® LR 8893), which was mainly used within the scope of this work, is shown in Fig. 39. The initiator of the acylphosphine oxide class has been developed for the curing of acrylic and styrene functionalities[152]. Upon UV-irradiation, the molecule likewise undergoes a Norrish type I cleavage, as in the case before. The resulting primary radicals, the highly reactive tetrahedral phosphinoyl radical in particular, add to olefinic double bonds to initiate the chain polymerization[149].

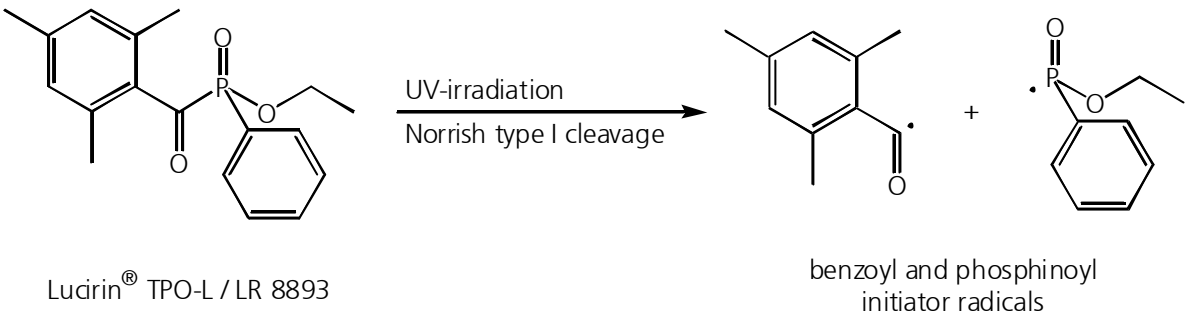

Fig. 39: Photo-induced Norrish type I cleavage of photo initiator Lucirin® TPO-L in analogy to the literature[149].

2.5.4 b59d – reference ORMOCER® for optical waveguide applications

The synthesis of ORMOCER® **b59d**, which has been developed as a low-loss optical waveguide material[32-34], incorporates MEMO and diphenylsilanediol as precursor silanes (Fig. 40). The material, also known as ORMOCER® I and ORMOCORE has been commercialized recently[153]. In contrast to formulation GMP2T (Figs. 35,36), which requires the addition of water to the initial silane mixture, the polycondensation reaction in the **b59d** case proceeds water-free upon base catalysis, as the diphenylsilanediol is effectively the product of a pre-hydrolysis reaction. Thus, the cocondensation with MEMO is limited to alcoxolation, which produces a material with very low silanol content. Waveguides prepared from the material exhibit low optical losses of 0.12 dB/cm at 1310 nm, and 0.55 dB/cm at 1550 nm, respectively[30,31]. However, before photochemical and thermal curing, the resin shows absorption values of 0.36 dB/cm at 1310 nm and 0.70 dB/cm at 1550 nm, respectively. Therefore, a considerable improvement is observed during processing. The refractive index also undergoes slight changes during processing due to network densification. Thus, at 633 nm, a value of 1.538 is found for the resin, which increases up to 1.552 in the cured material[33]. Upon admixture of low amounts of fluorinated resins, the index is tunable in a range from 1.47 to 1.56 at 633 nm[31]. The material shows good adhesion to a variety of substrates (Si/SiO_2, Glass, FR4, most oxidized surfaces) as well as thermal stability at 270 °C. Recent results prove excellent performance of the

material in the creation of complex three-dimensional micro-optical structures via 2PP technology, which has already been presented in the introductory section of this work (cf. Fig. 5)[30,154].

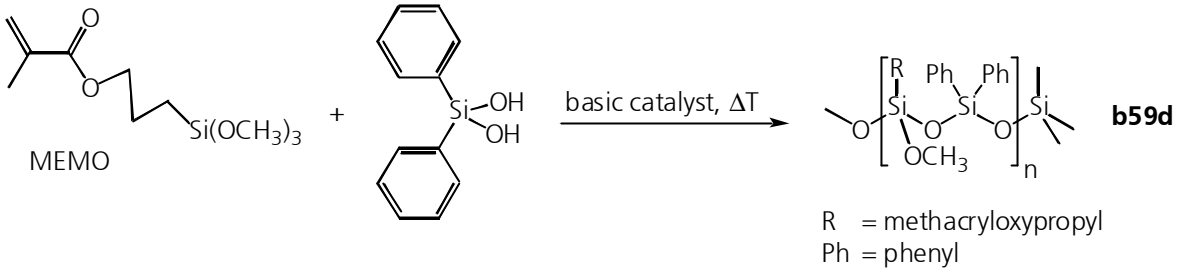

Fig. 40: Resin synthesis of **b59d** low silanol ORMOCER®[33,34].

2.5.5 Fluoroaryl modified ORMOCER®s – preliminary results

While ORMOCER® system **b59d** represents an unfluorinated low-loss optical material, the high transparency of which is primarily due to its low silanol content, also a route to fluorinated materials has been opened. Based on the Grignard reaction[155], a synthesis scheme to a variety of fluoroaryl modified alkoxysilanes has been established (Fig. 41)[50].

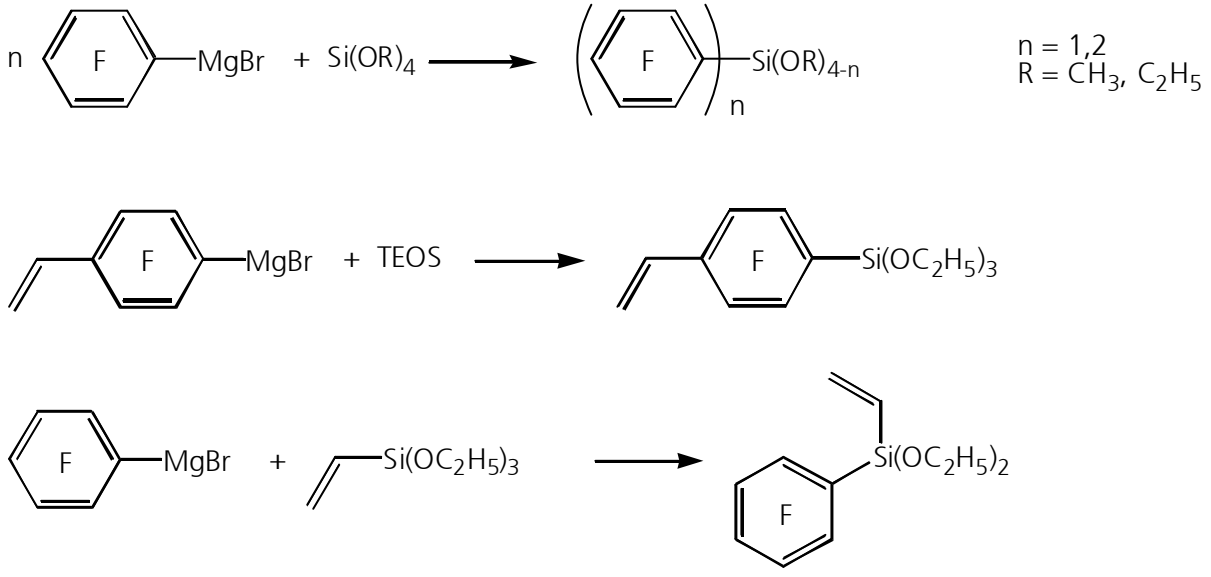

Fig. 41: Grignard synthesis routes to several exemplary fluoroarylalkoxysilanes[50].

Fluorinated ORMOCER®s derived from mixtures of precursor silanes pentafluorophenyltriethoxysilane and pentafluorophenyl(vinyl)diethoxysilane have shown low losses of 0.30 dB/cm at 1550 nm[41]. However, direct photolithographic patterning of the vinyl-substituted resins has presented major difficulties[156].

The great value of quantitative ^{29}Si-NMR spectroscopy in the analysis of sol-gel reactions and reaction products has been proven in a number of literature examples [5,157-160]. Thus, in order to allow for a better reaction control, first NMR experiments have been conducted on polycondensation reactions with fluoroarylmethoxysilanes[161,162]. In conjunction with computational results, a first insight into structural and reactivity details has been achieved. An important aspect herein is the fact that under non-acidic polycondensation conditions, the fluoroaryl substituent, which is directly bound to the silicon atom, easily undergoes Si-C bond cleavage. Thus, the fluoroaryl anion acts as the leaving group under nucleophilic attack on the silicon. Only under acidic catalysis, the methoxy groups are protonated to form the better leaving group methanol[161].

3 RESULTS AND DISCUSSION

The core part of this work comprises a number of subdivisions, following the multi-step task of ORMOCER® synthesis. Prior to the development of new fluoroaryl functionalized ORMOCER® systems for low-loss micro optics, it was considered useful to first assemble a collection of possible precursor silanes and characterize them with respect to optical absorption in the near-infrared spectral region (NIR) as well as with respect to the refractive index. Also, unfluorinated analogs were considered in order to find further evidence for the influence of fluorination by direct comparison of fluorinated and unfluorinated compounds. After an outline of the syntheses of new silanes that had not been reported in literature, as well as of commercially unavailable silanes, such a survey on optical properties is presented, which allows first conclusions concerning structure-property relations.

The next part of this work is the development of ORMOCER® resins suitable for further processing within micro technology. This involves the selection of precursor silanes and appropriate polycondensation reaction conditions, which is supported by in-depth studies of silane reactivities, particularly with time-resolved ^{29}Si-NMR. These studies on separate silanes are also crucial for the later spectral analysis of ORMOCER® resins, which consist of complex polysiloxane mixtures based on two or three different precursor silanes. These result in complicated NMR signal arrangements that can be assigned only with the help of prior spectral studies on condensation products based on single precursor silanes. Main targets in resin preparation are processibility and low absorption in the NIR. Visualization of structural characterization data is achieved with the help of molecular modeling tools.

Clean room processing of the produced ORMOCER® resins in order to manufacture waveguide patterns was the final task. Optimization of processing parameters such as coating, UV exposure, and thermal curing steps, as well as the choice of the appropriate photoinitiator is reported. Structural characterization and determination of optical properties close the circle to corresponding studies on ORMOCER® resins and precursor silanes, which allow general conclusions with respect to structure-property relations in fluoroaryl-functionalized ORMOCER®s for application in telecom and datacom micro-optics.

3.1 Precursor silane syntheses

The majority of organoalkoxysilanes used in this work for ORMOCER® preparation are commercially unavailable and were synthesized by conventional means of organic synthesis. A number of these silanes have been reported in literature, others were newly synthesized

applying modified literature syntheses, in particular via Grignard[155] and hydrosilylation[163] pathways.

3.1.1 Fluoroarylalkoxysilanes

Grignard syntheses have been found valuable for the preparation of fluoroarylalkoxysilanes, i.e. organomagnesium halides act as nucleophilic reagents on silanes bearing suitable leaving groups[41,50,161] (cf. chapter 2.5.5). More precisely, fluorinated aryl bromides are reacted with magnesium in order to generate the active nucleophile, which then is brought to reaction with either tetramethoxysilane or an alkyltrimethoxysilane. Whereas beside a number of methoxy silanes also ethoxy substituted ones have been reported in the cited literature, this work is mainly focused on syntheses of methoxy silanes. The reason for this is that the silanes are designed as precursors for hydrolysis and polycondensation under reaction conditions, which are not expected to result in completely alkoxy-free products. Thus, the nature of the alkoxy groups had to be considered in terms of low C-H content and hence the focus was drawn on methoxy silanes.

Figure 42 gives an overview of the highly fluorinated arylmethoxysilanes synthesized within this work following a Grignard route. Pentafluorophenyltrimethoxysilane (**1**) and bis-(pentafluorophenyl)dimethoxysilane (**2**) were synthesized according to literature[50] from bromopentafluorobenzene. In the first step, the Grignard reagent was formed by reaction of the bromine compound with magnesium. Thereafter, a stoichiometric amount of the electrophile, tetramethoxysilane, was added at once in order to minimize multiple substitution. As a result, a mixture of the two products was formed simultaneously, which could easily be separated by distillation to yield the monosubstituted silane **1** (67%) and the disubstituted byproduct **2** (21%).

The styrene-analogous compound 4-vinyltetrafluorophenyltrimethoxysilane (**4**) has also been reported[161]. Its synthesis starts from 1,4-dibromotetrafluorobenzene, which is first converted into 1-bromo-2,3,5,6-tetrafluoro-4-vinylbenzene (**3**) by Grignard reaction with acetaldehyde, followed by dehydration. The resulting aryl bromide **3** is then reacted with magnesium and excess tetramethoxysilane similarly to the synthesis described above to give silane **4** in a moderate overall yield of 23% ($46\%_{1st\ step} \times 50\%_{2nd\ step}$).

To my knowledge, not yet mentioned in literature are pentafluorophenyl(vinyl)dimethoxysilane (**5**) and pentafluorophenyl(methyl)dimethoxysilane (**6**). These D-silanes, i.e. diorganosilanes bearing two methoxy substituents that are susceptible to condensation reactions, could be prepared in a straightforward adaptation of the above mentioned Grignard synthesis from bromopentafluorobenzene as starting compound. After generation of the organomagnesium bromide, excess amounts of the electrophiles,

vinyltrimethoxysilane and methyltrimethoxysilane, respectively, were added at once to immediately provide a large reactant concentration, in order to prevent multiple substitution. In this way, the vinyl compound **5** could be prepared in good (73%), the methyl analog **6** in moderate (55%) yields.

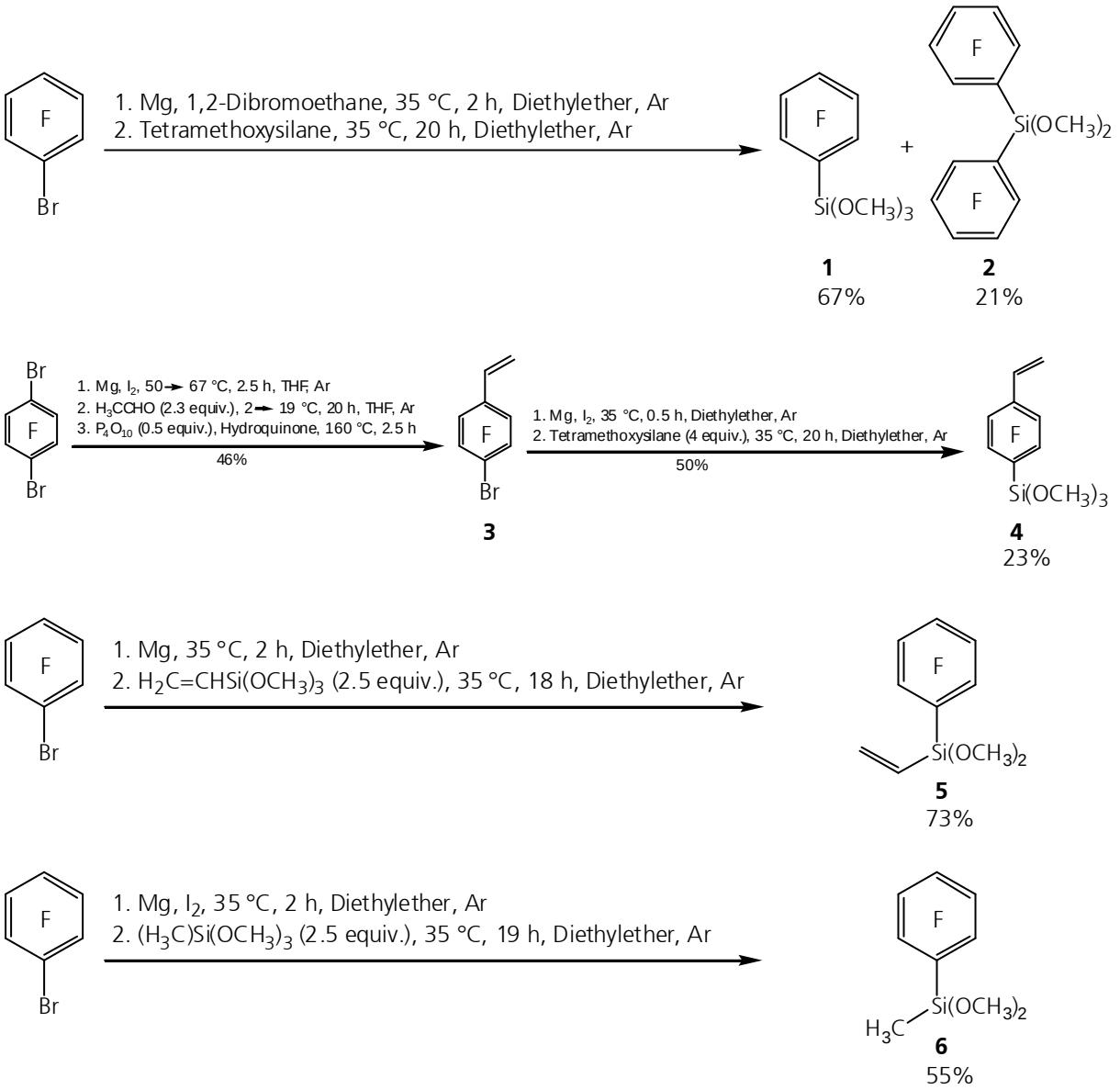

Fig. 42: Grignard syntheses of fluorinated arylalkoxysilanes.

3.1.2 Unfluorinated arylalkoxysilanes

Since this work deals with highly fluorinated ORMOCER® optical materials, the main focus with respect to precursor synthesis is on fluoroarylalkoxysilanes. Additionally, in order to examine the performance of fluorination itself with respect to optical properties, it was necessary to provide a non-fluorinated analogous material for comparison. This led to the

necessity to synthesize the unfluorinated analog of arylvinylsilane **5** due to its commercial unavailability. Via a similar Grignard approach as above, phenyl(vinyl)dimethoxysilane (**7**) was prepared from bromobenzene, magnesium and subsequent dropwise addition of vinyltrimethoxysilane in a moderate yield of 47% (Fig. 43). Upon silane addition at once rather than dropwise, also the disubstituted compound diphenyl(vinyl)methoxysilane (**8**) could be prepared as byproduct in a product mixture with silane **7**. Isolation of the two silanes was performed by vacuum distillation.

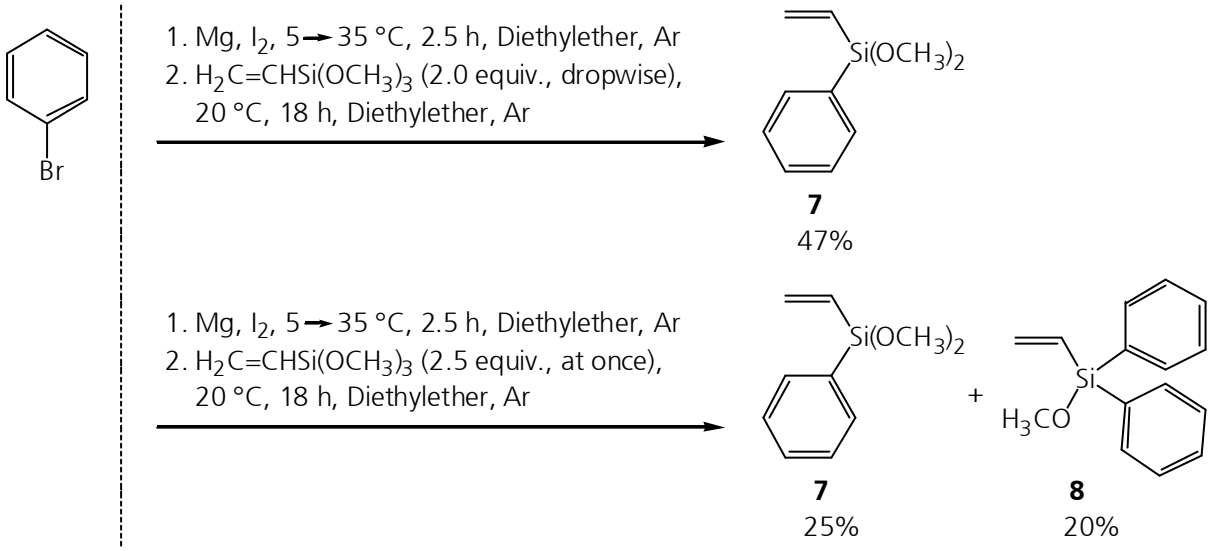

Fig. 43: Grignard syntheses of unfluorinated arylalkoxysilanes.

3.1.3 Methylene spacer silane via Grignard synthesis

In order to overcome the experienced weakness of the C-Si bond in highly fluorinated aryl alkoxysilanes[161,162] (cf. chapter 2.5.5), attempts were made to strengthen this bond by introducing a short alkyl spacer between the silicon atom and the fluoroaryl moiety. For the cost of few additional C-H bonds, the spacer should provide higher stability.

Motivated by the successful C-functionalization of alkoxysilanes with the Grignard approach, similar experiments were conducted with pentafluorobenzyl bromide as starting compound for the preparation of the organomagnesium halide (Fig. 44). However, the synthesis of methylene spacer silane **9** was found to be very difficult.

In a first approach, a common two-step Grignard pathway was tried, i.e. upon slow addition of the bromide to a suspension of magnesium together with some iodine in tetrahydrofuran, the organomagnesium bromide was prepared. After an extraordinarily strong exothermic reaction with a large amount of precipitates, tetramethoxysilane was added and refluxed overnight. However, spectral analysis of the crude product mixture clearly showed that only a Wurtz-type reaction between two (pentafluorophenylmethyl)bromide molecules had occurred, instead of an

organic functionalization of the silane. The product, 1,2-bis-(pentafluorophenyl)ethane (**10**), was not purified, because the crude product was doubtless characterizable and the desired silane **9** was not present.

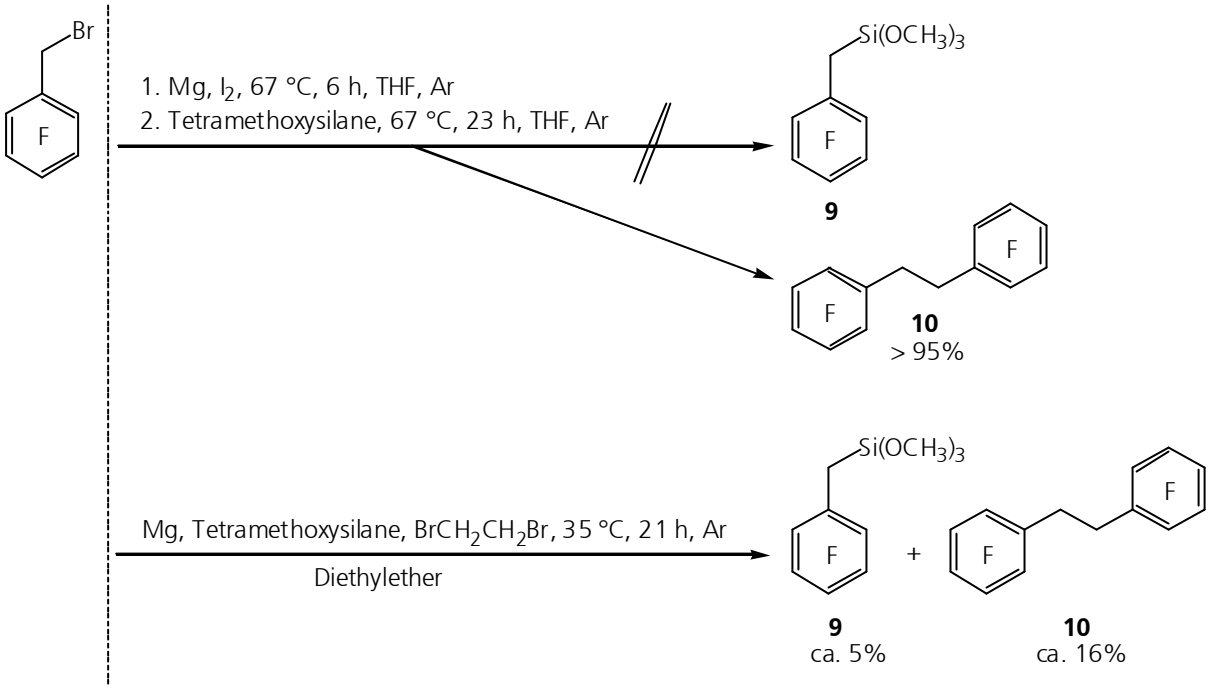

Fig. 44: Attempted synthesis of a methylene-spacer silane by Grignard reaction.

In another attempt, a one-pot synthesis, i.e. simultaneous addition of all reactants, yielded a product mixture which was analyzed by quantitative nuclear magnetic resonance spectroscopy (NMR). A number of NMR signals, among them a ^{29}Si-NMR signal at -51.0 ppm, could be assigned to (pentafluorophenylmethyl)trimethoxysilane (**9**). However, attempts to isolate the desired silane by distillation and crystallization, respectively, failed due to its low concentration. From cross-analysis of ^{29}Si-, ^{13}C-, and ^{1}H-NMR spectra including signal integration, a theoretical yield of 5% with respect to silane **9** could be estimated with a three times higher concentration of the Wurtz-product **10**.

Literature reports Grignard reactions performed with pentafluorobenzyl bromide as starting compound, which also suffer from the production of a large amount of **10** as secondary product[164]. However, such a high selectivity with respect to the Wurtz adduct **10**, as seen in the attempted synthesis of methoxysilane **9**, must be attributed to a relatively too low reactivity of tetramethoxysilane with respect to its leaving group, methoxy. As a consequence, a silane with better leaving groups, such as tetrachlorosilane, might be useful as electrophile. Additionally, inductive effects make the silane center of chlorosilanes more electrophilic. After generation of the organochlorosilane, this would have to be methoxy functionalized with methanol in a second step. The nucleophilic intermediate pentafluorobenzyl magnesium bromide, on the other

hand, could be stabilized by low temperature Grignard synthesis. However, this synthesis route was not further followed as it would have gone beyond the scope of this work.

3.1.4 Ethylene spacer silane by hydrosilylation of pentafluorostyrene

Hydrosilylation of olefins is a common method for the preparation of ethylene bridged organosilanes[163]. Therefore, hydrosilylation of pentafluorostyrene seemed to be a promising approach for the synthesis of 2-(pentafluorophenyl)ethylalkoxysilanes. The catalyst of choice was a platinum(0) divinyltetramethyldisiloxane complex, known as Karstedt's catalyst[165].

Figure 45 outlines the reaction conditions tried for the preparation of 2-(pentafluorophenyl)ethyltrimethoxysilane (**11**). The desired silane could only be produced in traces within a product mixture and was not isolated due to the high required cost. Still, NMR signals recorded from the product mixture could be attributed to **11**, among them the important ^{29}Si-NMR resonance at -45.1 ppm. Main product, however, was tetramethoxysilane together with its condensation products. This is attributed to a low thermal stability of trimethoxysilane.

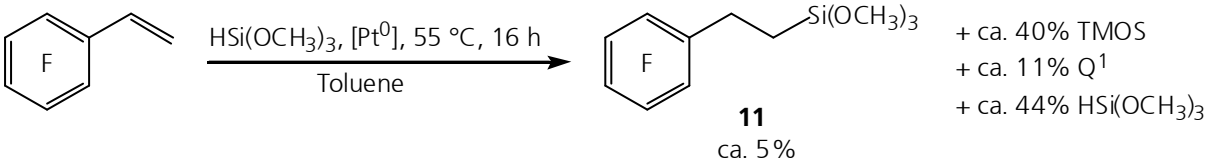

Fig. 45: Reaction of pentafluorostyrene with trimethoxysilane under hydrosilylation conditions.

In order to overcome this problem, the less reactive starting compound triethoxysilane was reacted with pentafluorostyrene under similar conditions (Fig. 46). Reaction control with NMR spectroscopy revealed the higher temperature resistance of the silane while, at the same time, conversion was incomplete at temperatures around 55 °C as applied in the trimethoxysilane case. Thus, the reaction was carried out at a higher temperature (80 °C), and finally yielded 23% of 2-(pentafluorophenyl)ethyltriethoxysilane (**12**). The product was isolated and characterized. The ^{29}Si-NMR resonance at -48.3 ppm also supports the characterization of the above mentioned crude reaction mixture containing traces of **11**, as the NMR signals are very similar.

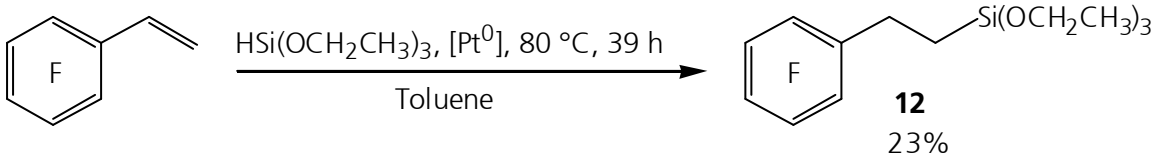

Fig. 46: Synthesis of 2-(pentafluorophenyl)ethyltriethoxysilane (**12**) via hydrosilylation.

3.2 Optical properties of precursor silanes

Table 7 outlines optical properties of the fluorinated and unfluorinated arylalkoxysilanes, which were synthesized in the framework of this work. The characterization is focused on their refractive indices and absorptions at telecom wavelengths 1310 nm and 1550 nm. In the following, trends are discussed with respect to influences of the chemical structure on the mentioned optical properties in order to facilitate the choice of suitable starting compounds for the synthesis of inorganic-organic hybrid waveguide materials. Beside the fluoroarylmethoxysilanes intended for the preparation of low-loss ORMOCER®s, the discussion also includes their unfluorinated analogs, and several compounds with other close similarities in chemical structure, as presented above (Tab 1, chapter 2.1). Additionally, some of the most important precursor silanes for ORMOCER®s for microsystems, such as 3-methacryloxypropyltrimethoxysilane (MEMO) and 3-glycidyloxypropyltrimethoxysilane (GLYMO), are considered.

Tab. 7: Refractive indices n_D^{20} and optical losses [dB/cm] of the fluorinated and unfluorinated arylalkoxysilanes synthesized within this work.

Silane	n_D^{20}	[dB/cm] at λ: 1310 nm	1550 nm
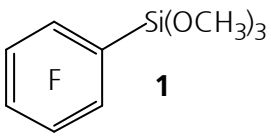 **1**	1.418	<0.02	0.18
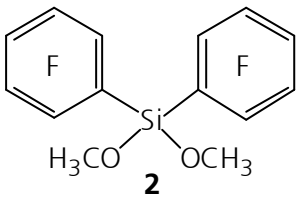 **2**	1.450	<0.02	0.10
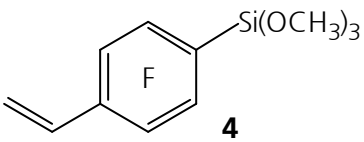 **4**	1.504	0.24	0.32
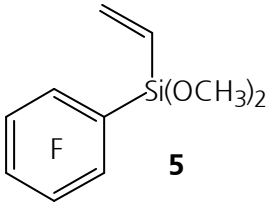 **5**	1.436	0.18	0.24

Tab. 7 continued:

Silane	n_D^{20}	[dB/cm] at λ: 1310 nm	1550 nm
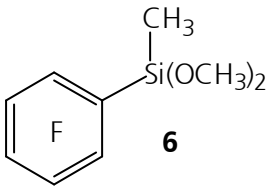 **6**	1.426	0.02	0.54
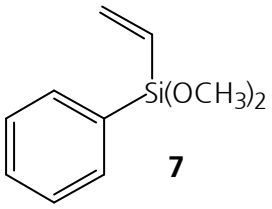 **7**	1.492	0.44	0.44
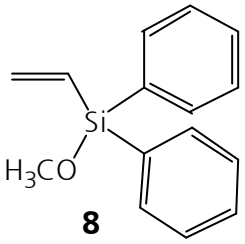 **8**	1.560		
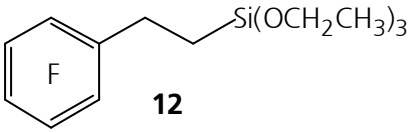 **12**	1.429		

3.2.1 Refractive indices

Regarding the influence of fluorination on refractive indices of organoalkoxysilanes, Tabs. 1 & 7 give several comparative examples of fluorinated silanes together with their unfluorinated analogs. In addition to that, also the influence of other substituents such as vinyl and methyl as well as phenyl groups, is shown.

By comparison of perfluorophenyl substituted silanes pentafluorophenyltrimethoxysilane (**1**), pentafluorophenyltriethoxysilane, pentafluorophenyl(vinyl)dimethoxysilane (**5**), and pentafluorophenyl(methyl)dimethoxysilane (**6**), with their unfluorinated analogs, fluorination results in lower refractive indices, as expected. The indices of the silanes are lowered by 0.043 to 0.056 due to perfluorination of a phenyl group. This trend is supported by an index difference of 0.095 between diphenyldimethoxysilane and bis-(pentafluorophenyl)dimethoxysilane (**2**), resulting in an index change of 0.048 per aryl moiety. However, the presented trend due to fluorination is not applicable to the silane pair 4-vinyltetrafluorophenyltrimethoxysilane (**4**) and its unfluorinated equivalent. In this case, the index lowering is only marginal, with a difference of 0.001.

Another well-accepted influence of chemical structure on refraction is reflected by comparison of alkoxy silanes with different degrees of aromatic substitution. By regarding the evolution of index values as outlined in Tabs. 1 & 7, an increase of the refractive index by 0.069 to 0.105 can be assumed due to replacement of a methoxy by a phenyl group. These values originate from three rows of analogous compounds: 1. vinyltrimethoxysilane → phenyl(vinyl)dimethoxysilane (**7**) → diphenyl(vinyl)methoxysilane (**8**); 2. TMOS → phenyltrimethoxysilane → diphenyldimethoxysilane; 3. methyltrimethoxysilane → phenyl(methyl)dimethoxysilane.

Concerning the difference between vinyl and methyl substituents, the comparison between fluoroarylsilanes **5** and **6**, and with their unfluorinated counterparts, respectively, gives evidence for the higher optical density of the vinyl group. Also the comparison between the most simple model compounds, vinyltrimethoxysilane and methyltrimethoxysilane, supports this trend. In the mentioned cases, substitution of a methyl by a vinyl group results in an increase in refractive index by 0.010 to 0.022.

The observed trends are in accordance to the accepted origins of refraction outlined in chapter 2.1. Fluorination leads to a decrease in refractive index due to lowering the electronic mode of polarization. Because of the high electronegativity difference between fluorine and carbon atoms relative to carbon and hydrogen[166], the electrons forming the C-F bonds are much more localized than in the C-H case, i.e. electron mobility is very much restricted due to the high electronegativity of fluorine. In addition to that, pentafluorophenyl groups have a higher steric volume than unfluorinated phenyl groups, because the high partial negative charge located on the rim of the pentafluorophenyl rings causes high Coulomb repulsion of pentafluorophenyl substituted molecules in the vicinity. Thus, less molecules per volume unit can contribute to refraction leading to a lower refractive index.

However, in the case of 4-vinyltetrafluorophenyltrimethoxysilane (**4**) and the unfluorinated 4-vinylphenyltrimethoxysilane, only a small index difference of less than 0.001 could be detected between fluorinated and unfluorinated equivalents. Therefore, it can be assumed that for these styrene-analogous systems, the vast majority of polarization is due to electron redistribution along the π-systems, which are similar in extension both in the fluorinated and for the unfluorinated case. The contribution of free volume enhancement due to Coulomb repulsion of strongly negatively charged fluorine atoms, which are in addition sterically more demanding than hydrogen atoms, is to be neglected. The size of the vinyl group being attached to the outermost carbon atom with respect to the silane functionality, plays the decisive role in terms of sterical demand. The fluorine atoms, however, do not show a significant steric effect due to their position away from the periphery of the molecule.

The detected trend concerning the index-rising effect of aromatic and olefinic groups compared to alkyl or alkoxy substituents also originates from enhanced electronic polarizability. The high electron densities within π-systems allow strong interactions between light and medium.

3.2.2 Optical losses at telecom wavelengths 1310 nm and 1550 nm

Optical losses at the relevant wavelengths 1310 nm and 1550 nm are known to originate chiefly from C-H and O-H overtone vibrational absorptions (see chapter 2.2). In order to quantify these absorptions, a number of fluorinated and unfluorinated silanes were analyzed with NIR absorption spectroscopy. Table 7 outlines, beside refractive indices, optical absorptions of the synthesized precursor silanes for ORMOCER®s intended for optical applications. In addition to that, Tab. 8 presents NIR results derived from either commercially available organoalkoxysilanes, or such kindly made available by colleagues.

Tab. 8: Optical loss values [dB/cm] of organosilanes for comparison with Tab. 7.

Silane	**[dB/cm] at λ:**	
	1310 nm	**1550 nm**
pentafluorophenyltriethoxysilane	0.02	0.28
phenyltrimethoxysilane	0.14	0.36
diphenyldimethoxysilane	0.18	0.36
4-vinylphenyltrimethoxysilane	0.22	0.46
MEMO	0.20	0.54
GLYMO	0.20	0.66

In direct comparison, the fluoroarylalkoxysilanes pentafluorophenyltrimethoxysilane (**1**), bis-(pentafluorophenyl)dimethoxysilane (**2**), 4-vinyltetrafluorophenyltrimethoxysilane (**4**), and pentafluorophenyl(vinyl)dimethoxysilane (**5**) exhibit considerably lower losses at both wavelengths than their unfluorinated counterparts. Particularly at 1310 nm, silanes **1** and **2** are transparent (<0.02 dB/cm), whereas their unfluorinated analogs show 0.14 dB/cm and 0.18 dB/cm attenuation, respectively. At 1550 nm, silanes **1** and **2** produce losses of 0.18 dB/cm and 0.10 dB/cm, respectively, whereas phenyltrimethoxysilane and diphenyldimethoxysilane both attenuate 0.36 dB/cm. Thus, as a first impression one can note that fluorination results in the expected reduction of optical loss at telecom wavelengths. From a comparison between pentafluorophenyltrimethoxysilane (**1**) and pentafluorophenyltriethoxysilane, also a loss-reducing effect due to utilization of methoxy rather than ethoxy silanes was measured. Particularly at 1550 nm, a considerable difference in transparency (Δ = 0.10 dB/cm) could be detected.

A difference in vinyl and methyl functionalization is shown in the comparison of pentafluorophenyl(vinyl)dimethoxysilane (**5**) with pentafluorophenyl(methyl)dimethoxysilane (**6**). The methyl silane absorbs relatively strongly at 1550 nm (0.54 dB/cm). In contrast, the loss in vinyl silane **5** is moderate with 0.24 dB/cm. In both cases, vinyl and methyl, the same number of C-H bonds are involved. The vinyl substituent, however, is larger in size due to the additional carbon center and therefore, less absorbing C-H bonds are present per volume unit. This accounts for lower losses in the 1550 nm range.

Two silanes, which are of importance for the synthesis of a number of ORMOCER® materials for microsystems[32], MEMO and GLYMO, were also added to the list in Tab. 8. Both exhibit relatively high losses at 1550 nm (MEMO: 0.54 dB/cm; GLYMO: 0.66 dB/cm). The methacryl silane MEMO is of particular interest for this study, because it is, together with diphenylsilanediol, the main compound in the reference ORMOCER® **b59d** for telecom applications[33]. Diphenylsilanediol itself, however, could not be included in the list, because in contrast to the other silanes, it is a solid under ambient conditions, and therefore spectroscopically not measurable under equal conditions as the liquid compounds. Thus, because all fluoroaryl modified alkoxysilanes outlined in Tab. 7 exhibit lower losses than the standard system MEMO, they are considered to be promising candidates as precursor compounds for the development of low-loss ORMOCER®s for telecom and datacom.

3.3 Development of ORMOCER® resins

A major part of this work was the development of ORMOCER® resins, which are ready for processing under clean room conditions in order to produce optical structures/devices. Therefore, a suitable mixture of starting compounds, i.e. highly fluorinated arylalkoxysilanes for hydrolytic polycondensation, had to be found, and polycondensation conditions had to be chosen. The polycondensation products had to meet several specifications to make them suitable candidates for use as ORMOCER® resins.

The first, most obvious necessity was the ability to form viscous resins, which could be diluted with a suitable solvent in order to adjust viscosity for further microsystems processing. The resulting ORMOCER® lacquers were to be storage stable at least for several weeks. Gelation, i.e. formation of insoluble condensates, was expressly undesired. For the achievement of this goal, an important consideration was the T/D ratio, i.e. the molar ratio of alkoxysilanes bearing three (T) and two (D) alkoxy groups, respectively, ready for polycondensation. Taking into account the so far best-performing ORMOCER® materials for telecom applications[33], which are based on an equimolar mixture of MEMO and diphenylsilanediol (cf. chapter 2.5.4), a T/D ratio of approximately 1:1 was the chosen starting value. Monoalkoxysilanes (M) and

tetraalkoxysilanes (Q) were left unconsidered. Beside the T/D ratio, also the reaction conditions play an important role. However, as experienced earlier[161,162] (cf. chapter 2.5.5), the choice of catalyst was limited due to the instability of the C-$Si_{fluoroaryl}$ bond under all but acidic reaction conditions.

A second crucially necessary property of the polycondensates was their photopatternability. Therefore, at least one of the precursor silanes had to bear an organically crosslinkable functionality susceptible to polymerization conditions, which occur during standard photolithographic processing.

The intended application of the resins as waveguide materials required that their properties had to be promising with respect to low optical loss. This particularly included minimized C-H and O-H contents, being controllable by appropriate selection of precursor silanes and reaction conditions. In addition to that, high thermal and mechanical resistance of the cured films was desirable in order to expand possible areas of application as well as the range of microsystem packaging methods.

Spectroscopic studies on promising precursor candidates and the search for suitable polycondensation conditions as well as detailed structural analyses of resulting resins are presented in the following sections of this work.

3.3.1 NMR analyses of polycondensation reactions

^{29}Si-NMR spectroscopic studies had already been found valuable for sol-gel reaction control in general[5,157-160], and of perfluoroarylalkoxysilanes[161,162], in particular. They also play a central role in the studies presented within this work. On the one hand, such spectroscopic investigations allow a detailed insight into the hydrolysis/polycondensation reaction itself, i.e. reaction intermediates can be quantitatively recorded with respect to chronological changes in reaction mixture composition. This allows valuable conclusions concerning sol-gel reactivities of precursor silanes and, consequently, suitable adjustments in terms of reaction conditions. On the other hand, such analyses result in signal assignments of reaction intermediates generated throughout the polycondensation of a silane under certain reaction conditions. In a later stage of ORMOCER® development, these assignments are of great value for the difficult spectroscopic analysis of polycondensates, which are based on mixtures of two or three precursor silanes, and show complex ^{29}Si-NMR spectra.

From the experimental point of view, hydrolysis/polycondensation experiments were carried out in a flask, and with ongoing reaction time, small samples were removed from the reaction mixture, shock frozen in liquid nitrogen, and subsequently analyzed with solution NMR at reduced temperature (-40 °C). In this way, the reaction was stopped at the defined reaction time and analyzed in its frozen state. The low-temperature procedure was necessary to stop the

reaction, because the collection of ^{29}Si-NMR is quite time-consuming due to the long relaxation time and the low sensitivity of the nuclei, and the reaction should not be allowed to proceed during analysis. As deuterated solvent for NMR spectroscopy, which is necessary in order to provide deuterons as an anchor for the instrument's lock signal, hexadeuteroacetone (d_6-acetone) was chosen for a number of reasons. First, one had to consider that the highest possible concentration of polycondensate had to be present in the solution to be analyzed, because the ^{29}Si nuclei are of relatively low NMR sensitivity. Additionally, such polycondensates were expected to contain a vast number of different species, all with different NMR chemical shifts, which again reduces sensitivity drastically. Thus, in order to maintain a high concentration of the polycondensate for a high signal-to-noise ratio on the one hand, and a sufficient amount of deuterons for the instrument to lock on on the other hand, a polydeuterated solvent had to be chosen. d_6-Acetone itself was used, because it is a suitable solvent for such polycondensates, and also is a preferred solvent for use in low-temperature experiments, due to its low melting point of -95 °C[167]. A detailed description of the method is given in the experimental section (chapter 4.2.1). Upon collecting a sequence of spectra at a number of discrete reaction times, the polycondensation reaction of a silane could be monitored in detail. ^{29}Si-, ^{13}C-, and ^{1}H-NMR chemical shifts were assigned in relation to the internal reference tetramethylsilane (TMS).

3.3.2 Polycondensation of bis-(pentafluorophenyl)dimethoxysilane (**2**)

Based on the above mentioned considerations resulting in a desired T/D silane ratio of 1:1 for new fluorinated ORMOCER® resins, a suitable D-type silane was to be found. Regarding the presented results for refractive index and optical loss (Tab. 7), bis-(pentafluorophenyl)dimethoxysilane (**2**) seemed a perfect D system to start with, exhibiting both relatively high index and exceptionally low losses. In order to learn more about the silane's polycondensation behavior, several hydrolysis/condensation experiments were carried out (Fig. 47) and the evolution of condensation intermediates analyzed with solution NMR spectroscopy.

However, neither acidic nor basic reaction conditions resulted in silicone-type linear D^2 condensation products. Instead, T and Q silanes were found by ^{29}Si-NMR, and ^{1}H- and ^{13}C-NMR revealed the presence of pentafluorobenzene in the reaction mixtures prior to the removal of volatiles. As the respective NMR chemical shifts for pentafluorobenzene, a multiplet in proton NMR at 7.45 – 7.30 ppm, and a number of broad ^{13}C signals at δ = 149.0 – 146.2 ppm, 144.3 – 141.4 ppm, 140.2 – 137.4 ppm, and 102.5 ppm, were identified. The carbon NMR signals were assigned according to literature[168]. A more detailed analysis of NMR data (exact assignment to the different carbon sites, plus carbon-fluorine coupling constants) is given in the experimental section of this work (chapters 4.4.1, 4.4.2).

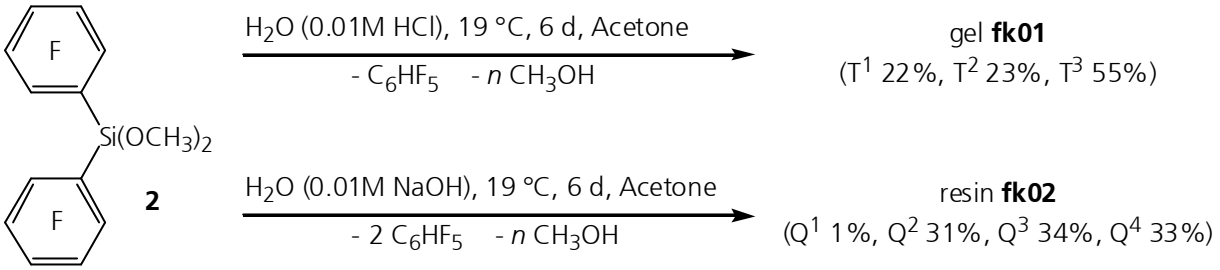

Fig. 47: Hydrolysis/condensation of bis-(pentafluorophenyl)dimethoxysilane.

In the alkaline reaction mixture, the presence of other than D-type silicon species was somewhat expected, because of the experiences made with dearylation of fluoroarylalkoxysilanes under non-acidic reaction conditions (see chapter 2.5.5[161,162]). It had been suggested that pentafluorophenyl is the better leaving group than the methoxy anion, and only upon protonation of the methoxy under acidic conditions, methanol as a good leaving group is formed. Thus, the exclusive formation of completely dearylated Q-type silicon species from **2** in alkaline medium can be understood.

The spectral analysis of the acidic reaction mixture, on the other hand, surprisingly also showed dearylation, as it exhibited only T instead of D species. Thus, even under acidic conditions, the first of the two perfluorophenyl substituents is still a better leaving group than the intended methoxy group. After the first dearylation, the polycondensation continues similarly to as if T silane **1** was the starting compound. Probably, due to the strongly electron-withdrawing pentafluorophenyl substituents in bis-(pentafluorophenyl)dimethoxysilane (**2**), the electron density on the silicon atom is so poor, that also electron density is withdrawn from the methoxy oxygen atoms. This in response leads to a lower basicity of the oxygen atoms, which complicates protonation with formation of the better leaving group methanol. Not before the first Si-(pentafluorophenyl) bond is cleaved, hydrolysis and condensation under production of alcohol occurs.

As a consequence of the presented results, bis-(pentafluorophenyl)dimethoxysilane (**2**) cannot be considered a suitable D-type precursor silane for the development of fluorinated ORMOCER® resins.

3.3.3 Polycondensation of pentafluorophenyl(vinyl)dimethoxysilane (**5**) – condensation stoichiometry

After the instability of bis-(pentafluorophenyl)dimethoxysilane (**2**) under the chosen polycondensation conditions had been discovered, reactivity investigations were focused on pentafluorophenyl(vinyl)dimethoxysilane (**5**) as the remaining fluoroaryl functionalized D-type silane candidate from Tab. 7.

In order to investigate the polycondensation behavior of silane **5**, it was first reacted with one molar equivalent of water, i.e. in condensation stoichiometry, with an acidic catalyst (Fig. 48). The reaction was carried out under ambient conditions in a way that the silane was stirred in a flask, and water and catalyst were added simultaneously in the form of 0.01 M hydrochloric acid as aqueous solution.

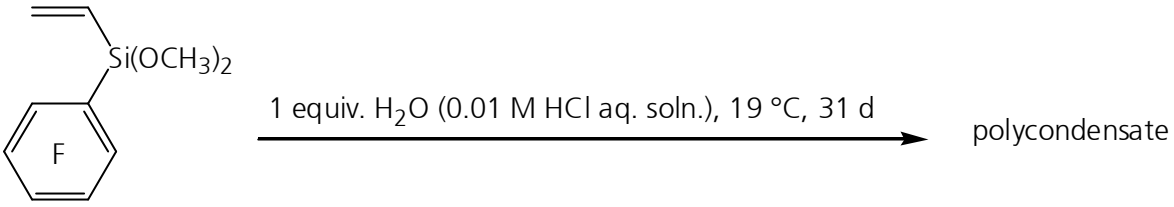

5

Fig. 48: Condensation-stoichiometric, acid-catalyzed hydrolysis/condensation of pentafluorophenyl(vinyl)dimethoxysilane (**5**).

After starting the reaction, ^{29}Si- as well as ^{1}H-NMR spectra were collected at predefined reaction times, following the low-temperature approach described above. Figure 49 shows the series of ^{29}Si-NMR spectra recorded at the marked reaction times. The quantitative analysis of the spectra, achieved by integration of the assigned NMR signals (Tab. 9), resulted in the plots shown in Figs. 50 & 51, for the chronological evolution of D^n silane species, and the conversion of methoxy groups into methanol, respectively.

Tab. 9: ^{29}Si-NMR signal assignments for polycondensates starting from silane **5**.

Signal: δ [ppm]	-36.4 – -41.4	-45.7 – -49.0	-55.1 – -56.1
Assignment	D^0	D^1	D^2

Because no solvent was added, the reaction mixture first exhibited a two-phase system, leading to a low reaction rate at the beginning of the experiment, because at this stage, reaction could only take place at the interface between the two liquid phases. Only after 1:44 h, enough methanol had been formed during hydrolysis, so that a homogeneous solution could be formed. From this point, the consumption of the educt silane as well as the production of condensates and methanol, was strongly accelerated. This effect is clearly seen in both silicon and proton NMR spectra, and in the resulting concentration plots (Figs. 49-51). The deduction of an exact kinetic theory, however, was not part of this work because of the multiple parameters that would have to be regarded. A semi-quantitative approach as presented was found to be sufficient for the reactivity investigations of relevance.

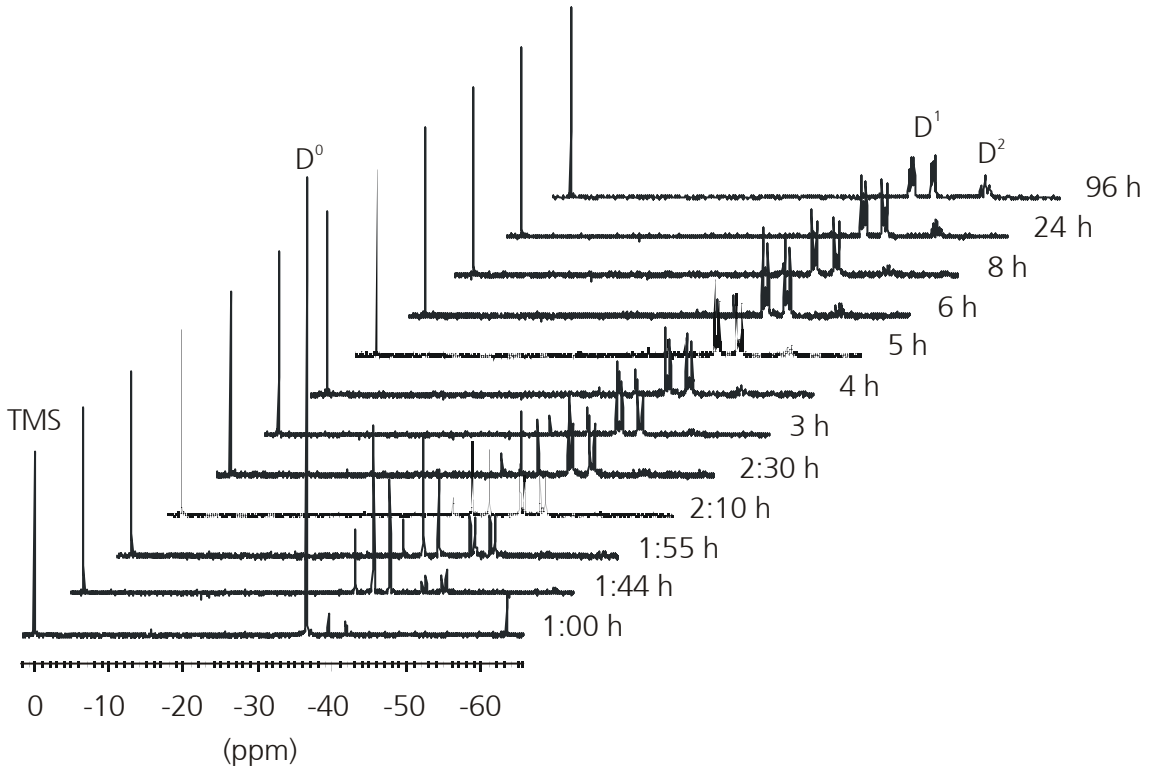

Fig. 49: Time-resolved ^{29}Si-NMR investigation of the acid-catalyzed hydrolysis/condensation of pentafluorophenyl(vinyl)dimethoxysilane (**5**) under condensation stoichiometry.

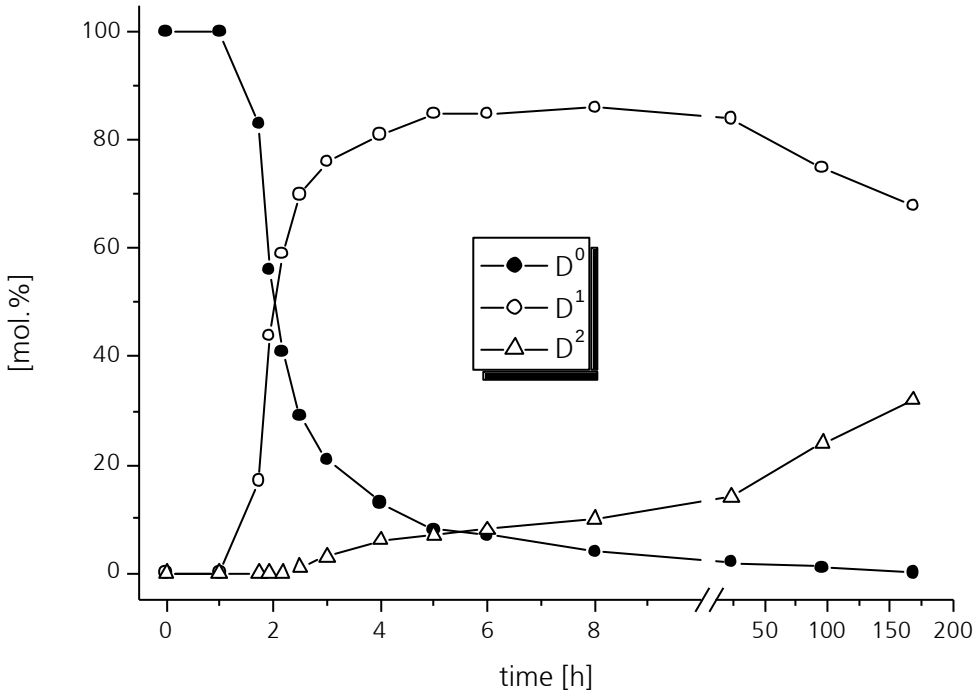

Fig. 50: Chronological development of D^n silane species concentrations during condensation stoichiometric polycondensation of **5** according to quantitative evaluation of ^{29}Si-NMR spectra as shown in Fig. 49.

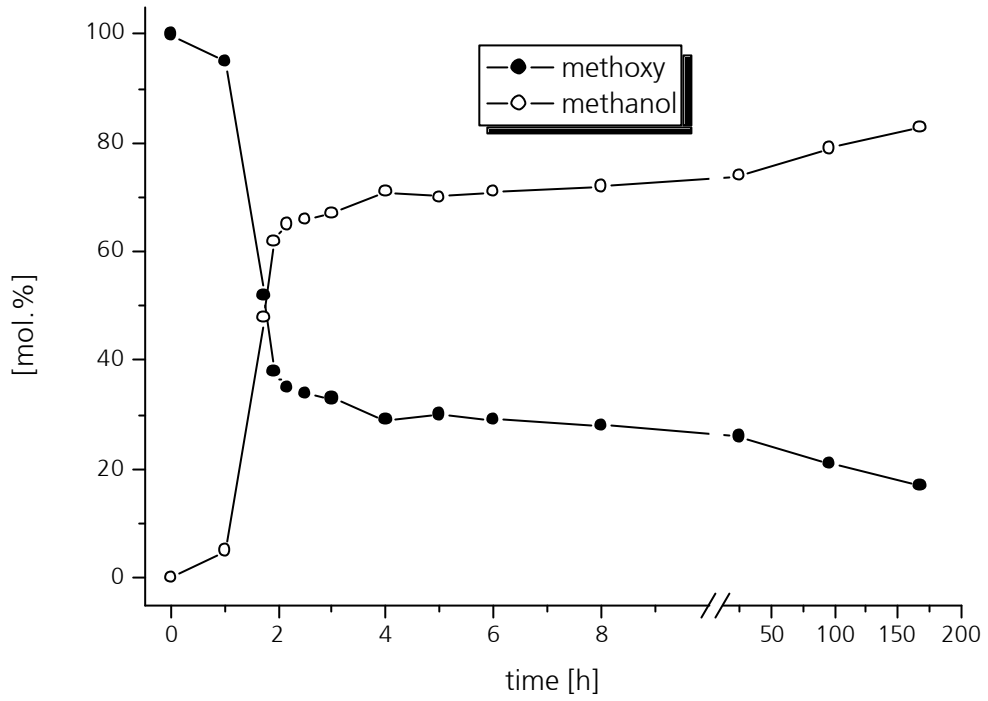

Fig. 51: Methoxy release and methanol production as derived from quantitative ^{1}H-NMR spectra, collected from condensation stoichiometric polycondensation reaction of **5**.

The ^{29}Si-NMR spectra show that after a homogeneous solution had been formed, the D^0 concentration, which includes the silane as well as both of its hydrolyzed stages, rapidly decreased. A value below 10% was reached after 5 h reaction time. Simultaneously, D^1 species evolved, reaching a concentration exceeding 80% after 4 h. A considerable amount of D^2 species in a quantity of more than 10%, however, was not detected before 8 h reaction time, i.e. up to this point the majority of the reaction mixture consisted of siloxane dimers. After these rapid changes within the reaction solution, further condensation occurred at a much reduced reaction rate, so that finally after 7 d (168 h) a $D^2/D^1/D^0$ ratio of 68:32:0 was achieved.

Regarding the quantitative analysis of the proton spectra, it can clearly be seen that after the point of homogeneity, methanol production went very fast, and after 2 h, more than 60% of the methoxy groups had been released. Taking into account that water had been added in condensation stoichiometry only, this means that water had already been widely consumed and from this point, methanol production was mainly due to condensation. Therefore, similarly to the results from ^{29}Si-NMR, further concentration changes happened with a much reduced rate. After 7 d (168 h), a methanol/methoxy concentration ratio of 83:17 was found.

Upon more detailed analysis of the evolution of ^{29}Si-NMR signals as outlined in the experimental part of this work (Tab. 25, chapter 4.4.3), a more detailed assignment of chemical shift values to reaction intermediates could be made. Although absolute quantitative

determination of ^{29}Si nuclei at concentrations below 5 – 10% was somewhat difficult due to low signal-to-noise ratios, relative evolutions of NMR signals could clearly be seen, and helped in signal assignment.

Starting from the precursor silane, symbolized by D_0^0, with a chemical shift of -36.4 ppm with respect to TMS, hydrolysis led to an upfield shift of -2.3 ppm to -2.7 ppm. In this context, it must be emphasized, that hydrolysis of D-type alkoxysilanes leads to upfield shifts, whereas hydrolysis of T-type alkoxysilanes results in downfield shifts. The latter trend had already been found in earlier experimental as well as computational studies on fluoroaryltrialkoxysilanes[50,161,162], and both trends are in accordance with literature[2,3,5,157,169]. Also of importance concerning the chemical shift values is a slight solvent effect. Whereas in deuterochloroform, the chemical shift for the precursor silane nucleus (D_0^0) was -36.9 ppm, the same signal in hexadeuteroacetone, which was the solvent in the NMR sequence experiments, was shifted downfield by 0.5 ppm.

Focusing back on the reaction, however, condensation of a D-type silicon center based on **5** with formation of a siloxane bond led to another upfield shift of approx. -8 ppm to -10 ppm. This is very similar to condensation of T silanes, as described for fluoroaryl-functionalized systems in preliminary work[50,161,162] as well as found for a variety of different T-type alkoxysilanes in literature[2,3,5,157,169]. An interesting detail was revealed in so far as the D^1 shift area could be resolved into six separate signals, divided into two groups of three. The downfield part between -45.4 ppm and -46.1 ppm represented D_0^1, the upfield shifted signals between -48.3 ppm and -49.0 ppm were due to D_1^1 silicon species. Thus, the shifts due to hydrolysis of a methoxy group were in the range of -2.9 ppm, very similar to the D^0 case. From regarding the chronological evolution of the three signals each, which the D_0^1 and D_1^1 groups consisted of, even the nature of the neighboring, siloxane-bound silicon center could be identified. The middle signals of each group, at -45.7 ppm and -48.6 ppm, respectively, continuously grew in intensity, while at the same time, the D^2 spectral region also became more intense. Therefore, the two signals could be assigned to D_0^1-(D^2) and D_1^1-(D^2) species, respectively, with connection to a D^2-type silicon atom. The assignments of the remaining four signals are explained within the next section of this work (chapter 3.3.4).

However, after a reaction period of 7 d, also traces of T species appeared in the solution, which after 31 d reached a concentration of 30% (4% T^1, 14% T^2, 12% T^3). Figure 52 compares the ^{29}Si-NMR spectra of the reaction mixture recorded after 4 d (Fig. 52a) and 31 d (Fig. 52b). The latter shows in addition to the expected signals for D_0^1 and D^2 species at -46 ppm and -56 ppm, respectively, also signals in a ppm region typical of T systems. Taking into account the weakness of the silicon-fluoroaryl bond, the obvious interpretation was the presence of T

condensates due to an aryl loss. Such a partial fragmentation in condensates based on pentafluorophenyl-(vinyl)-dimethoxysilane would lead to siloxanes with similarities to those based on vinyltrimethoxysilane. To support this idea, a control experiment, i.e. the hydrolytic polycondensation of vinyltrimethoxysilane, was carried out. The ^{29}Si-NMR spectrum of the resulting siloxane resin, which is shown in Fig. 52c, clearly reveals the correspondence to the signals found in the fluoroaryl experiment, proving the given interpretation of aryl loss.

Also an accumulation of signals at -52 – -54 ppm, i.e. with a downfield shift of approx. 3 ppm relative to the D^2 signal, strongly supports the appearance of T species. The newly found broad signal was assigned as D^2 species that are bound to one or two T-type silicon centers, symbolized by D^2-(T). This assignment is supported by a comparable result found in literature[159]: in the case of cocondensation of a D system, dimethyldiethoxysilane, with a Q silane, tetraethoxysilane, a new signal attributed to D^2 sites connected to Q sites was found with a downfield shift of about 4 ppm with respect to the major D^2 signal.

Besides the partial aryl loss, the ^{29}Si-NMR spectra also document a significant reduction of hydroxyl content as can be seen from the evolution of the D_1^1 signal (-49 ppm, D^1-OH) relative to D_0^1 (-46 ppm, D^1-OCH_3). Whereas after 4 d, the D^1-OH and the D^1-OCH_3 contents are equally distributed with amounts of 37% and 38%, respectively, the spectrum shows after 31 d only traces of D^1-OH compared to 17% D^1-OCH_3. This result strongly emphasizes the necessity to let the polycondensation mixture age for quite a long time – in the order of weeks – in order to minimize Si-OH content.

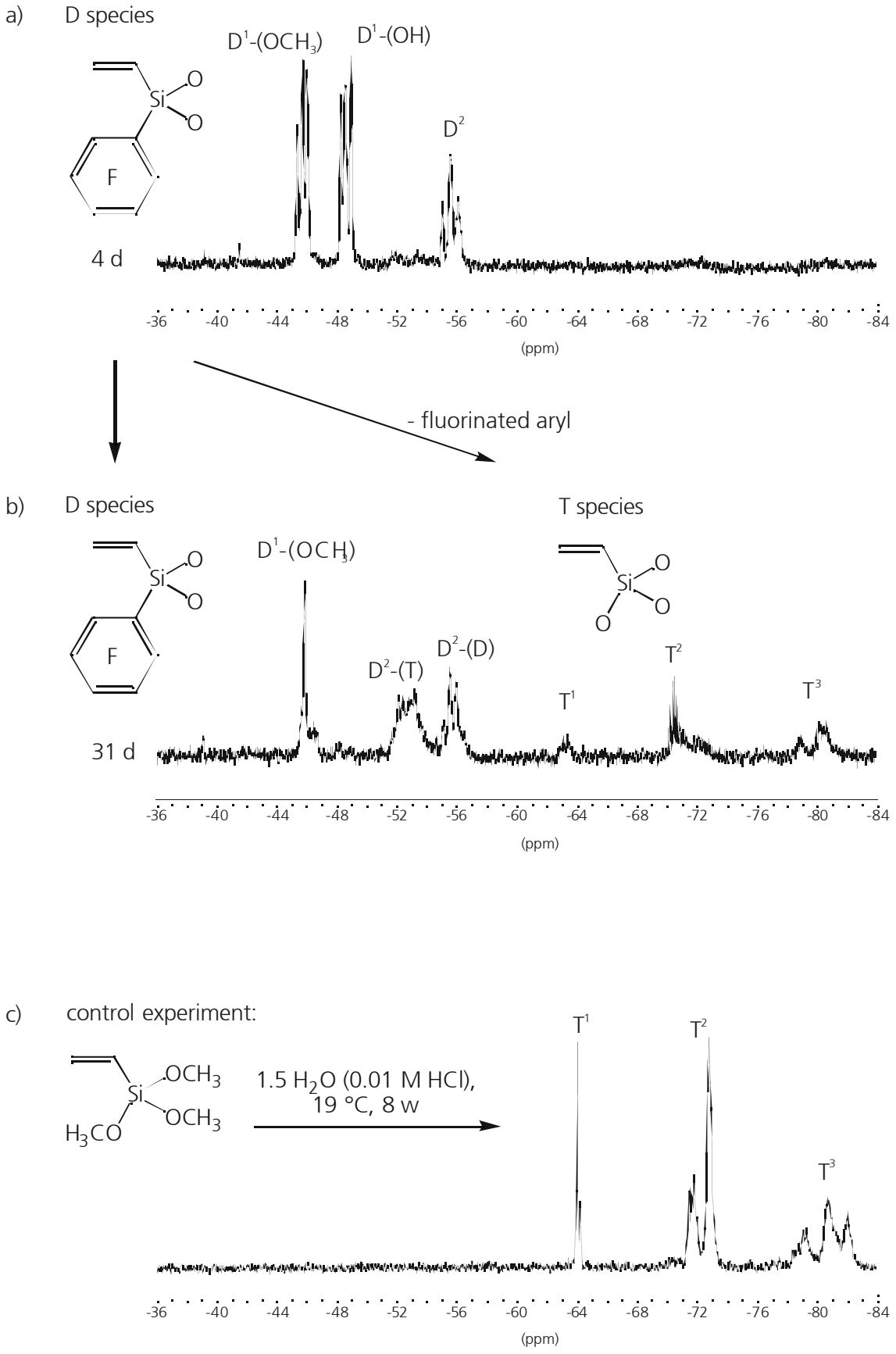

Fig. 52: ^{29}Si-NMR of polycondensation reaction mixtures starting from precursor silane **5** (cf. Fig. 48), recorded after a) 4 d and b) 31 d, compared to c) the polycondensation of vinyltrimethoxysilane.

3.3.4 Polycondensation of pentafluorophenyl(vinyl)dimethoxysilane (**5**) – hydrolysis stoichiometry

For further investigation of polycondensation reactivity of pentafluorophenyl(vinyl)dimethoxysilane (**5**), the silane was also reacted under hydrolysis stoichiometry, i.e. upon addition of two molar equivalents of water, and the reaction mixture was analyzed with the same method as in the condensation stoichiometric experiment presented above (see chapter 3.3.3). Time-resolved NMR analysis resulted in a series of ^{29}Si spectra (Fig. 53) and chronological plots for the evolution of silicon species (Fig. 54) as well as for the conversion of methoxy groups into methanol (Fig. 55). ^{29}Si-NMR signal assignments were made according to Tab. 27 (chapter 4.4.4).

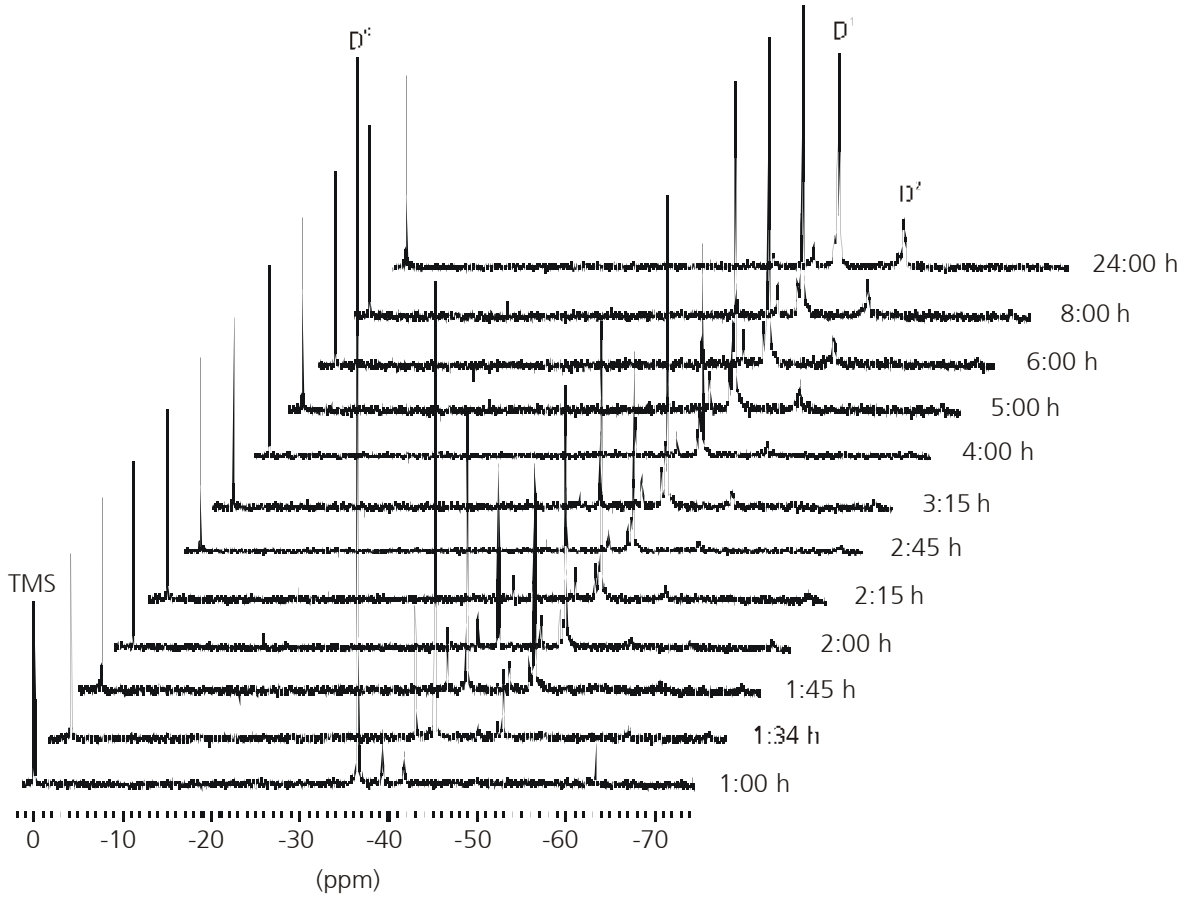

Fig. 53: Series of ^{29}Si-NMR spectra from acid-catalyzed hydrolysis/polycondensation of pentafluorophenyl(vinyl)dimethoxysilane (**5**) under hydrolysis stoichiometry.

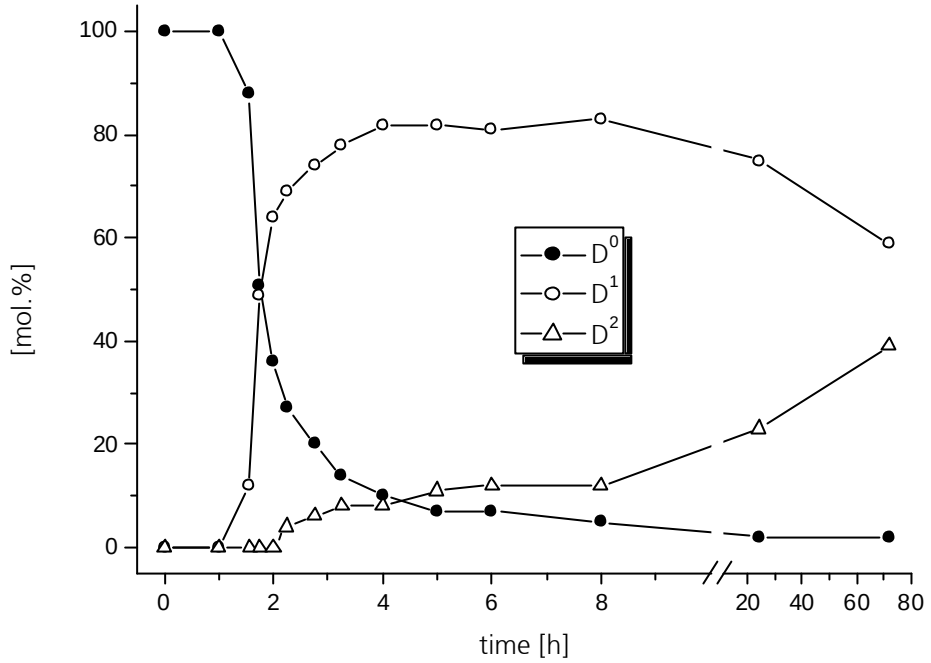

Fig. 54: Chronological development of D^n silane species concentrations during hydrolysis stoichiometric polycondensation of **5** according to quantitative evaluation of ^{29}Si-NMR spectra as shown in Fig. 53.

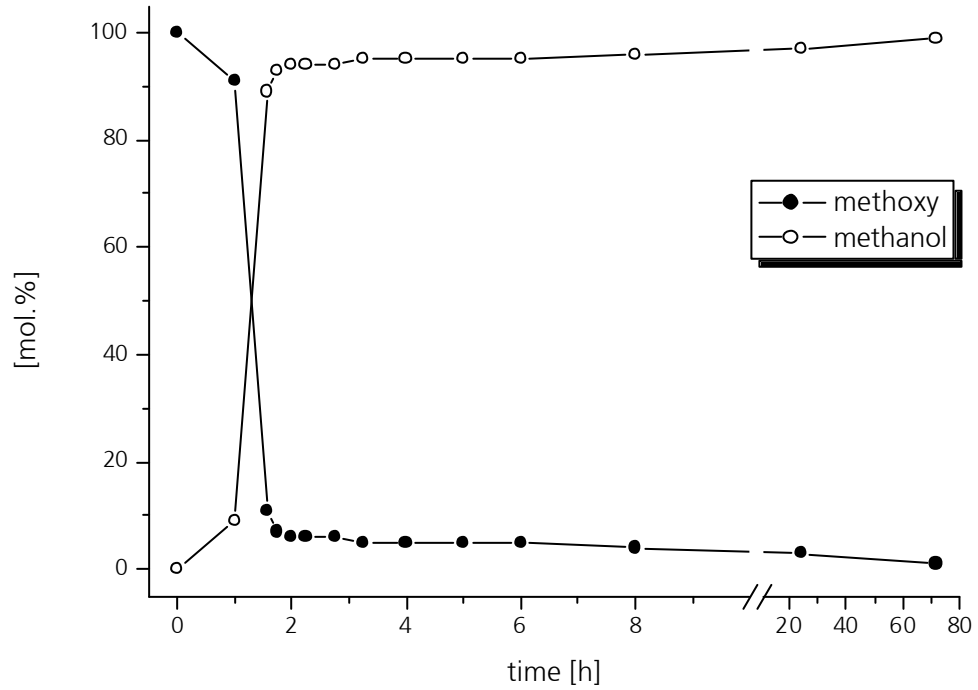

Fig. 55: Methoxy release and methanol production in the hydrolysis stoichiometric polycondensation of **5**, according to ^{1}H-NMR.

Quantitative analysis of ^{1}H-NMR (Fig. 55) shows that after homogenization (1:34 h), methanol production went very fast, so that after 1:45 h total reaction time, methoxy release was more than 90% completed. This means that during 45 min (1 h to 1:45 h total reaction time), methanol content increased from 9% to 93% with respect to 100% hydrolyzable methoxy groups. Afterwards, methanol production continued at a much slower rate. From analysis of the ^{29}Si-NMR spectra (Fig. 54) follows that from the point of homogeneity, condensation commences rapidly, reaching a D^1 content of more than 80% after 4 h, which is similar to the condensation stoichiometry case. D^2 species with a concentration of more than 10% were detectable after 5 h, compared to 8 h for reaction with condensation stoichiometry. After 24 h, a $D^2/D^1/D^0$ ratio of 23:75:2 (hydrolysis stoichiometry) as opposed to 14:84:2 (condensation stoichiometry) gives evidence for a slightly higher condensation reaction rate, which is a straightforward consequence from the higher concentration of reaction partners. Whereas in a completely hydrolyzed system all silane centers can react with each other, in a partly hydrolyzed system, condensation reactions are limited to silanol-alkoxysilane and silanol-silanol pairs, respectively. Two neighboring alkoxysilanes cannot react under the ambient polycondensation conditions applied.

Concerning the detailed assignment of ^{29}Si-NMR chemical shifts, the above mentioned results for the analysis of condensation stoichiometric polycondensation of **5** were supported and, additionally, the analysis of the two D^1 signal groups consisting of three sub-signals each, could be completed. The spectra in the hydrolysis stoichiometric case are more reduced, because particularly in the D^1 part, the signals are largely limited to fully hydrolyzed silane centers. This is of considerable help for the assignment. The complete quantitative analysis corresponding to the series of spectra outlined in Fig. 53 is given in the experimental section (Tab. 27, chapter 4.4.4). At first, D^1 signals in the region around -46 ppm are only sparsely resolvable, whereas between -48.2 ppm and -48.9 ppm, the same three-membered group of signals were detected as above. Therefore, the above found assignment of the high-field shifted signal group to D_1^1 silicon species and of the low-field shifted one to D_0^1 was supported, respectively.

In addition to that, evidence was found for the assignment of the remaining ^{29}Si-NMR signals in both D^1 groups. Table 27 (chapter 4.4.4) shows that in the D_1^1 signal group at -48.2 – -48.9 ppm, the intensity of the most high-field situated signal by far exceeds the other two. Because the middle signal at -48.6 ppm had already been identified as corresponding to D_1^1 species connected to D^2 silanes, the remaining one at -48.2 ppm was assigned to D_1^1-(D_0^1) species, which are present in the solution in only small concentrations among a vast majority of hydrolyzed silanes.

As a result from this detailed analysis, the NMR signal of a silane center, which forms a siloxane bond with a D_0^1 silicon atom, i.e. one with the methoxy group still attached, is shifted more towards the downfield region (-45.4 ppm, -48.3 ppm). A silicon center connected with a hydrolyzed D_1^1 species exhibits an upfield shifted resonance (-46.1 ppm, -49.0 ppm). Therefore, the already observed trend that hydrolysis of a D-type silane center results in an upfield shift of the respective ^{29}Si-NMR signal, is also reflected on the neighboring silicon atom.

The complete assignment of ^{29}Si-NMR signals to reaction intermediates, which occur in the polycondensation of pentafluorophenyl(vinyl)dimethoxysilane (**5**), as resulting from time-resolved ^{29}Si-NMR analysis, is presented in Tab. 10.

Tab. 10: Detailed ^{29}Si-NMR signal assignments for polycondensates starting from silane **5**, completing the simplified assignments in Tab. 9 (chapter 3.3.3).

Signal: δ [ppm]	-36.4	-39.1	-41.4	-45.4	-45.7	-46.1	-48.3	-48.6
Assignment	D_0^0	D_1^0	D_2^0	D_0^1-(D_0^1)	D_0^1-(D^2)	D_0^1-(D_1^1)	D_1^1-(D_0^1)	D_1^1-(D^2)

(continued)	-49.0	-51.8	-55.1	-55.6	-56.1
Assignment	D_1^1-(D_1^1)	D^2-(T)	D^2-(D_0^1)	D^2-(D_1^1)	D^2-(D^2)

As a concluding remark, although after longer reaction periods of several weeks, up to 30% aryl loss was detected, pentafluorophenyl(vinyl)dimethoxysilane (**5**) is considered a suitable D-type candidate for the development of fluoroaryl functionalized ORMOCER®s for telecom applications. A detailed assignment of ^{29}Si-NMR signals was achieved by time-resolved NMR experiments, which is expected to be a valuable contribution to following investigations on more complex polysiloxane systems.

3.3.5 Polycondensation of pentafluorophenyltrimethoxysilane (**1**)

After the presented investigations on D-type fluoroaryldimethoxysilanes **2** and **5**, the reactivities of suitable T-systems were investigated. The considerable presence of such trialkoxysilanes in the polycondensation mixture gives rise to the formation of a rigid three-dimensionally connected siloxane backbone, which is the basis for high thermal and mechanical resistance of ORMOCER®s. The most simple perfluoroarylalkoxysilane, pentafluorophenyltrimethoxysilane (**1**), had already been studied under several different reaction conditions[161,162]. In order to complete the reactivity investigations, the silane was reacted under acidic catalysis with water in hydrolysis stoichiometry, i.e. upon addition of three molar equivalents of water in the form of 0.01 M hydrochloric acid solution (Fig. 56). ^{29}Si- and ^{1}H-NMR spectra were recorded according to the method described above. Integration of the series of

^{29}Si-NMR signals presented in Fig. 57 resulted in a chronological plot (Fig. 58), which outlines the evolution of T^0, T^1, T^2, and T^3 silane species with increasing reaction time. Figure 59 shows the conversion of methoxy groups into methanol.

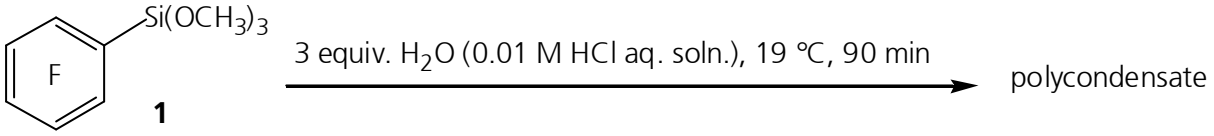

1

Fig. 56: Acid-catalyzed polycondensation of pentafluorophenyltrimethoxysilane (**1**) in hydrolysis stoichiometry.

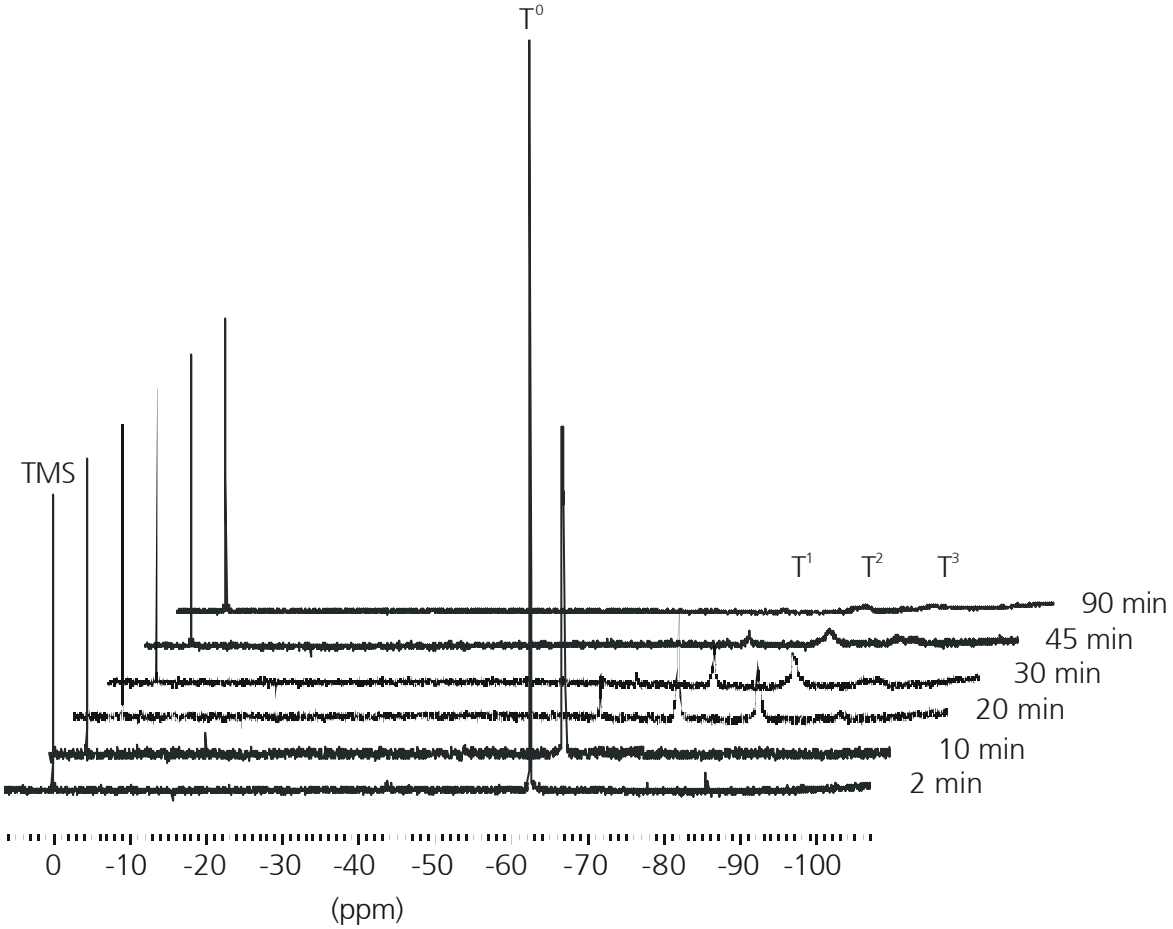

Fig. 57: ^{29}Si-NMR spectra from the polycondensation of pentafluorophenyltrimethoxysilane (**1**) under hydrolysis stoichiometry.

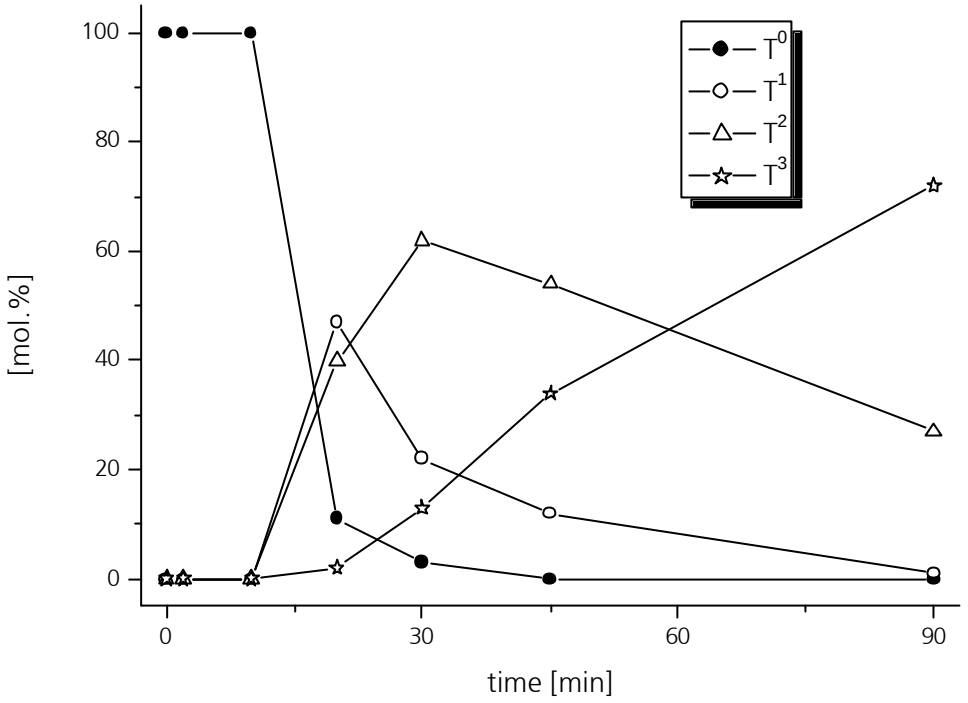

Fig. 58: Chronological evolution of polycondensation intermediates of **1**, based on ^{29}Si-NMR (Fig. 57).

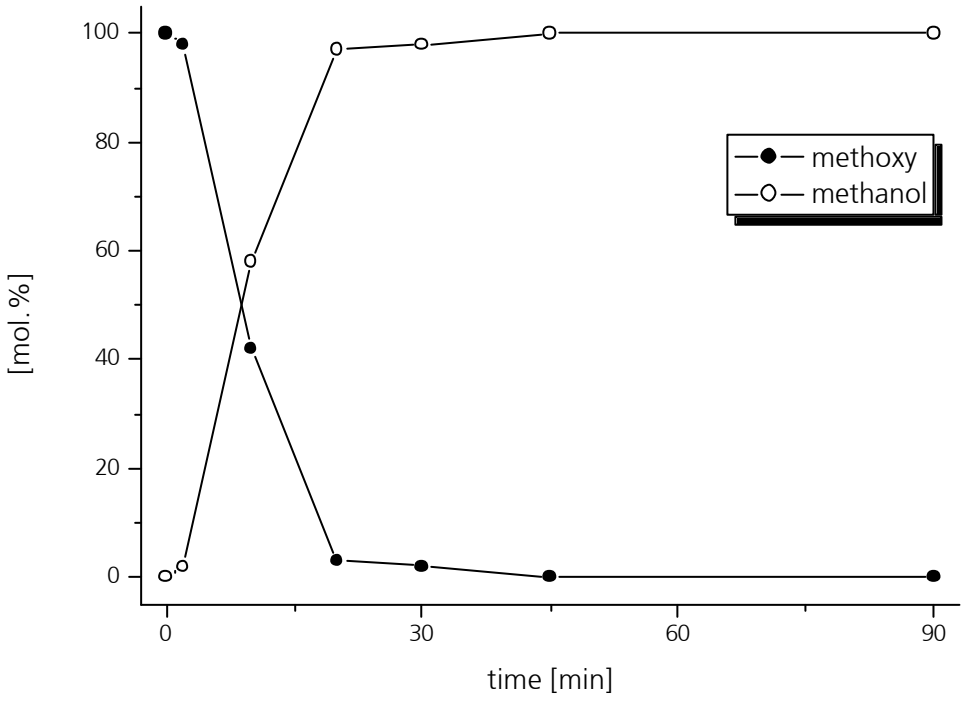

Fig. 59: Methoxy conversion to methanol during hydrolysis stoichiometric polycondensation of **1**, according to ^{1}H-NMR.

After mixing the reactants, the reaction mixture exhibited a two-phase system, similar to the experiments presented above. The mixture homogenized after 20 min and, immediately, T^1 and T^2 species were detected. The T^1 concentration reached a maximum of 47% after 20 min, i.e. even before homogenization, a considerable amount of silane molecules had undergone condensation. From ^{1}H-NMR, it could be seen that even during reaction at the interface between the two liquid phases, after 10 min, more than 50% of the methoxy groups had been released. At the point of homogeneity after 20 min, 97% conversion from methoxy to methanol was detected. With ongoing reaction time, the T^1 signal intensity in ^{29}Si-NMR decreased, while T^2 content reached its maximum of 62% at 30 min, when also T^3 species were detectable in a concentration above 10%. After 90 min, the polycondensate consisted of T^3, T^2 and T^1 silicon species in a ratio of 72:27:1.

In comparison with earlier results from reaction of **1** under condensation stoichiometric addition of water (1.5 molar equivalents)[161,162], the reaction mixture presented herein (hydrolysis stoichiometry) reached the point of homogeneity earlier, namely after 20 min compared to 30 min. Also, T^3 species could be detected after 30 min, in contrast to 3 h. From the methoxy conversion point of view, the reaction was more than 95% complete after 20 min, whereas in the condensation stoichiometry case, this happened not before 4 h. Thus, hydrolysis stoichiometry strongly enhanced the hydrolysis/condensation reaction rate.

The ^{29}Si-NMR signal assignments for reaction intermediates occurring in the polycondensation of pentafluorophenyltrimethoxysilane (**1**) are presented in Tab. 11 and are similar to the already published experiment in condensation stoichiometry[161,162].

Tab. 11: ^{29}Si-NMR signal assignments for polycondensates starting from silane **1**.

Signal: δ [ppm]	-62.0 – -62.8	-72.2 – -73.6	-82.1 – -85.0	-91.6 – -96.0
Assignment	T^0	T^1	T^2	T^3

In conclusion, pentafluorophenyltrimethoxysilane (**1**) is considered a promising candidate as T-type precursor silane for optical ORMOCER®s, particularly due to its low absorption at 1310 nm and 1550 nm as mentioned before (Tab. 7). The presented hydrolysis stoichiometric polycondensation experiment resulted in ^{29}Si-NMR shift assignments, which are supported by earlier results[161,162].

3.3.6 Polycondensation of 4-vinyltetrafluorophenyltrimethoxysilane (**4**)

Beside the D- and T-type silanes **1** and **5**, respectively, which are in particular considered useful for the alteration of the siloxane backbone of ORMOCER®s, a silane bearing a reactive functionality for organic cross-linking was needed. 4-Vinyltetrafluorophenyltrimethoxysilane (**4**)

as a fluorinated styrene-analogous compound was considered to be a candidate, which accounts for the photopatternability of ORMOCER® resins. In addition to earlier results on the polycondensation reactivity[161,162], the silane was studied by time-resolved NMR during hydrolysis stoichiometric reaction, according to the reaction carried out with pentafluorophenyltrimethoxysilane (**1**) (cf. Fig. 56).

Figure 60 gives the ^{29}Si-NMR spectra from the initial polycondensation phase up to a reaction time of 136 min. Similar to the above experiment with silane **1**, however, the ^{29}Si-NMR signals were of poorer resolution quality than the spectra recorded from reactions of the D-type silane **5**. This is attributed to the fact that the condensation stages of a T system involve more differently hydrolyzed silicon centers than in the D case. Thus, the total ^{29}Si signal intensity is distributed onto far more sub-signals, making the individual ones less intense. With increasing reaction time, more combinations are possible, to what kinds of species a silicon center can be connected to. Thus, the NMR signals become more and more diffuse due to a lower signal-to-noise ratio.

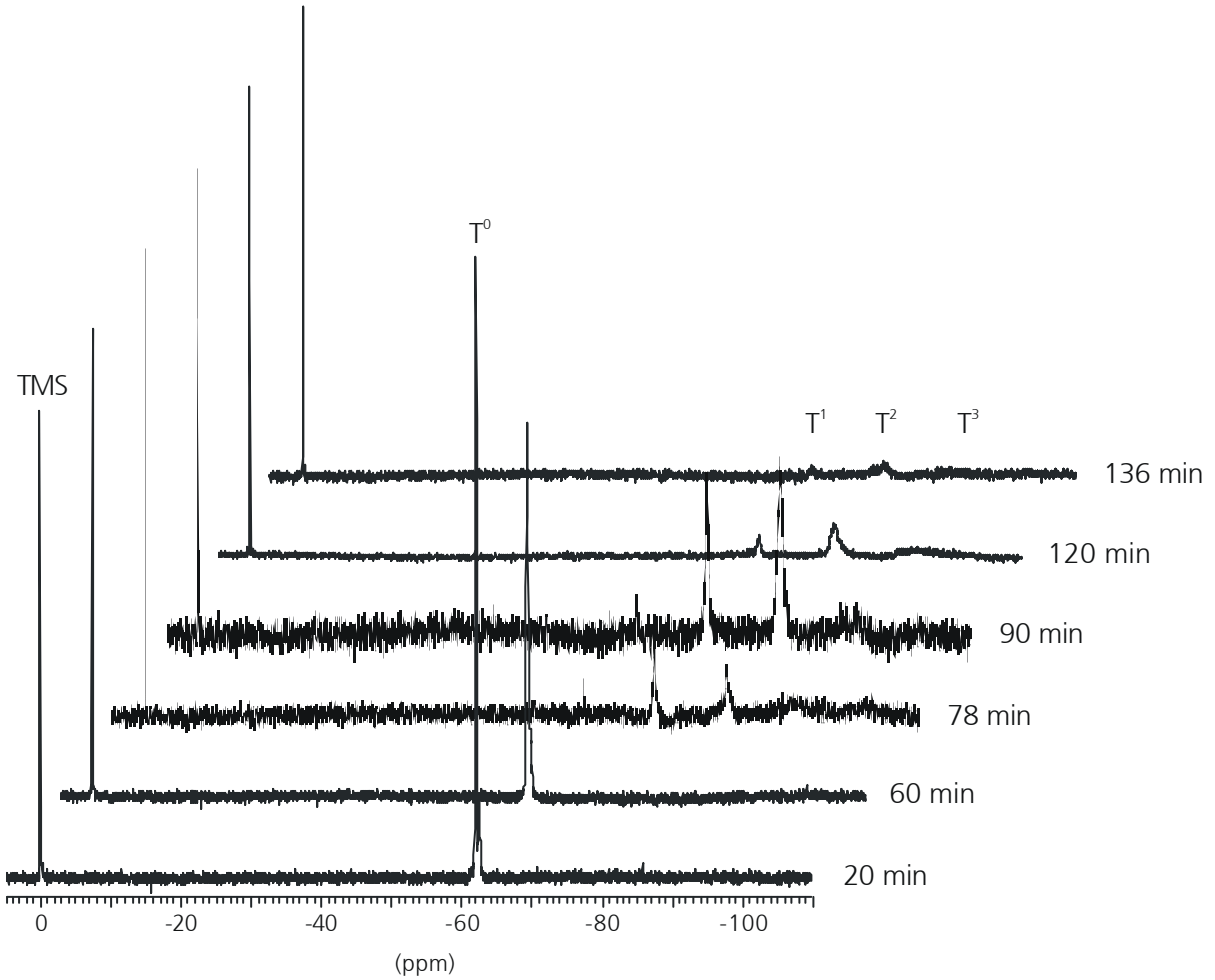

Fig. 60: ^{29}Si-NMR spectra from the polycondensation of 4-vinyltetrafluorophenyltrimethoxysilane (**4**) under hydrolysis stoichiometry.

Nevertheless, the spectral signals were integrated in an attempt to receive at least a semi-quantitative analysis, resulting in the chronological plot depicted in Fig. 61. The graph suffers from relatively high errors resulting from the poor NMR resolution. Being aware of this limitation, however, a coarse analysis of reaction mixtures could be given beside a signal assignment, which is believed to be sufficiently exact for the later analysis of highly condensed ORMOCER® resins.

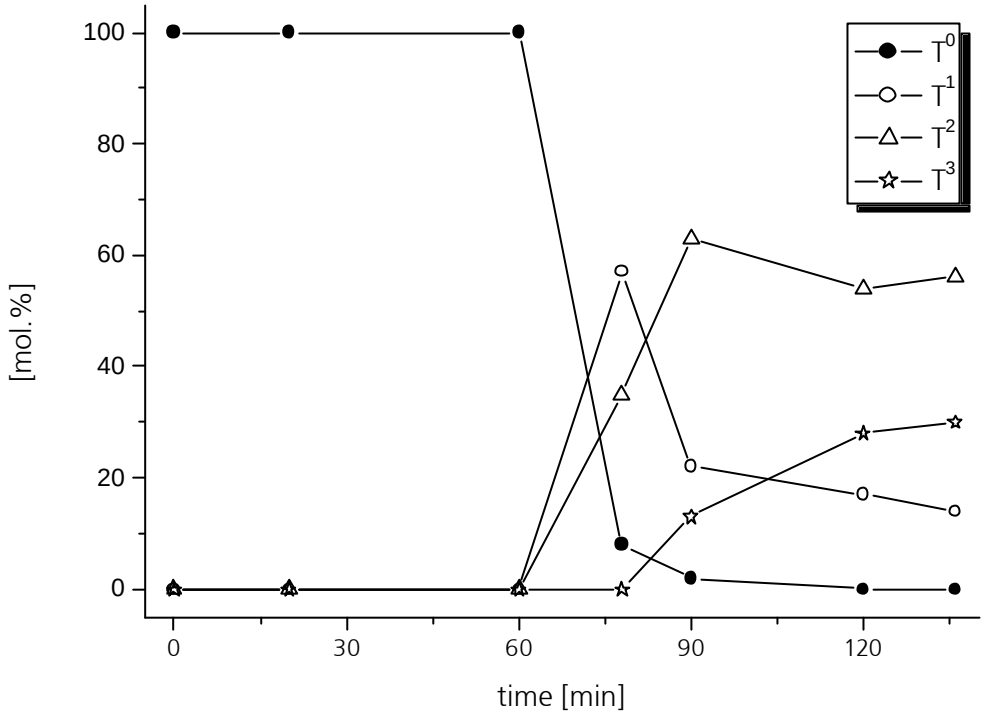

Fig. 61: Chronological evolution of polycondensation intermediates from starting compound **4**, according to ^{29}Si-NMR (Fig. 60).

Table 12 gives the ^{29}Si-NMR signal assignments for reaction intermediates, which occur in the hydrolysis/polycondensation reaction of 4vinyltetrafluorophenyltrimethoxysilane (**4**). They are almost identical with the ones for pentafluorophenyltrimethoxysilane (**1**).

Tab. 12: ^{29}Si-NMR signal assignments for polycondensates starting from silane **4**.

Signal: δ [ppm]	-61.8 – -62.7	-72.0 – -73.2	-82.2 – -84.6	-91.0 – -96.1
Assignment	T^0	T^1	T^2	T^3

In contrast to the analogous experiment with **1**, which homogenized after 20 min, the reaction with 4-vinyltetrafluorophenyltrimethoxysilane (**4**) required 78 min for homogenization, after which condensation quickly proceeded. The T^1 concentration reached a maximum of

approx. 60% after 78 min, when methoxy conversion had already been completed (Fig. 62). A maximum T^2 concentration of approx. 60% was determined after 90 min, and at the end of the experiment after 136 min, the last sample spectrum was recorded due to high viscosity of the mixture, a $T^3/T^2/T^1/T^0$ ratio of approx. 30:55:15:0 was measured.

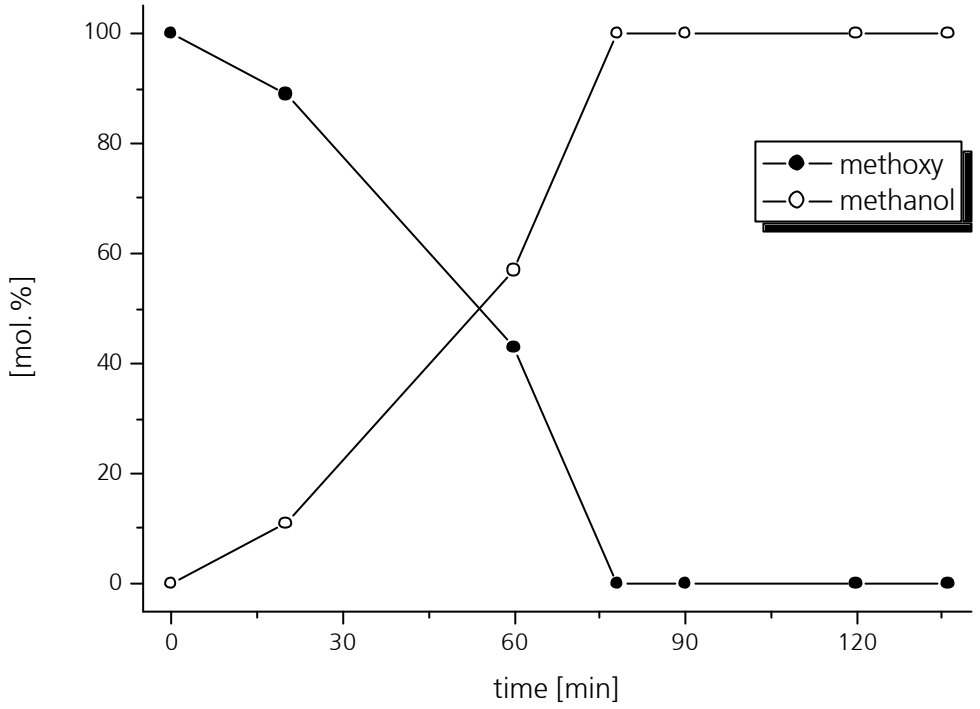

Fig. 62: Methoxy conversion to methanol during hydrolysis stoichiometric polycondensation of **4**, according to ^{1}H-NMR.

From this semi-quantitative approach, at least a reactivity of styrene-analogous silane **4** being slightly less than that of pentafluorophenyltrimethoxysilane (**1**) and higher than that of D-type silane **5**, can be deduced. Also, the presence of only T-type species in the solution gives rise to the assumption that the silane, like silane **1**, is stable under the chosen polycondensation conditions. Thus, 4-vinyltetrafluorophenyltrimethoxysilane (**4**) is a promising precursor candidate for ORMOCER® development.

3.3.7 Control experiments – polycondensation reactions of vinyltrimethoxysilane and tetramethoxysilane

Beside reactivity investigations, the above mentioned ^{29}Si-NMR investigations of fluoroarylalkoxysilane polycondensation reactions were conducted in order to find NMR chemical shift assignments for the polycondensation species attributed to the respective precursor compounds. These assignments were necessary for the analysis of complex ^{29}Si-NMR

spectra of polycondensates, which consist of combinations of these starting compounds. However, since partial fluoroaryl loss was involved in such reactions, also the NMR signals of decomposition products had to be considered.

The control reaction of vinyltrimethoxysilane under polycondensation conditions has already been mentioned within the scope of polycondensation investigations on pentafluorophenyl(vinyl)dimethoxysilane (**5**) (chapter 3.3.3). The partial dearylation of silane **5** was shown to result in condensates similar to those resulting from polycondensation of vinyltrimethoxysilane. Similar to silane **5**, also for the T-type silanes pentafluorophenyltrimethoxysilane (**1**) and 4-vinyltetrafluorophenyltrimethoxysilane (**4**), aryl loss was possible under acidic catalysis. Under non-acidic, i.e. neutral or basic conditions, such dearylation had already been detected[161,162]. In case of dearylation of T-systems, however, this did not result in condensates based on vinyltrimethoxysilane, as in case of silane **5**, but rather in Q-type orthosilicate species, as if tetramethoxysilane had been the precursor molecule.

Therefore, as model polycondensation precursors for these decomposition products, the condensates of vinyltrimethoxysilane and tetramethoxysilane were analyzed. It is true that numerous NMR investigations on these silanes are reported in literature[170], but the control experiments were necessary in order to record the spectra under similar conditions and acquisition parameters as in case of the resins. In this way, distortion due to solvent, temperature and concentration effects were excluded. Tables 13 & 14 outline the ^{29}Si-NMR signal assignments for polycondensates based on vinyltrimethoxysilane and tetramethoxysilane, respectively.

Tab. 13: ^{29}Si-NMR signal assignments for polycondensates starting from vinyltrimethoxysilane.

Signal: δ [ppm]	-62.9 – -63.8	-71.3 – -72.7	-79.1 – -81.9
Assignment	T^1	T^2	T^3

Tab. 14: ^{29}Si-NMR signal assignments for polycondensates starting from tetramethoxysilane.

Signal: δ [ppm]	-78.4	-83.9 – -85.9	-92.9 – -93.9	-100.1 – -104.1
Assignment	Q^0	Q^1	Q^2	Q^3

The individual T^n and Q^n regions, respectively, consist of groups of signals. However, the exact nature of the individual signals was not investigated in detail, because the task of the experiment was to find the ^{29}Si-NMR signal pattern for reaction intermediates in a phenomenological way. Detailed reactivity studies were focused on fluoroarylmethoxysilanes only within this work. Thus, no further experiments were conducted under varying reaction conditions. Interestingly, however, in the case of tetramethoxysilane, even after 8 w reaction

time, no Q^4 species could be found. This can be attributed to the acidic catalysis in combination with low water concentration, which generally results in more linearly than three-dimensionally connected siloxane networks[2].

3.4 Synthesis and characterization of ORMOCER® resins from precursor silane mixtures

Within the scope of the work presented so far, three promising precursor silanes for fluoroaryl functionalized ORMOCER®s for low-loss telecom applications have been identified. Pentafluorophenyltrimethoxysilane (**1**) exhibits low absorptions in the 1310 nm and 1550 nm telecom wavelength regions. As a T-type silane, **1** is expected to give rise to a dense inorganic network within the material. For the synthesis of liquid ORMOCER® resins, also the admixture of a D-type silane is crucial, as hydrolysis/condensation of pure T-type fluoroarylalkoxysilanes under the chosen acidic conditions inevitably leads to gelation of the polycondensates[161]. As the D-type fluoroaryl silane of choice, pentafluorophenyl(vinyl)dimethoxysilane (**5**) promises good performance both, for the build-up of a dense but soluble siloxane network, and for good optical properties. Bis-(pentafluorophenyl)dimethoxysilane (**2**), however, had to be excluded from the list, because NMR experiments revealed its instability even under acidic polycondensation conditions. Finally, 4vinyltetrafluorophenyltrimethoxysilane (**4**) recommends itself as T-type silane with a styrene-analogous substituent, which should ensure photopatternability of ORMOCER® resins.

The task of the following step in ORMOCER® development was to find a suitable mixture of the precursor silanes together with appropriate reaction conditions in order to produce liquid and in common solvents soluble, photopatternable ORMOCER® resins with low absorptions at 1310 nm and 1550 nm. All polycondensation reactions were carried out under acidic catalysis with dilute hydrochloric acid.

3.4.1 Preparation of soluble fluoroaryl-functionalized ORMOCER® resins

A first approach towards ORMOCER®s based on fluoroarylmethoxysilanes was the cocondensation of pentafluorophenyltrimethoxysilane (**1**) and 4-vinyltetrafluorophenyl-trimethoxysilane (**5**) in accordance to already published experiments with the respective ethoxy-substituted analogous compounds[41]. Within the literature reference, pentafluorophenyltriethoxysilane has been cocondensed with pentafluorophenyl(vinyl)-diethoxysilane in ethanolic solution. Following this route, mixtures of silanes **1** and **5** in methanol were reacted under hydrolysis stoichiometry (composition **fk11**) and condensation stoichiometry (composition **fk12**), respectively (Fig. 63).

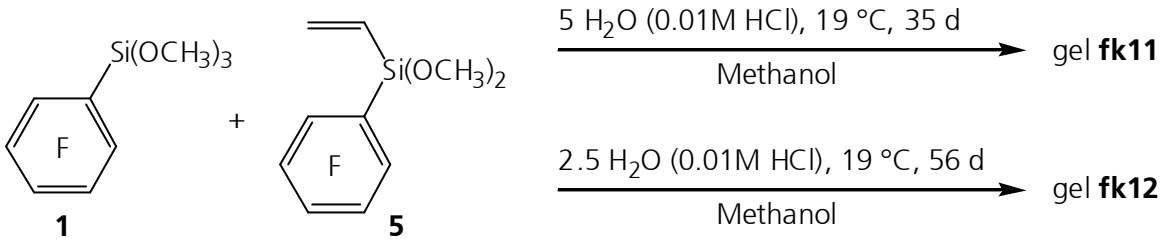

Fig. 63: Cocondensation of silanes **1** and **5** in methanol.

After 3 d reaction time, control NMR spectra were recorded from both mixtures. ^{29}Si-NMR detected instead of the expected D/T ratio of 50:50, which would reflect the initial composition, D/T/Q ratios of 30:54:16 in the **fk11** case, and of 23:74:3 for **fk12**. This shows considerable partial aryl loss, particularly for the D-type silane. Accordingly, in both cases proton and carbon spectra exhibited the respective signals for pentafluorobenzene. From the condensation stoichiometric polycondensation experiment conducted with pentafluorophenyl(vinyl)dimethoxysilane (**5**), the necessity of long reaction times in order to minimize Si-OH content has been deduced (see chapter 3.3.3). Therefore, compositions **fk11** and **fk12** were left reacting for 5 and 8 weeks, respectively. However, the experiments led to gelation in both cases.

Therefore, in order to examine solvent influence, additional experiments were carried out to find reaction conditions that result in liquid ORMOCER® resins. Figure 64 outlines further cocondensation reactions of silanes **1** and **5**, conducted in acetone as solvent as well as under solvent-free conditions. In both cases, the experiments were conducted in hydrolysis and condensation stoichiometry. The mixtures were allowed to react for 8 w in order to give the polycondensates time to age. Indeed, compositions **fk13**, **fk14**, and **fk16** led to highly viscous organopolysiloxane resins, which were soluble in solvents like acetone, propyl acetate and toluene, whereas the solvent-free hydrolysis stoichiometric composition **fk15** formed an insoluble gel after 8 d.

The two resins from the condensation stoichiometric compositions exhibited optical absorptions of 0.04 dB/cm at 1310 nm and 0.66 dB/cm at 1550 nm (**fk14**), and 0.10 dB/cm at 1310 nm and 0.18 dB/cm at 1550 nm (**fk16**), respectively. These low loss values, particularly for composition **fk16**, gave evidence that for the synthesis of ORMOCER®s for optical applications from fluoroarylalkoxysilanes, a D/T precursor silane ratio of 1:1, together with condensation stoichiometric addition of water under acidic catalysis and a long aging time are crucial polycondensation reaction parameters. From the solvent point of view, both, the addition of methanol and of acetone proved disadvantageous. Whereas methanol favors the undesirable gelation of the polycondensation mixture (**fk11**, **fk12**), acetone stabilizes reaction products,

which strongly absorb in the 1550 nm region (**fk14**). Conducting the reaction in condensation stoichiometry without an additional solvent gave the most promising results (**fk16**).

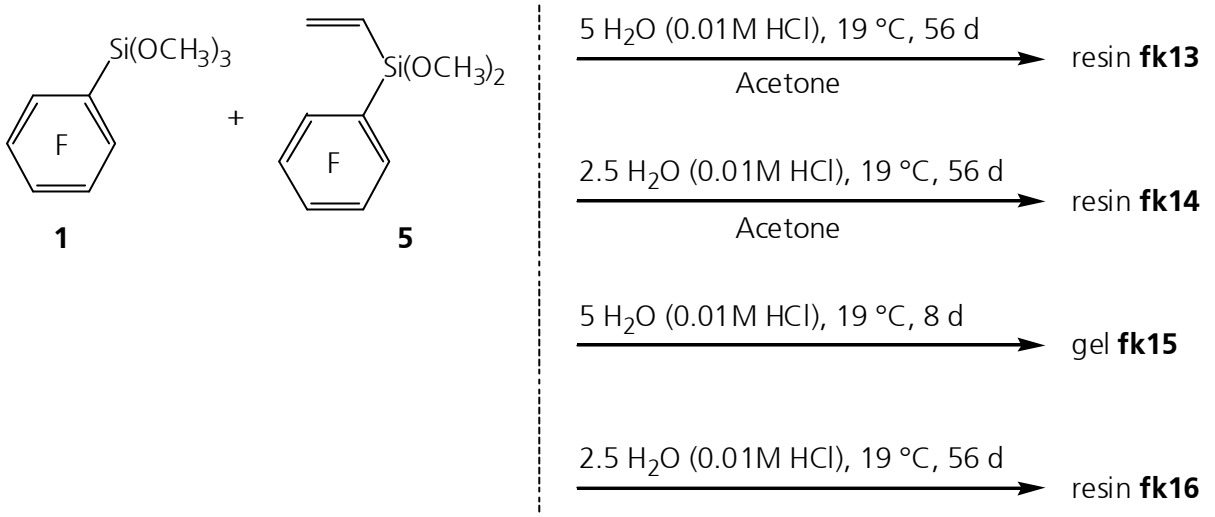

Fig. 64: Preparation of soluble resins by cocondensation of silanes **1** and **5** in acetone and solvent-free.

In order to test the precursor silane composition with regard to photopatternability, the resins **fk13**, **fk14**, and **fk16** were mixed with propyl acetate as diluting solvent and photo initiator Lucirin® LR 8893, which is suitable to initiate polymerization of olefinic systems, and processed with mask aligning equipment in an attempt to fabricate ORMOCER® patterns via photolithography. However, under common clean room processing conditions, the vinyl silane showed poor reactivity. With a photoinitiator concentration of 3 wt.% contained in the lacquers, which is common for lithographic patterning, even UV exposure times of 5 – 15 min were not sufficient to provide organic cross-linking of olefinic organosiloxane oligomers to a suitable degree. Micro-patterns, which had been reported in literature[41] for resins based on the ethoxy analogs of silanes **1** and **5**, could not be fabricated with photolithography. No further attempts were made to force the system to polymerize, e.g. by applying extremely high UV doses or thermal support, because an ORMOCER® system was to be developed, which ought to be processible under common conditions applicable in industrial processing. The tried exposure times of up to 15 min were already exceptionally long compared to usual UV exposure in the 30 s scale. Therefore, the decision was made to introduce a substituent of higher polymerization reactivity into the silane composition.

Recently, similarly poor UV polymerization reactivities of vinyl silanes have been reported for direct UV patterning of ethoxy analogous organopolysiloxane resins based on pentafluorophenyl(vinyl)diethoxysilane and pentafluorophenyltrimethoxysilane[156], thus supporting the present results.

3.4.2 First photopatternable fluoroaryl-functionalized ORMOCER®s

From the preceding series of experiments with mixtures of silanes **1** and **5**, the necessity has been deduced to introduce a functionality into the silane composition, which is much more reactive towards organic polymerization than a vinyl group directly attached to the silicon center. Thus, in order to achieve good photopatternability of fluoroaryl functionalized ORMOCER® resins, the styrene-analogous 4-vinyltetrafluorophenyltrimethoxysilane (**4**) was introduced as a precursor silane. Based on composition **fk16**, the T-type component pentafluorophenyltrimethoxysilane (**1**) was replaced by silane **4**, resulting in the preparation of ORMOCER® resin **fk18** depicted in Fig. 65. Additionally, the polycondensation reaction parameters catalyst concentration (composition **fk19**) and reaction temperature (**fk20**) have been varied in order to find an optimization.

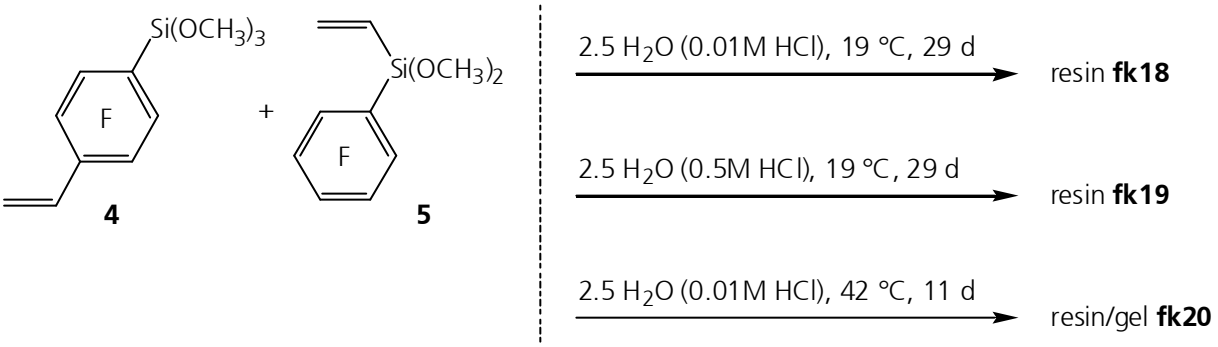

Fig. 65: Preparation of ORMOCER® resins **fk18**, **fk19**, and **fk20**.

The solvent-free polycondensation reaction following pathway **fk18** resulted in a resin exhibiting optical losses of 0.32 dB/cm at 1310 nm and 0.46 dB/cm at 1550 nm, respectively. Due to the long reaction times that were necessary to produce these ORMOCER® resins, attempts were made to speed up the reaction by higher catalyst concentration (**fk19**), and elevated temperature (**fk20**), respectively. Indeed, the reaction times needed for homogenization of the initially two-phase mixtures were much lower (**fk19**: 9 min, **fk20**: 30 min) than for composition **fk18** (55 min), which is an indication for a higher hydrolysis rate. However, after polycondensate **fk19** had been allowed to age for 29 d as in the case of **fk18**, it exhibited identical optical absorption in the telecom wavelengths (0.32 dB/cm at 1310 nm and 0.44 dB/cm at 1550 nm). Thus, the effect of a 50-fold higher hydrochloric acid concentration with respect to the inorganic network formation and thus the optical properties can be considered to be minimal.

An elevated temperature of 42 °C instead of 19 °C, on the other hand, led to the formation of a highly viscous polycondensate after 11 d, which was largely contaminated with gel particles. After removal of these particles, which otherwise would have contributed strongly to

scattering losses, the resulting resin **fk20** still showed absorption of 0.40 dB/cm at 1310 nm and 0.60 dB/cm at 1550 nm. Thus, another indication was found that the production of low-loss fluorinated ORMOCER® resins requires long aging at ambient temperature (cf. chapter 3.3.3).

This result is consistent with literature, where the acid-catalyzed synthesis of completely condensed polyhedral oligosilsesquioxanes $(RSiO_{3/2})_n$ (POSS)[171] from organoalkoxysilanes is reported to require several weeks at ambient conditions [172]. This is due to the fact that with acidic catalysis, hydrolysis of alkoxysilanes takes place at an elevated rate, but condensation is slowed down with rising degree of condensation[2]. The method of accelerating the condensation reaction by changing over to basic catalysis after hydrolysis as performed in several POSS routes[173], is impossible in the case of fluoroaryl alkoxysilanes. Upon contact with non-acidic conditions, the aryl substituent would be lost (cf. chapter 2.5.5). Therefore, the preparation of highly condensed fluoroaryl functionalized ORMOCER® resins with low Si-OH content for application in telecom and datacom requires long reaction periods in the order of weeks.

ORMOCER® resins **fk18**, **fk19**, and **fk20** were tested with respect to their photopatternability under conditions common for photolithographic processing with a mask aligner. After mixing with a diluting solvent (propyl acetate or toluene) and 3 wt.% photoinitiator Lucirin® LR 8893, micro-patterns could be produced by direct UV patterning through a mask. Exposure times of 60 s to 90 s were sufficient to induce enough cross-linking of oligomers to withstand the subsequent development step with a 4-methyl-2-pentanone/isopropanol solvent mixture, which was applied to wash away the unexposed area. Thus, the introduction of 4vinyltetrafluorophenyltrimethoxysilane into the silane composition was found crucial for photopatternability.

The differences in polymerization reactivity between resins of the types **fk16** and **fk18**, respectively, are attributed to the ability of the styrene-analogous 4-vinyltetrafluorophenyl substituent (in **fk18**) to stabilize free radicals, in contrast to the vinyl group directly attached to the silicon (in **fk16**). Such radical intermediates are present during free-radical polymerization of olefins, initiated by homolytic cleavage of a photoinitiator. After the primary initiator radical has attacked the olefinic bond and formed a secondary radical, propagation of the chain polymerization can only occur, if the lifetime of the intermediate radical is sufficient to react with another olefinic system. Otherwise, the chain polymerization is terminated. In siloxane oligomers functionalized with the 4-vinyltetrafluorophenyl substituent, a secondary radical is stabilized by conjugation throughout the arylic π-system, allowing for chain propagation upon collision with the next olefin (Fig. 66). In isolated vinyl systems, no such conjugated π-system can contribute to enhanced radical lifetime.

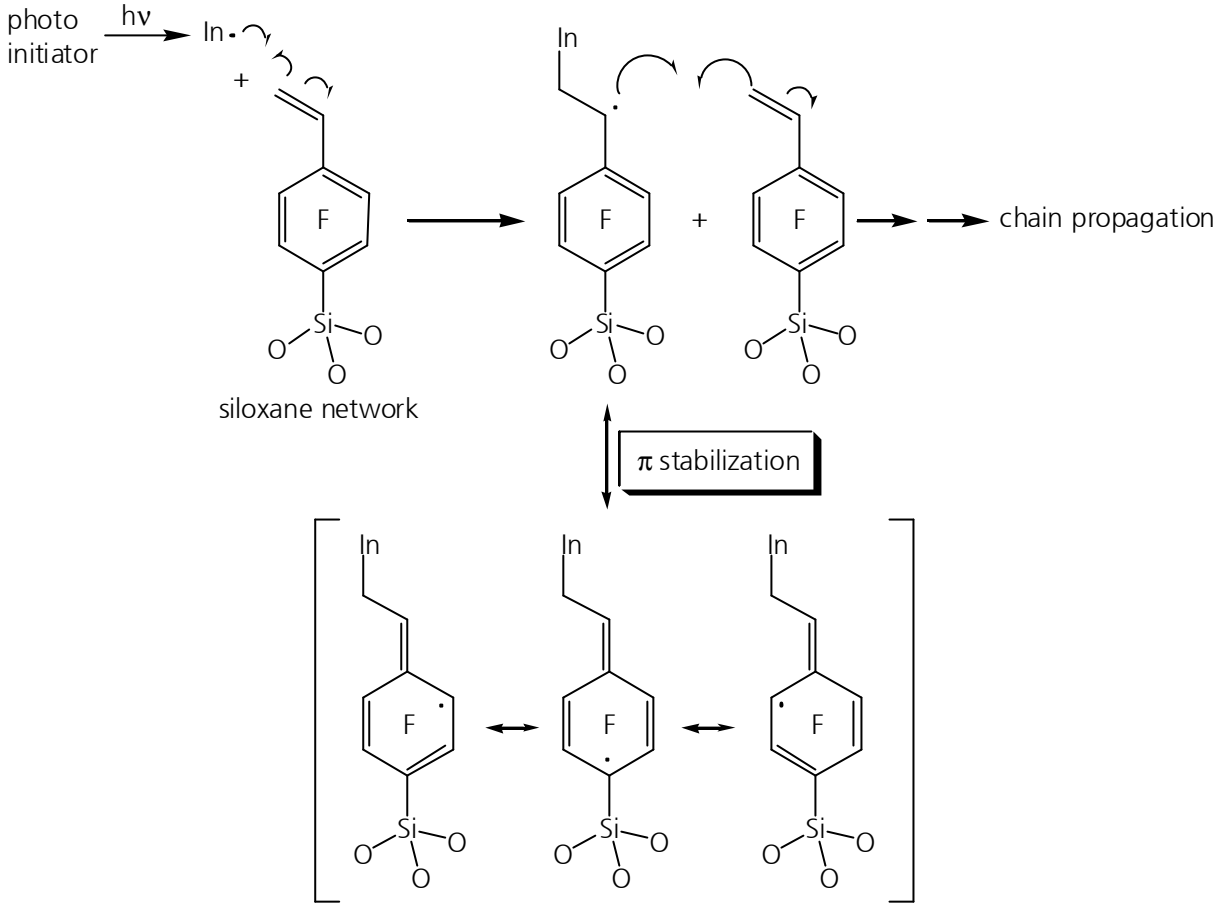

Fig. 66: Conjugation stabilization of intermediate free radicals present during organic cross-linking of organosiloxane oligomers bearing 4-vinyltetrafluorophenyl moieties.

With the cocondensation of silanes **4** and **5**, a photopatternable silane composition has been found with the 4-vinyltetrafluorophenyl substituent as the polymerization reactive compound. However, the identical optical loss values (0.32 dB/cm at 1310 nm and 0.44 dB/cm to 0.46 dB/cm at 1550 nm) of the favored compositions **fk18** and **fk19**, which differ in catalyst concentration, are considerably higher than those for the non-photopatternable resin composition **fk16** (0.10 dB/cm at 1310 nm and 0.18 dB/cm at 1550 nm). This reflects the higher absorptions of 4-vinyltetrafluorophenyltrimethoxysilane (**4**) compared to pentafluorophenyltrimethoxysilane (**1**) (see Tab. 7), which it replaces in order to provide photopatternability.

3.4.3 Synthesis of photopatternable ORMOCER® resins based on advanced formulations

On the one hand, the introduction of 4-vinyltetrafluorophenyltrimethoxysilane (**4**) into the ORMOCER® resin composition makes possible the manufacture of micropatterns by direct UV photolithography, but on the other hand significantly rises NIR absorption due to its additional C-H bonds. Thus, in order to profit from the photopatternability of composition **fk18** as well as

from the better optical transparency of composition **fk16**, these recipes were merged to result in cocondensates from one molar equivalent of silanes **1** and **4** each, plus two molar equivalents of silane **5**. In this way, the D/T ratio of 1:1, which has been proven necessary for the preparation of liquid resins rather than gels, is retained. The reduction of the photoactive compound concentration from 50% to 25% in the resins, however, was expected not to critically impair photopatternability, and thus not to be disadvantageous. In the opposite, because **4** is by far the most expensive among the precursor silanes presented within this work, a reduction also makes the ORMOCER® composition more attractive from the economical point of view. The high costs for silane **4** originate from the multi-step synthesis with only moderate yields (cf. chapter 3.3.1, Fig. 42) as well as from cost-intensive source compounds.

For the preparation of resins, silanes **1**, **4**, and **5** were mixed in the molar ratio of 1:1:2 and cocondensed employing acidic catalysis under various conditions (Fig. 67). The addition of water (in the form of 0.01M hydrochloric acid) in hydrolysis stoichiometry resulted in the viscous resin **fk34** after 10 d. Reaction with condensation stoichiometric water led to the formation of resins **fk35** and **fk37** after 21 d and 35 d, respectively, the former of which employed 50-fold catalyst concentration compared to the latter. Dissolution of the reactants in tetrahydrofuran (THF) before conducting the reaction resulted in the formation of resin **fk36**, which, however, was contaminated with gel particles. In addition to that, the ^{13}C-NMR spectrum of the resin reveals that still a considerable amount of THF was present in the condensate. Apparently, the solvent coordination is so strong, that it cannot be completely removed by vacuum evaporation. These results make the use of THF as solvent unfavorable.

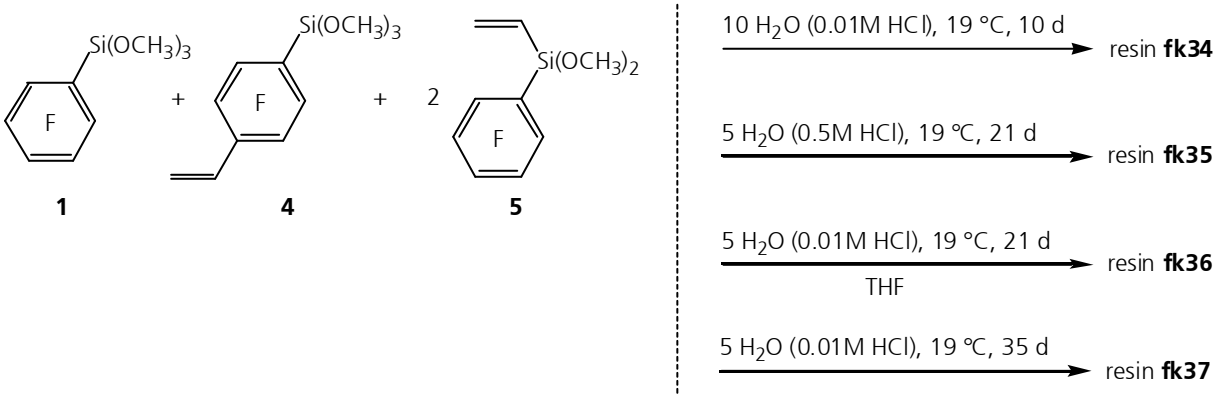

Fig. 67: Preparation of ORMOCER® resins **fk34**, **fk35**, **fk36**, and **fk37** from pentafluorophenyltrimethoxysilane (**1**), 4-vinyltetrafluorophenyltrimethoxysilane (**4**), and pentafluorophenyl(vinyl)dimethoxysilane (**5**).

First photopatternability tests, which were performed on ORMOCER® lacquers prepared from resin **fk34**, revealed good performance despite the reduced 4-vinyltetrafluorophenyl content. Comparable photopatternability can be expected for the analogous systems **fk35**,

fk36, and **fk37**. The detailed characterization of structure and properties of the polycondensates will be outlined in the following chapters.

Upon further reduction of silane **4** in the formulation, information was to be gained about possible effects on photopatternability. Simultaneously, the influence of a T/D ratio shifted to 30:70 on processibility as well as on optical properties was to be determined. Figure 68 depicts the synthesis of ORMOCER® resin **fk38**, based on silanes **1**, **4**, and **5** in a molar ratio of 15:15:70. Water was added in hydrolysis stoichiometry in order to make the results comparable to the **fk34** system.

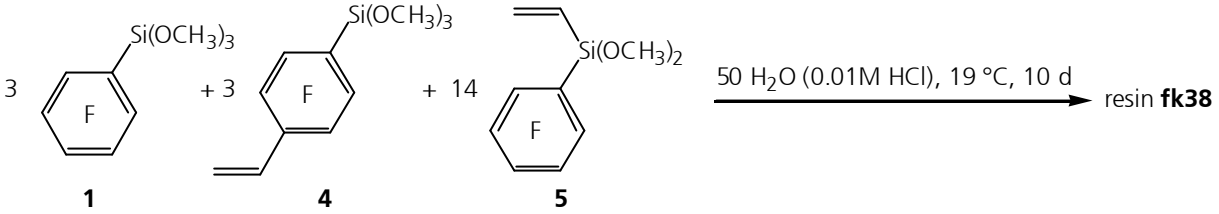

Fig. 68: Preparation of ORMOCER® resin **fk38**.

Even with the content of the 4-vinyltetrafluorophenyl moiety reduced to 15 mol.% with respect to the precursor silane concentration, first UV-patterning experiments with lacquers based on resin **fk38** were very promising.

In order to provide further variation of material properties, the D-type precursor silane **5** was replaced by pentafluorophenyl(methyl)dimethoxysilane (**6**) and cocondensed with **1** and **4**. ORMOCER® resin **fk48** was prepared by adoption of the polycondensation conditions applied in experiment **fk37** (Fig. 69).

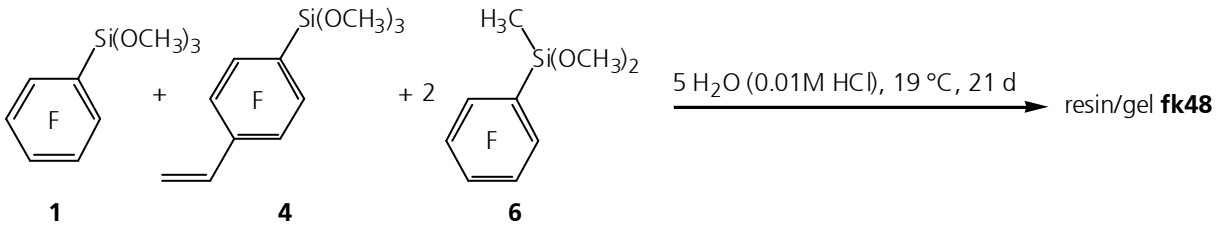

Fig. 69: Cocondensation of silanes **1** and **4** with pentafluorophenyl(methyl)-dimethoxysilane (**6**).

After characterization of the resin had been completed, photopatternability tests had to follow. However, after the resin had been mixed with a diluting solvent and photoinitiator, gelation occurred after 4 d. Thus, composition **fk48** cannot be considered suitable for the preparation of ORMOCER® resins, for which storage-stability is a basic necessity.

In order to be able to assess the influence of fluorination on optical properties, a comparative ORMOCER® resin was prepared from the unfluorinated analogs of silanes **1**, **4**, and

5, respectively. Phenyl(vinyl)dimethoxysilane (**7**) was cocondensed with 4-vinylphenyltrimethoxysilane and phenyltrimethoxysilane in a molar ratio of 2:1:1. Upon application of reaction conditions identical to those used for the preparation of resin **fk37**, the unfluorinated ORMOCER® resin **fk54** was synthesized (Fig. 70).

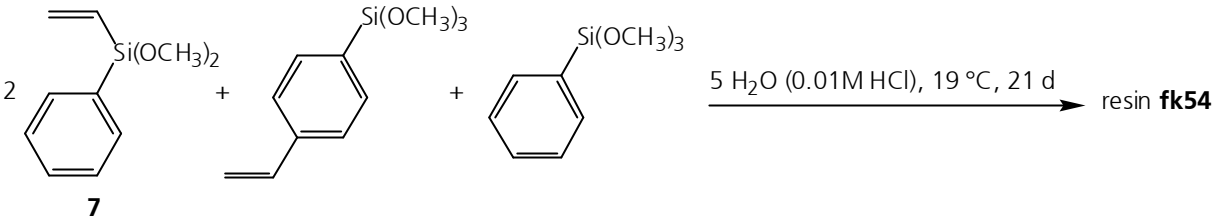

Fig. 70: Synthesis of unfluorinated ORMOCER® resin **fk54** in analogy to system **fk37**.

3.4.4 Characterization of selected ORMOCER® resins

ORMOCER® resins **fk34**, **fk35**, **fk36**, **fk37**, **fk38**, **fk48**, as well as the unfluorinated system **fk54** were thoroughly characterized. In particular, long-run solution ^{29}Si-NMR spectra were recorded in order to gain structural information about the established siloxane networks. Because of partial dearylation in the fluorinated cases, not only silicon centers originating from condensates of the precursor silanes pentafluorophenyltrimethoxysilane (**1**), 4-vinyltetrafluorophenyltrimethoxysilane (**4**), and pentafluorophenyl(vinyl)dimethoxysilane (**5**) were present in the resins but, in addition, also condensates analogous to vinyltrimethoxysilane and tetramethoxysilane. The resulting complex spectra were evaluated by applying the earlier achieved exact assignments of ^{29}Si-NMR resonances for polycondensates from isolated precursor silanes (see chapter 3.3). This is shown exemplarily in Fig. 71 for resin **fk34**. NMR signals in the resin spectrum (Fig. 71a) are assigned with support from single-precursor resin spectra assignments (Figs. 71b-e).

The figure shows the challenge connected with quantitative analysis of these spectra recorded from ORMOCER® resins. Due to the highly condensed states of the systems, signals are broadened, resulting in partial overlap as well as in poor signal-to-noise ratios particularly for low signal intensities. Only with the help of the comparative control spectra shown, the spectra could be analyzed, with utilization of calculations with the *dmfit2001* signal deconvolution program package[174] giving rise to an exact description of structural details within the organopolysiloxane network. Unfortunately, for resins **fk35** and **fk36**, the ^{29}Si-NMR spectra could not be unambiguously interpreted due to poor resolution.

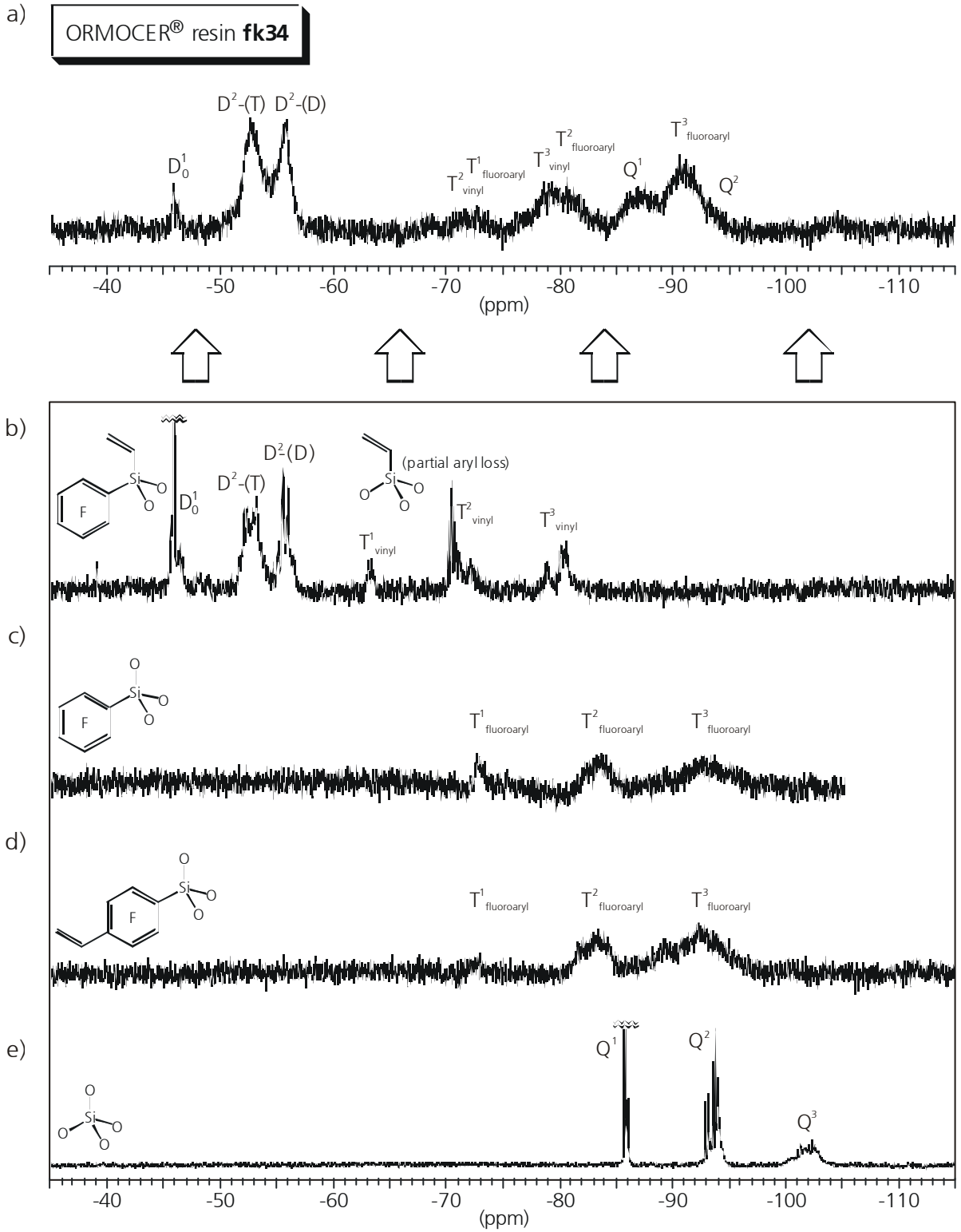

Fig. 71: ^{29}Si-NMR analysis of a) ORMOCER® resin **fk34** aided by assignments b) through e) of spectra recorded from polycondensates of isolated precursor silanes.

Further characterization included the determination of optical absorptions in the telecom wavelength regions 1310 nm and 1550 nm as well as refractive indices. Small angle X-ray scattering (SAXS) measurements provided information about the size of organosiloxane oligomers present in the resin solutions, assuming a spherical structure. This information refers

to the average diameter of the siloxane backbone. Fourier transform infrared (FT-IR) spectroscopy provided information about the Si-OH content. An exact quantitative evaluation of silanol groups, however, was hampered due to the lack of an internal reference vibration. The common method of taking the arylic C=C double bond vibrations around 1645 cm^{-1} as the internal reference, was not applicable because of the partial aryl loss. Table 15 summarizes the results for structural and optical characterization of ORMOCER® resins.

Tab. 15: Characterization of ORMOCER® resins. Gray-shaded: T_{vinyl} and Q silicon species originating from partial fluoroaryl loss of D and $T_{fluoroaryl}$ centers, respectively. **fk54**: unfluorinated.

resin	condensed silicon species [mol.%]									Æ [nm]	[Si-OH]	n_D^{20}	[dB/cm] at λ:	
	D_0^1	D^2-(T)	D^2-(D)	T^2 *vinyl*	T^3 *vinyl*	T^1 *fluoroaryl*	T^2 *fluoroaryl*	T^3 *fluoroaryl*	Q^1	Q^2				1310 nm	1550 nm
fk34	2	23	15	4	10	5	9	24	6	2	2.4	high	1.497	0.28	0.70
fk35												medium	1.496	0.36	0.52
fk36												medium	1.483	0.28	1.26
fk37	6	16	16	-	9	6	17	22	8	-	1.7	low	1.497	0.28	0.42
fk38	3	29	18	3	8	11	12	13	3	-	1.9	high	1.491	0.30	0.84
fk48	5	20	24	-	7	-	9	31	4	-		low	1.488	0.46	0.66
fk54	4	26	19	-	-	-	11	40	-	-	< 1.0	low	1.570	0.44	0.78

3.4.5 Interpretation of structural characterization data

Concerning the inorganic network structure, all given examples exhibit a high degree of condensation, which is documented by high portions of fully condensed D^2 and T^3 species, respectively. Highly condensed systems are preferential for ORMOCER®s intended for use as low-loss optical materials, because a high degree of condensation can account for low silanol content. In addition the significant presence of D^2-type silicon centers connected to T-type species, symbolized by D^2-(T), proves that from the different starting silanes, a cocondensation network was formed, and no separation into different phases based on different precursor silanes occurred. This meets a basic necessity for the subsequent establishment of an isotropic inorganic-organic hybrid network by crosslinking of the inorganic oligomers, which is crucial for low scattering loss passive optical waveguide materials.

However, the considerable concentration of D^2 species connected only to other D-type silicon atoms, depicted as D^2-(D), can only be explained by siloxane chains consisting of D species that are at least three (O-Si-O) units in length. The higher the proportion of D^2-(D)

centers compared to other D-type species, as for example in the case of **fk37**, the longer the chains must be. This result is in accordance with the observations of condensation reactivities of the different silanes (see section 3.3). During the initial phase of the reaction, condensation nuclei are formed primarily from the more reactive T-type silanes pentafluorophenyltrimethoxysilane (**1**) and 4-vinyltetrafluorophenyltrimethoxysilane (**4**), respectively. Only with ongoing reaction time, the less reactive D-silane pentafluorophenyl(vinyl)dimethoxysilane (**5**) is more and more involved in the establishment of the cocondensate network. Nevertheless, this process is believed to give rise to a cocondensate that is well suitable as an intermediate state in the build-up of a homogeneous, isotropic inorganic-organic hybrid network for use as a passive optical waveguide material. This will be discussed in more detail later, on the basis of a computational model of a typical oligomer (section 3.4.8). The model will also help to comprehend the SAXS measurement results by illustrating oligomer diameters of approx. 2 nm by means of a chemical structure drawing.

In all resins except for the unfluorinated system **fk54**, silicon species are detected which emerge from partial aryl loss. These species are marked in Tab. 15 by gray-shading of the respective columns. Upon aryl release from a D-type silicon center based on pentafluorophenyl(vinyl)dimethoxysilane (**5**), new T-type vinylsilane centers evolve, which are named T^2_{vinyl} and T^3_{vinyl}, respectively, in order to distinguish them from the original T-centers. Carbon-silicon bond cleavage in $T_{fluoroaryl}$-type silanes **1** and **4**, respectively, generates Q-type orthosilicate centers, which is in accordance to earlier considerations[161,162]. Within the earlier work, it has been proposed that upon nucleophilic attack on the silicon center during non-acidic hydrolysis/polycondensation of fluoroarylalkoxysilanes, the fluorinated aryl group is a better leaving group than the intended alkoxy substituents, resulting in dearylation (Fig. 72). Only under acidic conditions, the alkoxy functionalities are protonated, and thus generate the excellent leaving group, alcohol, which is released instead of the aryl.

Partial aryl loss during condensation and aging of the fluorinated ORMOCER® resins outlined in Tab. 15, however, occurs despite acidic catalysis. From the investigations on the polycondensation of pentafluorophenyl(vinyl)dimethoxysilane (**5**) (chapter 3.3.3), it could be seen that aryl loss did not happen during the initial reaction phase, but after the inorganic network had already been established to a considerable extent. Therefore, it can be deduced that aryl loss during aging of a fluoroaryl-functionalized polysiloxane occurs because of the high degree of immobilization within the system, leading to a hindered transport of protons towards the site of nucleophilic attack. Phase separation, i.e. segregation of polysiloxane and solvent methanol, strongly enhances this immobilization. Therefore, despite acidic conditions, partial aryl loss occurs in already highly condensed siloxanes.

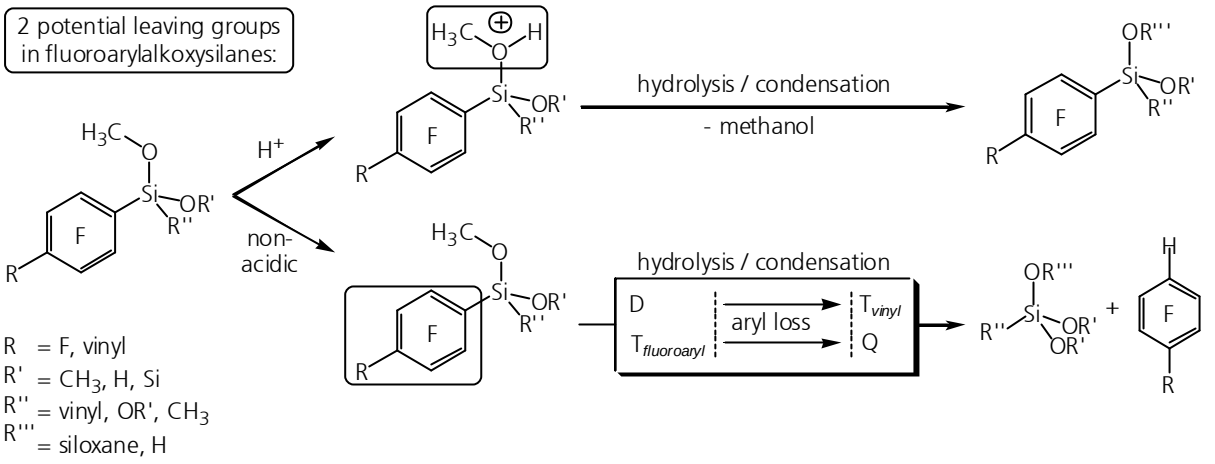

Fig. 72: Generation of methanol as leaving group under acidic hydrolysis/polycondensation conditions, as opposed to Si-$C_{fluoroaryl}$ bond cleavage (fluoroaryl loss) under non-acidic conditions.

In order to quantify aryl loss, the gray-shaded (Tab. 15) signal intensities of Q-species, generated by dearylation of fluoroaryl-functionalized $T_{fluoroaryl}$-type species, and of T_{vinyl} centers, emerged from dearylation of pentafluorophenyl(vinyl) functionalized D-type species, are added up. Thus, overall aryl losses during preparation of the presented ORMOCER® resins are in the range of 11% to 22% (22% for resin **fk34**, 17% for **fk37**, 14% for **fk38**, and 11% in resin **fk48**).

Beside aryl loss in fluorinated polycondensates, Tab. 15 shades light on further differences in polycondensation behavior of analogous fluorinated and unfluorinated ORMOCER® systems. Comparison of resin **fk37** (fluorinated, cf. Fig. 67) with **fk54** (unfluorinated, cf. Fig. 70) reveals, that the unfluorinated system exhibits a higher degree of condensation. This is illustrated by Tab. 16, which simplifies the more detailed structural characterization given above (Tab. 15) in a way that singly (≡Si-(OSi)), two-fold (=Si$(OSi)_2$), and three-fold (-Si$(OSi)_3$) condensed species are considered regardless of their origin (D-, T-, or Q-type).

Clearly, the higher proportion of three-fold condensed silicon centers as well as the significantly lower content of singly condensed end-groups in the unfluorinated resin **fk54**, compared to the fluorinated analog **fk37**, attest to a higher degree of condensation and therefore to a higher density of the polysiloxane network in the unfluorinated case. This result can be explained following a similar reasoning as presented already for the effect of fluorination on refractive indices of precursor alkoxy silanes (see chapter 3.2.1). The fluoroaryl moieties bound to the siloxane backbone are expected to interact strongly repulsive to each other, because the high partial negative charge located on the rim of the fluorinated aryl rings account for high Coulomb repulsion. Similar to the effect on refractive index, which is lowered due to a lower density of polarizable groups per volume unit, such a repulsion in oligosiloxane reaction intermediates leads to a lower degree of condensation, in a way that the higher steric volume of

the fluorinated compared to the unfluorinated aryl functionalities decrease the probability of a silanol–alkoxysilane collision with formation of a siloxane bond.

Tab. 16: Degree of condensation in analogous fluorinated (**fk34** and **fk37**), and unfluorinated (**fk54**) ORMOCER® resins: distribution of singly, two-fold, and three-fold condensed silicon species.

ORMOCER® resin	**condensed silicon species [mol.%]**		
	one-fold: ° **Si-(OSi)**	two-fold: **=Si(OSi)$_2$**	three-fold: **-Si(OSi)$_3$**
fk34 (high OH)	13	53	34
fk37 (low OH)	20	49	31
fk54 (unfluorinated, low OH)	4	56	40

ORMOCER® resin **fk34**, which originates from the same precursor silane mixture as system **fk37**, but has a high silanol (OH) content due to different polycondensation conditions, exhibits a slightly higher degree of condensation than **fk37** (Tab. 16). Considering that the reaction time in the **fk34** case was only 10 d compared to 35 d for **fk37** (cf. Fig. 67), this is evidence for a much higher condensation reaction rate for oxolation, i.e. condensation of two silanol groups upon release of water, than for alcoxolation, i.e. condensation of silanol and alkoxy upon release of alcohol.

Different silanol contents, which can only be quantified in terms of high, medium, and low Si-OH content, as mentioned above (chapter 3.4.4), originate from polycondensation reaction conditions. Because none of the systems discussed exhibits complete condensation, i.e. consists only of D^2 and T^3-type silicon centers, the result becomes straightforward, that those resins, which were prepared upon hydrolysis stoichiometric addition of water (**fk34**, **fk38**), show strong signals for hydroxyl groups in the IR spectra. Systems **fk37**, **fk48**, and **fk54**, which were prepared with condensation stoichiometric water addition, show low Si-OH contents, as expected. The remaining possible condensation sites on the silicon centers must be considered to be methoxy groups.

However, resins **fk35** and **fk36**, both reacted under condensation stoichiometry, exhibit silanol signals, which are of intermediate intensity, i.e. higher than in ORMOCER® resin **fk37**. In the **fk35** case, the polycondensation reaction was carried out with a 50-fold higher catalyst concentration, **fk36**, on the other hand, was prepared in tetrahydrofuran (THF) as solvent. Both reactions were stopped after 21 d (**fk37**: 35 d). This underlines again the necessity for long reaction periods in the production of low-loss ORMOCER® resins from fluoroarylalkoxysilanes.

3.4.6 Refractive indices of ORMOCER® resins

Regarding the influence of structural features on optical properties, Tab. 15 (chapter 3.4.4) gives a comparison of refractive indices determined from the different ORMOCER® resins. With a value of 1.570, the unfluorinated system **fk54** exhibits a refractive index significantly higher than for all fluorinated resins, e.g. 1.497 in the analogous **fk37** case. This reflects the results found for fluorinated and unfluorinated precursor silanes listed above (see chapter 3.2.1), and has to be equally interpreted with respect to impacts of fluorination on the electronic mode of polarization.

As already indicated, the Coulomb-repulsive effects of the fluorinated aryl moieties account for a lower network density within ORMOCER® resins, resulting in lower refraction. A higher density, as in the unfluorinated case, accounts for a higher amount of species per volume unit, which interact with light and therefore enhance refraction. In addition to that, also the partial aryl loss in the fluorinated systems accounts for a high index difference compared to the unfluorinated resin. Partial aryl loss in the fluorinated systems decreases the content of organic functions and shifts the material's properties more into the direction of low-index amorphous silica. For comparison, the control polycondensation reactions of tetramethoxysilane and vinyltrimethoxysilane, respectively, which were primarily conducted in order to identify ^{29}Si-NMR shifts of reaction intermediates (chapter 3.3.7), resulted in condensates exhibiting indices of n^D_{20} = 1.401 (orthosilicate) and n^D_{20} = 1.446 (vinylsiloxane), respectively.

Regarding the refractive indices of ORMOCER® resins **fk34**, **fk35**, and **fk37**, based on the same 1:1:2 mixture of fluorinated precursor silanes **1**, **4** and **5**, but prepared under different polycondensation reaction conditions, all exhibited the same n^D_{20} value of 1.496 to 1.497. The refraction of the high-vinyl system **fk38**, generated from a 15:15:70 mixture of silanes **1**, **4** and **5**, was with an n^D_{20} value of 1.491 slightly lower. The index difference of 0.005 to 0.006 compared to the aforementioned resins makes the material interesting as an associated *cladding* for the build-up of single-mode waveguides.

The methyl-substituted resin **fk48**, generated from silanes **1**, **4**, and pentafluorophenyl(methyl)dimethoxysilane (**6**) in a 1:1:2 ratio, has a refractive index of 1.488, which in comparison with resin **fk37** (n^D_{20} = 1.497) reflects the lower index of precursor silane **6** (n^D_{20} = 1.426) compared to silane **5** (n^D_{20} = 1.436). From the index difference point of view ($\Delta n_{\mathbf{fk37\text{-}fk48}}$ = 0.009), system **fk48** would also be a candidate as *cladding* material, but this is opposed by its poor storage stability (cf. chapter 3.4.3).

The refractive index of 1.483 measured for resin **fk36** is very low compared to the analogous resin **fk37**. This can be attributed to the coordination of residual solvent THF (n^D_{20} = 1.407[175]), which cannot be completely removed and thus significantly lowers refraction (cf. chapter 3.4.3). THF coordination also accounts for high absorption in the near-infrared. This underlines the

aforementioned argumentation, that the use of THF as solvent for the polycondensation reaction is disadvantageous.

In conclusion, it can be assumed that the major parameter for the manipulation of refractive indices of fluorinated ORMOCER® resins is the variation of the initial silane mixture. Refractive index differences of the precursor silanes, which are due to different organic functionalization, are reflected on the refraction of the resulting polycondensates. Variation of reaction parameters such as stoichiometry of water addition and catalyst concentration did not result in significant index differences for the resulting resins and was by far exceeded by the organic functionalization effects.

3.4.7 NIR absorption of photopatternable ORMOCER® resins

Besides the photopatternability, optical transparency in the telecommunication wavelength regions around 1310 nm and 1550 nm plays a central role in the development of ORMOCER® materials for telecom and datacom applications. Although the absorption of materials is primarily relevant for their cured, solid states, near-infrared (NIR) spectra of the intermediate resins allow a valuable insight into structure-property relations, which are expected to be reflected also on the solid state. Liquid-state measurements gain all the more importance in terms of easy availability of spectral data. Whereas resins can be easily analyzed by using a standard UV-VIS-NIR spectrometer setup with cuvettes, optical characterization of ORMOCER® films or embedded waveguides first requires the preparation of solid samples, which are suitable for absorption measurements followed by e.g. a cut-back analysis of the sample. For ORMOCER® **fk37**, the results are presented exemplarily in a later paragraph within this work (chapter 3.5.6). In case of ORMOCER® resins, however, NIR spectral investigations allow for easy comparability of systems with various structural characteristics.

Figure 73 depicts the NIR spectra of fluoroaryl-functionalized ORMOCER® resins **fk34**, **fk37**, and **fk38** as well as of the unfluorinated resin **fk54** in the range from 1080 nm to 1630 nm. Loss values at 1310 nm and 1550 nm, respectively, are explicitly given in Tab. 15 above. A reference spectrum of the unfluorinated low Si-OH ORMOCER® resin **b59d** (also known as ORMOCER® I and ORMOCORE, cf. chapter 2.5.4, Fig. 40), which had been developed at Fraunhofer ISC for optical applications, is added to the diagram. Within the shown spectral range, three main absorption regions can be recognized, one around 1100 – 1230 nm, the second one around 1350 – 1480 nm, and the final region above 1600 nm. From literature (see section 2.2.1, Tabs. 2-4), it is known that absorptions around 1140 – 1190 nm are due to second overtone C-H vibrations, and signals in the area above 1630 nm are due to C-H first overtones. C-H combination vibrations in the vicinity of siloxane have been found in the 1380 – 1420 nm range, in the vicinity of first overtone O-H vibrations, which are situated near

1438 nm. Based on these literature values and in combination with direct comparison of analogous systems, the NIR spectra of ORMOCER® resins will be discussed in the following.

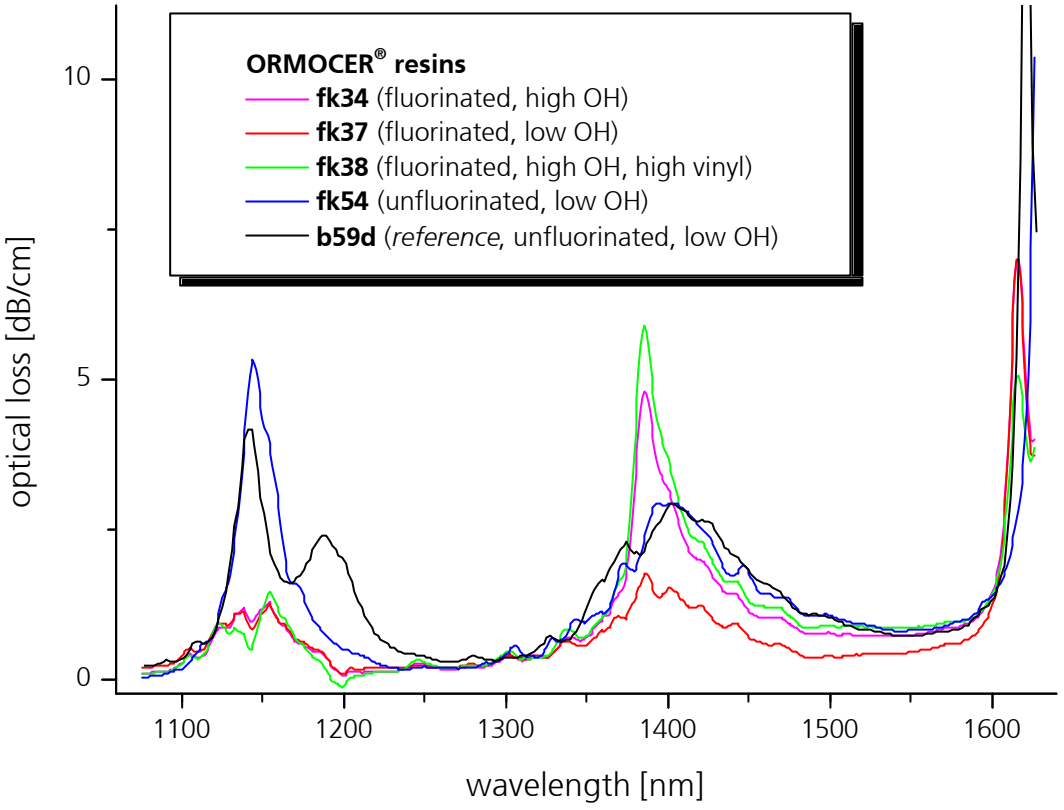

Fig. 73: NIR spectra of fluorinated ORMOCER® resins **fk34**, **fk37**, and **fk38** as well as of the unfluorinated analog **fk54** and the reference system **b59d** in the telecom wavelength regions around 1310 nm and 1550 nm.

Upon comparison of the spectra of resins **fk34** (Fig. 73, violet chart) and **fk37** (red chart), which primarily differ from each other in terms of high (**fk34**) and low (**fk37**) silanol content, the impact of Si-OH bonds on optical loss can directly be derived. Following the two curves along the wavelength scale, no difference in absorption can be noticed up to approximately 1340 nm. Loss values at 1310 nm are equally 0.28 dB/cm. Between 1340 nm and approx. 1480 nm, however, **fk34** shows high absorption with a signal maximum at 1387 nm, whereas **fk37** has significantly lower loss at the same wavelength. Thus, the observed absorption maxima can be assigned to first overtone (Si-)O-H vibrations in fluoroaryl-functionalized polysiloxanes. Whereas absorption of the low silanol resin **fk37** decreases with further increase of wavelength and reaches a value of 0.42 dB/cm at 1550 nm, the 1550 nm window is continuously affected by the **fk34** O-H absorption (loss: 0.70 dB/cm at 1550 nm). In accordance with literature[57], this is attributed to first overtone O-H vibrations of silanol groups, which take part in numerous

hydrogen bonds, whereas the silanol vibration at 1387 nm is due to free O-H. Above approx. 1580 nm, both spectra exhibit steep increases in absorption due to C-H first order overtone vibrations. First signal maxima of equal intensity are located at 1617 nm, which, with the help of precursor silane spectra, can be assigned to first order C-H overtones of the vinyl groups being part of 4-vinyltetrafluorophenyl substituents.

The absorption spectrum of the high vinyl containing system **fk38** (Fig. 73, green chart) essentially follows the characteristics of **fk34**. Only the absorption due to O-H is higher, with a maximum at 1386 nm. On the other hand, the absorption at 1617 nm is significantly lower than in the **fk34** and **fk37** cases, thus supporting the above mentioned assignment, as the initial silane composition for **fk38** included considerably less 4-vinyltetrafluorophenyltrimethoxysilane (**4**). The vinyl groups, which are directly connected to the silicon atoms, on the other hand, show first order C-H overtone vibration at 1643 nm, which is also in accordance with precursor silane spectra.

Thus, for the discussed materials, NIR absorption of 4-vinyltetrafluorophenyl moieties can be seen to close the 1550 nm telecom window towards higher wavelengths. Therefore, avoidance of this functionality might be worth considering, if in future times the necessity arises for an extension of the window into the 1600 nm region.

In order to examine the effect of fluorination, the spectra of resin **fk37** and its unfluorinated analog **fk54** (Fig. 73, blue chart) have to be compared. Particularly within the first absorption region around 1120 – 1220 nm, the unfluorinated resin shows by far higher absorption than the fluorinated system, with a signal maximum at 1145 nm. In accordance with literature[58], the absorption was assigned to the second overtone vibrations of aromatic C-H bonds. Therefore, fluorination unambiguously extends the 1310 nm window towards lower wavelengths. This also results in a **fk54** absorption at 1310 nm itself, which is higher (0.44 dB/cm) than that of the fluorinated system (0.28 dB/cm). Additionally, the curves show that also for attenuation in the 1350 – 1480 nm region, fluorination improves the transparency. Because for the two resins, similarly low silanol contents can be assumed, but **fk54** exhibits considerably higher absorption in this wavelength region, which has to be attributed to C-H vibrations. This corresponds to literature, where absorptions in the 1330 – 1436 nm region have been assigned to combination bands of C-H vibrations[176]. This effect is also reflected on the absorption loss of resin **fk54** at 1550 nm, which is with a value of 0.78 dB/cm significantly higher than for the fluorinated system **fk37** (0.42 dB/cm).

Finally, the NIR spectrum of reference ORMOCER® system **b59d**, which is a low-Si-OH cocondensate of diphenylsilanediol with 3-methacryloxypropyltrimethoxysilane (MEMO) (cf. chapter 2.5.4, Fig. 40), is shown for comparison (Fig. 73, black chart). The most striking difference to the spectra discussed before is a broad signal strongly affecting the 1310 nm

window. The absorption ranges from approx. 1160 nm to 1250 nm with a maximum at 1188 nm and can be assigned to second overtone vibrations of aliphatic C-H bonds, primarily due to the MEMO propylene groups as well as the remaining methoxy groups in the polycondensate. The absorption band corresponds with the net MEMO spectrum and the assignment is in consistency with literature values[57,58]. Absorption due to second order overtones of aromatic C-H within **b59d**, with a maximum at 1142 nm, is of slightly lower intensity than for resin **fk54**, due to the higher content of aromatic compounds in the latter. For the remaining wavelength regions, the NIR spectra of the two unfluorinated resins are very similar. ORMOCER® **b59d** has been designed primarily as a low-silanol material, whereas in **fk54** the content particularly of aliphatic C-H groups is lower. Thus, similar absorptions around 1400 nm are evidence of both, silanol and C-H contribution to optical loss in that wavelength region. Nevertheless, the central absorption values for resin **b59d** are 0.36 dB/cm at 1310 nm and 0.70 dB/cm at 1550 nm, respectively, which are slightly lower than for **fk54** (0.44 dB/cm at 1310 nm, and 0.78 dB/cm at 1550 nm).

Among the discussed photopatternable ORMOCER® compositions, resin **fk37** shows the overall lowest absorption among the photopatternable polycondensates, and exhibits the lowest loss values (0.28 dB/cm at 1310, and 0.42 dB/cm at 1550 nm) as well as the widest absorption windows at 1310 nm and 1550 nm (Fig. 73). This makes the resin a most promising candidate as a low-loss hybrid inorganic-organic material for telecom and datacom applications.

However, the lowest absorption losses measured on an ORMOCER® discussed within this work, were found in the non-photopatternable resin **fk16**, which was prepared from a 1:1 mixture of pentafluorophenyltrimethoxysilane (**1**) and pentafluorophenyl(vinyl)dimethoxy-silane (**5**) under similar polycondensation conditions as in the **fk37** case (chapter 3.4.1, Fig. 64). The resin absorption values of 0.10 dB/cm at 1310 nm, and 0.18 dB/cm at 1550 nm, respectively, are outstanding, but the vinyl group alone does not provide direct UV patternability. Nevertheless, the material might be very interesting as optical material for applications that do not require photopatternability. In comparison with resin **fk37**, it becomes clear that photopatternability is accompanied with higher absorption, due to the need for the 4-vinyltetrafluorophenyl groups for UV polymerization.

The impact of structural characteristics on the optical loss in the presented fluorinated and unfluorinated as well as high- and low-silanol containing ORMOCER® resins can be summarized as follows. Particularly the telecommunication window around 1310 nm is affected by C-H, where aliphatic moieties exert more influence than aromatic groups, insofar as aromatic C-H absorb at a lower wavelength (1145 nm compared to 1188 nm) and thus widen the window. Because aliphatic NIR absorption is also to be attributed to alkoxy groups, a low alkoxy content in the final material is desired. This can be achieved by a high degree of condensation, which

consumes the alkoxy groups and does not leave any silanol. The 1550 nm window is equally affected by O-H first overtone vibrations and C-H combination vibrations. Silanol groups account for a signal maximum at 1387 nm, along with further absorptions at higher wavelengths up to 1480 nm, which are due to O-H groups that are involved in hydrogen bonding. Combination vibrations of carbon-hydrogen bonds occur at similar wavelengths, so that the absorption region is likewise influenced by O-H and C-H.

3.4.8 Molecular modeling of a fluorinated organosiloxane oligomer

Based on the spectroscopic results outlined in Tab. 15, the molecular structure of a fluoroaryl functionalized siloxane oligomer has been visualized by computational molecular modeling. The polycondensate of choice was ORMOCER® resin **fk37**, exhibiting best performance as low-loss, photopatternable composition. Accelrys' *Materials Studio* program package[177], incorporating the COMPASS forcefield, was utilized as the actual simulation tool, as it has been reported to perform well in modeling polysiloxanes as well as aromatic and aliphatic hydrocarbons in condensed phase[178]. COMPASS (Condensed-phase Optimized Molecular Potentials for Atomistic Simulation Studies) is an *ab initio* forcefield, in which parameterization was achieved mostly on *ab initio* data, and has been designed specifically for atomistic simulations of materials in the condensed phase.

However, before an actual force field calculation could be performed, an initial geometric model had to be assumed, corresponding with the structural characterization data. Crucial information was given by ^{29}Si-NMR, which provided percentages of the various silicon species within the condensate as well as SAXS measurements, resulting in an average size of the oligomer. The step-wise modeling proceeded as follows.

(1) Taking into account earlier modeling studies on fluoroaryl-modified polysiloxanes[161,162], a respective oligomer with a silicate backbone of 1.7 nm in diameter, as determined for resin **fk37**, was expected to incorporate approximately 24 silicon centers. Thus, in order to maintain a 1:1:2 ratio of silicon species based on the precursor T- and D-type silanes **1**, **4**, and **5**, the oligomer composition outlined in Tab. 15 was converted to a 24 silicon atom model comprising 6 species each originating from pentafluorophenyltrimethoxysilane (**1**) and 4-vinyltetrafluorophenyltrimethoxysilane (**4**), plus 12 silicon centers descending from pentafluorophenyl(vinyl)dimethoxysilane (**5**) (Tab. 17).

(2) The next step was to find a skeletal siloxane structure, which represents the overall ratio of 7:5 with respect to three-fold to singly condensed species ($[2 \times T^3_{vinyl} + 5 \times T^3_{fluoroaryl}] / [2 \times D^1_0 + 1 \times T^1_{fluoroaryl} + 2 \times Q^1]$, cf. Tab. 16). This was feasible upon the assumption, that two cyclic structural features are present in the oligomer. By maintaining a

high degree of symmetry, the model skeleton, which is sketched in Fig. 74, was kept as simple as possible.

Tab. 17: Conversion of **fk37** spectroscopic data into a 24 silicon atom structural model.

	condensed silicon species in ORMOCER® resin fk37							
	D^1_0	D^2-(T)	D^2-(D)	T^3_{vinyl}	$T^1_{fluoroaryl}$	$T^2_{fluoroaryl}$	$T^3_{fluoroaryl}$	Q^1
[mol.%]	6	16	16	9	6	17	22	8
S = 24 Si	2	4	4	2	1	4	5	2

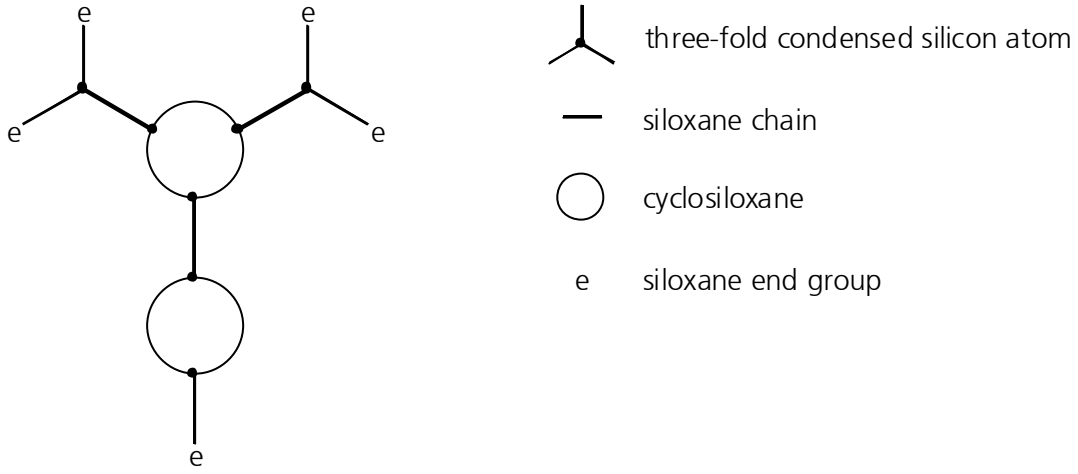

Fig. 74: Schematic representation of a model siloxane skeletal structure containing 7 three-fold condensed silicon species and 5 end groups.

(3) During discussion of the structural characterization of ORMOCER® resins (chapter 3.4.5), it has already been mentioned that a considerable amount of D^2-(D) species, i.e. two-fold condensed D-type silicon centers, which are only connected to other D-type species, can only be explained by siloxane chains consisting of at least three D-type O-Si-O units. For the setup of a structural model, this result was implemented in such a way that two peripheral chains (T)-D^2-D^2-D^2-D^1_0 consisting of four D-type species each were hypothesized. Thus, out of the 24 silicon atoms outlined in Tab. 17, not only the four D^2-(D) centers, but also the two D^1_0 end groups, and two of the D^2-(T) species, i.e. the bridges between the all-D-type chains and T-type connecting units, could be integrated into the model. The two D-chains were each attached to one of the two "Y"-shaped linear fragments sketched in Fig. 74, which are connected to the central cyclosiloxane feature. The peripheral attachment of D-type silicon species to a nucleus formed from T-type silanes is in accordance with the lower reactivity of the respective D-type precursor silanes compared to T systems.

(4) The remaining two-fold condensed siloxane centers as well as T^1-type and Q^1-type end-groups from Tab. 17 were randomly distributed within the limits of the siloxane skeleton sketch introduced above (Fig. 75). Finally, the model was completed by attachment of vinyl, pentafluorophenyl and 4-vinyltetrafluorophenyl groups to T-centers at random, resulting in the graphical model outlined in Fig. 75. For ease of depiction, the differently substituted siloxane centers were symbolized as shown in the picture, and simple lines between the symbols stand for siloxane (Si-O-Si) bonds. Residual, i.e. incompletely condensed (Si-O)-R sites are assumed to be filled up with methoxy groups.

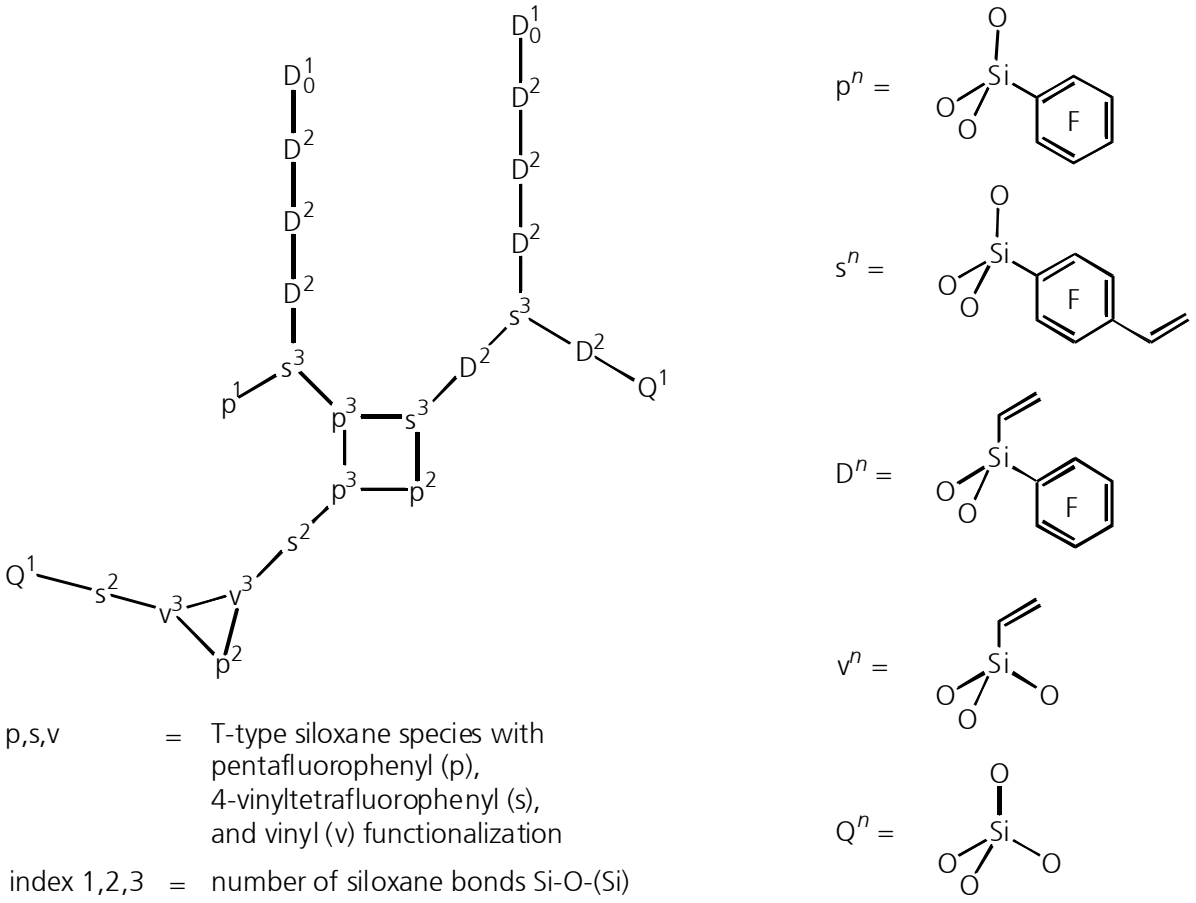

Fig. 75: Assembly of siloxane species based on the siloxane skeleton sketched in Fig. 74, according to ^{29}Si-NMR and SAXS characterization of ORMOCER® resin **fk37** (cf. Tabs. 15 & 16).

(5) So far, none of the presented modeling work involved actual computing, but was a logical assembly of structural features, which had been identified by means of ^{29}Si-NMR spectroscopy and SAXS oligomer size measurements on ORMOCER® resin **fk37**. In addition to the information originating from experimental characterization, a basic principle underlying this "paper model" of an average oligomer was symmetry and simplicity. The final step in creating a comprehensible image of a typical **fk37** oligomer molecular structure was the transformation of

the paper model into a three-dimensional display via a force field calculation. For this, the *Materials Studio* program was provided with a graphical input representing the model depicted in Fig. 75. In doing so, the structural model was intentionally fit out with several bends and twists, in order to deviate from an oversimplified image and to approximate the reality of an oligomer in condensed phase. The execution of a COMPASS force field geometry optimization calculation resulted in a structural model, which is visualized in the following by various means of presentation, all representing the same model, viewed from the same position, but being capable of clarifying different aspects of structural characteristics.

Figure 76 displays a stick model of the oligomer, which points up the basic structural conformation by reducing the image to the depiction of only the molecular bonds, i.e. atoms are located at the cross-over points of these bonds. The siloxane backbone is exposed in terms of bright colors, silicon atoms in violet, and oxygen in red. The organic moieties are easily identified with carbon atoms drawn in dark gray, fluorine in turquoise, and hydrogen atoms in white. C=C double bonds are recognizable by double lines between two carbon atoms, and aromatic systems are depicted as dotted inserts in the arylic six-membered carbon rings. The stick representation particularly shows the disordered arrangement of organic substituents within the oligomer. This accounts for isotropic behavior, which is favorable for passive optical waveguide materials. The two four-membered chains consisting of D-type siloxane species, which extend to the left and down right of the image, respectively, exhibit the above mentioned slight twisting, and possess no further short-range order, thus contributing to the isotropy of the material.

It is known from the literature[157] that cyclic organosiloxane trimers and tetramers exhibit very sharp and defined resonances in ^{29}Si-NMR spectra. As proposed, also the **fk37** model oligomer contains two cyclic features. The ^{29}Si-NMR spectra of the fluoroaryl-modified ORMOCER® resins presented within this work, however, only consist of broader, Gaussian-shaped signals, which seem to conflict with the model. However, from the image it is evident that the two proposed cyclic siloxane features, a cyclotetrasiloxane ring in the center of the model and a cyclotrisiloxane in the top right of the picture, suffer significantly from distortion due to unequal organic substitution on the individual silicon centers. Taking into account that the depicted model represents only one out of a vast variety of substitution patterns within the resin, all leading to differently distorted cycles, this results in broad ^{29}Si-NMR signals as seen in the experiment. Therefore, the stick representation of the model oligomer gives evidence that proposed siloxane ring structures and the lack of sharp ^{29}Si-NMR signals are not necessarily contradictory.

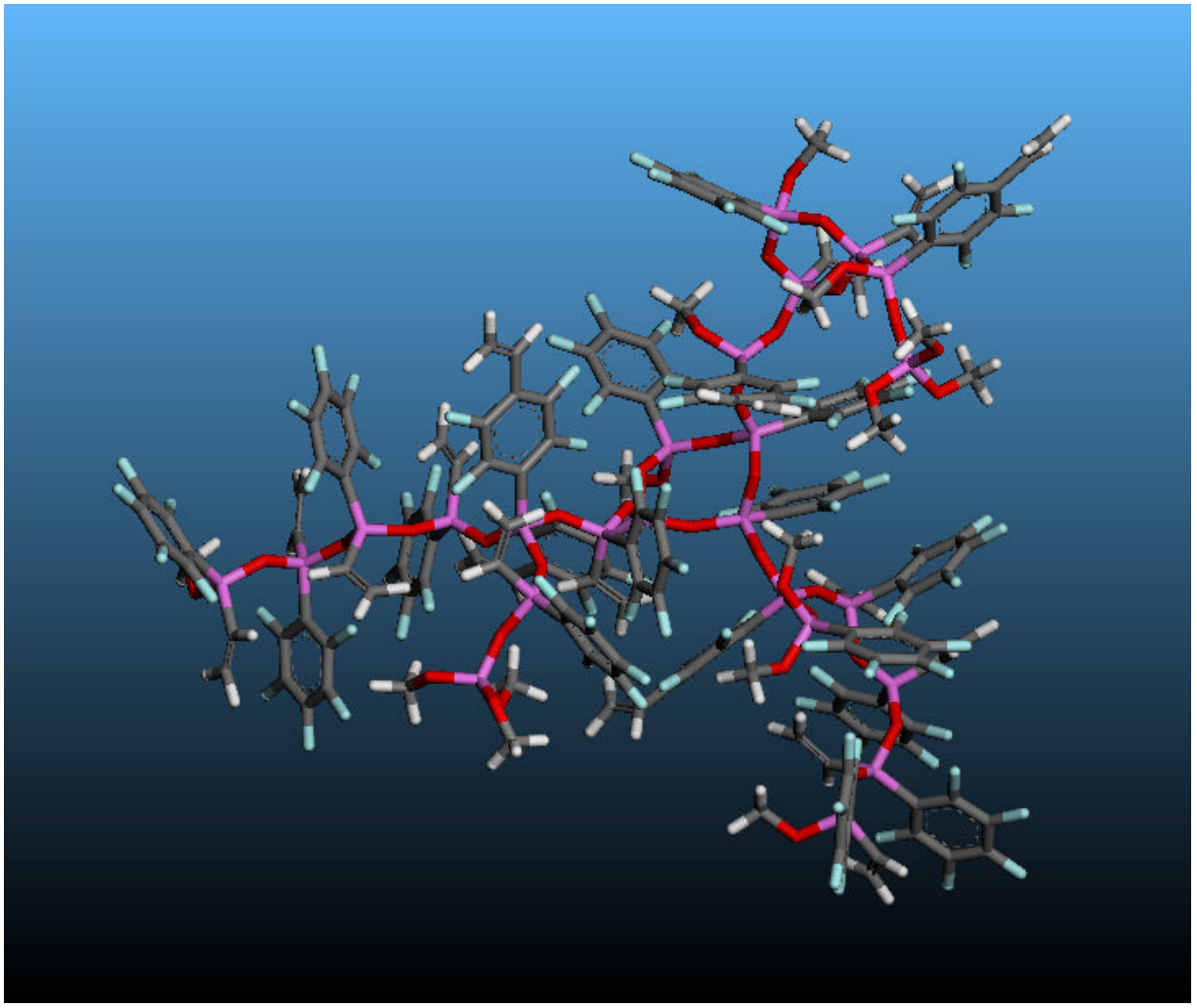

Fig. 76: Stick representation of the model oligomer generated by COMPASS forcefield geometry optimization of a paper model generated from structural characterization of ORMOCER® resin **fk37** as sketched in Fig. 75.

By displaying the $R_nSi(OR')_{4-n}$ centers as tetrahedra, while the organic moieties are outlined in the form of dots depicting atoms, special attention is drawn to the inorganic siloxane backbone (Fig. 77). The figure makes clear the primarily linear nature of the siloxane skeleton, with a cyclic center and pendant linear features. Distances between exterior silicon atoms are between 12 and 24 Ångstroms, and thus fit into SAXS experimental results. The observed star-like geometry results chiefly from a two-dimensional build-up of the siloxane network, i.e. condensation primarily occurs by addition of monomers to reactive sites in the periphery of the oligomer, rather than intramolecularly. On the one hand, this result is due to the high content (50 mol.%) of D-type silicon species within the system, allowing only for linear growth. On the other hand, application of acidic catalysis for the polycondensation reaction is known to activate mainly silicon centers in low condensation states[2]. Thus, peripheral alkoxysilyl and silanol groups are more reactive than those in the center of the molecule, which are already of higher condensation degree. From the picture, the disordered arrangement of siloxane centers can be

observed, which results in a large variation of chemical environment around the silicon atoms and in turn, is responsible for ^{29}Si-NMR signal broadening.

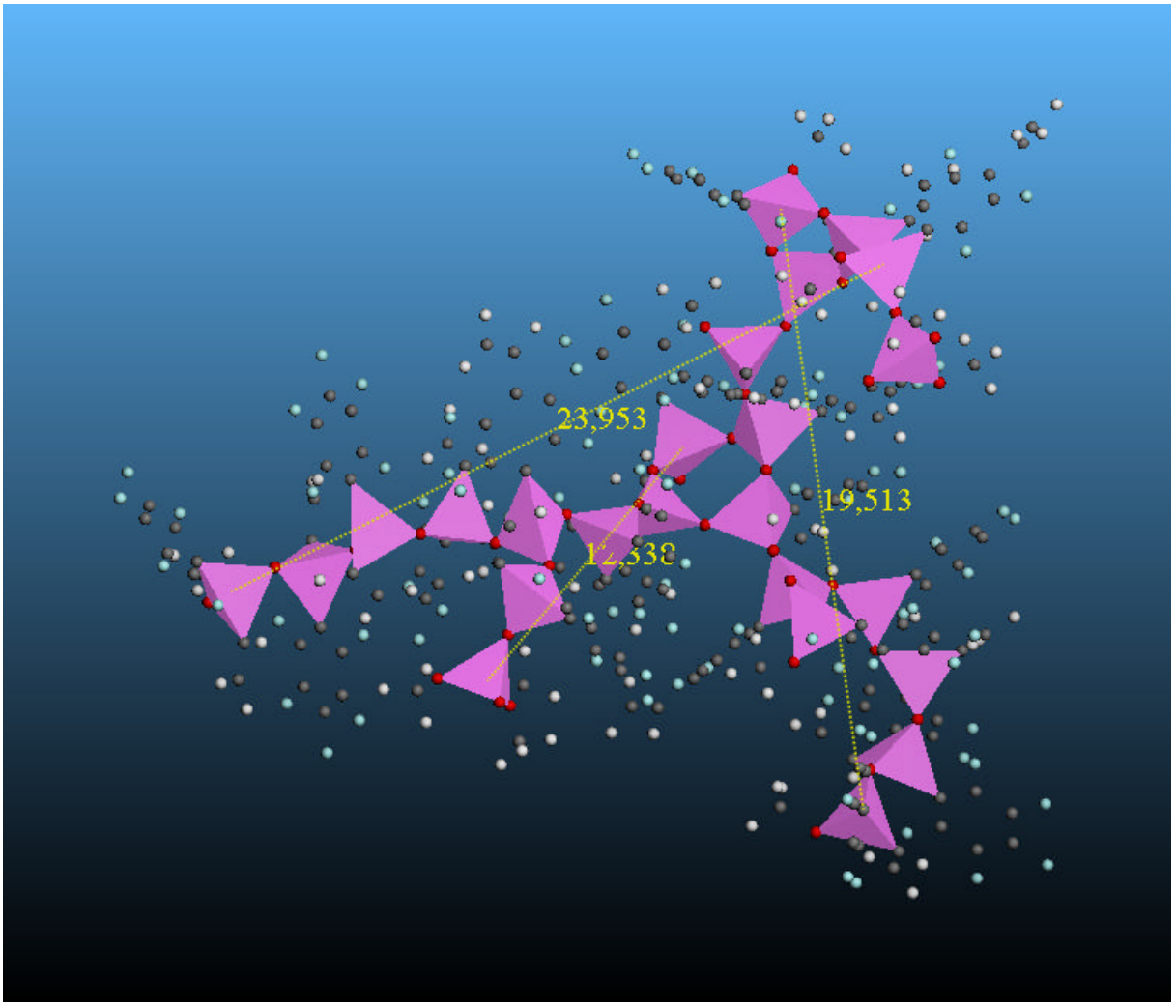

Fig. 77: **fk37** resin oligomer from Fig. 76, with silicon atoms depicted as tetrahedra. Atoms belonging to organic moieties are shown as dots, distances are measured in Ångstroms.

Rendering the model with space filling spheres (Fig. 78), i.e. depiction of atoms as spheres with radii related to their van der Waals radii, gives information about sterical demand of siloxane skeleton and substituents. In order to examine a possible impact of sterical characteristics on photopatternability, the vinyl groups of 4-vinyltetrafluorophenyl moieties, which are responsible for the UV patternability of the resin, are highlighted in yellow. Four of the five reactive groups within the model are visible, and the last one is situated on the backside of the molecule.

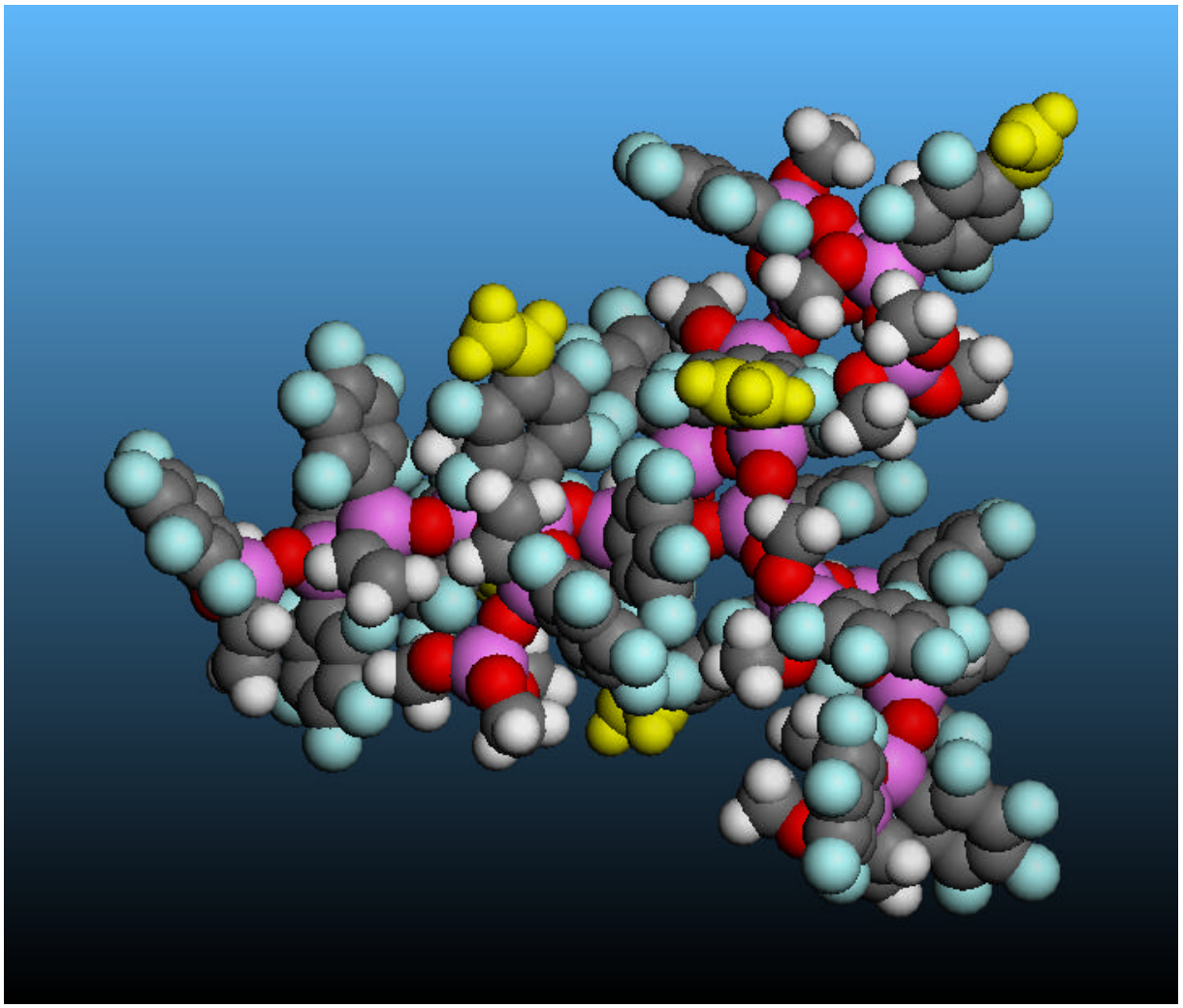

Fig. 78: **fk37** resin oligomer from Figs. 76 & 77, with atoms rendered as space-filling spheres. Vinyl groups being part of 4-vinyltetrafluorophenyl moieties are marked yellow in order to highlight the reactive sites for possible organic crosslinking with other oligomers.

It has been stated above (chapter 3.4.5) that the structural model of the oligomer somewhat mirrors the different reactivities of precursor alkoxy silanes. As a result, the core part of the oligomer chiefly consists of T-type silicon species, because the initial polycondensation phase mainly involved condensation of the more reactive T-systems. Pendant siloxane chains comprising D-type species originate from later addition of the less reactive D-centers. Considering that the organic functionality, 4vinyltetrafluorophenyl, which is responsible for organic cross-linking, is attached to T-silicon atoms, it is important to make sure that the reactive vinyl groups are not sterically hindered from reaction. As a matter of fact, the image gives evidence that even for 4-vinyltetrafluorophenyl groups attached to completely condensed siloxane species that are situated near the center of the molecule, the reactive functionality is well accessible for organic cross-linking.

The model also illustrates that due to the low number of organically crosslinkable moieties within the oligomer, photochemical crosslinking will in fact produce the desired inorganic-hybrid network, but the degree of polymerization will be low. Because of the high sterical demand of the siloxane backbone, which is attached to the 4vinyltetrafluorophenyl "monomers", the polystyrene analogous polymer chains will only be relatively short. A quantitative analysis, however, would require further molecular modeling studies, thus going beyond the scope of this work. Nevertheless, one can estimate that organic crosslinking will not include more than approx. five reactive 4-vinyltetrafluorophenyl groups.

In summary, it is important to emphasize that the given molecular structure cannot be considered an exact representation of an isolated molecule, but must be understood as an idealized model of an average **fk37** resin oligomer. Nevertheless, the model is in consistency with both, the ^{29}Si-NMR structural data and the SAXS measurement outlined in Tab. 15, and upon visualization by various means of rendering, different aspects of structural features could be analyzed.

3.5 Syntheses of ORMOCER® inorganic-organic hybrid polymers

The final step in ORMOCER® synthesis is the establishment of the inorganic-organic hybrid network by organic crosslinking of organosiloxane oligomers via organically polymerizable units. In general, this can be achieved by reaction under thermal and/or photochemical polymerization conditions, and normally involves the help of a suitable initiator, which is admixed to the resin in small amounts prior to reaction. Manufacture of ORMOCER® micropatterns, specifically, involves partial irradiation of a wet film with UV light by means of photolithography, i.e. partial photochemical cross-linking is achieved by the use of a mask (cf. chapter 2.3). ORMOCER® resins exhibit negative resist behavior. Thus, irradiated film areas are hardened, whereas during the subsequent development step, unexposed areas are washed away. By this, patterns according to the transparent sub-areas of the mask are formed. First successful photopatternability tests on 4-vinyltetrafluorophenyl functionalized ORMOCER® resins have already been mentioned earlier (cf. chapters 3.4.2, 3.4.3). The current section of this work gives a more detailed presentation of the manufactured ORMOCER® thin films and micropatterns. The individual samples are numbered according to the code described in chapter ii.ii.

3.5.1 General method for the manufacture of ORMOCER® micropatterns

All processes were performed in a clean room in order to provide a dust-free atmosphere, which is crucial for the manufacture of waveguide structures. Shaded windows as well as yellow light bulbs accounted for an exclusion of UV light in order to be able to handle the

photosensitive compounds. The preparation of ORMOCER® lacquers ready for processing generally involved dilution of the respective resins with a solvent (typically propyl acetate, 12.5 – 25 wt.% with respect to 100 wt.% resin), and admixture of a commercially available photo-initiator (1 – 3 wt.%). Pressure filtration over a 0.2 µm filter was performed in order to remove particles or contaminations resulting from the initiator. The resulting lacquers then were applied to a substrate by means of spin-coating. By variation of spinning speed on the one hand, and lacquer viscosity due to different diluting solvent concentrations on the other hand, film thicknesses ranging from approx. 2 µm to 20 µm could be achieved. Figure 79 outlines the consecutive processing steps, the sequence of which is typical of ORMOCER® micro patterning at Fraunhofer-ISC. Upon alteration of process parameters, pattern characteristics were varied.

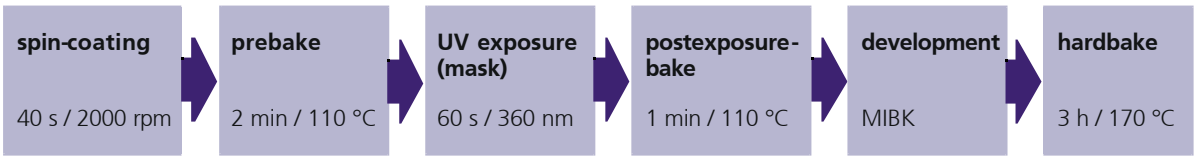

Fig. 79: Clean room processing steps for the manufacture of ORMOCER® micropatterns. The parameters are representative for the patterning of ORMOCER®s.

After spin-coating, a short prebake step was necessary in order to remove the diluting solvent. The prebake is also believed to enhance substrate adhesion. The core step within the patterning process was the UV irradiation of the prebaked film through a mask in order to induce crosslinking within the light-exposed areas. A postexposure bake step was to further improve substrate adhesion. The patterns were developed by removing unexposed lacquer and insufficiently crosslinked material with a solvent such as 4-methyl-2-pentanone (MIBK), leaving the patterns according to their negative resist behavior. Thermal curing finally ensured reaction completion, resulting in the patterned hybrid inorganic-organic ORMOCER® network.

3.5.2 Micropatterns of fluoroaryl functionalized ORMOCER®s

The manufacture of ORMOCER® micropatterns involved extended variation of processing parameters, as detailed in the experimental section (chapter 4.6.4). Only the optimization of parameters such as lacquer formulation (mixture: resin + diluter + photoinitiator), spin-coating speed, exposure dose, and baking steps, resulted in well-resolved micro-patterns. Figures 80-82 depict such test patterns from ORMOCER® formulations **fk34**, **fk37**, and **fk38**, respectively, demonstrating excellent photopatternability. Among the test structures were waveguide patterns (width: 5 µm, 10 µm, 25 µm, 50 µm), vias (width: 25 µm, 50 µm, 100 µm), and columns (width: 10 µm, 25 µm, 50 µm). The film thicknesses range from 2– 20 µm, which correspond to typical layer thicknesses in optical multilayers. Silicon wafers with a native oxide layer served as substrates.

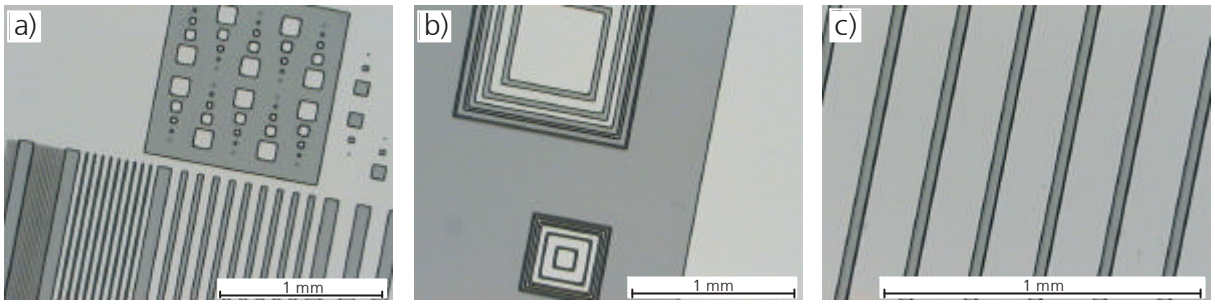

Fig. 80: **fk34** test patterns (dark gray) on silicon substrate (light gray): a) – c) sample **fk34a/2** (layer thickness: 2.3 µm).

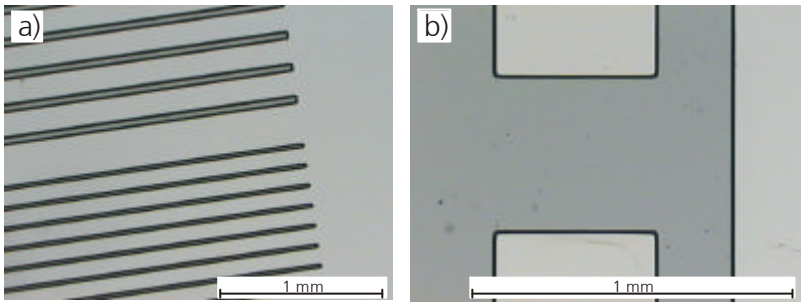

Fig. 81: **fk37** test patterns (dark gray) on silicon substrate (light gray): a) sample **fk37a/2** (thickness: 16 – 20 µm); b) sample **fk37-2a/4** (thickness: 3.5 µm).

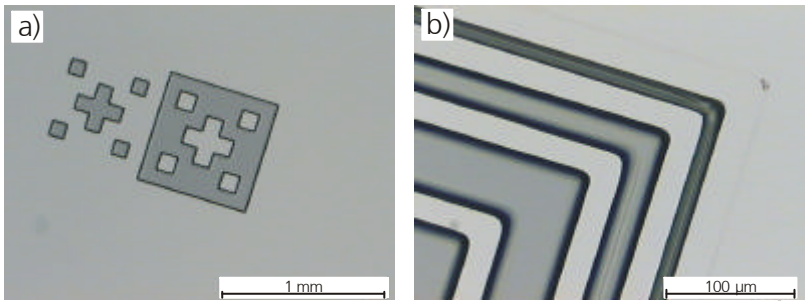

Fig. 82: **fk38** test patterns (dark gray) on silicon substrate (light gray): a) + b) sample **fk38a/1** (thickness: 8 – 9 µm).

A crucial requirement for ORMOCER®s, which are intended for use in microsystems technology, is their compatibility to SBU (sequential build-up) technology, i.e. their ability to form multilayers without cracking or delamination. In order to test this, a number of multilayer samples were prepared. Figure 83 illustrates patterns of system **fk37** on microstructures of unpublished, experimental ORMOCER® formulation **El20**, an unfluorinated material incorporating epoxy functionalities. The good adhesion not only between the two ORMOCER® layers, but also between **fk37** and the exposed silicon substrate, promise general applicability of the material in multilayers.

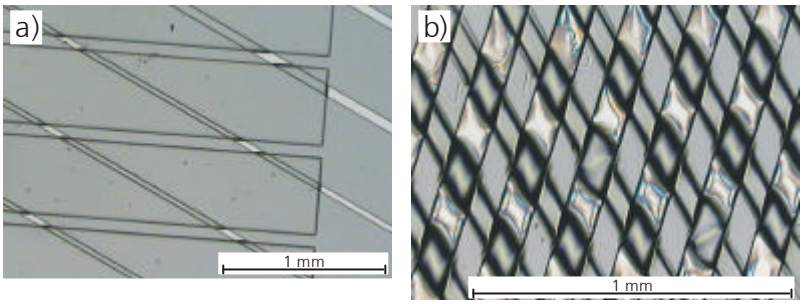

Fig. 83: fk37 microstructures on patterned ORMOCER® **El20** (upper left to lower right of the images; wide in a), narrow in b); substrate: silicon). a) Sample **fk37-3c/1** (thickness: 2 µm); b) sample **fk37-3c/2** (thickness: 17.5 µm).

Figure 84 demonstrates the formation of an embedded optical waveguide incorporating two **fk38** cladding layers with an **fk34** core layer in between. Figure 84a) shows the core pattern on the buffer (undercladding) layer, still without the uppercladding. The core profile of 10 x 10 µm is typical of thin multimode waveguides. Figure 84b) depicts the complete embedded strip waveguide, consisting of three ORMOCER® layers. However, the pinholes in the uppercladding layer show adhesion problems between the fully thermally cured **fk38** buffer film and the final uppercladding layer from the same material, which is more pronounced in Fig. 84c). First investigations have been made in order to overcome the adhesion problems. The use of surface-altering reagents such as ammonium hydroxide solution, which leaves the surface in a very well defined state with the silicon terminated by hydrogen[179,180] resulted in slight improvement. The use of more work- as well as cost-intensive processing methods such as plasma treatment would have gone beyond the scope of this work.

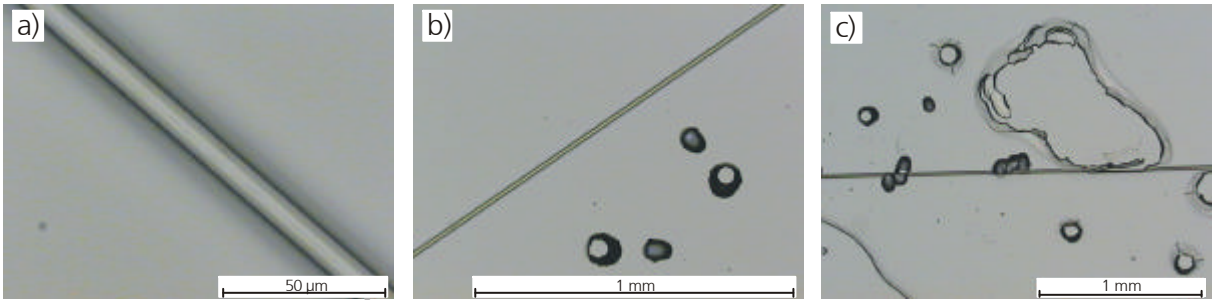

Fig. 84: **fk34** waveguide patterns on **fk38** film (thickness: 16 µm): a) sample **fk43/3b** (pattern profile: 10 x 10 µm); b) + c) sample **fk43/3c** (sample **fk43/3b** plus additional **fk38** uppercladding (thickness: 11 µm) with pin holes).

3.5.3 Oligosiloxane crosslinking via the styrene-analogous group

During photopatterning of ORMOCER® resins **fk34**, **fk37**, and **fk38**, oligomers of the type presented above (cf. Fig. 78, chapter 3.4.8) are organically crosslinked via the polymerizable

4-vinyltetrafluorophenyl groups. Upon UV exposure, hardening of the coating films occurs upon photoinduced cleavage of the photoinitiator into primary radicals (cf. Figs. 38 & 39, chapter 2.5.3), which initiate the radical chain polymerization of the reactive moieties within the organosiloxane oligomers. The crosslinking reaction is depicted schematically in Fig. 85.

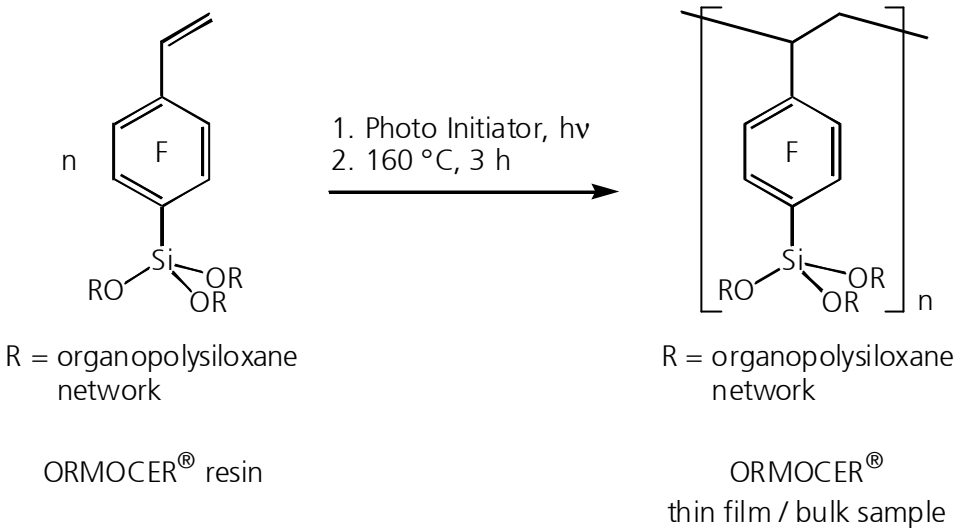

Fig. 85: Organic crosslinking of fluoroaryl ORMOCER® resin oligomers (schematic representation).

However, as derived from molecular modeling of a typical resin oligomer (see chapter 3.4.8), the degree of organic polymerization, as represented by the index *n* within Fig. 85, is expected to be low. This is due to steric demand within the oligomers. Therefore, the process differs from typical styrene polymerization insofar as the chain reaction, once initiated, does not produce long polystyrene chains from hundreds or thousands of monomer units, but must be rather considered as a crosslinking reaction between very few organic units. Thus, the photochemically induced hardening of the film is limited to only a small volume, which accounts for high resolution patterns, because the crosslinking does not propagate into the unexposed film area. By washing away the unexposed and therefore uncured resin with an organic solvent such as 4-methyl-2-pentanone (MIBK) or toluene, the ORMOCER® micropatterns are developed. Subsequent thermal hardbake completes the polymerization of residual 4-vinyltetrafluorophenyl groups, which have not reacted during photopatterning. Initiation of the chain reaction may occur by thermal decomposition of impurities starting either radical or ionic processes. Also possible is a mechanism as proposed for the thermal polymerization of styrene in the absence of an initiator[64,181]. In this case, the styrene-analogous compound undergoes a Diels-Alder-type [4+2]-cycloaddition with subsequent hydrogen migration from the adduct to another styryl group, thus generating the radical intermediate.

3.5.4 Structural characterization of ORMOCER® hybrid networks by magic angle spinning (MAS) solid state ^{29}Si-NMR

The inorganic siloxane network structure of completely photochemically and thermally cured ORMOCER® powder samples was analyzed with quantitative solid state ^{29}Si-MAS-NMR. Deconvolution of the spectra was performed by using the *dmfit2001* program[174] as for the resin NMR spectra (cf. chapter 3.4.4). However, compared to the solution spectra, the solid state results could not be derived with equal detail because of irresolvable overlaps of several signals, particularly of fluoroaryl-substituted $T^2_{fluoroaryl}$ with vinyl-functionalized T^3_{vinyl}. Nevertheless, the analyses allowed insight into the oxidic network structure of completely cured ORMOCER®s **fk34**, **fk35**, **fk37**, and **fk38**, respectively, which is summarized in Tab. 18. For comparison, the table also picks up (in brackets) the respective results for the resins, as presented in Tab. 15 (chapter 3.4.4). This allows to draw conclusions concerning inorganic network alteration during clean room processing of ORMOCER® resins/lacquers, particularly during thermal curing.

Tab. 18: Siloxane network structures of cured fluoroaryl ORMOCER®s **fk34**, **fk35**, **fk37**, and **fk38** according to quantitative analysis of ^{29}Si-MAS-NMR spectra. Comparative resin values from solution ^{29}Si-NMR are given in subscript brackets (cf. Tab. 15). Silanol (Si-OH) contents are given qualitatively according to FT-IR (subscript brackets: resin).

	condensed silicon species within inorganic network [mol.%]									Si-OH content
	D^1	D^2	$T^1_{fluoroaryl}$	T^2_{vinyl}	$T^2_{fluoroaryl}$ / T^3_{vinyl}	Q^1	$T^3_{fluoroaryl}$	Q^2	Q^3 / Q^4	
fk34	$0_{(2)}$	$34_{(38)}$	$0_{(5)}$	$1_{(4)}$	$19_{(19)}$	$3_{(6)}$	$27_{(24)}$	$8_{(2)}$	$8_{(0)}$	$medium_{(high)}$
fk35		36			17	4	29	5	9	$medium_{(medium)}$
fk37	$0_{(6)}$	$34_{(32)}$	$0_{(6)}$		$12_{(26)}$	$3_{(8)}$	$36_{(22)}$	$6_{(0)}$	$9_{(0)}$	$low_{(low)}$
fk38	$8_{(3)}$	$38_{(47)}$	$4_{(11)}$	$0_{(3)}$	$25_{(20)}$	$0_{(3)}$	$20_{(13)}$		$5_{(0)}$	$medium_{(high)}$

The distribution of signal intensities assigned to silicon centers with different degrees of condensation gives information about inorganic network densities. Accordingly, materials **fk34**, **fk35**, and **fk37**, which are based on the same initial precursor silane composition, bear large similarities in their established siloxane networks. Only by considering the difference in $T^3_{fluoroaryl}$ content, it may be assumed that system **fk37** possesses an inorganic network of a slightly higher degree of condensation than **fk34** and **fk35**. ORMOCER® **fk38** also exhibits a high degree of condensation, although direct comparison is impossible due to the difference in initial silane formulation.

In comparison to the respective resin characterization, each ORMOCER® system shows significant increase in degree of condensation due to clean room processing, i.e. during UV-lithography and subsequent thermal curing. This expresses itself in a general intensity shift

towards higher condensed species such as $T^3_{fluoroaryl}$ and $Q^2/Q^3/Q^4$. Simultaneously, signal intensities due to low states of condensation decrease, as for D^1, $T^1_{fluoroaryl}$, T^2_{vinyl}, and Q^1. Further reduction of silanol content as seen with FT-IR spectroscopy, supports the idea of post-condensation. However, the increase in siloxane network density can only be explained by thermal condensation reactions rather than photochemical processes, i.e. UV-lithography does not alter the inorganic condensate. The latter should only induce organic cross-linking, which has no effect on ^{29}Si-NMR shifts.

In close relation to network alteration due to condensation, the spectral analyses allow conclusions considering an aryl loss within the hybrid polymers. For this, the initial D/T ratios (**fk34**, **fk35**, **fk37**: 50/50; **fk38**: 70/30) are compared with the integrals of D- and Q-signals (resulting from dearylation of T species), respectively. Table 19 summarizes the results both for total aryl loss and the respective proportions for D- and T-silane decomposition. These amounts due to complete ORMOCER® processing are compared to those due to resin syntheses alone (cf. Tab. 15, chapter 3.4.4). The differences between these values are assigned to aryl losses during clean room processing of the resins, particularly during final thermal hardbake.

Tab. 19: Aryl losses during processing of fluorinated aryl ORMOCER®s.

	Aryl loss D (mol.%) in fluoroaryl ORMOCER® processing during:								
	resin synthesis (cf. Tab. 15)			**thermal curing after UV**			**total ORMOCER® process**		
	$\Delta_{D\rightarrow T}$	$\Delta_{T\rightarrow Q}$	D_{total}	$\Delta_{D\rightarrow T}$	$\Delta_{T\rightarrow Q}$	D_{total}	$\Delta_{D\rightarrow T}$	$\Delta_{T\rightarrow Q}$	D_{total}
fk34	14	8	**22**	2	11	**13**	16	19	**35**
fk35							14	18	**32**
fk37	9	8	**17**	7	10	**17**	16	18	**34**
fk38	11	3	**14**	13	2	**15**	24	5	**29**

The table shows that during thermal curing, fluoroaryl functionalized ORMOCER®s undergo further significant Si-$C_{fluoroaryl}$ bond cleavage, approximately of the same magnitude as during resin aging (cf. chapter 3.4.5). Thus, within the completely cured ORMOCER® hybrid networks, approx. 29 – 35 mol.% of the initially present Si-$C_{fluoroaryl}$ bonds have been cleaved. Fluoroarylsilane centers of D- and T-types, respectively, can be considered similarly susceptible to aryl loss, as the total amount of cleaved bonds is equally distributed to D species converted to T (D→T), and T centers converted to Q (T→Q), respectively. This also applies to **fk38**, considering the initial D/T ratio of 70:30, which leads to a proportional increase/decrease in D- and T-conversion, respectively.

Because of the simultaneous increase in siloxane network connectivity during aryl loss, one can deduce a correlation. Thus, thermally (160 °C) induced post-condensation largely involves

nucleophilic attack of residual Si-OH to silicon centers, which undergo Si-O-Si bond formation upon release of a fluoroaryl substituent as leaving group.

3.5.5 Thermal analysis

In order to get further insight into materials properties, samples of completely cured fluorinated ORMOCER®s **fk34**, **fk35**, and **fk37** were analyzed with thermogravimetry (TG) and differential thermal analysis (DTA) in an artificial air atmosphere. The resulting charts for the thermal decomposition of the materials in a temperature range of 60 °C – 1000 °C are depicted in Fig. 86.

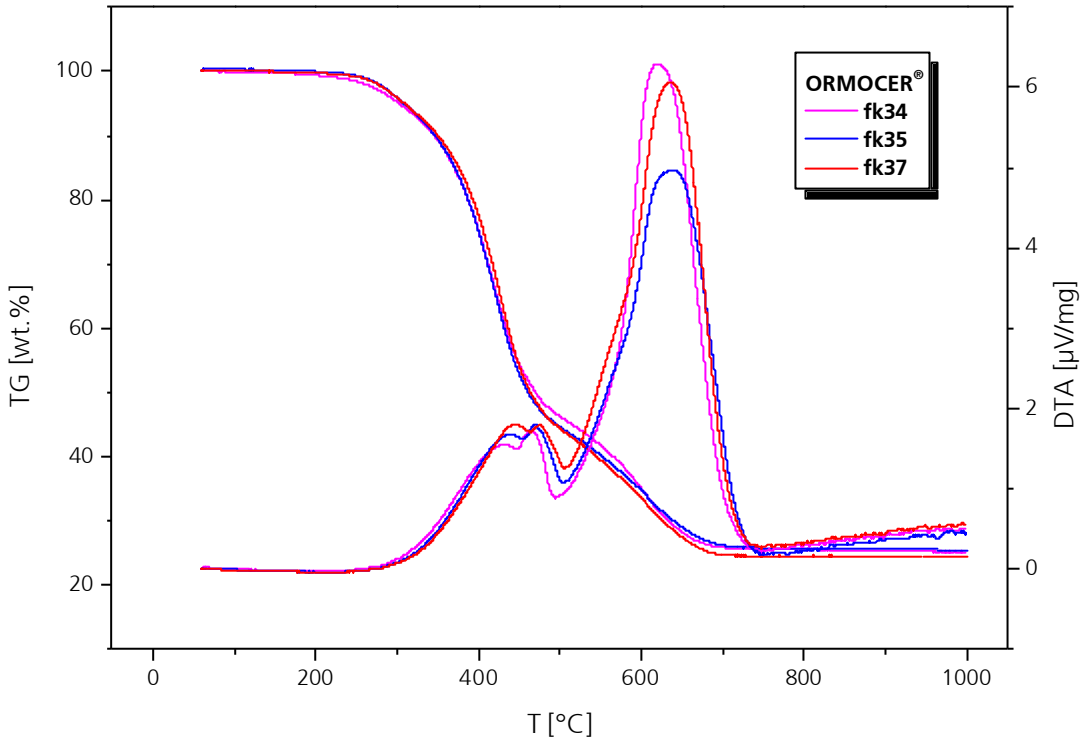

Fig. 86: TG (above) and DTA (below) curves during thermolysis of fluoroaryl modified ORMOCER® powder samples in an artificial air atmosphere.

Systems **fk34**, **fk35**, and **fk37** exhibit largely similar behavior, which is due to their identical precursor silane formulations. Obviously, the different polycondensation conditions, which were applied for resin syntheses, do not significantly affect the material properties when exposed to heat. This is in consistence with the solid state NMR investigations (see above), which suggest close similarities between the inorganic network structures of the three materials.

One aspect to be mentioned is the similar thermal resistance of the polymers. In accordance with literature[62], a maximum of 5% weight loss due to temperature impact was considered tolerable. Thus, the materials were found thermally stable up to approx. 300 °C (**fk34**: 303 °C;

fk35: 308 °C; **fk37**: 309 °C). The TG charts exhibit flat lines above approx. 750 °C, which indicate that above this temperature, the organic parts of the materials are completely removed, leaving only silicon dioxide, SiO_2. Total weight losses in **fk34** (75 wt.%), **fk35** (75 wt.%), and **fk37** (76 wt.%) are equal, giving additional evidence of the close similarities between the materials.

The first steep decrease in the TG plots is assigned to fluoroaryl decomposition. Thus, beside NMR, additional analytical access to fluoroaryl loss is offered by thermogravimetry. By comparison of the experimental weight loss due to fluoroaryl decomposition with the theoretically expected value, aryl loss can be quantified. The theoretical (without aryl loss) average molar mass of fluorinated aryls with respect to each silicon atom can be calculated according to precursor arylsilane ratios. Average molar mass within this context means that molar masses of pentafluorophenyl [167.06 g/mol] and vinyltetrafluorophenyl (175.10 g/mol) radicals, respectively, are considered according to their percentage in the silane mixture. Thus, in ORMOCER®s **fk34**, **fk35**, and **fk37**, the theoretical average molar mass $M_{theor.}$ of the fluoroaryl moiety equals 169.07 g/mol.

In order to quantify the TG experimental weight loss due to fluoroaryl degradation, the respective experimental percentage $\%_{exp.}$ [wt.%] (first descent in TG chart) is correlated with the amount of remaining inorganic silicon dioxide, $\%_{SiO2}$ [wt.%], the molar mass M_{SiO2} of which is 60.08 g/mol. Thus, the experimental average molar mass $M_{exp.}$ [g/mol] of fluoroaryl components within the materials is derived from the following equation (eq. 5).

$$M_{exp.} = \frac{M_{SiO2}}{\%_{SiO2}} \text{ x } \%_{exp.} \qquad \text{(eq. 5)}$$

In correlation with the theoretical values $M_{theor.}$ for average fluoroaryl molar mass, the fluoroaryl loss $\Delta_{fluoroaryl}$ [mol.%], which occurs during ORMOCER® processing (resin synthesis and photochemical/thermal curing), is quantified (eq. 6).

$$\Delta_{fluoroaryl} = \left(1 - \frac{M_{exp.}}{M_{theor.}}\right) \text{x } 100 \text{ mol.\%} \qquad \text{(eq. 6)}$$

Table 20 summarizes the results from thermal analysis of ORMOCER®s and compares the values $\Delta_{fluoroaryl}$ for aryl loss with the respective figures Δ_{NMR} derived from solid state ^{29}Si-NMR (cf. Tab. 19, chapter 3.5.4). The TG/DTA derived values for fluoroaryl loss are significantly lower than those resulting from NMR. This allows one to draw the conclusion that although approx. 32% to 35% of the Si-$C_{fluoroaryl}$ bonds are cleaved during ORMOCER® processing, still approximately one third of the involved aryl moieties remain attached to the hybrid network. This means that vinyltetrafluorophenyl groups, which had undergone organic cross-linking, may

in fact be victims of Si-$C_{fluoroaryl}$ bond breaking, but still are covalently connected to the organic part of the hybrid polymer network. Thus, combined thermal and NMR analyses of the materials shade new light on the phenomenon of fluoroaryl loss.

Tab. 20: Aryl loss $\Delta_{fluoroaryl}$ calculation according to thermal analysis of ORMOCER®s. Values Δ_{NMR} derived from solid state NMR (cf. Tab. 19) are added for comparison.

	$\%_{exp.}$	$\%_{SiO2}$	$M_{exp.}$	$M_{theor.}$	$D_{fluoroaryl}$	D_{NMR}
fk34	51 wt.%	25 wt.%	122.56 g/mol	169.07 g/mol	**28 mol.%**	35 mol.%
fk35	52 wt.%	25 wt.%	124.97 g/mol	169.07 g/mol	**26 mol.%**	32 mol.%
fk37	52 wt.%	24 wt.%	130.17 g/mol	169.07 g/mol	**23 mol.%**	34 mol.%

3.5.6 Optical properties

Besides photopatternability, the central concern for ORMOCER®s designed for telecom applications lies in the optical properties of the completely cured materials. In particular, refractive indices as well as optical losses of ORMOCER® thin-films in the telecommunication wavelength regions are the main characteristics of interest. Table 21 outlines thin-film optical properties of systems **fk34**, **fk37**, and **fk38** and correlates them with respective resin values. Some data are missing due to the high complexity of thin film preparation and analysis, which within the scope of this work limited the number of samples suitable for characterization. Nevertheless, the observed trends are obvious.

Tab. 21: Optical properties of fluoroaryl ORMOCER® thin-film samples **fk34c/1**, **fk37-4a/1**, and **fk38c/1**. Comparative resin values in subscript brackets.

Sample No.	Refractive index *n* at				Optical loss at 1550 nm
	635 nm	850 nm	1310 nm	1550 nm	
fk34c/1	1.493 $_{(1.497)}$	1.487	1.482	1.481	– $_{(0.70)}$ dB/cm
fk37-4a/1	– $_{(1.497)}$	–	–	1.475	0.51 $_{(0.42)}$ dB/cm
fk38c/1	1.491 $_{(1.491)}$	1.485	1.482	1.481	– $_{(0.84)}$ dB/cm

The fluorinated materials exhibit refractive indices below 1.500 (365 – 1550 nm), which are significantly lower than those of comparative unfluorinated ORMOCER®s for telecom applications (e.g. **b59d**[33]: *n* (633 nm) = 1.552, cf. chapter 2.5.4). This is due to their high degree of fluorination, which strongly decreases refraction. This effect has already been observed and discussed for the respective precursor silanes and resins (cf. chapters 3.2.1, 3.4.6) and also applies to solid state characteristics.

Unlike ORMOCER® **b59d**, however, which undergoes an increase of refractive index during ORMOCER® processing (from n_{resin} = 1.538 (633 nm) to $n_{SolidState}$ = 1.552 (633 nm[33]) due to network densification, refraction of fluoroaryl materials does not change significantly between resin and solid state. This different behavior is attributed to network alteration processes during thermal curing, but in case of the fluorinated hybrids, two competing processes must be considered. On the one hand, the siloxane network is densified due to post-condensation as well as completion of organic crosslinking, which leads to higher refraction. On the other hand, however, post-condensation of fluoroaryl functionalized organosiloxane networks also involves additional partial aryl loss (cf. chapters 2.5.5, 3.4.5), which on the contrary lowers refraction, because another portion of arylic π-systems is removed from the material. Obviously, neither of the effects outweighs the other, thus not resulting in significant index changes.

A frequency dependence of refraction, however, is clearly documented for systems **fk34** and **fk38** (Fig. 87). In the VIS/NIR range from 635 nm to 1550 nm, an index decrease with increasing wavelength is evident. Thus, according to theory, the materials exhibit normal dispersion[42].

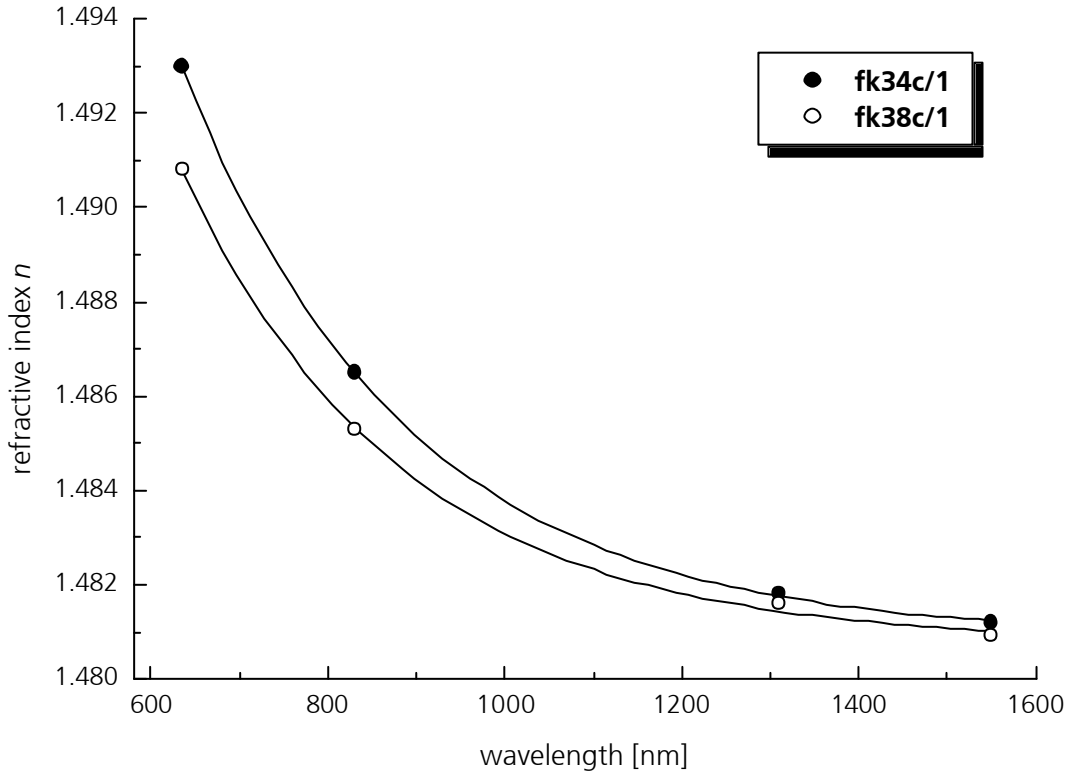

Fig. 87: Refractive indices of ORMOCER® thin film samples **fk34c/1** and **fk38c/1** at 635 nm, 850 nm, 1310 nm, and 1550 nm, measured with a laboratory-built prism coupler.

Considering absorption loss of waveguides at 1550 nm, the fluoroaryl functionalized ORMOCER® **fk37** shows an improvement of loss (0.51 dB/cm) compared to the reference ORMOCER® **b59d** (0.55 dB/cm[30]). Compared to the **fk37** resin absorption (0.42 dB/cm at 1550 nm), however, solid state processing of the fluorinated material did not result in lower signal attenuation, although literature suggests that within organosiloxane networks, post-condensation due to thermal baking leads to silanol decrease and therefore to loss reduction[30,182]. However, since the measurements presented in Tab. 21 were conducted on very first examples of **fk37** waveguides, it can be assumed that upon further optimization of processing parameters, particularly with respect to thermal hardbake (temperature/time), further reduction of absorption loss will be achieved. Thus, for a detailed discussion of fluorinated ORMOCER® waveguides, considerably more work has to be invested into waveguide processing, which requires intensive studies that may be conducted in future times.

3.5.7 Dielectrical properties

For dielectrical testing, capacitor multilayers with embedded ORMOCER® films were prepared. Figure 88 shows a 4'' silicon wafer with four copper platter capacitors embedding a thin (4.7 µm) **fk37** dielectric layer. The manufacture in SBU (sequential build-up) technology included as first step the patterning of copper capacitor plate patterns on the silicon substrate using a standard photoresist patterning – plasma deposition – wet etching sequence. Of this lower layer, only the T-shaped contacts are visible in the image. Afterwards, the dielectric ORMOCER® layer was applied and photo- as well as thermally cured, prior to the final addition of the top capacitor patterns.

The determined dielectric permittivity of the **fk37** material (ε = 3.7 at 10 kHz) is in the typical range for permittivities of ORMOCER®s (ε (10 kHz) = 3.1 – 4.0)[183]. This makes the material very promising for application in integrated electro-optical devices, as it can serve as optical waveguide and dielectric layer simultaneously. This ability is desired for high integration densities in such devices.

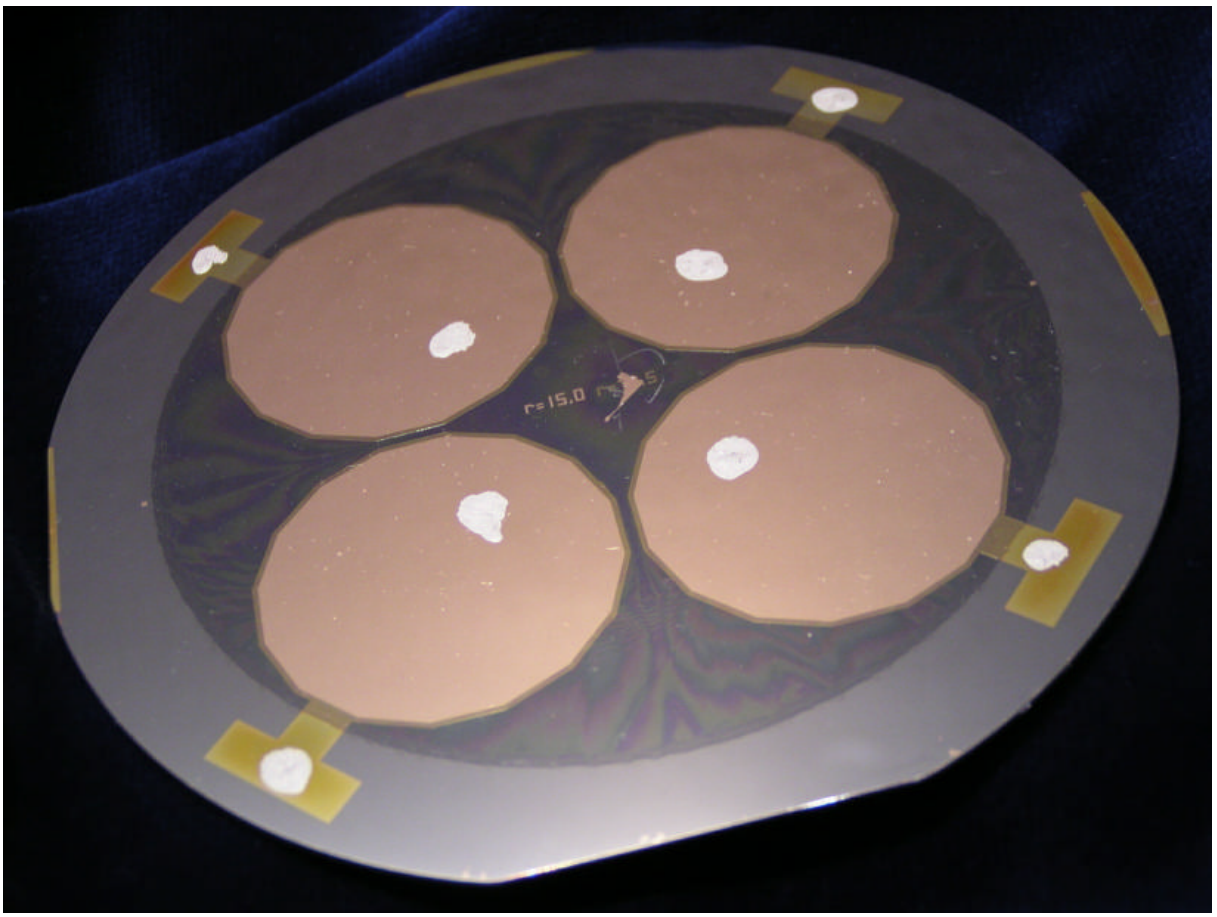

Fig. 88: 4'' silicon wafer with four copper capacitors embedding a 4.7 µm **fk37** thin film (dark, showing rainbow color reflexes) for dielectrical testing (sample **fk37-2e/1**). White spots due to contact paste denote the contact areas of the measurement apparatus.

3.5.8 Mechanical properties

As materials intended for use in integrated microsystems, mechanical properties such as microhardnesses and Young's moduli of fluorinated ORMOCER®s are application-relevant characteristics. Table 22 shows the results of micro indenter measurements on cured hybrid polymer samples **fk34c/1**, **fk37-2a/4**, and **fk38c/1**. The high micro-hardnesses as well as the low elasticities of the materials indicate high degrees of crosslinking for both, the inorganic polysiloxane network and the organic part. In accordance with the literature[184], the relatively low values for the **fk38** system compared to the other two systems are attributed to both, its higher content of D-type silicon species making the inorganic network more flexible, and the lower content of organically crosslinked vinyltetrafluorophenyl groups. Thus, the resulting overall lower degree of crosslinking leads to lower hardness and higher flexibility of the material.

The higher figures for **fk34** compared to the closely related **fk37** system result from the higher silanol content of the former, as determined with FT-IR spectroscopy (cf. Tab. 18, chapter 3.5.4), whereas the siloxane chains of the latter are predominantly terminated by

methoxy groups. The structural difference affects the rigidity of the network in two ways, leading to the same trend. On the one hand, increased silanol content as in **fk34** accounts for a higher network density and thus rigidity due to increased secondary network interactions by hydrogen bonding. On the other hand, the steric demand of the methoxy compared to the silanol groups leads to a less dense network and therefore lower rigidity in the **fk37** case. The higher refractive index of sample **fk34c/1** ($n_{1550\ nm}$ = 1.481) compared to sample **fk37-4a/1** ($n_{1550\ nm}$ = 1.475) as shown in Tab. 21 (chapter 3.5.6) supports the idea of network densification due to higher silanol instead of methoxy content. Although Tab. 18 (chapter 3.5.4) suggests that the less rigid material **fk37** has a slightly higher siloxane network connectivity, the difference to **fk34** is not significant, taking into account that the quantitative evaluation of the complex solid state ^{29}Si-NMR spectra of cured hybrid polymers is subject to a considerable error margin. Since also the thermal analyses presented in chapter 3.5.5 indicate similarities between the **fk34** and **fk37** networks to a large extent, the differences in hardness and Young's modulus have to be attributed primarily to silanol versus methoxy content.

Tab. 22: Mechanical properties at 20 °C of fluoroaryl functionalized ORMOCER® samples.

sample-No.	**Microhardness** [N/mm^2]	**Young's modulus** [GPa]
fk34c/1	218.3 +/- 16.67	7.96 +/- 0.69
fk37-2a/4	173.1 +/- 11.51	4.80 +/- 0.27
fk38c/1	139.1 +/- 3.52	3.54 +/- 0.16

Overall, the measurements suggest high mechanical toughness of the photopatternable ORMOCER®s **fk34**, **fk37**, and **fk38**, which is a requirement for materials designed for industrial microsystems fabrication processes such as flip-chip bonding[185].

4 EXPERIMENTAL SECTION

4.1 Chemicals

Commercially available reactants and solvents were purchased from chemical companies Gelest, Lancaster and Sigma-Aldrich and used without further purification. Deuterated solvents for NMR were purchased from Deutero, silicon wafers have been delivered by Wacker Siltronic, and UV initiators are from BASF (Lucirin® LR 8893 / TPO-L) and Ciba (Irgacure® 907). Positive Photoresist ma-P1215 and developer ma-D331 were purchased from micro resist technology corporation. Samples of experimental ORMOCER® systems **V32** and **El20** as well as small amounts of the commercially unavailable precursor silane 4-vinylphenyltrimethoxysilane were kindly made available by fellow members of the Competence Team "Hybrid Polymers (ORMOCER®s) for Microsystems" at Fraunhofer-ISC.

4.2 Analytical methods and apparatuses

4.2.1 Nuclear magnetic resonance spectroscopy (NMR) in solution

Routine ^{1}H-, ^{13}C-, and ^{29}Si-NMR spectroscopy in solution was carried out on a Bruker Avance DPX 400 NMR spectrometer with a 9.4 T magnetic field and equipped with a quaternary nuclear probehead. The setup uses the deuterium signal of typical NMR solvents as an internal locking vehicle. Therefore, the samples were dissolved in deuterated solvents deuterochloroform ($CDCl_3$) and deuterated acetone (d_6-acetone), respectively. The solutions were transferred into glass NMR sample tubes of 5 mm in diameter and 178 mm in length, mixed with a small amount of tetramethylsilane (TMS) as internal reference, and analyzed at 25 °C. All ^{1}H-, ^{13}C-, and ^{29}Si-NMR chemical shifts given in parts per million (ppm) refer to the according TMS signal. Table 23 shows a selection of typical acquisition parameters in routine ^{1}H-, ^{13}C-, and ^{29}Si-NMR.

Tab. 23: Typical parameters in routine solution NMR.

Parameter	^{1}H	^{13}C	^{29}Si
Frequency	400 MHz	101 MHz	79.5 MHz
Number of scans	128	1024	512
Delay time D1	1.00 s	2.00 s	30.0 s
Decoupling frequency	-	400 MHz	400 MHz

For the ^{29}Si-NMR analysis of a complex mixture of silane species, an ORMOCER® resin in particular, the number of scans was increased up to 3072 in order to optimize the signal-to-noise ratio. The addition of chromium(III) acetylacetonate (approx. 10 – 20 mmol/l) proved advantageous as the relaxation of the excited nuclei could considerably be accelerated and therefore the reduction of delay times D1 to 5– 10 s delay between two pulses was made possible. Without addition of the relaxation reagent, a delay time of 60.0 s was determined sufficient for reproducible quantitative ^{29}Si-NMR analyses.

Time-resolved ^{29}Si-NMR monitoring of ongoing polycondensation reactions was obtained by sequential analysis of reaction mixture samples at low temperatures. To this, small samples (0.5 ml) were extracted from the reacting polycondensation mixture at predefined reaction times and immediately frozen in liquid nitrogen to ensure the reaction was stopped. For the NMR experiments, the hard-frozen samples were briefly allowed to liquefy at room temperature, then mixed with a solution chromium(III) acetylacetonate (28.6 mmol/l) and TMS (1170 mmol/l) in d_6-acetone (0.2 ml) and filled into the NMR tube together with and. At -40 °C, 200 – 500 pulses were applied for each spectrum employing a delay time of 5 s for the ^{29}Si nuclei.

For the assignment of NMR chemical shifts, principles known in literature were adopted and modified. In the ^{29}Si case, fruitful considerations are given in references [57], [3], [5], [157], [159], [4], [2], and [169]. Considerable help in the assignment of ^{1}H- and ^{13}C-NMR data of solvents and reactants is found in references [167] and [186], as well as in databases accessible through the world wide web[187]. ^{13}C-NMR signals of pentafluorobenzene (HC_6F_5) were assigned directly according to literature[168].

4.2.2 Solid state NMR

Solid state ^{29}Si-MAS NMR experiments were executed at the Institut für Anorganische Chemie of the University of Würzburg on a Bruker DSX 400 and on a Bruker MSL 300 NMR spectrometer at the Laboratoire de Chimie de la Matière Condensée of Université Pierre et Marie Curie, Paris. 320 – 747 pulses were applied at resonance frequencies of 79.5 MHz (DSX 400) and 59.6 MHz (MSL 300), respectively. Chemical shifts given in [ppm] refer to the external reference, TMS. Quantitative analysis of ^{29}Si-MAS NMR spectra resulted from peak fitting utilizing the *dmfit2001* program package[174]. Line shapes were assumed as purely Gaussian.

4.2.3 Infrared spectroscopy (FT-IR)

FT-IR spectra were recorded on a Nicolet Magna-IR 760 FT-IR spectrometer. Liquid samples were analyzed as films between sodium chloride crystal plates. Solid samples were ground, mixed with potassium bromide (KBr), and analyzed as pellets, which were formed under pressure. Characteristic absorptions were assigned in wavenumbers [cm^{-1}] and characterized as

weak (w), *medium* (m), *strong* (s), or *broad* (br) signals. Assignments were made according to trends reported in the literature on infrared absorption bands in inorganic/organic hybrid polymers[188,176].

4.2.4 Ultraviolet / visible / near-infrared spectroscopy (UV/VIS/NIR)

Absorption spectra in the UV/VIS/NIR region were recorded on a Shimadzu UV-3100 spectrophotometer. For the determination of absorption losses in ORMOCER® resins and alkoxy silanes, samples were measured in Hellma® 10 mm fused silica cuvettes. Resins were pressure filtered over 0.45 µm syringe filters prior to measurement. The losses at 350 nm, 1310 nm, and 1550 nm were specified as dB/cm.

4.2.5 Refractive index measurements

Refractive indices of liquid samples and ORMOCER® resins were determined using an Abbé refractometer manufactured by Carl Zeiss company. For the analysis of solid ORMOCER® thin films, a custom-made prism coupler setup was used enabling measurements at 635 nm, 850 nm, 1310 nm, and 1550 nm. A droplet of methylene iodide acted as immersion agent between the film and the prism.

4.2.6 Small angle X-ray scattering (SAXS)

SAXS experiments were conducted on a Kratky compact camera setup manufactured by Anton Paar KG Company. Samples of ORMOCER® resins were measured as a solution in toluene and propyl acetate, respectively.

4.2.7 Thermogravimetry – differential thermal analysis (TG-DTA)

A Netzsch simultaneous thermal analyzer STA 429 was employed for TG-DTA thermal analyses. Ground samples (10 mg) were set into a platinum crucible and heated at a rate of 10.0 K/min from 20 °C up to 1000 °C under a synthetic air atmosphere. Weight loss (TG) and enthalpy change (DTA) were recorded simultaneously. In accordance to literature[62,92], the thermal stability of a material was determined by a maximum of 5% weight loss up to the respective temperature.

4.2.8 Determination of ORMOCER® thin film optical losses

Optical losses of thin films at 1550 nm were determined at the Fraunhofer Institute for Applied Optics and Precision Engineering (IOF) in Jena, utilizing the cutback method. Laser light was coupled into strip waveguides, and upon cutback of the sample, the outcoupled intensity at the end of the waveguide measured in order to obtain the propagation loss.

4.2.9 Micro indenter measurements

Mechanical properties of thin films were determined with a Fischerscope H100 coating thickness measurement apparatus by using a Berkovich indenter with a test load of 0.4 – 5 mN. The mechanical properties of interest were the universal microhardness HU [N/mm^2], and the elastic (Young's) modulus Y [GPa].

4.2.10 Dielectrical testing

Dielectric constants of ORMOCER® thin films were determined from capacitor multilayer demonstrators, in which the material film is embedded between two micro-patterned copper capacitor plates. The films were analyzed with a Solartron-Schlumberger 1260 Impedance/Gain Phase Analyzer equipped with custom-made analysis software in order to yield the dielectric constant.

4.3 Precursor syntheses

4.3.1 Concurrent synthesis of pentafluorophenyltrimethoxysilane (**1**) and bis-(pentafluorophenyl)dimethoxysilane (**2**)

Composition:

Bromopentafluorobenzene	[246.96 g/mol; 1.94 g/mL]	153 mL ? 296 g	(1200 mmol)
Magnesium turnings	[24.31 g/mol]	32.1 g	(1320 mmol)
1,2-Dibromoethane, some drops			
Diethylether		800 mL	
Tetramethoxysilane	[152.22 g/mol; 1.03 g/mL]	170 mL ? 175 g	(1150 mmol)
n-Heptane		500 mL	

Procedure corresponding to literature[161]:

Under an argon atmosphere and temperature controlled with an ice bath, a solution of bromobenzene (153 mL ? 296 g, 1200 mmol) in dried diethylether (100 mL), was added to an agitated suspension of magnesium turnings (32.1 g, 1320 mmol) and a few drops of 1,2-dibromoethane in dried diethylether (700 mL). The reaction mixture was stirred at 35 °C for 2 h and then cooled down to 0 °C prior to the addition of tetramethoxysilane (170 mL ? 175 g, 1150 mmol). After heating at reflux for an additional 20 h, *n*-heptane (500 mL) was admixed for the precipitation of residual magnesium salts and precipitates were removed by filtration. Volatiles were removed under reduced pressure (40 °C / 35 mbar) and the crude product (284 g brown oil) underwent fractionate vacuum distillation.

Yield (product distribution):

Pentafluorophenyltrimethoxysilane (**1**) [288.24 g/mol] *bp* 52 °C / 5.1 x 10^{-2} mbar:

187 g (649 mmol) ? 68% (primary product).

Bis-(pentafluorophenyl)dimethoxysilane (**2**) [424.26 g/mol] *bp* 75 °C / 5.2 x 10^{-2} mbar:

41.8 g (98.5 mmol) ? 21% (byproduct).

Supporting data:

Pentafluorophenyltrimethoxysilane (**1**)

($C_9H_9F_5O_3Si$) [288.24 g/mol]

(primary product):

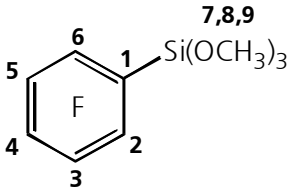

^{1}H-NMR (400 MHz, $CDCl_3$): δ = 3.68 (s, 9 H, 3 x O*C*H_3) ppm.

^{13}C-NMR (101 MHz, $CDCl_3$): δ = 150.9 – 148.1 (dm, 2 C, $|^1J$ (C,F)| = 245.9 Hz, C-3, C-5), 144.6 – 141.7 (dm, 1 C, $|^1J$ (C,F)| = 256.6 Hz, C-4), 138.9 – 136.0 (dm, 2 C, $|^1J$ (C,F)| = 251.7 Hz, C-2, C-6), 103.5 (td, 1 C, $|^2J$ (C,F)| = 31.1 Hz, $|^4J$ (C,F)| = 3.9 Hz, C-1), 51.3 (s, 3 C, 3 x O*C*H$_3$) ppm.

^{29}Si-NMR (79.5 MHz, $CDCl_3$): δ = -63.1 (t, $|^3J$ (Si,F)| = 3.9 Hz) ppm.

IR (film): $\tilde{\nu}$ = 2953 (m), 2852 (m), 1645 (m), 1519 (s), 1468 (s), 1386 (w), 1292 (m), 1196 (m), 1094 (s), 973 (s), 834 (m), 692 (m) cm^{-1}.

Refractive index: n_D^{20} = 1.418.

NIR:	**Wavelength**	1310 nm	1550 nm
	Absorption Loss	0.00 dB/cm	0.18 dB/cm

Bis-(pentafluorophenyl)dimethoxysilane (**2**)

($C_{14}H_6F_{10}O_2Si$) [424.26 g/mol]

(secondary product):

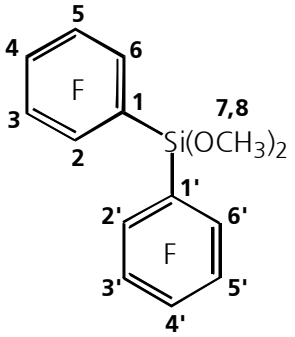

^{1}H-NMR (400 MHz, $CDCl_3$): δ = 3.77 (s, 6 H, 2 x OC*H*$_3$) ppm.

^{13}C-NMR (101 MHz, $CDCl_3$): δ = 150.8 – 148.0 (dm, 4 C, $|^1J$ (C,F)| = 246.9 Hz, C-3, C-3', C-5, C-5'), 145.2 – 142.3 (dtt, 2 C, $|^1J$ (C,F)| = 257.6 Hz, $|^2J$ (C,F)| = 13.6 Hz, $|^3J$ (C,F)| = 5.8 Hz, C-4, C-4'), 139.1 – 136.1 (dm, 4 C, $|^1J$ (C,F)| = 253.7 Hz, C-2, C-2', C-6, C-6'), 105.0 (tdm, 2 C, $|^2J$ (C,F)| = 30.1 Hz, $|^4J$ (C,F)| = 2.9 Hz, C-1, C-1'), 52.0 (s, 2 C, 2 x O*C*H$_3$) ppm.

^{29}Si-NMR (79.5 MHz, $CDCl_3$): δ = -44.5 ppm.

IR (film): $\tilde{\nu}$ = 2956 (w), 2855 (w), 1645 (s), 1518 (s), 1471 (s), 1381 (m), 1294 (s), 1196 (s), 1090 (s), 973 (s), 831 (m), 732 (m), 628 (w), 530 (m) cm^{-1}.

Refractive index: n_D^{20} = 1.450.

NIR:	**Wavelength**	1310 nm	1550 nm
	Absorption Loss	0.00 dB/cm	0.10 dB/cm

4.3.2 Synthesis of 1-bromo-2,3,5,6-tetrafluoro-4-vinylbenzene (**3**)

Composition:

1,4-Dibromotetrafluorobenzene	[307.88 g/mol]	154 g	(500 mmol)
Magnesium turnings	[24.31 g/mol]	12.2 g	(500 mmol)
Iodine, some crystals			
Acetaldehyde	[44.05 g/mol], 0.78 g/mL	65.0 mL ? 50.7 g	(1150 mmol)
Tetrahydrofuran		565 mL	
Ice		450 g	
Hydrochloric acid conc. aq. soln.		110 mL	
Diethylether		600 mL	
Sodium carbonate 10 wt.% aq. soln.		120 mL	
Water		500 mL	
Sodium sulfate, anhydrous			
2,5-Di-*tert.*-butylhydroquinone	[222.33 g/mol]	3.00 g	(13.5 mmol)
Phosphorous(V) oxide P_4O_{10}	[238.88 g/mol]	59.8 g	(250 mmol)

Procedure corresponding to literature[50]:

Under an argon atmosphere and cooled with an ice bath, to a solution of 1,4-dibromotetrafluorobenzene (154 g, 500 mmol) and some iodine crystals in tetrahydrofuran (500 mL), magnesium (12.2 g, 500 mmol) was added in portions over a period of 15 min. The strongly exothermic reaction was controlled using the ice bath to keep the reaction temperature at 50 °C for another 1¼ h prior to completing the forming of the Grignard reagent by heating to reflux for an additional 1 h. After cooling the solution to 2 °C, a solution of acetaldehyde (65.0 ml ? 50.7 g (1150 mmol) in tetrahydrofuran (65 mL) was added dropwise during 40 min so as to keep the reaction temperature below 15 °C. The solution was agitated at 0-10 °C for 1¾ h prior to stirring at room temperature (19 °C) for an additional 17 h. The brownish black mixture was poured onto hydrochloric acid (140 mL conc. aq. soln.) mixed with ice (550 g) and stirred for 15 min. Organic components were extracted with diethylether (5 x 125 mL), the combined organic extracts washed with sodium carbonate (2 x 125 mL 10 wt.% aq. soln.) and water (2 x 125 mL) and dried over anhydrous sodium sulfate. After addition of 2,5-di-*tert.*-butylhydroquinone (3.00 g, 13.5 mmol) as radical inhibitor, volatiles were removed under reduced pressure (52 °C / 38 mbar). The crude product (178 g viscous brown oil) was dehydrated without undergoing an extra isolation step by heating with phosphorous(V) oxide P_4O_{10} (59.8 g, 250 mmol) at 160 °C for 2.5 h. Isolation of the pure product was achieved by fractionate vacuum distillation and crystallization at -25 °C.

Yield:

1-Bromo-2,3,5,6-tetrafluoro-4-vinylbenzene (**3**) [254.81 g/mol] *bp* 37 °C / 0.9 mbar:

58.3 g (229 mmol) ? 46% (literature[50]: 52%).

Supporting data:

1-Bromo-2,3,5,6-tetrafluoro-4-vinylbenzene (**3**)

($C_8H_3BrF_4$) [254.81 g/mol]:

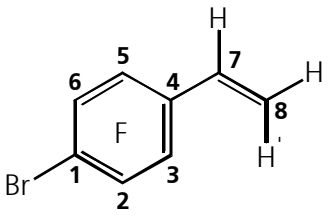

^{1}H-NMR (400 MHz, $CDCl_3$): δ = 6.66 (dd, 1 H, ^3J (E) = 18.1, ^3J (Z) = 11.6 Hz, 7-H), 6.13 (d, 1 H, ^3J (E) = 18.1 Hz, 8-H'), 5.76 (d, 1 H, ^3J (Z) = 11.6 Hz, 8-H) ppm.

^{13}C-NMR (101 MHz, $CDCl_3$): δ = 146.5 – 143.3 (dm, 4 C, $|^1J$ (C,F)| = 248.8 Hz, C-2, C-3, C-5, C-6), 124.4 (t, 1 C, $|^3J$ (C,F)| = 7.8 Hz, C-7), 122.1 (s, 1 C, C-8), 116.3 (t, 1 C, $|^2J$ (C,F)| = 13.6 Hz, C-4), 98.4 (t, 1 C, $|^2J$ (C,F)| = 22.4 Hz, C-1) ppm.

4.3.3 Synthesis of 4-vinyltetrafluorophenyltrimethoxysilane (**4**)

Composition:

1-Bromo-2,3,5,6-tetrafluoro-4-vinylbenzene (**3**)	[254.81 g/mol]	63.8 g	(250 mmol)
Magnesium turnings	[24.31 g/mol]	6.81 g	(280 mmol)
Iodine, some crystals			
Diethylether		250 mL	
Tetramethoxysilane	[152.22 g/mol]	152 g	(1000 mmol)
n-Heptane		200 mL	
2,5-Di-*tert*.-butylhydroquinone	[222.33 g/mol]	1.20 g	(5.40 mmol)

Procedure corresponding to literature[161]:

Under an argon atmosphere and temperature controlled with an ice bath, a solution of 1-bromo-2,3,5,6-tetrafluoro-4-vinylbenzene (**3**) (59.6 g, 234 mmol) in dried diethylether (50 mL), was added to an agitated suspension of magnesium turnings (6.81 g, 280 mmol) and a few iodine crystals in dried diethylether (200 mL). The reaction mixture was stirred at 35 °C for 30 min and then cooled down to 0 °C prior to the addition of tetramethoxysilane (152 g, 1000 mmol). After heating at reflux for an additional 20 h, *n*-heptane (200 mL) was admixed for the precipitation of residual magnesium salts and precipitates were removed by filtration. 2,5-Di-*tert*.-butylhydroquinone was added as radical inhibitor, volatiles were removed under

reduced pressure (40 °C / 20 mbar) and the pure compound isolated by fractionate vacuum distillation and crystallization at -25 °C.

Yield:

4-Vinyltetrafluorophenyltrimethoxysilane (**4**) [296.29 g/mol] *bp* 84 °C / 0.8 mbar:

36.7 g (124 mmol) ? 50% (literature[161]: 55%).

Supporting data:

4-Vinyltetrafluorophenyltrimethoxysilane (**4**)

($C_{11}H_{12}F_4O_3Si$) [296.29 g/mol]:

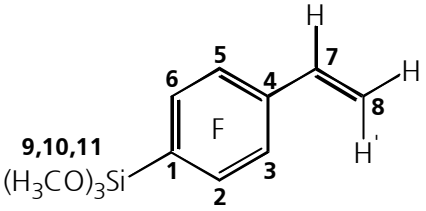

^{1}H-NMR (400 MHz, $CDCl_3$): δ = 6.70 (dd, 1 H, ^3J (E) = 18.1 Hz, ^3J (Z) = 12.1 Hz, 7-H), 6.15 (d, 1 H, ^3J (E) = 18.1 Hz, 8-H'), 5.74 (d, 1 H, ^3J (Z) = 12.1 Hz, 8-H), 3.65 (s, 9 H, 3 x OCH_3) ppm.

^{13}C-NMR (101 MHz, $CDCl_3$): δ = 150.6 – 147.8 (dtm, 2 C, $|^1J$ (C,F)| = 244.9 Hz, $|^2J$ (C,F)| = 13.6 Hz, C-3, C-5), 145.9 – 143.1 (dm, 1 C, $|^1J$ (C,F)| = 253.2 Hz, C-2, C-6), 124.5 (s, 1 C, $|^4J$ (C,F)| = 7.8 Hz, C-8), 122.8 (s, 1 C, C-7), 119.3 (t, 1 C, $|^1J$ (C,F)| = 13.1 Hz, C-4), (106.8 (t, 1 C, $|^2J$ (C,F)| = 31.1 Hz, C-1), 50.8 (s, 3 C, 3 x OCH_3) ppm.

^{29}Si-NMR (79.5 MHz, $CDCl_3$): δ = -62.5 ppm.

IR (film): $\tilde{\nu}$ = 2950 (m), 2850 (m), 1641 (m), 1460 (m), 1416 (s), 1277 (m), 1264 (s), 1196 (s), 1101 (s), 998 (m), 945 (s), 830 (s), 692 (m) cm^{-1}.

Refractive index: n_D^{20} = 1.504.

NIR:	**Wavelength**	1310 nm	1550 nm
	Absorption Loss	0.24 dB/cm	0.32 dB/cm

4.3.4 Synthesis of pentafluorophenyl(vinyl)dimethoxysilane (**5**)

Composition:

Bromopentafluorobenzene	[246.96 g/mol; 1.94 g/mL]	102 mL ? 198 g	(800 mmol)
Magnesium turnings	[24.31 g/mol]	21.8 g	(900 mmol)
Iodine, some crystals			
Diethylether		1100 mL	
Vinyltrimethoxysilane	[148.24 g/mol; 1.13 g/mL]	262 mL ? 296 g	(2000 mmol)
n-Heptane		500 mL	
2,5-Di-*tert.*-butylhydroquinone	[222.33 g/mol]	2.40 g	(10.8 mmol)

Procedure:

Under an argon atmosphere, bromobenzene (102 mL ? 198 g, 800 mmol), dissolved in dried diethylether (800 mL), was added dropwise to a suspension of magnesium turnings (21.8 g, 900 mmol) and a couple of iodine crystals in dried diethylether (100 mL) over a period of 45 min. An ice bath was used to control the exothermic reaction. After further stirring at 35 °C for 1½ h the reaction mixture was allowed to cool down to room temperature (19 °C). Vinyltrimethoxysilane (262 mL ? 296 g, 2000 mmol), dissolved in dried diethylether (200 mL), was added at once and the mixture heated at reflux for an additional 18 h. For the precipitation of residual magnesium salts, *n*-heptane (400 mL) was admixed and precipitates were removed by filtration and centrifugation (3000 min^{-1} / 15 min). After addition of 2,5-di-*tert.*-butylhydroquinone (2.40 g, 10.8 mmol) as radical inhibitor, volatiles were removed under reduced pressure (47 °C / 20 mbar) and the crude product (222 g viscous brown oil) underwent fractionate vacuum distillation.

Yield:

Pentafluorophenyl(vinyl)dimethoxysilane [284.26 g/mol] *bp* 73 °C / 5 mbar:

166 g (584 mmol) ? 73%.

Supporting data:

Pentafluorophenyl(vinyl)dimethoxysilane (**5**)

($C_{10}H_9F_5O_2Si$) [284.26 g/mol]:

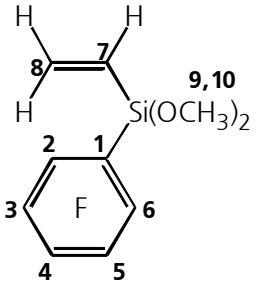

^{1}H-NMR (400 MHz, $CDCl_3$): δ = 6.30 - 6.03 (m, 3 H, Si-C*H*=C*H*$_2$), 3.68 (s, 9 H, 3 x OC*H*$_3$) ppm.

^{13}C-NMR (101 MHz, $CDCl_3$): δ = 151.1 – 148.0 (dm, 2 C, $|^1J$ (C,F)| = 244.9 Hz, C-3, C-5), 144.7 – 141.6 (dm, 1 C, $|^1J$ (C,F)| = 255.6 Hz, C-4), 139.2 – 136.0 (dm, 2 C, $|^1J$ (C,F)| = 252.7 Hz, C-2, C-6), 137.6 (s, 1 C, C-8), 129.9 (s, 1 C, C-7), 105.6 (t, 1 C, $|^2J$ (C,F)| = 32.1 Hz, C-1), 51.0 (s, 2 C, 2 x O*C*H$_3$) ppm.

^{29}Si-NMR (79.5 MHz, $CDCl_3$, $Cr(acac)_3$): δ = -36.9 ppm.

IR (film): $\tilde{\nu}$ = 3065 (w), 2951 m), 2847 (m), 1644 (s), 1598 (w), 1518 (s), 1456 (s), 1407 (m), 1381 (m), 1290 (s), 1194 (s), 1089 (s), 1009 (m), 970 (s), 822 (s), 785 (s), 745 (w), 662 (s), 625 (w), 585 (w), 550 (s) cm^{-1}.

Refractive index: n_D^{20} = 1.436.

NIR:	**Wavelength**	1310 nm	1550 nm
	Absorption Loss	0.18 dB/cm	0.24 dB/cm

4.3.5 Synthesis of pentafluorophenyl(methyl)dimethoxysilane (**6**)

Composition:

Bromopentafluorobenzene	[246.96 g/mol; 1.94 g/mL]	12.7 mL ?	24.7 g	(100 mmol)
Magnesium turnings	[24.31 g/mol]		2.67 g	(110 mmol)
Iodine, some crystals				
Diethylether			140 mL	
Methyltrimethoxysilane	[136.23 g/mol; 0.955 g/mL]	35.7 ml ?	34.1 g	(250 mmol)
n-Heptane			60 mL	

Procedure:

Under an argon atmosphere, bromobenzene (12.7 mL ? 24.7 g, 100 mmol), dissolved in dried diethylether (100 mL), was added dropwise to a suspension of magnesium turnings (2.67 g, 110 mmol) and some iodine crystals in dried diethylether (15 mL) over a period of 25 min. An ice bath was used to control the exothermic reaction. After further stirring at 35 °C for 1½ h the reaction mixture was allowed to cool down to room temperature (19 °C). Methyltrimethoxysilane (35.7 mL ? 34.1 g, 250 mmol), dissolved in dried diethylether (25 mL), was added at once and the mixture heated at reflux for an additional 19 h. For the precipitation of residual magnesium salts, *n*-heptane (60 mL) was admixed and precipitates were removed by filtration. Volatiles were removed under reduced pressure (43 °C / 7 mbar) and the crude product (22 g light-brown liquid) underwent fractionate vacuum distillation.

Yield:

Pentafluorophenyl(methyl)dimethoxysilane [272.25 g/mol] *bp* 51 °C / 2 mbar:

15.0 g (55.1 mmol) ? 55%.

Supporting data:

Pentafluorophenyl(methyl)dimethoxysilane (**6**)

($C_9H_9F_5O_2Si$) [272.25 g/mol]:

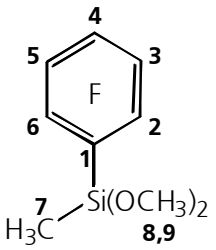

^{1}H-NMR (400 MHz, $CDCl_3$): δ = 3.62 (s, 6 H, 2 x OC*H*$_3$), 0.47 (t, 3 H, |^5J (H,F)| = 1.5 Hz, 7-H) ppm.

^{13}C-NMR (101 MHz, $CDCl_3$): δ = 150.7 – 147.9 (dm, 2 C, |^1J (C,F)| = 244.4 Hz, C-3, C-5), 144.4 – 141.4 (dtt, 1C, |^1J (C,F)| = 256.6 Hz, |^2J (C,F)| = 13.4 Hz, |^3J (C,F)| = 6.0 Hz, C-4), 138.9 – 136.0 (dm, 2 C, |^1J (C,F)| = 253.7 Hz, C-2, C-6), 107.1 – 106.3 (tm, 1 C, |^2J (C,F)| = 32.1 Hz, C-1), 50.7 (s, 2 C, 2 x OCH_3), -2.8 (s, 1 C, C-7) ppm.

^{29}Si-NMR (79.5 MHz, $CDCl_3$): δ = -20.6 (t, |^3J (Si,F)| = 3.1 Hz) ppm.

IR (film): $\tilde{\nu}$ = 2950 (w), 2847 (w), 1644 (m), 1519 (s), 1460 (s), 1379 (w), 1289 (w), 1266 (w), 1193 (m), 1091 (s), 972 (s), 850 (m), 809 (m), 769 (m), 665 (w) cm^{-1}.

Refractive index: n_D^{20} = 1.426.

NIR:	**Wavelength**	1310 nm	1550 nm
	Absorption Loss	0.02 dB/cm	0.54 dB/cm

4.3.6 Synthesis of phenyl(vinyl)dimethoxysilane (**7**)

Composition:

Bromobenzene	[157.02 g/mol; 1.494 g/mL]	42.0 mL ?	62.8 g	(400 mmol)
Magnesium	[24.31 g/mol]		10.9 g	(450 mmol)
Iodine, some crystals				
Diethylether			550 mL	
Vinyltrimethoxysilane	[148.24 g/mol; 1.13 g/mL]	106 mL ?	118 g	(800 mmol)
n-Heptane			250 mL	

Procedure:

Under an argon atmosphere, bromobenzene (42.0 mL ? 62.8 g, 400 mmol), dissolved in dried diethylether (400 mL), was added dropwise to a suspension of magnesium turnings (10.9 g, 450 mmol) and a couple of iodine crystals in dried diethylether (50 mL) over a period of 55 min. An ice bath was used to control the exothermic reaction. After further stirring at 35 °C for 1½ h the reaction mixture was transferred to a dropping funnel and within 2h added dropwise to a solution of vinyltrimethoxysilane (65.9 mL ? 74.1 g, 500 mmol) in dried diethylether (50 mL), cooled to 5 °C. The mixture was allowed to warm up to room temperature (19 °C) and left stirring for an additional 18 h. *n*-Heptane (250 mL) was admixed for the precipitation of residual magnesium salts and precipitates were removed by filtration. After addition of 2,5-di-*tert.*-butylhydroquinone (0.8 g) as radical inhibitor, volatiles were removed under reduced pressure (48 °C / 23 mbar) and the crude product (64.1 g yellowish liquid) underwent fractionate vacuum distillation over a Vigreux column.

Yield:

Phenyl(vinyl)dimethoxysilane (**7**) [194.31 g/mol] *bp* 45 °C / 1.9 x 10^{-1} mbar:

36.74 g (189 mmol) ? 47%.

Supporting data:

Phenyl(vinyl)dimethoxysilane (**7**)

($C_{10}H_{14}O_2Si$) [194.31 g/mol]:

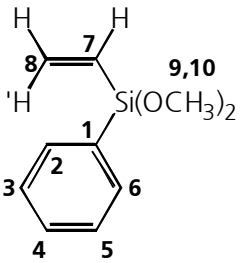

^{1}H-NMR (400 MHz, $CDCl_3$): δ = 7.63 (dd, 2H, ^3J (*ortho*) = 7.5, ^4J (*meta*) = 1.5 Hz, 2-H, 6-H), 7.44-7.33 (m, 3 H, 3-H, 4-H, 5-H), 6.20 (dd, 1 H, ^3J (E) = 15.1 Hz, ^3J (Z) = 5.0 Hz, 7-H), 6.13 (dd, 1 H, $|^2J$ (*geminal*)| = 19.6 Hz, ^3J (E) = 15.1 Hz, 8-H'), 5.96 (dd, 1 H, $|^2J$ (*geminal*)| = 19.6 Hz, ^3J (Z) = 5.0 Hz, 8-H), 3.58 (s, 6 H, 2 x OCH_3) ppm.

^{13}C-NMR (101 MHz, $CDCl_3$): δ = 137.3 (s, 1 C, C-8), 134.6 (s, 2 C, C-2, C-6), 132.2 (s, 1 C, C-1), 131.2 (s, 1 C, C-4), 130.4 (s, 1 C, C-7), 127.9 (s, 2 C, C-3, C-5), 50.7 (s, 3 C, 2 x OCH_3) ppm.

^{29}Si-NMR (79.5 MHz, $CDCl_3$): δ = -29.6 ppm.

IR (film): $\tilde{\nu}$ = 3071 (w), 3053 (w), 2940 (m), 2837 (m), 1594 (w), 1430 (m), 1405 (w), 1190 (m), 1122 (s), 1075 (s), 1009 (w), 967 (w), 808 (s), 769 (m), 739 (s), 727 (s), 701 (m), 641 (w), 548 (w) cm^{-1}.

Refractive index: n_D^{20} = 1.492.

NIR:	**Wavelength**	1310 nm	1550 nm
	Absorption Loss	0.44 dB/cm	0.44 dB/cm

4.3.7 Concurrent synthesis of phenyl(vinyl)dimethoxysilane (**7**) and diphenyl(vinyl)methoxysilane (**8**)

Composition:

Bromobenzene	[157.02 g/mol; 1.494 g/mL]	21.0 mL ? 31.4 g	(200 mmol)
Magnesium turnings	[24.31 g/mol]	5.47 g	(225 mmol)
Iodine, some crystals			
Diethylether		275 mL	
Vinyltrimethoxysilane	[148.24 g/mol; 1.13 g/mL]	65.9 mL ? 74.1 g	(500 mmol)
n-Heptane		125 mL	

Procedure:

Under an argon atmosphere, bromobenzene (21.0 mL ? 31.4 g, 200 mmol), dissolved in dried diethylether (200 mL), was added dropwise to a suspension of magnesium turnings (5.47 g, 225 mmol) and a couple of iodine crystals in dried diethylether (25 mL) over a period of 60 min. An ice bath was used to control the exothermic reaction. After further stirring at 35 °C for 1½ h the reaction mixture was allowed to cool down to room temperature (19 °C). Vinyltrimethoxysilane (65.9 mL ? 74.1 g, 500 mmol), dissolved in dried diethylether (50 mL), was added at once and the mixture stirred at room temperature for an additional 18 h. For the precipitation of residual magnesium salts, *n*-heptane (125 mL) was admixed and precipitates were removed by filtration. After addition of 2,5-di-*tert.*-butylhydroquinone (0.3 g) as radical inhibitor, volatiles were removed under reduced pressure (47 °C / 7 mbar) and the crude product (22.7 g yellow liquid) underwent fractionate vacuum distillation.

Yield (product distribution):

Phenyl(vinyl)dimethoxysilane (**7**) [194.31 g/mol] *bp* 45 °C / 1.9 x 10^{-1} mbar:

9.54 g (49 mmol) ? 25% (primary product).

Diphenyl(vinyl)methoxysilane (**8**) [240.38 g/mol] *bp* 105 °C / 6.5 x 10^{-1} mbar:

9.82 g (41 mmol) ? 20% (byproduct).

Supporting data:

Phenyl(vinyl)dimethoxysilane (**7**)

($C_{10}H_{14}O_2Si$) [194.31 g/mol]: [see above]

(primary product)

Diphenyl(vinyl)methoxysilane (**8**)

($C_{15}H_{16}OSi$) [240.38 g/mol]:

(byproduct)

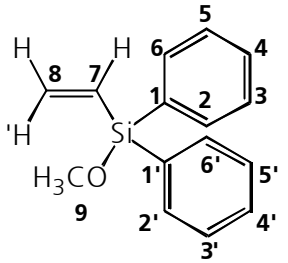

^{1}H-NMR (400 MHz, $CDCl_3$): δ = 7.60 (dd, 4H, ^3J (*ortho*) = 7.5, ^4J (*meta*) = 1.5 Hz, 2-H, 2'-H, 6-H, 6'-H), 7.43-7.30 (m, 6H, 3-H, 3'-H, 4-H, 4'-H, 5-H, 5'-H), 6.47 (dd, 1 H, $|^2J$ (*geminal*)| = 20.6 Hz, ^3J (E) = 15.1 Hz, 8-H'), 6.27 (dd, 1 H, ^3J (E) = 15.1 Hz, ^3J (Z) = 4.0 Hz, 7-H), 5.91 (dd, 1 H, $|^2J$ (*geminal*)| = 20.6 Hz, ^3J (Z) = 4.0 Hz, 8-H), 3.58 (s, 3 H, OCH_3) ppm.

^{13}C-NMR (101 MHz, $CDCl_3$): δ = 137.1 (s, 1 C, C-8), 135.0 (s, 4 C, C-2, C-2', C-6, C-6'), 134.0 (s, 2 C, C-1, C-1'), 133.1 (s, 2 C, C-4, C-4'), 130.1 (s, 1 C, C-7), 127.9 (s, 4 C, C-3, C-3', C-5, C-5'), 51.6 (s, 1 C, OCH_3) ppm.

^{29}Si-NMR (79.5 MHz, $CDCl_3$): δ = -13.0 ppm.

IR (film): $\tilde{\nu}$ = 3069 (m), 3051 (m), 3010 (m), 2943 (m), 2834 (m), 1591 (m), 1486 (w), 1429 (s), 1405 (m), 1264 (w), 1188 (m), 1119 (s), 1085 (s), 1009 (m), 965 (m), 777 (s), 739 (s), 712 (s), 700 (s), 648 (m), 554 (m) cm^{-1}.

Refractive index: n_D^{20} = 1.560.

4.3.8 Reaction of pentafluorobenzyl bromide with magnesium and tetramethoxysilane I (two-step approach)

Composition:

Pentafluorobenzyl bromide	[260.99 g/mol; 1.728 g/mL]	15.1 mL ?	26.1 g	(100 mmol)
Magnesium turnings	[24.31 g/mol]		2.67 g	(110 mmol)
Iodine, some crystals				
Tetramethoxysilane	[152.22 g/mol; 1.03 g/mL]	14.8 ml ?	15.2 g	(100 mmol)
Tetrahydrofuran			100 mL	
n-Heptane			35 mL	

Procedure:

Under an argon atmosphere, pentafluorobenzyl bromide (15.1 mL ? 26.1 g, 100 mmol), dissolved in tetrahydrofuran (40 mL) was added dropwise, over a period of 4 h, to a suspension of magnesium turnings (2.67 g, 110 mmol) and some iodine crystals in tetrahydrofuran (10 mL). The strongly exothermic reaction was controlled using an ice bath to keep the reaction temperature at 65 °C. After heating another 2 h to reflux and following cooling to room temperature (19 °C), tetramethoxysilane (14.8 mL ? 15.2 g, 100 mmol), dissolved in tetrahydrofuran (50 mL), was added prior to heating to reflux for an additional 23 h. For the precipitation of residual magnesium salts, *n*-heptane (25 mL) was admixed at ambient temperature and precipitates were removed by filtration and washed with *n*-heptane. Volatiles were removed under reduced pressure (50 °C / 4 mbar) and the crude product analyzed with ^{1}H-, ^{13}C-, and ^{29}Si-NMR. The crude product underwent no further purification.

Crude product:

19.9 g colorless solid.

Characterization:

1,2-Bis(pentafluorophenyl)ethane (**10**) ($C_{14}H_4F_{10}$) [362.17 g/mol], >90% purity:

approx. 17.9 g (49.5 mmol), >95% yield.

No silane compounds.

Supporting data:

1,2-Bis-(pentafluorophenyl)ethane (**10**)
($C_{14}H_4F_{10}$) [362.17 g/mol]:

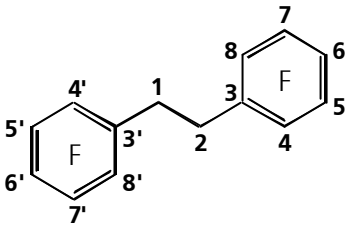

^{1}H-NMR (400 MHz, $CDCl_3$): δ = 3.01 (s, 4 H, 1-H, 2-H) ppm.

^{13}C-NMR (101 MHz, $CDCl_3$): δ = 146.4 – 143.7 (dm, 4 C, $|^{1}J$ (C,F)| = 251.7 Hz, C-4, C-4', C-8, C-8'), 141.6 – 138.4 (dm, 2 C, $|^{1}J$ (C,F)| = 248.8 Hz, C-6, C-6'), 138.0 – 136.0 (dm, 4 C, $|^{1}J$ (C,F)| = 251.7 Hz, C-5, C-5', C-7, C-7'), 112.3 (td, 2 C, $|^{2}J$ (C,F)| = 19.4 Hz, $|^{4}J$ (C,F)| = 4.9 Hz, C-3, C-3'), 21.8 (s, 2 C, C-1, C-2) ppm.

^{29}Si-NMR (79.5 MHz, $CDCl_3$): no signal.

^{1}H and ^{13}C-NMR peak assignments correspond to literature[164].

4.3.9 Reaction of pentafluorobenzyl bromide with magnesium and tetramethoxysilane II (one-pot approach)

Composition:

Pentafluorobenzyl bromide	[260.99 g/mol; 1.728 g/mL]	15.1 mL ?	26.1 g	(100 mmol)
Tetramethoxysilane	[152.22 g/mol; 1.03 g/mL]	14.8 ml ?	15.2 g	(100 mmol)
Magnesium turnings	[24.31 g/mol]		3.16 g	(130 mmol)
1,2-Dibromoethane	[187.89 g/mol]		4.70 g	(25 mmol)
Diethylether			40 mL	
n-Heptane			35 mL	

Procedure:

Under an argon atmosphere, pentafluorobenzyl bromide (15.1 mL ? 26.1 g, 100 mmol), tetramethoxysilane (14.8 mL ? 15.2 g, 100 mmol), magnesium turnings (3.16 g, 130 mmol) and 1,2-dibromoethane (4.70 g, 25 mmol) were mixed and diethylether (40 mL) was added. After applying heat for 30 min, the exothermal reaction commenced and the reaction mixture was agitated for another 30 min prior to heating at reflux for additional 20 h. For the precipitation of residual magnesium salts, *n*-heptane (35 mL) was admixed at ambient temperature and precipitates were removed by filtration and washed with *n*-heptane. Volatiles were removed under reduced pressure (50 °C / 24 mbar) and the crude product analyzed with ^{1}H-, ^{13}C-, and ^{29}Si-NMR. A number of NMR signals could be assigned to (pentafluorophenylmethyl)trimethoxysilane (**9**). Isolation by distillation or crystallization failed due to low concentration.

Crude product:

13.2 g viscous brown oil.

Characterization resulting from quantitative cross-analysis of spectra:

(Pentafluorophenylmethyl)trimethoxysilane (**9**)

(secondary product)

($C_{10}H_{11}F_5O_3Si$) [302.27 g/mol]:

approx. 5 mmol (1.4 g), 5%.

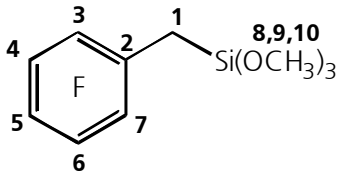

1,2-Bis-(pentafluorophenyl)ethane (**10**)

(primary product)

($C_{14}H_4F_{10}$) [362.17 g/mol]:

approx. 8 mmol (2.9 g), 16%.

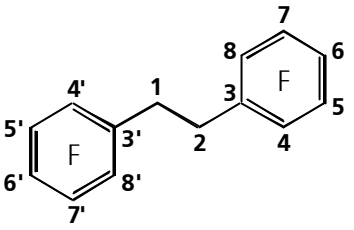

Supporting data:

^{1}H-NMR (400 MHz, $CDCl_3$): δ = 4.51 (s, C_6F_5-CH_2-Br), 3.64 – 3.51 (m, OCH_3), 3.04 (s, 1-H, 2-H [C_6F_5-CH_2CH_2-C_6F_5]), 2.26 – 2.17 (m, C_6F_5-CH_2-Si(OCH_3) ppm.

^{13}C-NMR (101 MHz, $CDCl_3$): δ = 146.6 – 136.1 (m, arylic *C*-F), 113.0 (td, $|^2J$ (C,F)| = 18.5 Hz, $|^4J$ (C,F)| = 3.9 Hz, quaternary arylic [C_6F_5-CH_2-Br]), 112.3 (td, $|^2J$ (C,F)| = 17.5 Hz, $|^4J$ (C,F)| = 3.9 Hz, C-3, C-3' [C_6F_5-CH_2CH_2-C_6F_5]), 51.4 (O-CH_3), 51.3 (TMOS), 51.0 (O-CH_3), 21.9 (s, C-1, C-2 [C_6F_5-CH_2CH_2-C_6F_5]), 16.0 (C_6F_5-CH_2-Br), 5.6 (traces, C_6F_5-CH_2-Si(OCH_3)$_3$) ppm.

^{29}Si-NMR (79.5 MHz, $CDCl_3$): δ = -51.0 ppm (C_6F_5-CH_2-*Si*(OCH_3)$_3$), -78.4 (TMOS), -85.1 – -86.2 (Q^1), -93.8 – -94.0 (Q^2).

^{1}H and ^{13}C-NMR peak assignments of 1,2-bis-(pentafluorophenyl)ethane (**10**) correspond to literature[164].

4.3.10 Reaction of pentafluorostyrene with trimethoxysilane under hydrosilylation conditions

Composition:

2,3,4,5,6-Pentafluorostyrene	[194.10 g/mol; 1.428 g/mL]	6.80 mL ? 9.71 g	(50.0 mmol)
Trimethoxysilane	[122.20 g/mol; 0.957 g/mL]	6.38 mL ? 6.11 g	(50.0 mmol)
Platinum(0) divinyltetramethyldisiloxane-complex in xylene (Karstedt's catalyst; 2.1-2.4 wt.% Pt^0 [195.08 g/mol])		0.05 – 0.50 g soln. (1 – 10 mg "Pt^0")	(0.005 – 0.05 mmol Pt^0)
Toluene		25 mL	

Procedure:

To a solution of 2,3,4,5,6-pentafluorostyrene (6.80 mL ? 9.71 g, 50.0 mmol) in toluene (15 mL), Karstedt's catalyst (0.05 g soln., 2.1-2.4 wt.% soln. in xylene, 0.005 mmol Pt^0) was added and the mixture stirred under air for 30 min. Subsequently, trimethoxysilane (6.38 mL ? 6.11 g, 50.0 mmol), dissolved in toluene (10 mL), was admixed dropwise over a period of 15 min prior to putting the solution under an argon atmosphere and stirring at 19 °C

for an additional 18 h. Because ^{1}H- and ^{29}Si-NMR of the reaction mixture showed educt conversion of less than 10%, the mixture was heated at 55 °C for 16 h. The mixture was analyzed by NMR and the reaction products underwent no further purification.

Characterization resulting from quantitative cross-analysis of spectra:

Tetramethoxysilane (TMOS, primary product)
($C_4H_{12}O_4Si$) [152.2 g/mol]:
approx. 20 mmol (3.04 g), 40%.

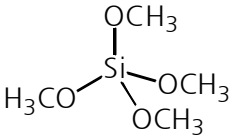

2-(Pentafluorophenyl)ethyltrimethoxysilane (**11**)
(secondary product)
($C_{11}H_{13}F_5O_3Si$) [316.30 g/mol]:
approx. 3 mmol (0.79 g), 5%.

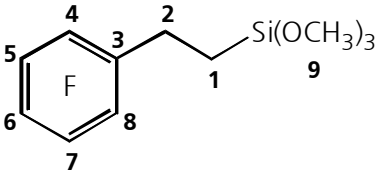

Supporting data:

^{1}H-NMR (400 MHz, Toluene, d_6-Acetone, $Cr(acac)_3$): δ = 6.53 (dd, *J* = 17.57, 11.52 Hz, 7-H [C_6F_5-CH=CH_2]), 5.97 (d, *J* = 17.57 Hz, 8-H' [C_6F_5-CH=CH_2]), 5.65 (d, *J* = 11.52 Hz, 8-H [C_6F_5-CH=CH_2]), 4.15 (*H*-Si [$HSi(OCH_3)_3$]), 3.50 (4 x OCH_3 [TMOS]), 3.49 (3 x OCH_3 [$HSi(OCH_3)_3$]), 3.33 (3 x OCH_3 [C_6F_5-CH_2CH_2-$Si(OCH_3)_3$]), 2.73 (m, 2-H [C_6F_5-CH_2CH_2-$Si(OCH_3)_3$]), 0.89 (1-H [C_6F_5-CH_2CH_2-$Si(OCH_3)_3$]) ppm.

^{13}C-NMR (101 MHz, Toluene, d_6-Acetone, $Cr(acac)_3$): δ = 146 – 136 (m, C-4, C-5, C-6, C-7, C-8 [C_6F_5-CH_2CH_2-$Si(OCH_3)_3$]), 146.9 – 144.1 (m, C-3, C-5 [C_6F_5-CH=CH_2]), 142.1 – 139.5 (m, C-4 [C_6F_5-CH=CH_2]), 139.5 – 136.8 (m, C-2, C-6 [C_6F_5-CH=CH_2]), 124.1 (s, C-8 [C_6F_5-CH=CH_2]), 121.9 (s, C-7 [C_6F_5-CH=CH_2]), 118.3 – 117.7 (m (w), C-3 [C_6F_5-CH_2CH_2-$Si(OCH_3)_3$]), 113.0 (m, C-1 [C_6F_5-CH=CH_2]), 51.7 (s, C-9 [C_6F_5-CH_2CH_2-$Si(OCH_3)_3$]), 51.2 (OCH_3 [TMOS]), 50.6 (s, OCH_3 [Q^1]), 50.0 (s, OCH_3 [$HSi(OCH_3)_3$]), 16.3 (s, C-2 [C_6F_5-CH_2CH_2-$Si(OCH_3)_3$]), 14.0 (s, C-1 [C_6F_5-CH_2CH_2-$Si(OCH_3)_3$]) ppm.

^{29}Si-NMR (79.5 MHz, Toluene, d_6-Acetone, $Cr(acac)_3$): δ = -45.1 (5%, C_6F_5-CH_2CH_2-$Si(OCH_3)_3$), -55.3 (44%, $HSi(OCH_3)_3$), -78.4 (40%, TMOS), -85.4 – -85.7 (11%, Q^1) ppm.

4.3.11 Synthesis of 2-(pentafluorophenyl)ethyltriethoxysilane (**12**)

Composition:

2,3,4,5,6-Pentafluorostyrene	[194.10 g/mol; 1.428 g/mL]	6.80 mL ? 9.71 g	(50.0 mmol)
Triethoxysilane	[164.30 g/mol; 0.896 g/mL]	9.17 mL ? 8.22 g	(50.0 mmol)
Platinum(0) divinyltetramethyldisiloxane-complex in xylene		0.17 g soln.	(0.02 mmol Pt^0)
(Karstedt's catalyst; 2.1-2.4 wt.% Pt^0 [195.08 g/mol])		? 4 mg "Pt^0"	
Toluene		25 mL	

Procedure:

To a solution of 2,3,4,5,6-pentafluorostyrene (6.80 mL ? 9.71 g, 50.0 mmol) in toluene (15 mL), Karstedt's catalyst (0.17 g soln., 2.1-2.4 wt.% soln. in xylene, 0.02 mmol Pt^0) was added and the mixture stirred under air for 30 min. Subsequently, triethoxysilane (9.17 mL ? 8.22 g, 50.0 mmol), dissolved in toluene (10 mL), was admixed dropwise over a period of 15 min prior to putting the solution under an argon atmosphere and heating at 80 °C for an additional 38.5 h. Volatiles were removed under reduced pressure (46 °C / 1 mbar) and the product isolated by fractionate vacuum distillation.

Yield:

2-(Pentafluorophenyl)ethyltriethoxysilane (**12**) [358.38 g/mol] *bp* 50 °C / 2.8 x 10^{-2} mbar:

4.13 g (11.5 mmol) ? 23%.

Supporting data:

2-(Pentafluorophenyl)ethyltriethoxysilane (**12**)
($C_{14}H_{19}F_5O_3Si$) [358.38 g/mol]:

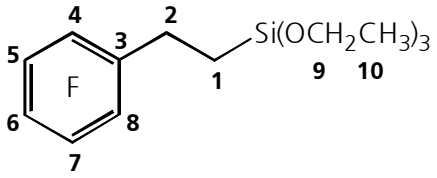

^{1}H-NMR (400 MHz, $CDCl_3$): δ = 3.84 (q, 6 H, ^3J = 7.03 Hz, 9-H), 2.80 (m, 2-H), 1.24 (t, 9 H, ^3J = 7.03 Hz, 10-H), 0.94 (m, 1-H) ppm.

^{13}C-NMR (101 MHz, $CDCl_3$): δ = 146.4 – 143.7 (dm, 2 C, $|^1J$ (C,F)| = 244.0 Hz, C-5, C-7), 140.9 – 138.2 (dm, 1 C, $|^1J$ (C,F)| = 250.8 Hz, C-6), 139.0 – 136.2 (dm, 2 C, $|^1J$ (C,F)| = 251.7 Hz, C-4, C-8), 117.7 (td, 1 C, $|^2J$ (C,F)| = 18.5 Hz, $|^4J$ (C,F)| = 3.9 Hz, C-3), 58.5 (s, 3 C, C-9), 18.3 (s, 3 C, C-10), 16.2 (s, 1 C, C-2), 11.1 (s, 1 C, C-1) ppm.

^{29}Si-NMR (79.5 MHz, $CDCl_3$): δ = -48.3 ppm.

IR (film): $\tilde{\nu}$ = 2978 (m), 2930 (w), 2897 (w), 1656 (w), 1518 (s), 1501 (s), 1392 (w), 1299 (w), 1197 (w), 1167 (m), 1155 (m), 1067 (s), 988 (m), 954 (s), 898 (w), 802 (m) cm^{-1}.

Refractive index: n_D^{20} = 1.429.

4.4 Polycondensation reactions

4.4.1 Reaction of bis-(pentafluorophenyl)dimethoxysilane (**2**) with dilute hydrochloric acid in acetone

Composition:

Bis-(pentafluorophenyl)dimethoxysilane (**2**)	[424.26 g/mol]	2.12 g	(5.00 mmol)
Water (hydrochloric acid 0.01 M aq. soln.)	[18.02 g/mol]	0.09 mL	(5.00 mmol water)
Acetone		1.84 mL	

Procedure:

At ambient temperature (19 °C), to a stirred solution of bis-(pentafluorophenyl)dimethoxysilane (**2**) (2.12 g, 5.00 mmol) in acetone (1.84 mL), hydrochloric acid (0.09 mL 0.01 M aq. soln. ? 5.00 mmol water) was added and the solution left stirring. The ongoing reaction was monitored by NMR (samples analyzed after 1 d and 6 d). After 6 d, volatile compounds were removed *in vacuo* (0.1 mbar) leading to gelation of the reaction mixture.

Characterization after 1 d reaction time:

^{1}H-NMR (400 MHz, Acetone-d_6, Cr(acac)$_3$): δ = 7.46 – 7.32 (m, *H*C$_6$F$_5$), 3.83 – 3.48 (m, Si-OC*H*$_3$), 3.32 (s, C*H*$_3$OH) ppm.

^{13}C-NMR (101 MHz, Acetone-d_6, Cr(acac)$_3$): δ = 152.1 – 148.9 (dm, |^1J (C,F)| = 245.3 Hz, C-3, C-5 [C$_6$F$_5$Si(OR)$_3$, R = CH$_3$,H]), 148.9 – 146.1 (dm, |^1J (C,F)| = 246.9 Hz, C-1, C-4 [HC$_6$F$_5$]), 144.2 – 141.4 (dm, |^1J (C,F)| = 251.7 Hz, C-3 [HC$_6$F$_5$], C-4 [C$_6$F$_5$Si(OR)$_3$, R = CH$_3$, H]), 140.2 – 137.3 (dm, |^1J (C,F)| = 249.8 Hz, C-2, C-4 [HC$_6$F$_5$]), 140.0 – 137.0 (dm, |^1J (C,F)| = 252.7 Hz, C-2, C-6 [C$_6$F$_5$Si(OR)$_3$, R = CH$_3$,H]), 52.0 – 51.2 (m, Si-O*C*H$_3$), 50.0 (s, *C*H$_3$OH) ppm.

^{29}Si-NMR (79.5 MHz, Acetone-d_6, Cr(acac)$_3$): δ = -66.3 – -73.9 (27%, T^1), -75.5 – -83.2 (36%, T^2), -84.4 – -92.1 (37%, T^3) ppm; no D-species.

Characterization after 6 d reaction time, prior to removal of volatiles:

^{1}H-NMR (400 MHz, Acetone-d_6, Cr(acac)$_3$): δ = 7.53 – 7.26 (m, *H*C$_6$F$_5$), 3.80 – 3.48 (m, Si-OC*H*$_3$), 3.32 (s, C*H*$_3$OH) ppm.

^{13}C-NMR (101 MHz, Acetone-d_6, Cr(acac)$_3$): δ = 152.1 – 149.0 (dm, $|^1J$(C,F)| = 248.8 Hz, C-3, C-5 [$C_6F_5Si(OR)_3$, R = CH_3,H]), 149.0 – 146.1 (dm, $|^1J$(C,F)| = 246.9 Hz, C-1, C-4 [HC_6F_5]), 144.3 – 141.3 (dm, $|^1J$(C,F)| = 251.7 Hz, C-3 [HC_6F_5], C-4 [$C_6F_5Si(OR)_3$, R = CH_3,H]), 140.3 – 137.3 (dm, $|^1J$(C,F)| = 248.8 Hz, C-2, C-4 [HC_6F_5]), 140.0 – 137.0 (dm, $|^1J$(C,F)| = 251.7 Hz, C-2, C-6 [$C_6F_5Si(OR)_3$, R = CH_3,H]), 104.4 – 103.1 (C-1 [$C_6F_5Si(OR)_3$, R = CH_3,H]), 102.5 (td, $|^2J$(C,F)| = 23.3 Hz, $|^4J$(C,F)| = 2.9 Hz, C-6 [HC_6F_5]), 52.2 – 51.2 (m, Si-OCH_3), 50.0 (s, CH_3OH) ppm.

^{29}Si-NMR (79.5 MHz, Acetone-d_6, Cr(acac)$_3$): δ = -67.0 – -74.2 (22%, T^1), -74.9 – -81.7 (23%, T^2), -84.3 – -91.1 (55%, T^3) ppm; no D-species.

4.4.2 Reaction of bis-(pentafluorophenyl)dimethoxysilane (**2**) with dilute sodium hydroxide solution in acetone

Composition:

Bis-(pentafluorophenyl)dimethoxysilane (**2**)	[424.26 g/mol]	2.12 g	(5.00 mmol)
Water (sodium hydroxide 0.01 M aq. soln.)	[18.02 g/mol]	0.09 mL	(5.00 mmol water)
Acetone		1.84 mL	

Procedure:

At ambient temperature (19 °C), to a stirred solution of bis-(pentafluorophenyl)dimethoxysilane (**2**) (2.12 g, 5.00 mmol) in acetone (1.84 mL), sodium hydroxide solution (0.09 mL 0.01 M aq. soln. ≙ 5.00 mmol water) was added leading to a strongly exothermic reaction. While the solution was kept stirred the ongoing reaction was monitored by NMR (samples analyzed after 1 d, 6 d and after removal of volatiles). After 6 d, volatile compounds were removed *in vacuo* (40 °C / 5 mbar) leading to the viscous resin **fk02**.

Characterization after 1 d reaction time:

^{1}H-NMR (400 MHz, Acetone-d_6, Cr(acac)$_3$): δ = 7.45 – 7.30 (m, HC_6F_5), 3.64 – 3.55 (m, Si-OCH_3), 3.33 (s, CH_3OH) ppm.

^{13}C-NMR (101 MHz, Acetone-d_6, Cr(acac)$_3$): δ = 149.0 – 146.2 (dm, $|^1J$(C,F)| = 247.8 Hz, C-1, C-4 [HC_6F_5]), 144.3 – 141.4 (dm, $|^1J$(C,F)| = 251.7 Hz, C-3 [HC_6F_5]), 140.2 – 137.4 (dm, $|^1J$(C,F)| = 249.7 Hz, C-2, C-4 [HC_6F_5]), 102.5 (td, $|^2J$(C,F)| = 23.3 Hz, $|^4J$(C,F)| = 2.9 Hz, C-6 [HC_6F_5]), 51.6 – 51.3 (m, Si-OCH_3), 50.0 (s, CH_3OH) ppm.

^{29}Si-NMR (79.5 MHz, Acetone-d_6, Cr(acac)$_3$): δ = -78.4 (13%, Q^0), -85.5 – -86.4 (26%, Q^1), -92.8 – -94.7 (28%, Q^2), -100.9 – -103.6 (33%, Q^3) ppm; no D-/T-species.

Characterization after 6 d reaction time:

^{1}H-NMR (400 MHz, Acetone-d_6, Cr(acac)$_3$): δ = 7.48 – 7.29 (m, *H*C$_6$F$_5$), 3.71 – 3.55 (Si-OC*H*$_3$), 3.33 (C*H*$_3$OH) ppm.

^{13}C-NMR (101 MHz, Acetone-d_6, Cr(acac)$_3$): δ = 149.0 – 146.2 (dm, |^{1}J (C,F)| = 247.0 Hz, C-1, C-4 [HC$_6$F$_5$]), 144.3 – 141.4 (dm, |J (C,F)| = 251.7 Hz, C-3 [HC$_6$F$_5$]), 140.2 – 137.4 (dm, |^{1}J (C,F)| = 248.8 Hz, C-2, C-4 [HC$_6$F$_5$]), 102.5 (td, |^{2}J (C,F)| = 23.3 Hz, |^{4}J (C,F)| = 2.9 Hz, C-6 [HC$_6$F$_5$]), 51.7 – 51.4 (m, Si-O*C*H$_3$), 50.0 (s, *C*H$_3$OH) ppm.

^{29}Si-NMR (79.5 MHz, Acetone-d_6, Cr(acac)$_3$): δ = -78.4 (11%, Q^0), -85.6 – -86.3 (24%, Q^1), -92.9 – -94.8 (35%, Q^2), -100.5 – -104.5 (30%, Q^3) ppm; no D-/T-species.

Characterization after 6 d reaction time and removal of volatiles:

^{1}H-NMR (400 MHz, $CDCl_3$, Cr(acac)$_3$): δ = 3.69 – 3.52 (m, Si-OC*H*$_3$) ppm.

^{13}C-NMR (101 MHz, $CDCl_3$, Cr(acac)$_3$): δ = 51.4 – 50.6 (m, Si-O*C*H$_3$) ppm.

^{29}Si-NMR (79.5 MHz, $CDCl_3$, Cr(acac)$_3$): δ = -78.5 (1%, Q^0), -85.7 – -86.9 (31%, Q^1), -93.0 – -95.6 (34%, Q^2), -100.4 – -104.9 (33%, Q^3) ppm; no D-/T-species.

4.4.3 Reaction of pentafluorophenyl(vinyl)dimethoxysilane (**5**) with dilute hydrochloric acid – condensation stoichiometry

Composition:

Pentafluorophenyl(vinyl)dimethoxysilane (**5**)	[284.26 g/mol]	14.2 g	(50.0 mmol)
Water (hydrochloric acid 0.01 M aq. soln.)	[18.02 g/mol; d=1.00 g/mL]	0.90 mL	(50.0 mmol water)

Procedure:

At ambient temperature (20 °C), to pentafluorophenyl(vinyl)dimethoxysilane (**5**) (14.2 g, 50.0 mmol) hydrochloric acid (0.90 mL 0.01 M aq. soln. ? 50.0 mmol water) was added. Initially, the vigorously stirred mixture exhibited a two-phase system, which homogenized after 1 h 44 min. For the time-resolved NMR experiments, samples (0.5 mL each) were drawn at selected reaction times (1 h, 1:44 h, 1:55 h, 2:10 h, 2:30 h, 3 h, 4 h, 5 h, 6 h, 8 h, 24 h, 4 d, 7 d) and analyzed by ^{1}H- (Tab. 24) and ^{29}Si-NMR (Tab. 25) according to the method described above. A last ^{29}Si-NMR spectrum was recorded after 31 d reaction time.

Characterization of the reaction mixture after 31 d reaction time:

^{29}Si-NMR (79.5 MHz, Acetone-d_6): δ = -39.1 [1%, D_1^0], -45.9 [17%, D_0^1], -47.8 – -49.2 [3%, D_1^1], -51.7 – -54.0 [30%, D^1-(T)], -55.2 – -56.5 [19%, D^2-(D)], -63.2 [4%, T^1], -70.5 – -73.0 [14%, T^2], -78.5 – -81.2 [12%, T^3] ppm.

Characterization of polycondensation intermediates:

^{1}H-NMR (400 MHz, Acetone-d_6, Cr(acac)$_3$): δ = 6.35 – 6.03 (m, (H_2C=CH)-Si), 3.66 – 3.56 (m, Si-OCH_3), 3.39 – 3.30 (CH_3OH) ppm.

^{29}Si-NMR (79.5 MHz, Acetone-d_6, Cr(acac)$_3$): δ = -36.4 [D_0^0], -39.1 [D_1^0], -41.4 [D_2^0], -45.4 [D_0^1-(D_0^1)], -45.7 [D_0^1-(D^2)], -46.1 [D_0^1-(D_1^1)], -48.3 [D_1^1-(D_0^1)], -48.6 [D_1^1-(D^2)], -49.0 [D_1^1-(D_1^1)], -51.8 [D^2-(T)], -55.1 [D^2-(D_0^1)], -55.6 [D^2-(D_1^1)], -56.1 [D^2-(D^2)] ppm.

Tab. 24: Methoxy and methanol contents [mol.%] according to their relative ^{1}H-NMR peak intensities at selected reaction times.

time:	**0 h**	**1 h**	**1:44 h**	**1:55 h**	**2:10 h**	**2:30 h**	**3 h**
[methoxy]	100	95	52	38	35	34	33
[methanol]		5	48	62	65	66	67

(continued)	**4 h**	**5 h**	**6 h**	**8 h**	**24 h**	**4 d**	**7 d**
[methoxy]	29	30	29	28	26	21	17
[methanol]	71	70	71	72	74	79	83

Tab. 25: Relative ^{29}Si-NMR peak intensities [mol.%] at selected reaction times.

time	D^0_0	D^0_1	D^0_2	D^0_{total}	D^1_0-(D^1_0)	D^1_0-(D^2)	D^1_0-(D^1_1)	D^1_1-(D^1_0)	D^1_1-(D^2)	D^1_1-(D^1_1)	D^1_{total}	D^2-(T)	D^2-(D^1_0)	D^2-(D^1_1)	D^2-(D^2)	D^2_{total}
0 h	100			**100**												
1 h	93	4	3	**100**												
1:44 h	13	38	32	**83**	2		4	5		6	**17**					
1:55 h	7	26	23	**56**	10		12	10	1	11	**44**					
2:10 h	4	19	18	**41**	15	1	14	13	3	13	**59**					
2:30 h	4	13	12	**29**	18	2	18	15	3	14	**70**			1		**1**
3 h	4	10	7	**21**	20	4	18	16	5	13	**76**		1	2		**3**
4 h	1	5	7	**13**	18	5	20	17	6	15	**81**		2	3	1	**6**
5 h	1	3	4	**8**	21	6	20	17	7	14	**85**		2	4	1	**7**
6 h	1	3	3	**7**	19	6	21	16	8	15	**85**		2	4	2	**8**
8 h		2	2	**4**	18	7	21	16	9	15	**86**		3	5	2	**10**
24 h		1	1	**2**	15	10	20	14	11	14	**84**		3	7	4	**14**
4 d			1	**1**	8	14	16	9	16	12	**75**		4	12	8	**24**
7 d					3	13	13	6	22	11	**68**	3	3	12	14	**32**

4.4.4 Reaction of pentafluorophenyl(vinyl)dimethoxysilane (**5**) with dilute hydrochloric acid – hydrolysis stoichiometry

Composition:

Pentafluorophenyl-(vinyl)-dimethoxysilane	[284.26 g/mol]	14.2 g	(50.0 mmol)
Water (hydrochloric acid 0.01 M aq. soln.)	[18.02 g/mol; d=1.00 g/mL]	1.80 mL	(100 mmol water)

Procedure:

At ambient temperature (20 °C), to pentafluorophenyl(vinyl)dimethoxysilane (**5**) (14.2 g, 50.0 mmol) hydrochloric acid (1.80 mL 0.01 M aq. soln. ≙ 100 mmol water) was added. Initially, the vigorously stirred mixture exhibited a two-phase system, which homogenized after 1 h 34 min. For the time-resolved NMR experiments, samples (0.5 mL each) were drawn at selected reaction times (1 h, 1:34 h, 1:45 h, 2 h, 2:15 h, 2:45 h, 3:15 h, 4 h, 5 h, 6 h, 8 h, 24 h, 3 d) and analyzed by ^{1}H- (Tab. 26) and ^{29}Si-NMR (Tab. 27) according to the method described above.

Characterization of polycondensation intermediates:

^{1}H-NMR (400 MHz, Acetone-d_6, Cr(acac)$_3$): δ = 6.40 – 5.85 (m, (*H*$_2$C=C*H*)-Si), 3.66 – 3.61 (m, Si-OC*H*$_3$), 3.38 – 3.33 (C*H*$_3$OH) ppm.

^{29}Si-NMR (79.5 MHz, Acetone-d_6, Cr(acac)$_3$): δ = -36.5 [D_0^0], -38.9 [D_1^0], -41.1 [D_2^0], -46.0 [D_0^1-(D_1^1)], -48.2 [D_1^1-(D_0^1)], -48.6 [D_1^1-(D^2)], -48.9 [D_1^1-(D_1^1)], -51.8 [D^2-(T)], -55.6 [D^2-(D_1^1)], -56.2 [D^2-(D^2)] ppm.

Tab. 26: Methoxy and methanol contents [mol.%] according to their relative ^{1}H-NMR peak intensities at selected reaction times.

time:	**0 h**	**1 h**	**1:34 h**	**1:45 h**	**2 h**	**2:15 h**	**2:45 h**
[methoxy]	100	91	11	7	6	6	6
[methanol]		9	89	93	94	94	94

(continued)	**3:15 h**	**4 h**	**5 h**	**6 h**	**8 h**	**24 h**	**3 d**
[methoxy]	5	5	5	5	4	3	1
[methanol]	95	95	95	95	96	97	99

Tab. 27: Relative ^{29}Si-NMR peak intensities [mol.%] at selected reaction times.

time	D^0_0	D^0_1	D^0_2	D^0_{total}	D^1_0-(D^1_1)	D^1_1-(D^1_0)	D^1_1-(D^2)	D^1_1-(D^1_1)	D^1_{total}	D^2-(T)	D^2-(D^1_1)	D^2-(D^2)	D^2_{total}
0 h	100			**100**									
1 h	88	7	5	**100**									
1:34 h		18	70	**88**	1	1		10	**12**				
1:45 h		9	42	**51**	5	5		39	**49**				
2 h		5	31	**36**	7	7	2	48	**64**				
2:15 h		4	23	**27**	8	7	3	51	**69**			4	**4**
2:45 h		3	17	**20**	8	7	5	54	**74**			6	**6**
3:15 h		2	12	**14**	8	7	10	53	**78**		2	6	**8**
4 h		1	9	**10**	8	7	13	54	**82**		1	7	**8**
5 h			7	**7**	8	6	15	53	**82**		3	8	**11**
6 h			7	**7**	7	7	14	53	**81**		3	9	**12**
8 h			5	**5**	8	5	19	51	**83**		1	11	**12**
24 h			2	**2**	7	4	26	38	**75**		4	19	**23**
3 d			2	**2**	6	2	15	36	**59**	2	3	34	**39**

4.4.5 Reaction of pentafluorophenyltrimethoxysilane (**1**) with dilute hydrochloric acid – hydrolysis stoichiometry

Composition:

Pentafluorophenyltrimethoxysilane	[288.24 g/mol]	14.4 g	(50.0 mmol)
Water (hydrochloric acid 0.01 M aq. soln.)	[18.02 g/mol; d=1.00 g/mL]	2.70 mL	(150 mmol water)

Procedure:

At ambient temperature (20 °C), to pentafluorophenyltrimethoxysilane (**1**) (14.4 g, 50.0 mmol) hydrochloric acid (2.70 mL 0.01 M aq. soln. ? 150 mmol water) was added. Initially, the vigorously stirred mixture exhibited a two-phase system, which homogenized after 20 min. For the time-resolved NMR experiments, samples (0.5 mL each) were drawn at selected reaction times (2 min, 10 min, 20 min, 30 min, 45 min, 90 min) and analyzed by ^{1}H- (Tab. 28) and ^{29}Si-NMR (Tab. 29) according to the method described above. After 90 min, the reaction mixture became too viscous for quantitative NMR spectroscopy.

Characterization of polycondensation intermediates:

^{1}H-NMR (400 MHz, Acetone-d_6, $Cr(acac)_3$): δ = 3.67 – 3.62 (m, Si-OCH_3), 3.40 – 3.33 (CH_3OH) ppm.

^{29}Si-NMR (79.5 MHz, Acetone-d_6, $Cr(acac)_3$): δ = -62.0 – -62.8 (m, T^0), -72.2 – -73.6 (m, T^1), -82.1 – -85.0 (m, T^2), -91.6 – -96.0 (m, T^3) ppm.

Tab. 28: Methoxy and methanol contents [mol.%] according to their relative ^{1}H-NMR peak intensities at selected reaction times.

time:	0 min	2 min	10 min	20 min	30 min	45 min	90 min
[methoxy]	100	98	42	3	2		
[methanol]		2	58	97	98	100	100

Tab. 29: Relative ^{29}Si-NMR peak intensities [mol.%] at selected reaction times.

time:	0 min	2 min	10 min	20 min	30 min	45 min	90 min
T^0	100	100	100	11	3		
T^1				47	22	12	1
T^2				40	62	54	27
T^3				2	13	34	72

4.4.6 Reaction of 4-vinyltetrafluorophenyltrimethoxysilane (**4**) with dilute hydrochloric acid – hydrolysis stoichiometry

Composition:

4-Vinyltetrafluorophenyltrimethoxysilane (**4**)	[296.29 g/mol]	13.1 g	(44.2 mmol)
Water (hydrochloric acid 0.5 M aq. soln.)	[18.02 g/mol; d=1.00 g/mL]	2.39 mL	(133 mmol water)

Procedure:

At ambient temperature (20 °C), to 4-vinyltetrafluorophenyltrimethoxysilane (**4**) (13.1 g, 44.2 mmol) hydrochloric acid (2.70 mL 0.01 M aq. soln. ≙ 150 mmol water) was added. Initially, the vigorously stirred mixture exhibited a two-phase system, which homogenized after 1:18 h. For the time-resolved NMR experiments, samples (0.5 mL each) were drawn at selected reaction times (20 min, 1 h, 1:18 h, 1:30 h, 2 h, 2:16 h) and analyzed by ^{1}H- (Tab. 30) and ^{29}Si-NMR (Tab. 31) according to the method described above.

Characterization of polycondensation intermediates:

^{1}H-NMR (400 MHz, Acetone-d_6, $Cr(acac)_3$): δ = 3.71 – 3.70 (m, Si-OCH_3), 3.44 – 3.33 (CH_3OH) ppm.

^{29}Si-NMR (79.5 MHz, Acetone-d_6, $Cr(acac)_3$): δ = -61.8 – -62.7 (m, T^0), -72.0 – -73.2 (m, T^1), -82.2 – -84.6 (m, T^2), -91.0 – -96.1 (m, T^3) ppm.

Tab. 30: Methoxy and methanol contents [mol.%] according to their relative ^{1}H-NMR peak intensities at selected reaction times.

time:	0 min	20 min	1 h	1:18 h	1:30 h	2 h	2:16 h
[methoxy]	100	89	43				
[methanol]		11	57	100	100	100	100

Tab. 31: Relative ^{29}Si-NMR peak intensities [mol.%] at selected reaction times.

time:	0 min	20 min	1 h	1:18 h	1:30 h	2 h	2:16 h
T^0	100	100	100	8	2		
T^1				57	22	17	14
T^2				35	63	54	56
T^3					13	28	30

4.4.7 Reaction of vinyltrimethoxysilane with dilute hydrochloric acid – ^{29}Si-NMR study

Composition:

Vinyltrimethoxysilane	[148.24 g/mol]	7.41 g	(50.0 mmol)
Water (hydrochloric acid 0.01 M aq. soln.)	[18.02 g/mol; d=1.00 g/mL]	0.90 mL	(50.0 mmol water)
Toluene		5 mL	

Procedure:

At ambient temperature (20 °C), to vinyltrimethoxysilane (7.41 g, 50.0 mmol) hydrochloric acid (0.90 mL 0.01 M aq. soln. ? 50.0 mmol water) was added. Initially, the vigorously stirred mixture exhibited a two-phase system, which homogenized after 2 min. After stirring for 8 w, the viscous sol was diluted with toluene (6 mL) and volatiles removed under reduced pressure (48 °C / 12 mbar). ^{29}Si-NMR experiments were carried out on the polycondensation mixture after 6 h, 3 d 18 h, and 10 d (Tab. 32) as well as on the resulting resin.

Characterization of polycondensation intermediates after 6 h reaction time:

^{29}Si-NMR (79.5 MHz, Acetone-d_6): δ = -62.9 (m, 6%, T^{1a}), -63.4 (m, 22%, T^{1b}), -63.9 (m, 13%, T^{1c}), -71.4 (m, 28%, T^{2a}), -72.7 (m, 28%, T^{2b}), -80.6 (m, 3%, T^{3}) ppm.

Characterization after 3 d 18 h reaction time:

^{29}Si-NMR (79.5 MHz, Acetone-d_6): δ = -62.9 (m, 3%, T^{1a}), -63.3 (m, 8%, T^{1b}), -63.8 (m, 7%, T^{1c}), -71.3 (m, 39%, T^{2a}), -72.7 (m, 25%, T^{2b}), -79.1 (m, 7%, T^{3a}), -80.6 (m, 9%, T^{3b}), -81.9 (m, 2%, T^{3c}) ppm.

Characterization after 10 d reaction time:

^{29}Si-NMR (79.5 MHz, Acetone-d_6): δ = -62.9 (m, 3%, T^{1a}), -63.9 (m, 4%, T^{1b}), -71.4 (m, 30%, T^{2a}), -72.7 (m, 27%, T^{2b}), -79.1 (m, 12%, T^{3a}), -80.7 (m, 17%, T^{3b}), -82.0 (m, 7%, T^{3c}) ppm.

Characterization of the resin after removal of volatiles:

^{29}Si-NMR (79.5 MHz, Acetone-d_6): δ = -64.0 (m, 10%, T^{1}), -71.4 (m, 17%, T^{2a}), -72.8 (m, 33%, T^{2b}), -79.1 (m, 11%, T^{3a}), -80.8 (m, 19%, T^{3b}), -82.0 (m, 10%, T^{3c}) ppm.

Refractive index: n_D^{20} = 1.446.

Tab. 32: Relative ^{29}Si-NMR peak intensities [mol.%] at selected reaction times.

time:	6 h	3 d 18 h	10 d	resin (8 w)
T^0				
T^{1a-c}	41	18	7	10
T^{2a-b}	56	64	57	61
T^{3a-c}	3	18	36	29

4.4.8 Reaction of tetramethoxysilane with dilute hydrochloric acid – ^{29}Si-NMR study

Composition:

Tetramethoxysilane	[152.22 g/mol]	7.61 g	(50.0 mmol)
Water (hydrochloric acid 0.01 M aq. soln.)	[18.02 g/mol; d=1.00 g/mL]	1.80 mL	(100 mmol water)
Toluene		6 mL	

Procedure:

At ambient temperature (20 °C), to tetramethoxysilane (7.61 g, 50.0 mmol) hydrochloric acid (1.80 mL 0.01 M aq. soln. ≙ 100 mmol water) was added. Initially, the vigorously stirred mixture exhibited a two-phase system, which soon homogenized. After stirring for 8 w, the viscous sol was diluted with toluene (6 mL) and volatiles removed under reduced pressure (47 °C / 2 mbar). ^{29}Si-NMR experiments were carried out on the polycondensation mixture after 6 h, 3 d 10 h, and 10 d (Tab. 33) as well as on the resulting resin.

Characterization of polycondensation intermediates after 6 h reaction time:

^{29}Si-NMR (79.5 MHz, Acetone-d_6): δ = -78.4 (m, 14%, Q^0), -83.9 (1%, Q^{1a}), -84.0 (1%, Q^{1b}), -85.8 (m, 34%, Q^{1c}), -93.6 (m, 27%, Q^2), -101.0 – -103.3 (m, 23%, Q^3) ppm.

Characterization after 3 d 13 h reaction time:

^{29}Si-NMR (79.5 MHz, Acetone-d_6): δ = -78.4 (m, 11%, Q^0), -83.9 (1%, Q^{1a}), -84.0 (1%, Q^{1b}), -85.9 (m, 34%, Q^{1c}), -92.9 – -93.9 (m, 31%, Q^2), -100.1 – -104.1 (m, 22%, Q^3) ppm.

Characterization after 10 d reaction time:

^{29}Si-NMR (79.5 MHz, Acetone-d_6): δ = -76.2 (1%, Q^0), -82.5 (3%, Q^{1a}), -83.9 (13%, Q^{1b}), -85.7 (m, 11%, Q^{1c}), -91.2 – -94.9 (m, 45%, Q^2), -99.0 – -103.4 (m, 27%, Q^3) ppm.

Characterization of the resin after removal of volatiles:

^{29}Si-NMR (79.5 MHz, Acetone-d_6): δ = -85.6 – -86.3 (m, 29%, Q^1), -92.9 – -94.6 (m, 39%, Q^2), -100.1 – -103.6 (m, 32%, Q^3) ppm.

Refractive index: n_D^{20} = 1.401.

Tab. 33: Relative ^{29}Si-NMR peak intensities [mol.%] at selected reaction times.

time:	6 h	3 d 13 h	10 d	resin (8 w)
Q^0	14	11	1	
Q^{1a-c}	36	36	27	29
Q^2	27	31	45	39
Q^3	23	22	27	32
Q^4	not detected			

4.4.9 Reaction of pentafluorophenyltrimethoxysilane (**1**) mixed with pentafluorophenyl(vinyl)dimethoxysilane (**5**) with dilute hydrochloric acid in methanol

Composition (fk11):

Pentafluorophenyltrimethoxysilane (**1**)	[288.24 g/mol]	5.76 g	(20.0 mmol)
Pentafluorophenyl(vinyl)dimethoxysilane (**5**)	[284.26 g/mol]	5.67 g	(20.0 mmol)
Water (hydrochloric acid 0.01 M aq. soln.)	[18.02 g/mol; d=1.00 g/mL]	1.80 mL	(100 mmol water)
Methanol	[32.04 g/mol; d=0.791 g/mL]	6.84 mL	(160 mmol)

Composition (fk12):

Pentafluorophenyltrimethoxysilane (**1**)	[288.24 g/mol]	5.76 g	(20.0 mmol)
Pentafluorophenyl(vinyl)dimethoxysilane (**5**)	[284.26 g/mol]	5.67 g	(20.0 mmol)
Water (hydrochloric acid 0.01 M aq. soln.)	[18.02 g/mol; d=1.00 g/mL]	0.90 mL	(50.0 mmol water)
Methanol	[32.04 g/mol; d=0.791 g/mL]	6.84 mL	(160 mmol)

Procedure:

At ambient temperature (19 °C), to solutions of pentafluorophenyltrimethoxysilane (**1**) (5.76 g, 20.0 mmol) and pentafluorophenyl(vinyl)dimethoxysilane (**5**) (5.67 g, 20.0 mmol) in methanol (6.48 mL, 160 mmol), hydrochloric acid (**fk11**: 1.80 mL 0.01 M aq. soln. ? 100 mmol water; **fk12**: 0.90 mL 0.01 M aq. soln. ? 50.0 mmol water) was added and the solutions left stirring. After 28 d (**fk11**) and 31 d (**fk12**), respectively, the reaction mixtures appeared milky white due to phase separation. After 35 d (**fk11**) and 56 d (**fk12**), respectively, the polycondensates were without success tried to redissolve in toluene, acetone, and propyl acetate, respectively, upon heating (50 °C). Gelation had occurred in both cases.

Characterization of reaction mixture fk11 after 3 d reaction time:

^{1}H-NMR (400 MHz, Acetone-d_6, Cr(acac)$_3$): δ = 7.40 – 7.23 (m, *H*C_6F_5), 6.35 – 5.65 (m, H_2C=C*H*-Si), 3.39 (CH_3OH) ppm.

^{13}C-NMR (101 MHz, Acetone-d_6, Cr(acac)$_3$): δ = 152.0 – 131.8 (m, C_{arylic}, C_{vinyl}), 102.4 (tm, $|^2J$ (C,F)| = 23.3 Hz, C-6 [HC_6F_5]), 50.1 (s, CH_3OH) ppm.

^{29}Si-NMR (79.5 MHz, Acetone-d_6, Cr(acac)$_3$): δ = -47.4 – -49.9 (7%, D^1_1), -51.6 – -55.1 (12%, D^2-(T)), -55.3 – -57.6 (11%, D^2-(D)), -62.3 – -63.1 (4%, $T^0_{fluoroaryl}$), -69.8 – -72.8 (16%, $T^1_{fluoroaryl}$), -77.6 – -78.7 (8%, Q^0), -79.0 – -84.1 (17%, $T^2_{fluoroaryl}$, T^3_{vinyl}), -85.8 – 88.2 (8%, Q^1), -88.7 – -92.0 (17%, $T^3_{fluoroaryl}$) ppm.

Characterization of reaction mixture fk12 after 3 d reaction time:

^{1}H-NMR (400 MHz, Acetone-d_6, Cr(acac)$_3$): δ = 7.39 – 7.25 (m, *H*C_6F_5), 6.34 – 5.72 (m, H_2C=C*H*-Si), 3.38 (CH_3OH) ppm.

^{13}C-NMR (101 MHz, Acetone-d_6, Cr(acac)$_3$): δ = 152.2 – 130.6 (m, C_{arylic}, C_{vinyl}), 102.4 (tm, $|^2J$ (C,F)| = 23.2 Hz, C-6 [HC_6F_5]), 50.1 (s, CH_3OH) ppm.

^{29}Si-NMR (79.5 MHz, Acetone-d_6, Cr(acac)$_3$): δ = -45.4 – -46.9 (3%, D^1_0), -47.4 – 49.4 (6%, D^1_1), -51.7 – -54.2 (6%, D^2-(T)), -54.4 – -57.4 (8%, D^2-(D)), -62.3 – -63.9 (4%, $T^0_{fluoroaryl}$), -70.4 – -73.5 (14%, $T^1_{fluoroaryl}$), -79.2 – -80.2 (12%, T^3_{vinyl}), -80.5 – -83.8 (14%, $T^2_{fluoroaryl}$), -85.4 – -88.1 (3%, Q^1), -88.4 – -94.5 (30%, $T^3_{fluoroaryl}$) ppm.

4.4.10 Preparation of ORMOCER® resins fk13 and fk14

Composition (fk13):

Pentafluorophenyltrimethoxysilane (**1**)	[288.24 g/mol]	5.76 g	(20.0 mmol)
Pentafluorophenyl(vinyl)dimethoxysilane (**5**)	[284.26 g/mol]	5.67 g	(20.0 mmol)
Water (hydrochloric acid 0.01 M aq. soln.)	[18.02 g/mol; d=1.00 g/mL]	1.80 mL	(100 mmol water)
Acetone	[58.08 g/mol; d=0.791 g/mL]	11.8 mL	(160 mmol)
Toluene		15 mL	

Composition (fk14):

Pentafluorophenyltrimethoxysilane (**1**)	[288.24 g/mol]	5.76 g	(20.0 mmol)
Pentafluorophenyl(vinyl)dimethoxysilane (**5**)	[284.26 g/mol]	5.67 g	(20.0 mmol)
Water (hydrochloric acid 0.01 M aq. soln.)	[18.02 g/mol; d=1.00 g/mL]	0.90 mL	(50.0 mmol water)
Acetone	[58.08 g/mol; d=0.791 g/mL]	11.8 mL	(160 mmol)
Toluene		15 mL	

Procedure:

At ambient temperature (19 °C), to solutions of pentafluorophenyltrimethoxysilane (**1**) (5.76 g, 20.0 mmol) and pentafluorophenyl(vinyl)dimethoxysilane (**5**) (5.67 g, 20.0 mmol) in acetone (11.8 mL, 160 mmol), hydrochloric acid (**fk13**: 1.80 mL 0.01 M aq. soln. ? 100 mmol water; **fk14**: 0.90 mL 0.01 M aq. soln. ? 50.0 mmol water) was added and the solutions left stirring. After 56 d, toluene (15 mL) was added and volatile components were removed under reduced pressure (**fk13**: 55 °C / 24 mbar; **fk14**: 55 °C / 4 mbar) resulting in the colorless, highly viscous ORMOCER® resins **fk13** and **fk14**. Both resins were well soluble in acetone, toluene, and propyl acetate.

Characterization of reaction mixture fk13 after 3 d reaction time:

^{1}H-NMR (400 MHz, Acetone-d_6, Cr(acac)$_3$): δ = 7.48 – 7.34 (m, *H*C_6F_5), 6.34 – 5.83 (m, H_2C=C*H*-Si), 3.34 (CH_3OH) ppm.

^{13}C-NMR (101 MHz, Acetone-d_6, Cr(acac)$_3$): δ = 151.8 – 131.5 (m, C_{arylic}, C_{vinyl}), 102.4 (td, $|^2J$ (C,F)| = 23.3 Hz, $|^4J$ (C,F)| = 2.9 Hz, C-6 [HC_6F_5]), 49.9 (s, *C*H_3OH) ppm.

Characterization of reaction mixture fk14 after 3 d reaction time:

^{1}H-NMR (400 MHz, Acetone-d_6, Cr(acac)$_3$): δ = 7.46 – 7.34 (m, *H*C_6F_5), 6.32 – 5.88 (m, H_2C=C*H*-Si), 3.64 (Si-OCH_3), 3.33 (CH_3OH) ppm.

^{13}C-NMR (101 MHz, Acetone-d_6, Cr(acac)$_3$): δ = 151.8 – 104.0 (m, C_{arylic}, C_{vinyl}), 102.4 (traces, C-6 [HC_6F_5]), 51.5 – 51.2 (m, Si-O*C*H$_3$), 49.9 (s, *C*H_3OH) ppm.

Characterization of ORMOCER® resin fk14:

^{1}H-NMR (400 MHz, Acetone-d_6, Cr(acac)$_3$): δ = 7.46 – 7.37 (m, *H*C_6F_5), 6.45 – 5.66 (m, H_2C=C*H*-Si), 3.77 – 3.36 (m, Si-OCH_3), 3.31 (CH_3OH) ppm.

^{13}C-NMR (101 MHz, Acetone-d_6, Cr(acac)$_3$): δ = 151.8 – 103.3 (m, C_{arylic}, C_{vinyl}), 102.3 (td, $|^2J$ (C,F)| = 23.3 Hz, $|^4J$ (C,F)| = 2.9 Hz, C-6 [HC_6F_5]), 51.8 – 51.0 (m, traces, Si-O*C*H$_3$) ppm.

^{29}Si-NMR (79.5 MHz, Acetone-d_6, Cr(acac)$_3$): δ = -44.8 – -46.7 (2%, D^1_0), -49.7 – -54.5 (34%, D^2-(T)), -54.6 – -56.8 (8%, D^2-(D)), -69.7 – -73.2 (4%, T^1), -74.7 – -82.8 (38%, T^2), -84.7 – -87.7 (5%, Q^1), -87.9 – -91.4 (9%, T^3) ppm.

NIR (filtered over 0.45 µm filter)**:**

Wavelength	1310 nm	1550 nm
Absorption Loss	0.04 dB/cm	0.66 dB/cm

4.4.11 Preparation of gel fk15 and ORMOCER® resin fk16

Composition (fk15):

Pentafluorophenyltrimethoxysilane (**1**)	[288.24 g/mol]	5.76 g	(20.0 mmol)
Pentafluorophenyl(vinyl)dimethoxysilane (**5**)	[284.26 g/mol]	5.67 g	(20.0 mmol)
Water (hydrochloric acid 0.01 M aq. soln.)	[18.02 g/mol; d=1.00 g/mL]	1.80 mL	(100 mmol water)

Composition (fk16):

Pentafluorophenyltrimethoxysilane (**1**)	[288.24 g/mol]	5.76 g	(20.0 mmol)
Pentafluorophenyl(vinyl)dimethoxysilane (**5**)	[284.26 g/mol]	5.67 g	(20.0 mmol)
Water (hydrochloric acid 0.01 M aq. soln.)	[18.02 g/mol; d=1.00 g/mL]	0.90 mL	(50.0 mmol water)
Toluene		15 mL	

Procedure:

At ambient temperature (19 °C), to vigorously stirred mixtures of pentafluorophenyltrimethoxysilane (**1**) (5.76 g, 20.0 mmol) and pentafluorophenyl(vinyl)dimethoxysilane (**5**) (5.67 g, 20.0 mmol), hydrochloric acid (**fk15**: 1.80 mL 0.01 M aq. soln. ? 100 mmol water; **fk16**: 0.90 mL 0.01 M aq. soln. ? 50.0 mmol water) was added. Initially, the reaction mixtures formed two-phase systems, which homogenized after 35 min (**fk15**), and 40 min (**fk16**), respectively, to exhibit colorless lucent solutions that, in the **fk15** case, underwent phase separation again after 1 d and turned into a gel after 8 d that could not be redissolved in propyl acetate, acetone, nor toluene, respectively. The **fk16** polycondensate, however, remained a clear solution, to which after 56 d, toluene (15 mL) was added. Volatile components were removed under reduced pressure (48 °C / 5 mbar) resulting in the colorless, highly viscous ORMOCER® resin **fk16**. The resin was well soluble in acetone and propyl acetate, and upon warming (50 °C) also in toluene.

Characterization of reaction mixture fk15 (viscous phase) after 3 d reaction time:

^{1}H-NMR (400 MHz, Acetone-d_6, Cr(acac)$_3$): δ = 7.27 (m, *H*C$_6$F$_5$), 6.50 – 5.61 (m, *H*$_2$C=C*H*-Si), 3.38 (C*H*$_3$OH) ppm.

^{13}C-NMR (101 MHz, Acetone-d_6, Cr(acac)$_3$): δ = 152.3 – 103.2 (m, C_{arylic}, C_{vinyl}), 102.4 (tm, $|^2J$ (C,F)| = 24.3 Hz, C-6 [HC_6F_5]), 51.9 – 51.5 (m, Si-O*C*H$_3$), 50.2 (s, *C*H$_3$OH) ppm.

^{29}Si-NMR (79.5 MHz, Acetone-d_6, Cr(acac)$_3$): δ = -45.4 – -46.6 (2%, D_0^1), -47.2 – -49.4 (8%, D_1^1) -51.3 – -54.4 (17%, D^2-(T)), -54.5 – -57.8 (22%, D^2-(D)), -70.0 – -72.6 (3%, $T^1_{fluoroaryl}$), -78.5 – -84.0 (14%, $T^2_{fluoroaryl}$, T^3_{vinyl}), -85.5 – -88.8 (4%, Q^1), -89.2 – -92.6 (20%, $T^3_{fluoroaryl}$), -92.7 – -95.5 (10%, Q^2) ppm.

Characterization of reaction mixture fk16 after 3 d reaction time:

^{1}H-NMR (400 MHz, Acetone-d_6, Cr(acac)$_3$): δ = 7.28 (m, *H*C_6F_5), 6.42 – 5.69 (m, H_2C=C*H*-Si), 3.74 – 3.49 (Si-OCH_3), 3.38 (CH_3OH) ppm.

^{13}C-NMR (101 MHz, Acetone-d_6, Cr(acac)$_3$): δ = 152.1 – 104.0 (m, C_{arylic}, C_{vinyl}), 51.8 – 51.5 (m, Si-OCH_3), 50.1 (s, CH_3OH) ppm.

^{29}Si-NMR (79.5 MHz, Acetone-d_6, Cr(acac)$_3$): δ = -44.3 – -47.0 (8%, D_0^1), -47.7 – -48.7 (9%, D_1^1), -51.8 – -54.0 (12%, D^2-(T)), -54.7 – -57.3 (15%, D^2-(D)), -71.6 – -72.3 (4%, $T^1_{fluoroaryl}$), -79.5 – -81.5 (7%, T^3_{vinyl}), -81.7 – -84.3 (14%, $T^2_{fluoroaryl}$), -85.2 – -89.3 (5%, Q^1), -89.6 – -93.0 (18%, $T^3_{fluoroaryl}$), 93.1 – -95.5 (8%, Q^2) ppm.

Characterization of ORMOCER® resin fk16:

NIR (filtered over 0.45 µm filter)**:**

Wavelength	1310 nm	1550 nm
Absorption Loss	0.10 dB/cm	0.18 dB/cm

4.4.12 Preparation of ORMOCER® resins fk18 and fk19

Composition (fk18):

4-Vinyltetrafluorophenyltrimethoxysilane (**4**)	[296.29 g/mol]	5.93 g	(20.0 mmol)
Pentafluorophenyl(vinyl)dimethoxysilane (**5**)	[284.26 g/mol]	5.67 g	(20.0 mmol)
Water (hydrochloric acid 0.01 M aq. soln.)	[18.02 g/mol; d=1.00 g/mL]	0.90 mL	(50.0 mmol water)
Toluene		15 mL	

Composition (fk19):

4-Vinyltetrafluorophenyltrimethoxysilane (**4**)	[296.29 g/mol]	5.93 g	(20.0 mmol)
Pentafluorophenyl(vinyl)dimethoxysilane (**5**)	[284.26 g/mol]	5.67 g	(20.0 mmol)
Water (hydrochloric acid 0.5 M aq. soln.)	[18.02 g/mol; d=1.00 g/mL]	0.90 mL	(50.0 mmol water)
Toluene		15 mL	

Procedure:

At ambient temperature (19 °C), to vigorously stirred mixtures of 4-vinyltetrafluorophenyltrimethoxysilane (**4**) (5.93 g, 20.0 mmol) and pentafluorophenyl(vinyl)dimethoxysilane (**5**) (5.67 g, 20.0 mmol), hydrochloric acid (**fk18**: 0.90 mL 0.01 M aq. soln. ? 50.0 mmol water; **fk19**: 0.90 mL 0.5 M aq. soln. ? 50.0 mmol water) was added. Initially, the reaction mixtures formed two-phase systems, which homogenized after 55 min (**fk18**), and 9 min (**fk19**), respectively, to exhibit colorless lucent solutions. In the **fk19** case, phase separation occurred again after 3 d. After 29 d, the polycondensates were dissolved in toluene (15 mL) and volatile components were removed under reduced pressure (**fk18**: 44 °C / 4 mbar; **fk19**: 45 °C / 5 mbar) resulting in the colorless, highly viscous ORMOCER® resin **fk18**.

Characterization of ORMOCER® resin fk18:

NIR (filtered over 0.45 µm filter)**:**

Wavelength	1310 nm	1550 nm
Absorption Loss	0.32 dB/cm	0.46 dB/cm

Characterization of ORMOCER® resin fk19:

NIR (filtered over 0.45 µm filter)**:**

Wavelength	1310 nm	1550 nm
Absorption Loss	0.32 dB/cm	0.44 dB/cm

4.4.13 Preparation of ORMOCER® resin fk20

Composition:

4-Vinyltetrafluorophenyltrimethoxysilane (**4**)	[296.29 g/mol]	5.93 g	(20.0 mmol)
Pentafluorophenyl(vinyl)dimethoxysilane (**5**)	[284.26 g/mol]	5.67 g	(20.0 mmol)
Water (hydrochloric acid 0.01 M aq. soln.)	[18.02 g/mol; d=1.00 g/mL]	0.90 mL	(50.0 mmol water)
Toluene		15 mL	

Procedure:

To a vigorously stirred mixture of 4-vinyltetrafluorophenyltrimethoxysilane (**4**) (5.93 g, 20.0 mmol) and pentafluorophenyl(vinyl)dimethoxysilane (**5**) (5.67 g, 20.0 mmol), hydrochloric acid (0.90 mL 0.01 M aq. soln. ? 50.0 mmol water) was added at 42 °C. Initially, the reaction

mixtures formed a two-phase systems which homogenized after 30 min to exhibit a colorless lucent solution. After 11 d, the polycondensate was dissolved in toluene (15 mL) and volatile components were removed under reduced pressure (50 °C / 8 mbar) resulting in the colorless, highly viscous ORMOCER® resin **fk20**, that was largely contaminated with gel particles, which were removed by filtering prior to characterization.

Characterization of ORMOCER® resin fk20:

NIR (filtered over 0.45 µm filter)**:**

Wavelength	1310 nm	1550 nm
Absorption Loss	0.40 dB/cm	0.60 dB/cm

4.4.14 Preparation of ORMOCER® resin fk34

Composition:

Pentafluorophenyltrimethoxysilane (**1**)	[288.24 g/mol]	14.4 g	(50.0 mmol)
4-Vinyltetrafluorophenyltrimethoxysilane (**4**)	[296.29 g/mol]	14.8 g	(50.0 mmol)
Pentafluorophenyl(vinyl)dimethoxysilane (**5**)	[284.26 g/mol]	28.4 g	(100 mmol)
Water (hydrochloric acid 0.01 M aq. soln.)	[18.02 g/mol; d=1.00 g/mL]	9.01 mL	(500 mmol water)
Toluene		50 mL	

Procedure:

At ambient temperature (19 °C), to a vigorously stirred mixture of pentafluorophenyltrimethoxysilane (**1**) (14.4 g, 50.0 mmol), 4-vinyltetrafluorophenyltrimethoxysilane (**4**) (14.8 g, 50.0 mmol) and pentafluorophenyl(vinyl)dimethoxysilane (**5**) (28.4 g, 100 mmol), hydrochloric acid (9.01 mL 0.01 M aq. soln. ? 500 mmol water) was added. Initially, the reaction mixture formed a two-phase system, which homogenized after 25 min to exhibit a colorless lucent solution. After 2 d, the reaction mixture appeared milky white due to phase separation. After 10 d, toluene (50 mL) was added and volatile components were removed under reduced pressure (43 °C / 5 mbar) resulting in the colorless, highly viscous ORMOCER® resin **fk34** (54.4 g).

Characterization of ORMOCER® resin fk34:

^{13}C-NMR (101 MHz, Acetone-d_6): δ = 151.9 – 106.3 (m, C_{arylic}, C_{vinyl}), 102.2 (td, traces, $|^2J$ (C,F)| = 23.3 Hz, $|^4J$ (C,F)| = 3.2 Hz, C-6 [HC_6F_5]), 51.6 (m, traces, Si-OCH_3) ppm.

^{29}Si-NMR (79.5 MHz, Acetone-d_6): δ = -45.6 – -46.2 (2%, D^1_0), -51.4 – -54.1 (23%, D^2-(T)), -54.5 – -56.9 (15%, D^2-(D)), -69.8 – -71.5 (4%, T^2_{vinyl}), -72.3 – -74.5 (5%, $T^1_{fluoroaryl}$), -76.4 – -80.0 (10%, T^3_{vinyl}), -80.1 – -83.7 (9%, $T^2_{fluoroaryl}$), -84.5 – -88.8 (6%, Q^1), -88.9 – -92.9 (24%, $T^3_{fluoroaryl}$), -93.0 – -94.0 (2%, Q^2) ppm.

IR (film): $\tilde{\nu}$ = 3380 cm^{-1} (broad peak, high intensity): high Si-OH content.

Refractive index: n_D^{20} = 1.497.

NIR (filtered over 0.45 µm filter):

Wavelength	350 nm	1310 nm	1550 nm
Absorption Loss	2.30 dB/cm	0.28 dB/cm	0.70 dB/cm

SAXS (toluene): Average size of oligomers = 2.4 nm.

Dynamic viscosity (20 °C): η = 139 Pa s.

4.4.15 Preparation of ORMOCER® resins fk35 and fk37

Composition (fk35):

Pentafluorophenyltrimethoxysilane (**1**)	[288.24 g/mol]	2.88 g	(10.0 mmol)
4-Vinyltetrafluorophenyltrimethoxysilane (**4**)	[296.29 g/mol]	2.96 g	(10.0 mmol)
Pentafluorophenyl(vinyl)dimethoxysilane (**5**)	[284.26 g/mol]	5.68 g	(20.0 mmol)
Water (hydrochloric acid 0.5 M aq. soln.)	[18.02 g/mol; d=1.00 g/mL]	0.90 mL	(50.0 mmol water)
Toluene		15 mL	

Composition (fk37):

Pentafluorophenyltrimethoxysilane (**1**)	[288.24 g/mol]	11.53 g	(40.0 mmol)
4-Vinyltetrafluorophenyltrimethoxysilane (**4**)	[296.29 g/mol]	11.85 g	(40.0 mmol)
Pentafluorophenyl(vinyl)dimethoxysilane (**5**)	[284.26 g/mol]	22.74 g	(80.0 mmol)
Water (hydrochloric acid 0.01 M aq. soln.)	[18.02 g/mol; d=1.00 g/mL]	3.60 mL	(200 mmol water)
Toluene		60 mL	

Procedure:

At ambient temperature (19 °C), to a vigorously stirred mixture of pentafluorophenyltrimethoxysilane (**1**) (**fk35**: 2.88 g, 10.0 mmol; **fk37**: 11.5 g, 40.0 mmol),

4-vinyltetrafluorophenyltrimethoxysilane (**4**) (**fk35**: 2.96 g, 10.0 mmol; **fk37**: 11.9 g, 40.0 mmol) and pentafluorophenyl(vinyl)dimethoxysilane (**5**) (**fk35**: 5.68 g, 20.0 mmol; **fk37**: 22.7 g, 80.0 mmol), hydrochloric acid (**fk35**: 0.90 mL 0.5 M aq. soln. ? 50.0 mmol water; **fk37**: 3.60 mL 0.01 M aq. soln. ? 200 mmol water) was added. Initially, the reaction mixtures formed two-phase systems, which homogenized after 25 min (**fk35**), and 50 min (**fk37**), respectively, to exhibit colorless lucent solutions.

In the **fk35** case, the reaction mixture appeared milky white due to phase separation after 8 d. After 21 d, toluene (15 mL) was added and volatile components were removed under reduced pressure (49 °C / 7 mbar) resulting in the colorless, highly viscous ORMOCER® resin **fk35**.

As for **fk37**, after 25 d Karl-Fischer titration detected 89% water conversion (0.78 wt.% water; initially 7.24 wt.%), after 35 d 90% conversion (0.75 wt.% water). After 35 d, toluene (60 mL) was added and volatile components were removed under reduced pressure (42 °C / 1 mbar) resulting in the colorless, highly viscous ORMOCER® resins **fk37**, **fk37-2**, **fk37-3** and **fk37-4**, respectively (36.9 g).

Characterization of ORMOCER® resin fk35:

IR (film): $\tilde{\nu}$ = 3400 cm^{-1} (broad peak, medium intensity): medium Si-OH content.

Refractive index: n_D^{20} = 1.496.

NIR (filtered over 0.45 µm filter):

Wavelength	350 nm	1310 nm	1550 nm
Absorption Loss	4.14 dB/cm	0.36 dB/cm	0.52 dB/cm

Characterization of ORMOCER® resin fk37:

^{13}C-NMR (101 MHz, Acetone-d_6): δ = 151.8 – 106.3 (m, C_{arylic}, C_{vinyl}), 102.3 (td, traces, $|^2J$ (C,F)| = 23.3 Hz, $|^4J$ (C,F)| = 3.9 Hz, C-6 [HC_6F_5]), 51.7 – 51.1 (Si-OCH_3) ppm.

^{29}Si-NMR (79.5 MHz, Acetone-d_6): δ = -45.5 – -46.4 (6%, D_0^1), -51.7 – -54.3 (16%, D^2-(T)), -54.8 – -57.0 (16%, D^2-(D)), -70.7 – -73.5 (6%, $T^1_{fluoroaryl}$), -78.2 – -80.0 (9%, T^3_{vinyl}), -81.2 – -84.0 (17%, $T^2_{fluoroaryl}$), -84.7 – -88.7 (8%, Q^1), -89.5 – -93.3 (22%, $T^3_{fluoroaryl}$) ppm.

IR (film): $\tilde{\nu}$ = 3400 cm^{-1} (broad peak, low intensity): low Si-OH content.

Refractive index: n_D^{20} = 1.497.

NIR (filtered over 0.45 µm filter):

Wavelength	350 nm	1310 nm	1550 nm
Absorption Loss	2.40 dB/cm	0.28 dB/cm	0.42 dB/cm

SAXS (toluene): Average size of oligomers = 1.7 nm.

Dynamic viscosity (20 °C): η = 4030 Pa s.

4.4.16 Preparation of ORMOCER® resin fk36

Composition:

Pentafluorophenyltrimethoxysilane (**1**)	[288.24 g/mol]	2.88 g	(10.0 mmol)
4-Vinyltetrafluorophenyltrimethoxysilane (**4**)	[296.29 g/mol]	2.96 g	(10.0 mmol)
Pentafluorophenyl(vinyl)dimethoxysilane (**5**)	[284.26 g/mol]	5.68 g	(20.0 mmol)
Water (hydrochloric acid 0.01 M aq. soln.)	[18.02 g/mol; d=1.00 g/mL]	0.90 mL	(50.0 mmol water)
Tetrahydrofuran	[72.11 g/mol; d=0.887 g/mL]	32.5 mL	(400 mmol)
Toluene		45 mL	

Procedure:

At ambient temperature (19 °C), to a solution of pentafluorophenyltrimethoxysilane (**1**) (2.88 g, 10.0 mmol), 4-vinyltetrafluorophenyltrimethoxysilane (**4**) (2.96 g, 10.0 mmol) and pentafluorophenyl(vinyl)dimethoxysilane (**5**) (5.68 g, 20.0 mmol) in tetrahydrofuran (32.5 mL, 400 mmol), hydrochloric acid (0.90 mL 0.01 M aq. soln. ? 50.0 mmol water) was added. After 21 d, toluene (45 mL) was added and volatile components were removed under reduced pressure (43 °C / 6 mbar) resulting in the colorless, viscous ORMOCER® resin **fk36**, which was contaminated with gel particles.

Characterization of ORMOCER® resin fk36:

^{13}C-NMR (101 MHz, Acetone-d_6, Cr(acac)$_3$): δ = 151.5 – 105.6 (m, C_{arylic}, C_{vinyl}), 102.3 (td, traces, $|^2J$ (C,F)| = 23.3 Hz, $|^4J$ (C,F)| = 3.9 Hz, C-6 [HC_6F_5]), 68.2 (traces, CH_2 [THF]), 52.6 – 50.5 (Si-OCH_3), 26.3 (traces, CH_2O [THF]) ppm.

IR (film): $\tilde{\nu}$ = 3400 cm^{-1} (broad peak, medium intensity): medium Si-OH content.

Refractive index: n_D^{20} = 1.483.

NIR (filtered over 0.45 µm filter):

Wavelength	350 nm	1310 nm	1550 nm
Absorption Loss	2.58 dB/cm	0.28 dB/cm	1.26 dB/cm

4.4.17 Preparation of ORMOCER® resin fk38

Composition:

Pentafluorophenyltrimethoxysilane (**1**)	[288.24 g/mol]	8.65 g	(30.0 mmol)
4-Vinyltetrafluorophenyltrimethoxysilane (**4**)	[296.29 g/mol]	8.89 g	(30.0 mmol)
Pentafluorophenyl(vinyl)dimethoxysilane (**5**)	[284.26 g/mol]	39.8 g	(140 mmol)
Water (hydrochloric acid 0.01 M aq. soln.)	[18.02 g/mol; d=1.00 g/mL]	9.01 mL	(500 mmol water)
Toluene		50 mL	

Procedure:

At ambient temperature (19 °C), to a vigorously stirred mixture of pentafluorophenyltrimethoxysilane (**1**) (8.65 g, 30.0 mmol), 4-vinyltetrafluorophenyltrimethoxysilane (**4**) (8.89 g, 30.0 mmol) and pentafluorophenyl(vinyl)dimethoxysilane (**5**) (39.8 g, 140 mmol), hydrochloric acid (9.01 mL 0.01 M aq. soln. ? 500 mmol water) was added. Initially, the reaction mixture formed a two-phase system, which homogenized after 125 min to exhibit a colorless lucent solution, which underwent phase separation after 2 d. After 10 d, toluene (50 mL) was added and volatile components were removed under reduced pressure (47 °C / 1 mbar) resulting in the colorless, highly viscous ORMOCER® resin **fk38** (46.5 g).

Characterization of ORMOCER® resin fk38:

^{13}C-NMR (101 MHz, Acetone-d_6): δ = 151.5 – 106.0 (m, C_{arylic}, C_{vinyl}), 102.3 (td, traces, $|^2J$ (C,F)| = 23.3 Hz, $|^4J$ (C,F)| = 3.9 Hz, C-6 [HC_6F_5]), 51.4 (m, traces, Si-OCH_3) ppm.

^{29}Si-NMR (79.5 MHz, Acetone-d_6): δ = -45.7 – -46.2 (3%, D^1_0), -51.4 – -54.3 (29%, D^2-(T)), -54.9 – -56.7 (18%, D^2-(D)), -68.0 – -69.5 (3%, T^2_{vinyl}), -69.8 – -73.4 (11%, $T^1_{fluoroaryl}$), -76.3 – -79.6 (8%, T^3_{vinyl}), -79.7 – -81.1 (12%, $T^2_{fluoroaryl}$), -84.3 – -87.5 (3%, Q^1), -88.6 – -92.4 (13%, $T^3_{fluoroaryl}$) ppm.

IR (film): $\tilde{\nu}$ = 3380 cm^{-1} (broad peak, high intensity): high Si-OH content.

Refractive index: n_D^{20} = 1.491.

NIR (filtered over 0.45 µm filter):

Wavelength	350 nm	1310 nm	1550 nm
Absorption Loss	1.76 dB/cm	0.30 dB/cm	0.84 dB/cm

SAXS (toluene): Average size of oligomers = 1.9 nm.

Dynamic viscosity (20 °C): η = 104 Pa s.

4.4.18 Preparation of ORMOCER® resin fk48

Composition:

Pentafluorophenyltrimethoxysilane (**1**)	[288.24 g/mol]	2.88 g	(10.0 mmol)
4-Vinyltetrafluorophenyltrimethoxysilane (**4**)	[296.29 g/mol]	2.96 g	(10.0 mmol)
Pentafluorophenyl(methyl)dimethoxysilane (**6**)	[272.25 g/mol]	5.45 g	(20.0 mmol)
Water (hydrochloric acid 0.01 M aq. soln.)	[18.02 g/mol; d=1.00 g/mL]	0.90 mL	(50.0 mmol water)
Toluene		15 mL	

Procedure:

At ambient temperature (19 °C), to a vigorously stirred mixture of pentafluorophenyltrimethoxysilane (**1**) (2.88 g, 10.0 mmol), 4-vinyltetrafluorophenyltrimethoxysilane (**4**) (2.96 g, 10.0 mmol) and pentafluorophenyl(methyl)dimethoxysilane (**6**) (5.45 g, 20.0 mmol), hydrochloric acid (0.90 mL 0.01 M aq. soln. ? 50 mmol water) was added and the reaction mixture left stirring. Initially, the reaction mixture formed a two-phase system, which homogenized after 45 min to exhibit a colorless lucent solution. After 7 d of reaction time, separation into two liquid phases occurred. Having the mixture stirred for 21 d, the resulting highly viscous two-phase system was dissolved in toluene (15 mL). At this stage, the water content was measured by Karl-Fischer titration (0.52 wt.%, relative to 7.38 wt.% initial water admixture) and determined a water conversion of 93%. Volatiles were removed under reduced pressure (49 °C / 1 mbar) resulting in the colorless, viscous ORMOCER® resin **fk48** (9.46 g), which was then stored at -25 °C.

Characterization of ORMOCER® resin fk48:

^{13}C-NMR (101 MHz, Acetone-d_6): δ = 151.0 – 103.0 (m, C_{arylic}, C_{vinyl}), 101.5 (m, traces, C-6 [HC_6F_5]), 50.4 (m, traces, Si-OCH_3) ppm.

^{29}Si-NMR (79.5 MHz, Acetone-d_6): δ = -29.2 – -30.7 (5%, D^1), -35.7 – -38.3 (20%, D^2-(T)), -38.4 – -41.0 (24%, D^2-(D)), -78.0 – -80.5 (7%, T^3_{vinyl}), -80.6 – -83.4 (9%, $T^2_{fluoroaryl}$), -85.2 – -89.1 (4%, Q^1), -89.6 – -94.3 (31%, $T^3_{fluoroaryl}$) ppm.

IR (film): $\tilde{\nu}$ = 3400 cm^{-1} (broad peak, low intensity): low Si-OH content.

Refractive index: n_D^{20} = 1.488.

NIR (filtered over 0.45 µm filter):

Wavelength	350 nm	1310 nm	1550 nm
Absorption Loss	11.98 dB/cm	0.46 dB/cm	0.66 dB/cm

For further processing, resin **fk48** (7.44 g, 100 wt.%) was mixed with propyl acetate (1.86 g, 25 wt.%) and the solution filtered (0.2 µm syringe filter). The filtrate (5.80 g) was then mixed with pre-filtered photoinitiator Lucirin® LR 8893 (0.123 g, 3.4 wt.%) and allowed to settle for a few days. However, gelation occurred after 4 d.

4.4.19 Preparation of ORMOCER® resin fk54

Composition:

Phenyl(vinyl)dimethoxysilane (**7**)	[194.31 g/mol]	11.66 g	(60.0 mmol)
4-Vinylphenyltrimethoxysilane	[224.33 g/mol]	6.73 g	(30.0 mmol)
Phenyltrimethoxysilane	[198.29 g/mol]	5.95 g	(30.0 mmol)
Water (hydrochloric acid 0.01 M aq. soln.)	[18.02 g/mol; d=1.00 g/mL]	2.70 mL	(150 mmol water)
Toluene		45 mL	

Procedure:

At ambient temperature (19 °C), to a vigorously stirred mixture of phenyl(vinyl)dimethoxysilane (**7**) (11.66 g, 60.0 mmol), 4-vinylphenyltrimethoxysilane (6.73 g, 30.0 mmol) and phenyltrimethoxysilane (5.95 g, 30.0 mmol), hydrochloric acid (2.70 mL 0.01 M aq. soln. ? 150 mmol water) was added. Initially, the reaction mixture formed a two-phase system, which homogenized after 30 min to exhibit a colorless lucent solution. After 16 d, the reaction mixture appeared cloudy, another 2 d later it was milky white due to phase separation. Karl-Fischer titration after 34 d detected 86% water conversion (1.42 wt.% water; initially 9.99 wt.%), after 40 d 87% conversion (1.26 wt.% water). After 42 d (Karl-Fischer titration: 1.21 wt.% water, 87% conversion), toluene (45 mL) was added and volatile components were removed under reduced pressure (50 °C / 7 mbar) resulting in the colorless, viscous ORMOCER® resin **fk54** (17.82 g).

Characterization of ORMOCER® resin fk54:

^{1}H-NMR (400 MHz, Acetone-d_6): δ = 7.94 – 6.87 (m, 19 H, H_{arylic}), 6.69 (m, 1 H, Ar-C*H*=CH_2), 6.37 – 5.44 (m, 7 H, H_{vinyl}), 5.23 (m, 1 H, Ar-C*H*=C*H*H') ppm.

^{13}C-NMR (101 MHz, Acetone-d_6): δ = 140.7 – 114.6 (m, C_{arylic}, C_{vinyl}), 50.9 – 50.4 (m, Si-OCH_3), 49.7 (traces, CH_3OH) ppm.

^{29}Si-NMR (79.5 MHz, Acetone-d_6): δ = -37.8 – -38.6 (4%, D^1), -42.4 – -45.8 (26%, D^2-(T)), -46.0 – -48.0 (19%, D^2-(D)), -68.9 – -72.5 (11%, T^2), -75.3 – -81.5 (40%, T^3) ppm.

IR (film): $\tilde{\nu}$ = 3410 cm^{-1} (broad peak, low intensity): low Si-OH content.

Refractive index: n_D^{20} = 1.570.

NIR (filtered over 0.45 µm filter):

Wavelength	350 nm	1310 nm	1550 nm
Absorption Loss	2.00 dB/cm	0.44 dB/cm	0.78 dB/cm

SAXS (toluene): Size of oligomers below detection limit (< 1 nm in diameter).

Dynamic viscosity (20 °C): η = 45.7 Pa s.

4.5 Syntheses of ORMOCER® inorganic-organic hybrid polymers

4.5.1 General method for clean room processing of ORMOCER® resins

Processing of ORMOCER® resins to form bulk samples or thin films was performed in a clean room with a specification of 100 / 1000 / 10000 particles per cubic meter (three areas). The clean room was equipped with yellow light bulbs to prevent untimely decomposition of the photo initiator.

For the preparation of ORMOCER® lacquers ready for coating and UV-exposure, the respective ORMOCER® resin (3.00 g – 35.1 g) was diluted with propyl acetate (0.513 g – 8.76 g), propylene glycol monomethyl ether acetate (PGMEA), and toluene (0.523 g – 3.28 g), respectively, and mixed with commercially available photo initiators Lucirin® LR 8893 (now renamed as Lucirin® TPO-L, 0.069 g – 1.10 g) and Irgacure® 907 (0.360 g – 0.826 g), respectively. The viscous lacquer underwent pressure filtration (0.2 µm PTFE, 4 bar) in order to remove impurity particles.

For the preparation of ORMOCER® bulk and powder samples, the respective ORMOCER® lacquer (1.00 g – 2.98 g) was poured into an aluminum platter of 5 cm in diameter, and silica glass slides, respectively, and exposed to UV light emitted by a Bluepoint 3 lamp (405 nm, 20 mW/cm^2, 60 s – 600 s). Finally, the sample was thermally cured at 110 °C – 170 °C for 5 min – 3 h. Bulk samples were ground for analysis with solid state NMR (^{29}Si) and FT-IR spectroscopy.

ORMOCER® thin film processing on substrates (silicon wafer 4'', silica glass, silicon wafer with 8 µm silicon dioxide layer, or in multilayer processing another ORMOCER® layer) followed typical procedures employed in micro systems technology[66]. The substrates were coated with the respective ORMOCER® lacquers by spin-coating on a Fairchild 501 or Convac 1001s spinner system (400 – 2500 rpm, 40 s). After edge bead removal with acetone, the samples underwent a prebake step on a hot plate (80 – 110 °C, 0 – 120 s), prior to UV exposure in an MA 45 mask aligner (350 nm, 17 mW/cm^2, 60 – 300 s). Exposure through a mask (ISC-Eichmaske, LWL, or D-PT) occurred at proximities of 80 – 200 µm. The samples then underwent postexposurebake (110 °C, 60 – 600 s). Unexposed lacquer was washed away with a developer (4-methyl-2-pentanone, isopropanol, toluene, or a mixture of these, 30 – 120 s) and the developed microstructures were rinsed with solvent (isopropanol, ethyl acetate, 4-methyl-2-pentanone, toluene, or acetone). The reaction was completed by thermal curing at 150 – 170 °C for 2 h – 3 h in an oven. Thin films were analyzed by optical microscopy (Leica INM20), Alpha Step 200 profilometer, prism coupler, and micro indenter. Optical loss values were measured at Fraunhofer-IOF on strip waveguides with the cut-back method. For dielectrical testing with a modified impedance analyzer, capacitor multilayers were

manufactured with embedded ORMOCER® thin films between copper capacitor plates, which were deposited using von Ardenne LS 730 S sputter equipment..

4.5.2 Preparation of ORMOCER® lacquers

Table 34 details ORMOCER® lacquer compositions. Photo initiator and diluter were added in measures of weight percent as a commonly used dimension in industrial applications. The amount of resin was taken as reference (100 wt.%). Thus, the overall percentage of a ready-made lacquer equals the sum of all percentages (e.g. 100 wt.% resin + 25 wt.% diluter + 3 wt.% starter = 128 wt.% lacquer). This method is common practice among the technological/industrial partners of Fraunhofer-ISC, and therefore also adopted within this work. Liquid photo initiator Lucirin® LR 8893 / Lucirin® TPO-L was pressure filtered (0.2 µm PTFE, 4 bar) prior to addition to likewise filtered (0.2 µm PTFE, 4 bar) ORMOCER® resin / diluter mixture. Solid photo starter Irgacure® 907 was admixed prior to filtering. Weight loss due to filtering of the diluted resin was taken into account in the addition of photo initiators. ORMOCER® lacquer **fk37-4a** was prepared at Fraunhofer-IOF, Jena. Lacquers **fk37-2b** and **fk37-2c** contain mixtures (50:50 wt.%) of resin **fk37-2** with experimental non-aromatic, methacrylate-based ORMOCER® resin composition **V32-8**, which was kindly provided by members of the KF5 competence team at ISC.

Tab. 34: ORMOCER® lacquer compositions.

lacquer	resin		diluter		photo initiator	
fk13a	**fk13**	1.00 g 100 wt.%	propyl acetate	1.00 g 100 wt.%	Lucirin® LR 8893	0.03 g 3 wt.%
fk14a	**fk14**	1.00 g 100 wt.%	propyl acetate	1.00 g 100 wt.%	Lucirin® LR 8893	0.03 g 3 wt.%
fk16a	**fk16**	1.00 g 100 wt.%	propyl acetate	0.45 g 45 wt.%	Lucirin® LR 8893	0.03 g 3 wt.%
fk18a	**fk18**	1.01 g 100 wt.%	propyl acetate	0.200 g 20 wt.%	Lucirin® LR 8893	0.01 g 1 wt.%
fk18b	**fk18**	3.30 g 100 wt.%	propyl acetate	0.661 g 20 wt.%	Lucirin® LR 8893	0.100 g 3 wt.%
fk19a, fk19c	**fk19**	2.77 g 100 wt.%	toluene	0.555 g 20 wt.%	Lucirin® LR 8893	0.097 g 3 wt.%
fk19d	**fk19**	2.09 g 100 wt.%	toluene	0.523 g 25 wt.%	Lucirin® LR 8893	0.073 g 3 wt.%

Tab. 34 continued (1):

lacquer	resin		diluter		photo initiator	
fk20a	**fk20**	1.64 g 100 wt.%	toluene	3.28 g 200 wt.%	Lucirin® LR 8893	0.048 g 3 wt.%
fk34a	**fk34**	8.00 g 100 wt.%	propyl acetate	2.00 g 25 wt.%	Lucirin® LR 8893	0.244 g 3 wt.%
fk34b	**fk34**	8.00 g 100 wt.%	propyl acetate	1.00 g 12.5 wt.%	Lucirin® LR 8893	0.242 g 3 wt.%
fk34c	**fk34**	8.14 g 100 wt.%	propyl acetate	2.07 g 25 wt.%	Lucirin® LR 8893	0.251 g 3 wt.%
fk34d	**fk34**	3.00 g 100 wt.%	propyl acetate	0.750 g 25 wt.%	Lucirin® LR 8893	0.069 g 3 wt.%
fk34e	**fk34**	8.00 g 100 wt.%	propyl acetate	1.00 g 12.5 wt.%	Lucirin® LR 8893	0.171 g 3 wt.%
fk34f	**fk34**	9.49 g 100 wt.%	propyl acetate	1.19 g 12.5 wt.%	Lucirin® LR 8893	0.228 g 3 wt.%
fk35a	**fk35**	3.69 g 100 wt.%	propyl acetate	0.460 g 12.5 wt.%	Lucirin® LR 8893	0.092 g 3 wt.%
fk37a	**fk37**	4.04 g 100 wt.%	propyl acetate	0.513 g 12.5 wt.%	Lucirin® LR 8893	0.099 g 3 wt.%
fk37-2a	**fk37-2**	8.07 g 100 wt.%	propyl acetate	2.05 g 25 wt.%	Lucirin® LR 8893	0.190 g 3 wt.%
fk37-2b	**fk37-2** **V32-8**	6.89 g 100 wt.%	propyl acetate	0.876 g 12.5 wt.%	Lucirin® LR 8893	0.197 g 3 wt.%
fk37-2c	**fk37-2** **V32-8**	4.82 g 100 wt.%	propyl acetate	1.21 g 25 wt.%	Lucirin® LR 8893	0.145 g 3 wt.%
fk37-2e	**fk37-2**	17.6 g 100 wt.%	propyl acetate	4.40 g 25 wt.%	Lucirin® TPO-L	0.44 g 2.5 wt.%
fk37-3a	**fk37-3**	35.1 g 100 wt.%	propyl acetate	8.76 g 25 wt.%	Irgacure® 907	0.360 g 1 wt.%
fk37-3b	**fk37-3**	27.5 g 100 wt.%	propyl acetate	6.88 g 25 wt.%	Irgacure® 907	0.826 g 3 wt.%
fk37-3c	**fk37-3**	19.3 g 100 wt.%	propyl acetate	4.83 g 25 wt.%	Irgacure® 907	0.579 g 3 wt.%
fk37-4a	**fk37-4**	100 wt.%	PGMEA		Lucirin® TPO-L	2 wt.%

Tab. 34 continued (2):

lacquer	resin		diluter		photo initiator	
fk38a	**fk38**	9.32 g 100 wt.%	propyl acetate	1.21 g 12.5 wt.%	Lucirin® LR 8893	0.291 g 3 wt.%
fk38b	**fk38**	3.00 g 100 wt.%	propyl acetate	0.75 g 25 wt.%	Lucirin® LR 8893	0.067 g 3 wt.%
fk38c	**fk38**	8.00 g 100 wt.%	propyl acetate	1.00 g 12.5 wt.%	Lucirin® LR 8893	0.320 g 5 wt.%
fk38d	**fk38**	26.9 g 100 wt.%	propyl acetate	1.68 g 6.25 wt.%	Lucirin® LR 8893	1.10 g 5 wt.%

4.5.3 Preparation and characterization of ORMOCER® powder samples

Table 35 depicts in detail the parameters used in the preparation of ORMOCER® powder samples for solid-state NMR and FT-IR measurements. The samples were prepared from lacquers ready for clean room processing (Tab. 34). UV exposure data apply to utilization of a Bluepoint 3 lamp. Irradiation intensities were determined at 405 nm.

Tab. 35: ORMOCER® powder samples.

sample	lacquer		substrate	UV exposure	thermal curing
fk19/2	**fk19c**	(1.00 g)	silica glass slide	20 mW/cm^2, 600 s	110 °C, 5 min
fk34d/1	**fk34d**	(2.77 g)	aluminum platter	20 mW/cm^2, 60 s	170 °C, 3 h
fk35a/3	**fk35a**	(1.82 g)	aluminum platter	20 mW/cm^2, 60 s	170 °C, 3 h
fk37a/4	**fk37a**	(1.90 g)	aluminum platter	20 mW/cm^2, 60 s	170 °C, 3 h
fk38b/1	**fk38b**	(2.98 g)	aluminum platter	20 mW/cm^2, 180 s	170 °C, 3 h

Characterization of ORMOCER® sample fk19/2:

^{29}Si-NMR (59.6 MHz, solid state): δ = -53.9 (41%, D^2), -80.7 (10%, T^2), -90.2 (49%, T^3), ppm.

Characterization of ORMOCER® sample fk34d/1:

^{29}Si-NMR (79.5 MHz, solid state): δ = -55.3 (34%, D^2), -71.0 (1%, T^2_{vinyl}), -81.1 (19%, $T^2_{fluoroaryl}$, T^3_{vinyl}), -87.0 (3%, Q^1), -90.1 (27%, $T^3_{fluoroaryl}$), -94.2 (8%, Q^2), -110.8 (8%, Q^3, Q^4) ppm.

IR (film): $\tilde{\nu}$ = 3420 cm^{-1} (broad peak, medium intensity): medium Si-OH content.

Characterization of ORMOCER® sample fk35a/3:

^{29}Si-NMR (79.5 MHz, solid state): δ = -54.3 (36%, D^2), -80.2 (17%, $T^2_{fluoroaryl}$, T^3_{vinyl}), -85.7 (4%, Q^1), -90.2 (29%, $T^3_{fluoroaryl}$), -93.2 (5%, Q^2), -100.0 – -112.3 (9%, Q^3, Q^4) ppm.

IR (film): $\tilde{\nu}$ = 3400 cm^{-1} (broad peak, medium intensity): medium Si-OH content.

Characterization of ORMOCER® sample fk37a/4:

^{29}Si-NMR (79.5 MHz, solid state): δ = -54.3 (34%, D^2), -82.1 (12%, $T^2_{fluoroaryl}$, T^3_{vinyl}), -85.0 (3%, Q^1), -91.1 (36%, $T^3_{fluoroaryl}$), -94.2 (6%, Q^2), -110.8 (9%, Q^3, Q^4) ppm.

IR (film): $\tilde{\nu}$ = 3400 cm^{-1} (broad peak, low intensity): low Si-OH content.

Characterization of ORMOCER® sample fk38b/1:

^{29}Si-NMR (79.5 MHz, solid state): δ = -47.0 (8%, D^1), -55.0 (38%, D^2), -72.8 (4%, $T^1_{fluoroaryl}$), -80.9 (25%, $T^2_{fluoroaryl}$, T^3_{vinyl}), -91.0 (20%, $T^3_{fluoroaryl}$), -105.3 (1%, Q^3), -112.4 (4%, Q^4) ppm.

IR (film): $\tilde{\nu}$ = 3420 cm^{-1} (broad peak, medium intensity): medium Si-OH content.

4.5.4 ORMOCER® thin films and multilayers

Table 36 details process parameters chosen for the preparation of ORMOCER® thin films and multilayers. Numerations of lacquers refer to the lacquer compositions outlined in Tab. 34. All exposure data refer to processing in a MA 45 mask aligner (350 nm, 17 mW/cm^2). ORMOCER® thin films **fk37-4a/1** and **fk37-4a/2** were kindly prepared and analyzed at Fraunhofer-IOF, Jena.

Abbreviations used in Tab. 36:

BlueP	UV exposure with Bluepoint 3 lamp, 100 mW/cm^2
curing	thermal curing parameters
D-PT	Dielektrikum PT (mask)
expos.	UV exposure time
flood	UV flood exposure, without the use of a mask
glass	silica glass slide
ISC	ISC-Eichmaske (mask)
LWL	Lichtwellenleiter (mask)
MIBK	4-methyl-2-pentanone (methyl isobutyl ketone)
PGMEA	propylene glycol monomethyl ether acetate
postexp.	postexposurebake
^{i}PrOH	2-propanol (isopropanol)
Si	silicon wafer
Si/El20	silicon wafer, coated with epoxy-functionalized, non-fluorinated ORMOCER® **El20**
Si/SiO_2	silicon wafer with 8 µm oxide layer grown on top
substr.	substrate

Tab. 36: Process parameters for the preparation of ORMOCER® thin film and multilayer samples.

sample	lacquer	substr.	spin-on	prebake	expos.	mask	postexp.	developer	rinse	curing	film thickness	notes
fk13a/1	**fk13a**	Si	250 rpm	80 °C 120 s	300 s	D-PT	110 °C 120 s	MIBK/^{i}PrOH 1:1, 30 s	^{i}PrOH			film completely removed during development
fk13a/2	**fk13a**	Si	250 rpm	80 °C 120 s	900 s	D-PT	110 °C 120 s	MIBK/^{i}PrOH 1:1, 30 s	^{i}PrOH			film completely removed during development
fk14a/1	**fk14a**	Si	250 rpm	80 °C 120 s	300 s	D-PT	110 °C 120 s	MIBK/^{i}PrOH 1:1, 30 s	^{i}PrOH			film completely removed during development
fk14a/2	**fk14a**	Si	250 rpm	80 °C 120 s	900 s	D-PT	110 °C 120 s	MIBK/^{i}PrOH 1:1, 30 s	^{i}PrOH			film completely removed during development
fk16a/1	**fk16a**	Si	250 rpm	80 °C 120 s	900 s	D-PT	110 °C 120 s	MIBK/^{i}PrOH 1:1, 30 s	^{i}PrOH			film completely removed during development
fk18a/1	**fk18a**	Si	1000 rpm	110 °C 120 s	60 s	ISC	110 °C 120 s	MIBK/^{i}PrOH 1:3, 45 s	^{i}PrOH	170 °C 2 h	15 – 18 µm	film largely cracked
fk18a/2	**fk18a**	Si	1000 rpm	110 °C 120 s	90 s	ISC	110 °C 120 s	MIBK/^{i}PrOH 1:3, 30 s	^{i}PrOH	170 °C 3 h	23 µm	film largely cracked
fk18b/1	**fk18b**	Si	1000 rpm	110 °C 120 s	60 s	ISC	110 °C 120 s	MIBK/^{i}PrOH 1:1, 30 s	^{i}PrOH	170 °C 3 h	10 µm	removal of most structures during development
fk19a/1	**fk19a**	Si	1000 rpm	110 °C 120 s	90 s	ISC	110 °C 120 s	MIBK/^{i}PrOH 1:3, 45 s	^{i}PrOH	170 °C 3 h	17 µm	largely cracked
fk19d/1	**fk19d**	glass	500 rpm	110 °C 120 s	90 s	flood	110 °C 120 s	MIBK/^{i}PrOH 1:3, 30 s	^{i}PrOH	170 °C 3 h		completely cracked, no adhesion to substrate
fk20a/1	**fk20a**	Si	manual application	110 °C 120 s	90 s	ISC	110 °C 120 s	MIBK/^{i}PrOH 1:3, 45 s	^{i}PrOH	170 °C 3 h	5 – 15 µm	thicker than 5 µm cracked, particles

Tab. 36 continued (1).

sample	lacquer	substr.	spin-on	prebake	expos.	mask	postexp.	developer	rinse	curing	film thickness	notes
fk34a/1	**fk34a**	Si	1000 rpm	110 °C 120 s	90 s	ISC	110 °C 120 s	MIBK/^{i}PrOH 1:3, 150 s	^{i}PrOH	170 °C 3 h	5.1 – 5.5 µm	well resolved, little residual lacquer
fk34a/2	**fk34a**	Si	1000 rpm	110 °C 60 s	60 s	ISC	110 °C 60 s	MIBK/^{i}PrOH 1:3, 30 s	^{i}PrOH	170 °C 3 h	2.3 µm	very well resolved
fk34a/3	**fk34a**	glass	1000 rpm	110 °C 60 s	60 s	flood	110 °C 60 s	MIBK/^{i}PrOH 1:3, 30 s	^{i}PrOH	170 °C 3 h	6 – 8 µm	film rough, wetting problems
fk34a/4	**fk34a**	glass	1000 rpm	110 °C 120 s	60 s	flood	110 °C 120 s	MIBK/^{i}PrOH 1:1, 30 s	^{i}PrOH	170 °C 3 h	4 – 5 µm	wetting problems
fk34a/5	**fk34a**	glass	1000 rpm	110 °C 120 s	60 s	flood	110 °C 120 s	MIBK/^{i}PrOH 1:1, 30 s	^{i}PrOH	170 °C 3 h	10 – 11 µm	wetting problems
fk34b/1	**fk34b**	Si	1000 rpm	110 °C 60 s	60 s	ISC	110 °C 60 s	MIBK/^{i}PrOH 1:1, 30 s	^{i}PrOH	170 °C 3 h	17 – 18 µm	structures largely displaced
fk34b/2	**fk34b**	Si	2000 rpm	110 °C 60 s	90 s	ISC	110 °C 120 s	MIBK/^{i}PrOH 1:1, 30 s	^{i}PrOH	170 °C 3 h	9 – 11 µm	structures largely displaced, 10% shrinkage due to thermal curing
fk34c/1	**fk34c**	Si	1000 rpm	110 °C 60 s	60 s	ISC	110 °C 60 s	MIBK/^{i}PrOH 1:1, 30 s	^{i}PrOH	170 °C 3 h	5 µm	excellent film and structures
fk34c/2	**fk34c**	Si	500 rpm	110 °C 60 s	60 s	ISC	110 °C 60 s	MIBK/^{i}PrOH 1:1, 30 s	^{i}PrOH	170 °C 3 h	8 – 10 µm	well resolved, little displacement
fk34c/3	**fk34c**	glass	1000 rpm	110 °C 60 s	60 s	flood	110 °C 60 s	MIBK/^{i}PrOH 1:1, 30 s	^{i}PrOH	170 °C 3 h	6.3 µm	film rough, wetting problems
fk34c/4	**fk34c**	glass	1000 rpm	110 °C 60 s	60 s	flood	110 °C 60 s	MIBK/^{i}PrOH 1:1, 30 s	^{i}PrOH	170 °C 3 h	7.4 µm	film rough, wetting problems
fk34e/1	**fk34e**	Si	2000 rpm	110 °C 60 s	60 s	LWL	110 °C 60 s	MIBK/^{i}PrOH 1:3, 30 s	^{i}PrOH	170 °C 3 h	3.5 – 6 µm	structures well resolved

Tab. 36 continued (2).

sample	lacquer	substr.	spin-on	prebake	expos.	mask	postexp.	developer	rinse	curing	film thickness	notes
fk34f/1	**fk34f**	Si	1500 rpm	110 °C 60 s	30 s	LWL	110 °C 120 s	MIBK, 30 s	MIBK	170 °C 3 h	2.5 µm	very well resolved
fk34f/2	**fk34f**	Si	1500 rpm	110 °C 60 s	60 s	LWL	110 °C 120 s	MIBK, 30 s	MIBK	170 °C 3 h	18 µm	well resolved, high aspect ratio
fk34f/3	**fk34f**	Si	1000 rpm	110 °C 60 s	30 s	LWL	110 °C 120 s	MIBK, 30 s	MIBK	170 °C 3 h	2 µm	only large structures remain on substrate
fk35a/1	**fk35a**	Si	1000 rpm	110 °C 60 s	60 s	ISC	110 °C 120 s	MIBK, 60 s	MIBK	170 °C 3 h	17 – 20 µm	small items resolved, large 60% removed
fk35a/2	**fk35a**	Si	2000 rpm	110 °C 60 s	60 s	ISC	110 °C 120 s	MIBK, 30 s	MIBK	170 °C 3 h	12 – 14 µm	small items resolved, large 30% removed
fk37a/1	**fk37a**	Si	1000 rpm	110 °C 60 s	60 s	ISC	110 °C 120 s	MIBK/^{i}PrOH 1:1, 30 s	MIBK	170 °C 3 h	16 µm	rinse causes removal of most structures
fk37a/2	**fk37a**	Si	1000 rpm	110 °C 60 s	60 s	ISC	110 °C 120 s	MIBK/^{i}PrOH 1:1, 60 s	^{i}PrOH	170 °C 3 h	16 – 20 µm	fine structures resolved, large cracked
fk37a/3	**fk37a**	glass	1000 rpm	110 °C 120 s	60 s	flood	110 °C 240 s	MIBK/^{i}PrOH 1:1, 60 s	^{i}PrOH	170 °C 3 h	30 – 45 µm	film completely cracked
fk37-2a/1	**fk37-2a**	glass	2000 rpm	110 °C 120 s	60 s	flood	110 °C 240 s	MIBK/^{i}PrOH 1:1, 30 s	^{i}PrOH, EtOAc	170 °C 3 h	6 µm	rinse with ^{i}PrOH causes precipitation
fk37-2a/4	**fk37-2a**	Si	2000 rpm	110 °C 60 s	60 s	D-PT	110 °C 120 s	toluene, 30 s	toluene	170 °C 3 h	3.2 – 3.5 µm	slight wetting problems
fk37-2b/2	**fk37-2b**	glass	2000 rpm	110 °C 120 s	60 s	flood	110 °C 240 s	toluene, 30 s	toluene	170 °C 3 h	18 µm	film completely cracked
fk37-2b/3	**fk37-2b**	Si	2000 rpm	110 °C 60 s	60 s	D-PT	110 °C 120 s	toluene, 30 s	toluene	170 °C 3 h	19 µm	50% of small, 90% of large structures cracked

Tab. 36 continued (3).

sample	lacquer	substr.	spin-on	prebake	expos.	mask	postexp.	developer	rinse	curing	film thickness	notes
fk37-2c/2	**fk37-2c**	glass	2000 rpm	110 °C 120 s	60 s	flood	110 °C 240 s	toluene, 30 s	toluene	170 °C 3 h	7.5 µm (pre-curing)	no adhesion to substrate
fk37-2c/22	**fk37-2c**	Si	2000 rpm	110 °C 60 s	60 s	D-PT	110 °C 120 s	toluene, 30 s	toluene	170 °C 3 h	13.8 µm	removal of most structures during development
fk37-2c/23	**fk37-2c**	glass	2000 rpm	110 °C 120 s	60 s	flood	110 °C 240 s	toluene, 30 s	toluene	170 °C 3 h		no adhesion to substrate
fk37-3a/4	**fk37-3a**	Si	2000 rpm	110 °C 60 s	30 s	ISC	110 °C 120 s	toluene on spinner				good wetting, film completely removed during development
fk37-3a/5	**fk37-3a**	Si	2000 rpm	110 °C 120 s	60 s	ISC	110 °C 120 s	toluene on spinner				film completely removed during development
fk37-3a/6	**fk37-3a**	Si	2000 rpm	110 °C 120 s	300 s	ISC	110 °C 120 s	toluene on spinner				film completely removed during development
fk37-3b/4	**fk37-3b**	Si	1000 rpm	110 °C 60 s	300 s	flood	110 °C 60 s	toluene on spinner		150 °C 3 h	1 µm	structures appear extremely thin
fk37-3b/5	**fk37-3b**	Si	400 rpm	110 °C 60 s	300 s	flood	110 °C 60 s	toluene on spinner		150 °C 3 h	4.5 µm	removal of most structures during development
fk37-3b/6	**fk37-3b**	Si	1000 rpm	110 °C 60 s	300 s	flood	110 °C 300 s	toluene on spinner		150 °C 3 h		removal of most structures during development
fk37-3b/7	**fk37-3b**	Si	400 rpm	110 °C 60 s	BlueP 30 s		110 °C 60 s	toluene on spinner				film completely removed during development

Tab. 36 continued (4).

sample	lacquer	substr.	spin-on	prebake	expos.	mask	postexp.	developer	rinse	curing	film thickness	notes
fk37-3b/8	**fk37-3b**	Si/El20	1000 rpm	110 °C 60 s	30 s	ISC	110 °C 60 s	toluene on spinner				film completely removed during development
fk37-3b/9	**fk37-3b**	Si/El20	1000 rpm	110 °C 60 s	300 s	ISC	110 °C 60 s	toluene on spinner				removal of most structures during development
fk37-3b/10	**fk37-3b**	Si/El20	1000 rpm	110 °C 60 s	300 s	ISC	110 °C 300 s	toluene on spinner				removal of most structures during development
fk37-3c/1	**fk37-3c**	Si/El20	800 rpm	110 °C 60 s	300 s	ISC	110 °C 60 s	toluene on spinner		150 °C 3 h	2 µm	well resolved
fk37-3c/2	**fk37-3c**	Si/El20	400 rpm		300 s	ISC	110 °C 60 s	toluene on spinner		150 °C 3 h	17.5 µm	well resolved
fk37-3c/3	**fk37-3c**	glass	600 rpm		300 s	flood	110 °C 240 s	toluene on spinner		150 °C 3 h		removal of most structures during development, residues cracked after curing
fk37-3c/4	**fk37-3c**	Si/El20	600 rpm		300 s	flood	110 °C 60 s	toluene on spinner		150 °C 3 h	10 µm	good film quality
fk37-3c/5	**fk37-3c**	Si/El20	650 rpm		300 s	LWL	80 °C 60 s	toluene on spinner		150 °C 3 h		structures well resolved, substrate film polluted with particles
fk37-4a/1	**fk37-4a**	Si/SiO_2			1 J/cm^2, N_2	flood				180 °C 1 h, N_2	6 µm	0.51 dB/cm at 1550 nm, n_f = 1.475
fk37-4a/2	**fk37-4a**	Si/SiO_2			1 J/cm^2, N_2	flood				150 °C 1 d, N_2	6 µm	0.55 dB/cm at 1550 nm, n_f = 1.473

Tab. 36 continued (5).

sample	lacquer	substr	spin-on	prebake	expos.	mask	postexp.	developer	rinse	curing	film thickness	notes
fk38a/1	**fk38a**	Si	1000 rpm	110 °C 60 s	60 s	ISC	110 °C 60 s	MIBK/^{i}PrOH 1:3, 20 s	^{i}PrOH	170 °C 3 h	8 – 9 µm	well resolved, sparsely cracked
fk38a/2	**fk38a**	Si	500 rpm	110 °C 60 s	60 s	ISC	110 °C 60 s	MIBK/^{i}PrOH 1:3, 20 s	^{i}PrOH	170 °C 3 h	18 – 20 µm	cracked after curing
fk38a/3	**fk38a**	glass	500 rpm	110 °C 120 s	60 s	flood	110 °C 240 s	MIBK/^{i}PrOH 1:3, 20 s	^{i}PrOH	170 °C 3 h	20 µm	completely cracked, no adhesion to substrate
fk38a/4	**fk38a**	glass	1000 rpm	110 °C 120 s	60 s	flood	110 °C 240 s	MIBK/^{i}PrOH 1:3, 20 s	^{i}PrOH	170 °C 3 h	10 µm	completely cracked, no adhesion to substrate
fk38c/1	**fk38c**	Si	1000 rpm	110 °C 60 s	60 s	flood	110 °C 60 s	MIBK/^{i}PrOH 1:1, 30 s	^{i}PrOH	170 °C 3 h	3.7 µm	well resolved
fk38d/1	**fk38d**	Si	1000 rpm	110 °C 60 s	30 s	ISC	110 °C 60 s	MIBK/^{i}PrOH 1:1, 30 s	^{i}PrOH, MIBK	170 °C 3 h	11 µm (fine) 18 µm (large)	fine structures well resolved, large ones mostly cracked
fk38d/2	**fk38d**	Si	1000 rpm	110 °C 60 s	60 s	flood	110 °C 60 s	MIBK/^{i}PrOH 1:1, 20 s	^{i}PrOH	170 °C 3 h	20 µm	rinse with ^{i}PrOH causes precipitation, film widely cracked after curing
fk38d/3	**fk38d**	Si	2000 rpm	110 °C 60 s	60 s	flood	110 °C 60 s	MIBK, 30 s	MIBK	170 °C 3 h	11 µm	cracked after curing
fk38d/4	**fk38d**	Si	2000 rpm	110 °C 60 s	60 s	flood	110 °C 60 s	MIBK, 30 s	MIBK	170 °C 3 h	8.3 µm	cracked after curing

Tab. 36 continued (6).

sample	lacquer	substr.	spin-on	prebake	expos.	mask	postexp.	developer	rinse	curing	film thickness	notes
fk43/1a	**fk38c**	Si	1500 rpm	110 °C 60 s	60 s	flood	110 °C 60 s	MIBK/^{i}PrOH 1:3, 30 s	^{i}PrOH	170 °C 0.5 h	2.2 µm	good adhesion to substrate
fk43/1b	**fk38c**	sample **fk43/1a**	1500 rpm	110 °C 60 s	60 s	flood	110 °C 60 s	MIBK/^{i}PrOH 1:3, 30 s	^{i}PrOH	170 °C 0.5 h	1.9 µm	good adhesion to substrate film
fk43/1c	**fk34e**	sample **fk43/1b**	2500 rpm	110 °C 60 s	60 s	LWL	110 °C 240 s	MIBK/^{i}PrOH 1:3, 30 s	^{i}PrOH, EtOAc	170 °C 3 h	4 µm	rinse with ^{i}PrOH causes precipitation, insoluble particles remain
fk43/2a	**fk38d**	Si	2000 rpm	110 °C 60 s	60 s	flood	110 °C 60 s	MIBK/^{i}PrOH 1:1, 30 s	EtOAc, MIBK	170 °C 0.5 h	8 µm	small areas are lifted off during development
fk43/2b	**fk38d**	sample **fk43/2a**	2000 rpm	110 °C 60 s	60 s	flood	110 °C 60 s	MIBK/^{i}PrOH 1:1, 30 s	MIBK	170 °C 3 h	8 µm	after curing both films together cracked as if one, no adhesion to Si
fk43/3a	**fk38d**	Si	2000 rpm	110 °C 300 s	60 s	flood	110 °C 60 s	MIBK, 30 s	MIBK	170 °C 3 h	16 µm	good adhesion to substrate
fk43/3b	**fk34f**	sample **fk43/3a**	2000 rpm	110 °C 60 s	60 s	LWL	110 °C 60 s	MIBK, 30 s	acetone	170 °C 3 h	10 – 11 µm	well resolved, but many waveguides removed or displaced during development
fk43/3c	**fk38d**	sample **fk43/3b**	2000 rpm		60 s	flood	110 °C 600 s	MIBK, 30 s	acetone	170 °C 3 h	11 µm	30% film remain on substrate film, widely cracked after curing, small embedded waveguides

Characterization of ORMOCER® thin film fk18b/1:

Microhardness: HU = 181.4 N/mm^2 +/- 10.18 N/mm^2.

Young's Modulus: Y = 4.34 GPa +/- 0.26 GPa.

Characterization of ORMOCER® thin film fk34c/1:

Refractive index (prism coupler):

λ **[nm]**	635	830	1310	1550
n	1.4930	1.4865	1.4818	1.4812

Microhardness: HU = 218.3 N/mm^2 +/- 16.67 N/mm^2.

Young's Modulus: Y = 7.96 GPa +/- 0.69 GPa.

Characterization of ORMOCER® thin film fk37-2a/4:

Microhardness: HU = 173.1 N/mm^2 +/- 11.51 N/mm^2.

Young's Modulus: Y = 4.80 GPa +/- 0.27 GPa.

Characterization of ORMOCER® thin film fk37-4a/1:

Optical loss (cut back): 0.51 dB/cm at 1550 nm.

Refractive index: *n* = 1.475 at 1550 nm.

Characterization of ORMOCER® thin film fk37-4a/2:

Optical loss (cut back): 0.55 dB/cm at 1550 nm.

Refractive index: *n* = 1.473 at 1550 nm.

Characterization of ORMOCER® thin film fk38c/1:

Refractive index (prism coupler):

λ **[nm]**	635	830	1310	1550
n	1.4908	1.4853	1.4816	1.4809

Microhardness: HU = 139.1 N/mm^2 +/- 3.52 N/mm^2.

Young's Modulus: Y = 3.54 GPa +/- 0.16 GPa.

4.5.5 Capacitors with embedded ORMOCER® fk37 thin films for dielectrical testing

Silicon wafers with copper capacitor patterns (bottom platters) were spin-coated with a silanizing agent (solution of 3-methacryloxypropyltrimethoxysilane in isopropanol), followed by subsequent thermal curing at 100 °C for 3 min and washing with isopropanol. On top of this thin adhesion promoter film, ORMOCER® lacquer **fk37-2e** was coated, applying the processing parameters below:

spin-on	Fairchild 501 spinner, 900 rpm, 40 s > 0
prebake	110 °C, 60 s
exposure	MA45 mask aligner, 350 nm, 60 s, 17 mW/cm^2, flood exposure
postexposure bake	110 °C, 120 s
developer	toluene on spinner
thermal curing	160 °C, 3 h
film thickness	4.5 – 5.0 µm
notes	excellent film

Film thicknesses before development were 16 – 17 µm, i.e. an inhibition layer of 11 – 12 µm ? approx. 70% could be demonstrated.

For the application of the top copper patterns, the samples were spin-coated (1000 rpm) with positive photoresist ma-P 1215. After prebake (100 °C, 90 s) and UV exposure (MA 45, 17 mW/cm^2, 35 s), the photoresist negatives of the capacitor patterns were developed (developer ma-D 331, 25 s). A sputtered thin film (several angstroms) of titanium/tungsten was applied as adhesion promoter prior to plasma deposition of a copper layer of approx. 135 nm thickness. Final stripping of the residual photoresist covered with metal by treatment with acetone in an ultrasonic bath (5 min) accounted for isolation of the capacitor plates (samples **fk37-2e/1**, **fk37-2e/2**).

Characterization of ORMOCER® thin films fk37-2e/1 and fk37-2e/2:

Dielectric permittivity: ε (10 kHz) = 3.7.

5 SUMMARY

The development and in-depth characterization of new fluoroaryl functionalized ORMOCER® materials (inorganic-organic hybrid polymers) for optical waveguide applications in telecommunication is presented. The preparation of the materials included precursor silane synthesis, hydrolysis/polycondensation of organoalkoxysilane mixtures, and photolithographic processing of the resulting oligosiloxane resins in order to establish the inorganic-organic hybrid network. During all stages of ORMOCER® preparation, structure-property relations were deduced from characterization data, particularly with respect to low optical loss in the important near-infrared spectral region as well as refractive index. With the aid of molecular modeling, structural characteristics of oligomeric intermediates were visualized, which was found valuable in the fundamental understanding of the material class.

The material development started with the syntheses of a variety of commercially unavailable fluorinated and unfluorinated arylalkoxysilanes by means of Grignard and hydrosilylation pathways, respectively. A survey of silane optical properties, particularly their absorptions at the telecom wavelengths 1310 nm and 1550 nm, gave an impulse to the choice of suitable precursors for the preparation of low-loss ORMOCER® resins. Accordingly, precursor silane mixtures and hydrolysis/polycondensation reaction conditions were chosen and optimized with regard to low contents of C-H and Si-OH functions. Thus, absorptions as low as 0.04 dB/cm at 1310 nm and 0.18 dB/cm at 1550 nm, respectively, could be obtained from an oligosiloxane resin based on pentafluorophenyltrimethoxysilane (**1**) mixed with pentafluorophenyl(vinyl)-dimethoxysilane (**5**). In order to improve the organic crosslinkability under photolithographic processing conditions, further resins on the basis of the aforementioned were prepared, which additionally incorporated the styrene-analogous precursor 4-vinyltetrafluorophenyl-trimethoxysilane (**4**). Thus, ORMOCER® resins with low optical losses of 0.28 dB/cm at 1310 nm and 0.42 dB/cm at 1550 nm, respectively, were prepared, which exhibited excellent photopatternability. The manufacture of micropatterns such as optical waveguide structures by UV-photolithography under clean room conditions was the final stage of material synthesis. The optimization of processing parameters allowed the preparation of test patterns for the determination of optical, dielectrical and mechanical properties. A low optical loss of 0.51 dB/cm at 1550 nm could be measured on a waveguide manufactured from a photopatternable fluoroaryl functionalized ORMOCER®.

The structural characterization of liquid resins as well as cured ORMOCER® samples was accomplished chiefly with solution and solid state ^{29}Si-NMR spectroscopy, respectively. Particularly for polycondensates incorporating species based on more than one precursor silane, the spectra showed a high degree of complexity. An additional challenge arouse from the partial

loss of fluoroaryl groups during ORMOCER® condensation and curing, which resulted in even more condensation products. Thus, in order to provide a basis for resin analysis, first the hydrolysis/condensation reactions of the isolated precursors were investigated under reaction time-resolution with NMR spectroscopy at low temperature. Backed by signal assignments in these single-precursor systems, the respective species could also be identified in the complex resin spectra, allowing for their quantitative interpretation. The structural characterization was rounded out by IR spectroscopy and SAXS analyses.

With the help of molecular modeling, the experimental data were finally transferred into a three-dimensional image of an organosiloxane oligomer, which is representative for a photopatternable fluoroaryl functionalized ORMOCER® resin. The combination of low-temperature NMR, which made the characterization of polycondensates possible, with oligomer modeling paved the way to a further understanding of ORMOCER® resin systems. On the basis of this visualization of structural characteristics, e.g. properties such as organic crosslinkability of oligomers were discussed in the light of steric features within the molecular structure. Thus, new possibilities were established for the systematic optimization of ORMOCER® formulations.

Structure-property relations with respect to optical loss and refraction, as determined within this work, follow trends, which are in accordance with the literature. Particularly the direct comparison of data derived from analogous fluorinated and unfluorinated ORMOCER® resins showed that fluorination results in significant decrease in NIR optical loss. Additionally, different unfluorinated aryl functionalized systems with varying aliphatic C-H content were compared. In case of a lower aliphatic content, a widening effect on the 1310 nm window was found. This is due to a shift of arylic C-H vibrations (1145 nm) towards lower wavelengths compared to aliphatic C-H (1188 nm). Finally, on the basis of NIR spectra of analogous fluorinated resins with low and high silanol content, respectively, a significant impact of (Si)O-H groups on the 1550 nm window was demonstrated, while the 1310 nm window was unaffected. This is due to O-H vibrations with a maximum at 1387 nm and further bands at higher wavelength. The index of refraction was drastically lowered due to fluorination. Thus, the analogous fluorinated and unfluorinated ORMOCER® resins had indices of 1.497 and 1.570, respectively, in the VIS region. For the fluorinated systems, refraction did not change significantly during organic cross-connection and hardbake.

In conclusion, the new fluoroaryl functionalized ORMOCER® systems represent low-loss materials for telecom applications. In addition, in-depth characterization during material development allowed the proposal of structure-property relations, particularly with respect to optical properties, which are of considerable importance for future developments.

6 ZUSAMMENFASSUNG – SUMMARY IN GERMAN

Die vorliegende Arbeit befasste sich mit der Entwicklung und detaillierten Charakterisierung von fluorarylmodifizierten ORMOCER®en (anorganisch-organischen Hybridpolymeren) für optische Wellenleiteranwendungen in der Tele- und Datenkommunikation. Die Materialsynthese erstreckte sich von der Darstellung von kommerziell nicht erhältlichen Arylalkoxysilanen, die als molekulare Vorstufen dienten, über deren Hydrolyse/Polykondensationsreaktion bis hin zur abschließenden photochemischen Prozessierung zum Aufbau des hybriden Polymernetzwerkes. Zu jedem dieser Entwicklungsstadien wurden Struktur-Eigenschaftsbeziehungen ermittelt. Hauptaugenmerk hierbei lag auf der optischen Dämpfung im relevanten Nah-Infrarotspektralbereich und der Brechzahl. Details in der Molekülstruktur von oligomeren Zwischenstufen schließlich wurden basierend auf spektroskopischen Daten mit Hilfe von Molecular Modeling visualisiert.

Die Synthesen der fluorierten und unfluorierten Arylalkoxysilane stützten sich wesentlich auf Grignard- und Hydrosilylierungsrouten. Bereits die Ermittlung von optischen Eigenschaften der Vorläufersilane lieferte wichtige Impulse für den einzuschlagenden Weg bei der Entwicklung von verlustarmen ORMOCER®-Harzen. Zur Erreichung geringer Schwingungsabsorptionen bei 1310 nm und 1550 nm wurden somit sowohl die initialen Silangemische als auch die Bedingungen der Polykondensationsreaktionen hinsichtlich geringem Gehalt an C-H und Si-OH Gruppen optimiert. Auf diese Weise konnten geringe optische Verluste von 0.04 dB/cm bei 1310 nm und 0.18 dB/cm bei 1550 nm an einem ORMOCER®-Harz gemessen werden, das ausgehend von Pentafluorphenyltrimethoxysilan (**1**) und Pentafluorphenyl(vinyl)-dimethoxysilan (**5**) dargestellt wurde. In der Folge wurden weitere Harzsysteme entwickelt, um die organische Vernetzbarkeit der Materialien unter photolithographischen Prozessierungsbedingungen zu erhöhen. Hierzu wurde basierend auf der vorgenannten Silanzusammensetzung das Styrol-analoge 4-Vinyltetrafluorphenyltrimethoxysilan (**4**) zum Ausgangsgemisch hinzugefügt. Damit konnten ORMOCER®-Harze von ausgezeichneter Photostrukturierbarkeit dargestellt werden, die geringe optische Verluste von bis zu 0.28 dB/cm bei 1310 nm und 0.42 dB/cm bei 1550 nm aufwiesen. Die Materialsynthese wurde vervollständigt durch die photolithographische Darstellung von optischen Wellenleitern und anderen Mikrostrukturen unter Ausbildung des anorganisch-organischen Hybridnetzwerks. Unter Reinraumbedingungen konnten Prozessierungsparameter dahingehend optimiert werden, dass die Präparation von ORMOCER®-Teststrukturen für die optische, dielektrische und mechanische Charakterisierung ermöglicht wurde. An einem optischen Schichtwellenleiter aus einem photostrukturierbaren fluorarylfunktionalisierten ORMOCER® wurde bei 1550 nm eine optische Dämpfung von 0.51 dB/cm gemessen.

Die Strukturaufklärung von flüssigen Harzen und ausgehärteten ORMOCER®-Proben erfolgte größtenteils mittels ^{29}Si-NMR Spektroskopie. Die Polykondensatspektren setzten sich aus einer Vielzahl von Signalen zusammen, die einerseits die Ausgangssilangemische und andererseits deren unterschiedliche Kondensationsstufen widerspiegelten. Eine zusätzliche Herausforderung ergab sich aus der partiellen Abspaltung der Fluorarylfunktionalität während der Prozessierung, die zu weiteren Kondensationsprodukten führte. Aufgrund der damit gegebenen Komplexität der Spektren wurden zunächst die Ausgangssilane isoliert einer Hydrolyse/Kondensationsreaktion unterworfen und die Reaktionsgemische zeitaufgelöst mittels Tieftemperatur-Messreihen analysiert. Auf Grundlage der damit getroffenen Signalzuordnungen für die Reaktionsintermediate konnten in der Folge ebenfalls die komplexen Kondensatspektren quantitativ aufgeschlüsselt werden. Die Strukturaufklärung wurde mittels Infrarotspektroskopie und Röntgenkleinwinkelstreuung (im Fall der Harze) vervollständigt.

Die Veranschaulichung der molekularen Struktur eines Siloxanoligomers in einem photopolymerisierbaren fluorarylfunktionalisierten ORMOCER®-Harz erfolgte mittels Molecular Modeling. Hierbei ist zu betonen, dass das resultierende Modell wesentlich auf experimentell ermittelten Strukturkenndaten basierte. Mit der Kombination Tieftemperatur-NMR / Harzcharakterisierung / Oligomermodeling wurde somit ein wichtiger Zugang zum weiteren Verständnis von ORMOCER®-Harzsystemen eröffnet. Als Beispiel konnten gestützt auf die Visualisierung von sterischen Charakteristika Eigenschaften wie die organische Vernetzbarkeit des Siloxanoligomers diskutiert werden. Hieraus eröffnen sich zukünftig neue Möglichkeiten zur gezielten Optimierung von ORMOCER®-Formulierungen.

Aus Charakterisierungsdaten wurden Struktur-Eigenschaftsbeziehungen hinsichtlich optischer Dämpfung und Brechzahl abgeleitet, die literaturkonformen Trends folgten. Insbesondere im direkten Vergleich von analogen fluorierten und unfluorierten Materialien wurde der Effekt des Ersatzes von C-H durch C-F Bindungen deutlich. Optische Dämpfungswerte im NIR wurden durch Fluorierung signifikant verringert. Darüber hinaus konnte im Vergleich von unfluorierten Hybridpolymeren mit unterschiedlich hohem Anteil an aliphatischen und aromatischen C-H Bindungen gezeigt werden, wie durch einen geringeren Anteil an Aliphaten das Telekommunikationsfenster bei 1310 nm erweitert wird. Dies ist durch die unterschiedliche Lage von Obertonschwingungen für aliphatische (1188 nm) und aromatische C-H (1145 nm) begründet. Schließlich konnte anhand von analogen fluorierten Harzen mit unterschiedlichem Silanolgehalt eine signifikante Erhöhung der Dämpfung bei 1550 nm durch (Si)O-H Obertonschwingungen nachgewiesen werden, während die Absorption bei 1310 nm unbeeinflusst blieb. Hierfür war ein Absorptionsmaximum bei 1387 nm sowie eine Reihe schwächerer Banden bei höheren Wellenlängen verantwortlich. Die Brechzahl der Materialien wurde durch Fluorierung drastisch verringert. So wurden im VIS-Spektralbereich bei

analogen fluorierten und unfluorierten Harzen Werte von 1.497 bzw. 1.570 ermittelt. Für den Fall der fluorierten Harzsysteme wurde keine signifikante Brechzahlveränderung im Zuge der organischen Quervernetzung festgestellt.

Die neuentwickelten fluorarylfunktionalisierten ORMOCER®e eignen sich im Fazit als niedrig dämpfende Materialien für Telekomanwendungen. Zudem konnten mit Hilfe einer detaillierten Strukturaufklärung Struktur-Eigenschaftsbeziehungen herausgearbeitet werden, die wichtige Impulse für zukünftige Entwicklungen auf dem Gebiet liefern.

7 REFERENCES

[1] ORMOCER® is a registered trademark of the Fraunhofer-Gesellschaft zur Förderung der angewandten Forschung e.V., Munich.

[2] (a) C.J. Brinker, G.W. Scherer, *Sol-Gel Science. The Physics and Chemistry of Sol-Gel Processing*. Academic Press, San Diego **1990**. (b) F.D. Osterholtz, E.R. Pohl, *J. Adhesion Sci. Technol.* **1992**, *6*, 127-149. (c) R.K. Iler, *The Chemistry of Silica*. Wiley, New York **1979**.

[3] J. Méndez-Vivar, A. Mendoza-Bandala, *J. Non-Cryst. Solids* **2000**, *261*, 127-136.

[4] Y. Sugahara, S. Okada, K. Kuroda, C. Kato, *J. Non-Cryst. Solids* **1992**, *139*, 25-34.

[5] (a) S.E. Rankin, C.W. Macosko, A.V. McCormick, *J. Polym. Sci., Part A: Polym. Chem.* **1997**, *35*, 1293-1302. (b) S.E. Rankin, C.W. Macosko, A.V. McCormick, *AIChE J.* **1998**, *44*, 1141-1156. (c) S.E. Rankin, C.W. Macosko, A.V. McCormick, *Chem. Mater.* **1998**, *10*, 2037-2040.

[6] J.L. Cruz Rivera, T.K. Gaylord, E.N. Glytsis in *Fundamentals of Microsystems Packaging* (ed.: R.R. Tummala). McGraw-Hill, New York **2001**, 466-499.

[7] H.J.R. Dutton, *Understanding Optical Communications*. Prentice-Hall, Upper Saddle River NJ **1998**.

[8] W. Daum, J. Krauser, P.E. Zamzow, O. Ziemann, *POF – Optische Polymerfasern für die Datenkommunikation*. Springer-Verlag, Berlin **2001**.

[9] M. Young, *Optik, Laser, Wellenleiter*. Springer-Verlag, Berlin **1997**.

[10] *Truemode Backplane™ – Enabling Optical Backplanes*. Terahertz Photonics Ltd., Livingston (GB) **2003**.

[11] M. Hikita, R. Yoshimura, M. Usui, S. Tomaru, S. Imamura, *Thin Solid Films* **1998**, *331*, 303-308.

[12] H. Zarschizky, A. Richter, *Physik Journal* **2003**, *2*, 33-39.

[13] H. Ma, A.K.-Y. Jen, L.R. Dalton, *Adv. Mater.* **2002**, *14*, 1339-1365.

[14] M. Zhou, *Opt. Eng.* **2002**, *41*, 1631-1643.

[15] (a) L. Eldada in *Organic Photonic Materials and Devices IV* (eds.: B. Kippelen, D.D. Bradley), *Proc. SPIE* **2002**, *4642*, 11-22. (b) L. Eldada, *Opt. Eng.* **2001**, *40*, 1165-1178.

[16] (a) N. Keil, H.H. Yao, C. Zawadzki, *Appl. Phys. B* **2001**, *73*, 619-622. (b) N. Keil, H.H. Yao, C. Zawadzki, J. Bauer, M. Bauer, C. Dreyer, J. Schneider, *Electron. Lett.* **2001**, *37*, 579-580.

[17] J.-F. Viens, C.L. Callender, J.P. Noad, L. Eldada, *IEEE Photon. Technol. Lett.* **2000**, *12*, 1010-1012.

[18] J.-F. Viens, C.L. Callender, J.P. Noad, L. Eldada, R.A. Norwood, in *Organic Photorefractives, Photoreceptors, Waveguides, and Fibers* (eds.: S. Ducharme, D.H. Dunlap, R.A. Norwood). *Proc. SPIE* **1999**, *3799*, 202-213.

[19] C.L. Callender, J.-F. Viens, J.P. Noad, L. Eldada, *Electron. Lett.* **1999**, *35*, 1839-1840.

[20] Y. Hida, Y. Inoue, S. Imamura, *Electron. Lett.* **1994**, *30*, 959-960.

[21] L. Friedrich, P. Dannberg, C. Wächter, T. Henning, A. Bräuer, W. Karthe, *Opt. Commun.* **1997**, *137*, 239-243.

[22] M.-C. Oh, M.-H. Lee, H.-J. Lee, *IEEE Photon. Technol. Lett.* **1999**, *11*, 1144-1146.

[23] J.-W. Kang, E. Kim, J.-J. Kim, *Opt. Mater.* **2002**, *21*, 543-548.

[24] (a) N. Keil, H.H. Yao, C. Zawadzki, B. Strebel, *Electron. Lett.* **1994**, *30*, 639-640. (b) N. Keil, B. Strebel, R. Türck, H.H. Yao, C. Zawadzki in *Micro System Technologies '94 / 4th International Conference on Micro Electro, Opto, Mechanical Systems and Components, Berlin, October 19-21, 1994* (eds.: H. Reichl, A. Heuberger). vde-Verlag GmbH, Berlin **1994**, 1097-1106.

[25] S.-W. Ahn, S.-Y. Shin, S.-S. Lee, *Electron. Lett.* **2001**, *37*, 172-174.

[26] S. Toyoda, N. Ooba, T. Kitoh, T. Kurihara, T. Maruno, *Electron. Lett.* **2001**, *37*, 1130-1132.

[27] S. Toyoda, A. Kaneko, N. Ooba, M. Hikita, H. Yamada, T. Kurihara, K. Okamoto, S. Imamura, *IEEE Photon. Technol. Lett.* **1999**, *11*, 1141-1143.

[28] K. Ziemelis, *Nature* **1998**, *393*, 619-620.

[29] W.H. Steier, A. Chen, S.-S. Lee, S. Garner, H. Zhang, V. Chuyanov, L.R. Dalton, F. Wang, A.S. Ren, C. Zhang, G. Todorova, A. Harper, H.R. Fetterman, D. Chen, A. Udupa, D. Bhattacharya, B. Tsap, *Chem. Phys.* **1999**, *245*, 487-506.

[30] R. Houbertz, L. Fröhlich, M. Popall, U. Streppel, P. Dannberg, A. Bräuer, J. Serbin, B.N. Chichkov, *Adv. Eng. Mater.* **2003**, *5*, 551-555.

[31] R. Houbertz, G. Domann, C. Cronauer, A. Schmitt, H. Martin, J.-U. Park, L. Fröhlich, R. Buestrich, M. Popall, U. Streppel, P. Dannberg, C. Wächter, A. Bräuer, *Thin Solid Films* **2003**, *442*, 194-200.

[32] M. Popall, R. Buestrich, F. Kahlenberg, A. Andersson, J. Haglund, M.E. Robertsson, G. Blau, M. Gale, O. Rösch, A. Dabek, J. Neumann-Rodekirch, L. Cergel, D. Lambert, in *Hybrid Organic/Inorganic Materials – 2000* (eds.: R.M. Laine, C. Sanchez, E. Giannelis, C.J. Brinker). *Mat. Res. Soc. Symp. Proc.* **2001**, *628*, CC9.4.1-CC9.4.12.

[33] (a) R. Buestrich, F. Kahlenberg, M. Popall, P. Dannberg, R. Müller-Fiedler, O. Rösch, *J. Sol-Gel Sci. Technol.* **2001**, *20*, 181-186. (b) R. Buestrich, F. Kahlenberg, M. Popall, A. Martin, O. Rösch in *Hybrid Organic/Inorganic Materials – 2000* (eds.: R.M. Laine, C. Sanchez, E. Giannelis, C.J. Brinker). *Mat. Res. Soc. Symp. Proc.* **2001**, *628*, CC9.8.1-CC9.8.6.

[34] R. Buestrich, C. Roscher, *DE 19932629 A1*. Fraunhofer-Gesellschaft zur Förderung der angewandten Forschung e.V., Munich **2001**.

[35] (a) M. Popall, J. Kappel, J. Schulz, H. Wolter in *Micro System Technologies '94 / 4th International Conference on Micro Electro, Opto, Mechanical Systems and Components, Berlin, October 19-21, 1994* (eds.: H. Reichl, A. Heuberger). vde-Verlag GmbH, Berlin **1994**, 271-280. (b) P. Dannberg, A. Bräuer, W. Karthe, R. Waldhäusl, H. Wolter, *ibid.*, 281-287. (c) M. Popall, J. Kappel, M. Pilz, J. Schulz, *J. Sol-Gel Sci. Technol.* **1994**, *2*, 157-160.

[36] P. Dannberg, L. Erdmann, A. Krehl, C. Wächter, A. Bräuer, *Mater. Sci. Semicond. Process.* **2000**, *3*, 437-441.

[37] M.E. Robertsson, O.-J. Hagel, G. Gustavsson, A. Dabek, M. Popall, L. Cergel, P. Wennekers, P. Kiely, M. Lebby, T. Lindahl, *48th IEEE Electronic Components and Technology Conference* (Cat.No.98CH36206). Seattle, WA (US) May 25-28, **1998**, 1413-1421.

[38] W. Groh, *Makromol. Chem.* **1988**, *189*, 2861-2874.

[39] A. Rousseau, B. Boutevin, D. Bosc in *Proceedings of the First Plastic Optical Fibres and Application Conference, Paris, 1992*, IGI Europe, Boston MA, **1992**, 33-37.

[40] L.A. Hornak (ed.), *Polymers for Lightwave and Integrated Optics – Technology and Applications*. Marcel Dekker, New York **1992**.

[41] C. Roscher, R. Buestrich, P. Dannberg, O. Rösch, M. Popall in *Organic/Inorganic Hybrid Materials* (eds.: R.M. Laine, C. Sanchez, C.J. Brinker, E. Giannelis). *Mat. Res. Soc. Symp. Proc.* **1998**, *519*, 239-244.

[42] B.M. Jaworski, A.A. Detlaf, *Physik griffbereit Band 2*. Rowohlt, Hamburg **1974**.

[43] (a) G. Wedler, *Lehrbuch der Physikalischen Chemie*, 4. Auflage, Wiley-VCH, Weinheim **1997**. (b) P.W. Atkins, *Quanten: Begriffe und Konzepte für Chemiker*. VCH, Weinheim **1993**. (c) P.W. Atkins, *Physikalische Chemie*, VCH, Weinheim **1990**. (d) W.J. Moore, *Grundlagen der Physikalischen Chemie*. Walter de Gruyter, Berlin **1990**.

[44] (a) G. Hougham, G. Tesoro, A. Viehbeck, J.D. Chapple-Sokol, *Macromolecules* **1994**, *27*, 5964-5971. (b) G. Hougham, G. Tesoro, A. Viehbeck, *Macromolecules* **1996**, *29*, 3453-3456.

[45] D.W. van Krevelen, *Properties of Polymers*. 3rd edition, Elsevier, Amsterdam **1990**.

[46] T. Knoche, L. Müller, R. Klein, A. Neyer, *Electron. Lett.* **1996**, *32*, 1284-1285.

[47] W. Kleber, *Einführung in die Kristallographie*. 15. Auflage, VEB Verlag Technik, Berlin **1983**.

[48] J.-W. Kang, J.-S. Kim, J.-J. Kim, *Jpn. J. Appl. Phys.* **2001**, *40*, 3215-3219.

[49] H.-J. Lee, E.-M. Lee, M.-H. Lee, M.-C. Oh, J.-H. Ahn, S.G. Han, H.G. Kim, *J. Polym. Sci. Part A: Polym. Chem.* **1998**, *36*, 2881-2887.

[50] (a) C. Roscher, *PhD thesis*. University of Würzburg **1998**. (b) C. Roscher, M. Popall in *Better Ceramics Through Chemistry VII: Organic/Inorganic Hybrid Materials* (eds.: B.K. Coltrain, C. Sanchez, D.W. Schaefer, G.L. Wilkes). *Mat. Res. Soc. Symp. Proc.* **1996**, *435*, 547-552.

[51] Gelest-ABCR GmbH, Karlsruhe **2001**.

[52] S. Cochet, private communication.

[53] (a) *Pure Appl. Chem.* **1996**, *68*, 2223-2286. (b) A.D. McNaught, A. Wilkinson, *IUPAC Compendium of Chemical Terminology. Second Edition*, Blackwell Science **1997**.

[54] R.M. Blomquist, *US 2003/0055120 A1*. Corning Inc., Corning NY (US) **2003**.

[55] C. Zha, G. Atkins, *US 2002/0165339 A1*, **2002**.

[56] W. Groh, D. Lupo, H. Sixl, *Adv. Mater.* **1989**, *11*, 366-377.

[57] M. Oubaha, M. Smaïhi, P. Etienne, P. Coudray, Y. Moreau, *J. Non-Cryst. Solids* **2003**, *318*, 305-313.

[58] A. Skumanich, C.R. Moylan, *Chem. Phys. Lett.* **1990**, *174*, 139-144.

[59] J.S. Wong, C.B. Moore, *J. Chem. Phys.* **1982**, *77*, 603-615.

[60] C. Emslie, *J. Mater. Sci.* **1988**, *23*, 2281-2293.

[61] L.W. Shacklette, R. Blomquist, J.M. Deng, P.M. Ferm, M. Maxfield, J. Mato, H. Zou, *Adv. Funct. Mater.* **2003**, in press.

[62] H.-J. Lee, M.-H. Lee, M.-C. Oh, J.-H. Ahn, S.G. Han, *J. Polym. Sci. Part A : Polym. Chem.* **1999**, *37*, 2355-2361.

[63] B. Lotz, J.-C. Wittmann in *Materials Science and Technology : A Comprehensive Treatment* (eds. : R.W. Cahn, P. Haasen, E.J. Kramer), *Volume 12: Structure and Properties of Polymers* (vol. ed. : E.L. Thomas), VCH, Weinheim **1993**, 79-151.

[64] J. Ulbricht, *Grundlagen der Synthese von Polymeren*. 2. Auflage, Hüthing & Wepf, Basel **1992**.

[65] R.A. Norwood, R. Gao, J. Sharma, C.C. Teng in *Design, Manufacturing, and Testing of Planar Optical Waveguide Devices* (ed.: R.A. Norwood). *Proc. SPIE* **2001**, *4439*, 19-28.

[66] S. Büttgenbach, *Mikromechanik*. B.G. Teubner, Stuttgart **1991**.

[67] W.M. Moreau, *Semiconductor Lithography*. Third Printing, Plenum Press, New York **1991**.

[68] H. Nishihara, M. Haruna, T. Suhara, *Optical Integrated Circuits*. McGraw-Hill, New York **1989**.

[69] P. Demmer, E. Griese, A. Neyer, *DE 100 65 563 A1*. Siemens AG, Munich **2002**.

[70] K.Y. Suh, Y.S. Kim, H.H. Lee, *Adv. Mater.* **2001**, *13*, 1386-1389.

[71] S.Y. Chou, P.R. Krauss, P.J. Renstrom, *Science* **1996**, *272*, 85-87.

[72] E. Schäffer, T. Thurn-Albrecht, T.P. Russell, U. Steiner, *Nature* **2000**, *403*, 874-877.

[73] Y. Huang, G.T. Paloczi, J. Scheuer, A. Yariv, *Opt. Express* **2003**, *11*, 2452-2458.

[74] T. Shioda, *US 6,500,603 B1*. Mitsui Chemicals Inc., Tokyo (JP) **2002**.

[75] M. Wang, H.-G. Braun, T. Kratzmüller, E. Meyer, *Adv. Mater.* **2001**, *13*, 1312-1317.

[76] Y. Xia, G.M. Whitesides, *Angew. Chem.* **1998**, *110*, 568-594.

[77] B.A. Grzybowski, R. Haag, N. Bowden, G.M. Whitesides, *Anal. Chem.* **1998**, *70*, 4645-4652.

[78] J.A. Rogers, M. Meier, A. Dodabalapur, *Appl. Phys. Lett.* **1998**, *73*, 1766-1768.

[79] A. Aoki, P. Ghosh, R.M. Crooks, *Langmuir* **1999**, *15*, 7418-7421.

[80] G. Chen, Y. Ito, Y. Imanish, *Macromolecules* **1997**, *30*, 7001-7003.

[81] G. Wiegand, T. Jaworek, G. Wegner, E. Sackmann, *Langmuir* **1997**, *13*, 3563-3569.

[82] M.-H. Wu, G.M. Whitesides, *Adv. Mater.* **2002**, *14*, 1502-1506.

[83] *MA6 / MA8 Manuelle Mask Aligner: Bedienungsanleitung*. SUSS MicroTec Lithography GmbH, Garching **2002**.

[84] M. Popall, A. Dabek, M.E. Robertsson, G. Gustafsson, O.-J. Hagel, B. Olsowski, R. Buestrich, L. Cergel, M. Lebby, P. Kiely, J. Joly, D. Lambert, M. Schaub, H. Reichl, *48th IEEE Electronic Components and Technology Conference* (Cat.No.98CH36206). Seattle, WA (US) May 25-28, **1998**, 1018-1025.

[85] *Laser-Assisted Fabrication of Thin Films and Microstructures* (ed.: I.W. Boyd). *Proc. SPIE* **1994**, *2045*.

[86] A.K. Das, B.S. Chaudhari, S. Ghosh, *Appl. Opt.* **1998**, *37*, 6779-6786.

[87] M.A. Roberts, J.S. Rossier, P. Bercier, H. Girault, *Anal. Chem.* **1997**, *69*, 2035-2042.

[88] R. Srinivasan, B. Baren, *Chem. Rev.* **1989**, *89*, 1303-1316.

[89] H.-G. Rubahn, *Laseranwendung in der Oberflächenphysik und Materialbearbeitung*. B.G. Teubner, Stuttgart **1996**.

[90] M. Kagami, H. Ito, T. Ichikawa, S. Kato, M. Matsuda, N. Takahashi, *Appl. Opt.* **1995**, *34*, 1041-1046.

[91] B.L. Booth, J.E. Marchegiano, C.T. Chang, R.J. Furmanak, D.M. Graham, R.G. Wagner, in *Optoelectronic Interconnects and Packaging* (eds.: R.T. Chen, P.S. Guilfoyle). *Proc. SPIE* **1997**, *3005*, 238-253.

[92] L. Eldada, S. Yin, R.A. Norwood, J.T. Yardley, in *Design and Manufacturing of WDM Devices* (eds.: R.T. Chen, L.S. Lome). *Proc. SPIE* **1998**, *3234*, 161-174.

[93] R. A. Norwood, R. Blomquist, L. Eldada, C. Glass, C. Poga, L.W. Shacklette, B. Xu, S. Yin, J.T. Yardley in *Polymer Photonic Devices* (eds.: B. Kippelen, D.D. Bradley). *Proc. SPIE* **1998**, *3281*, 2-13.

[94] F. Tooley, N. Suyal, F. Bresson, A. Fritze, J. Gourlay, A. Walker, M. Emmery, *Opt. Mater.* **2001**, *17*, 235-241.

[95] N. Suyal, I. McEwan, *WO 01/94430 A1*. Terahertz Photonics Ltd., Livingston (GB) **2001**.

[96] M. Jöhnck, L. Müller, A. Neyer, J.W. Hofstraat, *Polymer* **1999**, *40*, 3631-3640.

[97] M. Jöhnck, L. Müller, A. Neyer, J.W. Hofstraat, *Eur. Polym. J.* **2000**, *36*, 1251-1264.

[98] J. Liang, E. Toussaere, R. Hierle, R. Levenson, J. Zyss, A.V. Ochs, A. Rousseau, B. Boutevin, *Opt. Mater.* **1998**, *9*, 230-235.

[99] J.P.D. Cook, G.O. Este, F.R. Shepherd, W.D. Westwood, J. Arrington, W. Moyer, J. Nurse, S. Powell, *Appl. Opt.* **1998**, *37*, 1220-1226.

[100] (a) J.D. Gelorme, R.J. Cox, S.A.R. Gutierrez, *US 4,882,245*. International Business Machines Corporation, Armonk, NY (US) **1989**. (b) L.M. Brown, J.D. Gelorme, J.P. Kuczinski, W.H. Lawrence, *US 4,940,651*. International Business Machines Corporation, Armonk, NY (US) **1990**. (c) N. LaBianca, J.D. Gelorme in *Advances in Resist Technology and Processing XII* (ed.: R.D. Allen). *Proc. SPIE* **1995**, *2438*, 846-852. (d) J.M. Shaw, J.D. Gelorme, N.C. LaBianca, W.E. Conley, S.J. Holmes, *IBM J. Res. Develop. 1997*, *41*, 81-94. (e) R.J. Hurditch, D.J. Nawrocki, D.W. Johnson, *US 6,391,523 B1*. MicroChem Corp., MA (US) **2002**.

[101] T.C. Sum, A.A. Bettiol, J.A. van Kan, F. Watt, E.Y.B. Pun, K.K. Tung, *Appl. Phys. Lett.* **2003**, *83*, 1707-1709.

[102] A. Borreman, S. Musa, A.A.M. Kok, M.B.J. Diemeer, A. Driessen, *Proc. Symp. IEEE/LEOS Benelux Chapter*, Amsterdam **2002**, 83-86.

[103] C.A. Langhoff, T. Stokich, B. Heistand, in *Optoelectronic Interconnects* (ed.: R.T. Chen). *Proc. SPIE* **1993**, *1849*, 336-341.

[104] G. Fischbeck, R. Moosburger, M. Töpper, K. Petermann, *Electron. Lett.* **1996**, *32*, 212-213.

[105] Y.-H. So, P. Garrou, J.-H. Im, D.M. Scheck, *Chem. Tech.* **2001**, *31*, 40-47.

[106] Y.-G. Zhao, W.-K. Lu, Y. Ma, S.-S. Kim, S.T. Ho, T.J. Marks, *Appl. Phys. Lett.* **2000**, *77*, 2961-2963.

[107] C.F. Kane, R.R. Krchnavek, *IEEE Photon. Technol. Lett.* **1995**, *7*, 535-537.

[108] J. Kobayashi, T. Matsuura, S. Sasaki, T. Maruno, *Appl. Opt.* **1998**, *37*, 1032-1037.

[109] T. Matsuura, J. Kobayashi, S. Ando, T. Maruno, S. Sasaki, F. Yamamoto, *Appl. Opt.* **1999**, *38*, 966-971.

[110] K.-H. Kim, S. Jang, F.W. Harris, *Macromolecules* **2001**, *34*, 8925-8933.

[111] C.-C. Chang, W.-C. Chen, *Chem. Mater.* **2002**, *14*, 4242-4248.

[112] (a) R.H. Woudenberg, T.O. Boonstra, J.W. Ladage, U.E. Wiersum, *US 5,872,882*. Akzo Nobel NV **1999**. (b) R.H. Woudenberg, T.O. Boonstra, *US 6,376,639 B1*. JDS Uniphase Photonics C.V., Arnhem (NL) **2002**.

[113] M.-H. Hung, *Macromolecules* **1993**, *26*, 5829-5834.

[114] (a) P.R. Resnick, *US 3,865,845* **1975**. (b) P.R. Resnick, *US 3,978,030*. E.I. Du Pont de Nemours and Company, Wilmington, Del. (US) **1976**. (c) P.R. Resnick, W.H. Buck in *Modern Fluoropolymers* (ed.: J. Scheirs). *Wiley Series in Polymer Science*, Wiley, Chichester **1997**, 397-419.

[115] P.K. Dasgupta, Z. Genfa, S.K. Poruthoor, S. Caldwell, S. Dong, S.-Y. Liu, *Anal. Chem.* **1998**, *70*, 4661-4669.

[116] G. Fischbeck, R. Moosburger, C. Kostrzewa, A. Achen, K. Petermann, *Electron. Lett.* **1997**, *33*, 518-519.

[117] D.W. Smith, Jr., S. Chen, S.M. Kumar, J. Ballato, C. Topping, H.V. Shah, S.H. Foulger, *Adv. Mater.* **2002**, *14*, 1585-1589.

[118] W. Shi, Y.J. Ding, C. Fang, Q. Pan, Q. Gu, *Opt. Las. Eng.* **2002**, *38*, 361-371.

[119] C. Pitois, R. Vestberg, M. Rodlert, E. Malmström, A. Hult, M. Lindgren, *Opt. Mater.* **2002**, *21*, 499-506.

[120] (a) S.B. Dawes, M.E. DeRosa, R.J. Hagerty, J. Wang, *US 2002/0198281 A1*. Corning Inc., Corning NY (US) **2002**. (b) J. Wang, P.J. Shustack, J.A. Chalk, *US 6,503,421 B1*. Corning Inc., Corning NY (US) **2003**.

[121] J.-P. Kim, W.-Y. Lee, J.-W. Kang, S.-K. Kwon, J.-J. Kim, J.-S. Lee, *Macromolecules* **2001**, *34*, 7817-7821.

[122] C. Pitois, S. Vukmirovic, A. Hult, D. Wiesmann, M. Robertsson, *Macromolecules* **1999**, *32*, 2903-2909.

[123] H.R. Allcock, J.D. Bender, Y. Chang, M. McKenzie, M.M. Fone, *Chem. Mater.* **2003**, *15*, 473-477.

[124] E.W. Bohannan, X. Gao, K.R. Gaston, C.D. Doss, C. Sotiriou-Leventis, N. Leventis, *J. Sol-Gel Sci. Technol.* **2002**, *23*, 235-245.

[125] M. Usui, S. Imamura, S. Sugawara, S. Hayashida, H. Sato, M. Hikita, T. Izawa, *Electron. Lett.* **1994**, *30*, 958-959.

[126] T. Watanabe, N. Ooba, S. Hayashida, T. Kurihara, S. Imamura, *J. Lightwave Technol.* **1998**, *16*, 1049-1055.

[127] S. Toyoda, N. Ooba, M. Hikita, T. Kurihara, S. Imamura, *Thin Solid Films* **2000**, *370*, 311-314.

[128] C. Xu, L. Eldada, C. Wu, R.A. Norwood, L.W. Shacklette, J.T. Yardley, *Chem. Mater.* **1996**, *8*, 2701-2703.

[129] P.J. Shustack, Z. Wang, *US 2003/0021566 A1*. Corning Inc., Corning NY (US) **2003**.

[130] W.-C. Chen, L.-H. Lee, B.-F. Chen, C.-T. Yen, *J. Mater. Chem.* **2002**, *12*, 3644-3648.

[131] S. Toyoda, S. Imamura, S. Tomaru, T. Kurihara, K. Enbutsu, S. Hayashida, T. Maruno, *US 6,537,723 B1*. Nippon Telegraph and Telephone Corp., Tokyo (JP) **2003**.

[132] M. Casalboni, F. Belli, M. Cirillo, F. de Matteis, P. Proposito, R. Russo, R. Pizzoferrato, *J. Sol-Gel Sci. Technol.* **2003**, *26*, 937-941.

[133] *Cyclotene® 4022-35 Advanced Electronics Resin. Materials Safety Data Sheet*. The Dow Chemical Company, Midland, MI (US) **2001**.

[134] Y.Y. Maruo, S. Sasaki, T. Tamamura, *Appl. Opt.* **1995**, *34*, 1047-1052.

[135] S. Singh, A. Kapoor, S.C.K. Misra, K.N. Tripathi, *Solid State Commun.* **1996**, *100*, 503-506.

[136] S.M. Grayson, J.M.J. Fréchet, *Chem. Rev.* **2001**, *101*, 3819-3867.

[137] C. Pitois, D. Wiesmann, M. Lindgren, A. Hult, *Adv. Mater.* **2001**, *13*, 1483-1487.

[138] K.A. Horn, T.M. Leslie, J.V. Suggs, M. He, *US 6,470,131 B1*. Corning Inc., Corning, NY (US) **2002**.

[139] (a) G. Philipp, H. Schmidt, *J. Non-Cryst. Solids* **1984**, *63*, 283-292. (b) H. Schmidt, *J. Non-Cryst. Solids* **1985**, *73*, 681-691. (c) H.K. Schmidt in *Better Ceramics Through Chemistry IV* (eds.: B.J.J. Zelinski, C.J. Brinker, D.E. Clark, D.R. Ulrich). *Mater. Res. Soc. Symp. Proc.* **1990**, *180*, 961-973.

[140] (a) K.-H. Haas, S. Amberg-Schwab, T. Ballweg in *Advances in Science and Technology* (ed.: P. Vincenzini) **2003**, *31*, 581-592. (b) K.-H. Haas, K. Rose, *Rev. Adv. Mater. Sci.* **2003**, *5*, 47-52. (c) G. Schottner, *Chem. Mater.*, **2001**, *13*, 3422-3435. (d) K.-H. Haas, H. Wolter, *Curr. Opin. Solid State Mater. Sci.* **1999**, *4*, 571-580.

[141] (a) K.-H. Haas, S. Amberg-Schwab, K. Rose, G. Schottner, *Surf. Coat. Technol.* **1999**, *111*, 72-79. (b) S. Amberg-Schwab, E. Arpac, W. Glaubitt, K. Rose, G. Schottner, U. Schubert in *High Performance Ceramic Films and Coatings* (ed.: P. Vincenzini). Elsevier, Amsterdam **1991**.

[142] G. Schottner, J. Kron, K.-J. Deichmann, *J. Sol-Gel Sci. Technol.* **1998**, *13*, 183-187.

[143] (a) M. Pilz, H. Römich, *J. Sol-Gel Sci. Technol.* **1997**, *8*, 1071-1075. (b) S. Amberg-Schwab, M. Hoffmann, H. Bader, M. Gessler, *J. Sol-Gel Sci. Technol.* **1998**, *2*, 141-146. (c) S. Amberg-Schwab, H. Katschorek, U. Weber, M. Hoffmann, A. Burger, *J. Sol-Gel Sci. Technol.* **2000**, *19*, 125-129.

[144] (a) H. Wolter, W. Storch, *J. Sol-Gel Sci. Technol.* **1994**, *2*, 93-96. (b) C. Gellermann, W. Storch, H. Wolter, *J. Sol-Gel Sci. Technol.* **1997**, *8*, 173-176.

[145] H. Wolter, W. Storch, H. Ott in *Better Ceramics through Chemistry VI* (eds.: A.K. Cheetham, C.J. Brinker, M.L. Mecartney, C. Sanchez). *Mat. Res. Soc. Symp. Proc.* **1994**, *346*, 143-149.

[146] (a) M. Popall, M. Andrei, J. Kappel, J. Kron, K. Olma, B. Olsowski, *Electrochim. Acta*, **1998**, *43*, 1155-1161. (b) L. Depre, J. Kappel, M. Popall, *Electrochim. Acta* **1998**, *43*, 1301-1306. (c) S. Skaarup, K. West, B. Zachau-Christiansen, M. Popall, J. Kappel, J. Kron, G. Eichinger, G. Semrau, *Electrochim. Acta* **1998**, *43*, 1589-1592.

[147] (a) M. Popall, X.-M. Du, *Electrochim. Acta* **1995**, *40*, 2305-2308. (b) L. Depre, M. Ingram, C. Poinsignon, M. Popall, *Electrochim. Acta* **2000**, *45*, 1377-1383. (c) S. Jacob, S. Cochet, C. Poinsignon, M. Popall, *Electrochim. Acta* **2003**, *48*, 2181-2186. (d) S. Jacob, M. Popall, L. Fröhlich, F. Kahlenberg, K. Olma,

DE 10163518A1. Fraunhofer-Gesellschaft zur Förderung der angewandten Forschung e.V., Munich **2003**.

[148] E.J.A. Pope, J.D. Mackenzie, *J. Non-Cryst. Solids* **1986**, *87*, 185-198.

[149] C.-H. Chang, A. Mar, A. Tiefenthaler, D. Wostratzky *in Handbook of Coatings Additives: Volume 2* (ed.: L.J. Calbo). Marcel Dekker, Inc., **1992**.

[150] C.G. Roffey, *Photogeneration of Reactive Species for UV Curing*. John Wiley & Sons, Chichester **1997**.

[151] *Ciba® IRGACURE® 907 Photoinitiator*. Ciba Specialty Chemicals, Basel **1999**.

[152] *Lucirin® TPO-L. Technical Information TI/ED 1787 e*. BASF Aktiengesellschaft, Ludwigshafen **1999**.

[153] *Inorganic-organic Hybride Polymers (ORMOCER®s) for Application in Optical Devices*. micro resist technology GmbH, Berlin **2003**.

[154] U. Streppel, P. Dannberg, C. Wächter, A. Bräuer, L. Fröhlich, R. Houbertz, M. Popall, *Opt. Mater.* **2002**, *21*, 475-483.

[155] (a) V.F.A. Grignard, *Compt. Rend.* **1900**, *130*, 1322. (b) V.F.A. Grignard, *Ann. Chim.* **1901**, *24*, 433-490. (c) P. Barbier, *Compt. Rend.* **1899**, *128*, 110.

[156] G.R. Atkins, R.B. Charters, *J. Sol-Gel Sci. Technol.* **2003**, *26*, 919-923.

[157] R.J. Hook, *J. Non-Cryst. Solids* **1996**, *195*, 1-15.

[158] F. Rousseau, C. Poinsignon, J. Garcia, M. Popall, *Chem. Mater.* **1995**, *7*, 828-839.

[159] T. Iwamoto, K. Morita, J.D. Mackenzie, *J. Non-Cryst. Solids* **1993**, *159*, 65-72.

[160] A.H. Boonstra, T.N.M. Bernards, *J. Non-Cryst. Solids* **1989**, *108*, 249-259.

[161] F. Kahlenberg, *Diplomarbeit*. University of Würzburg **1999**.

[162] F. Kahlenberg, R. Buestrich, M. Popall in *Hybrid Organic/Inorganic Materials – 2000* (eds.: R.M. Laine, C. Sanchez, E. Giannelis, C.J. Brinker). *Mat. Res. Soc. Symp. Proc.* **2001**, *628*, CC11.6.1-CC11.6.6.

[163] B. Marciniec, *Comprehensive Handbook on Hydrosilylation*. Pergamon Press, Oxford **1992**.

[164] R. Krafczyk, H. Thönnessen, P.G. Jones, R. Schmutzler, *J. Fluorine Chem.* **1997**, *83*, 159-166.

[165] B.D. Karstedt, *US 3,775,452*. General Electric Co., Scotia, NY (US) **1973**.

[166] (a) L. Pauling, *The Nature of the Chemical Bond*. 3rd. ed., Cornell University Press, Ithaca, NY **1960**. (b) G. Simons, M.E. Zandler, E.R. Talaty, *J. Am. Chem. Soc.* **1976**, *98*, 7869-7870. (c) R.T. Sanderson, *J. Am. Chem. Soc.* **1983**, *105*, 2259-2261. (d) R.T Sanderson, *J. Chem. Educ.* **1988**, *65*, 112-118. (e) S.G. Bratsch, *J. Chem. Educ.* **1988**, *65*, 223-227.

[167] M. Hesse, H. Meier, B. Zeeh, *Spektroskopische Methoden in der organischen Chemie*. 4., überarbeitete Auflage, Georg Thieme Verlag, Stuttgart **1991**.

[168] J.M. Briggs, E.W. Randall, *J. Chem. Soc., Perkin Trans. II* **1973**, 1789-1791.

[169] H.C. Marsmann in *NMR 17: Oxygen-17 and Silicon-29* (eds.: P. Diehl, E. Fluck, R. Kosfeld). Springer-Verlag, Berlin **1981**, 65-235.

[170] (a) G. Engelhardt, W. Altenberg, D. Hoebbel, W. Wieker, *Z. Anorg. Allg. Chem.* **1977**, *428*, 43-52. (b) D. Hoebbel, G. Garzó, G. Engelhardt, A. Till, *Z. Anorg. Allg. Chem.* **1979**, *450*, 5-20. (c) I. Artaki, S. Sinha, A.D. Irwin, J. Jonas, *J. Non-Cryst. Solids* **1985**, *72*, 391-402. (d) L.W. Kelts, N.J. Armstrong, *J. Mater. Res.* **1989**, *4*, 423-433. (e) Y. Dubitsky, A. Zaopo, G. Zannoni, L. Zetta, *Mat. Chem. Phys.* **2000**, *64*, 45-53.

[171] (a) F.J. Feher, R. Terroba, R-Z. Jin, S. Lücke, F. Nguyen, R. Brutchey, K.D. Wyndham in *Organic/Inorganic Hybrid Materials – 2000* (eds.: R.M. Laine, C. Sanchez, C.J. Brinker, E. Giannelis). *Mat. Res. Soc. Symp. Proc.* **2001**, *628*, CC2.1.1-CC2.1.6. (b) S.H. Phillips, R.L. Blanski, S.A. Svejda, T.S. Haddad, A. Lee, J.D. Lichtenhan, F.J. Feher, P.T. Mather, B.S. Hsiao in *Organic/Inorganic Hybrid Materials – 2000* (eds.: R.M. Laine, C. Sanchez, C.J. Brinker, E. Giannelis). *Mat. Res. Soc. Symp. Proc.* **2001**, *628*, CC4.6.1-CC4.6.10. (c) F.J. Feher, T.A. Budzichowski, *J. Organomet. Chem.* **1989**, *379*, 33-40.

[172] (a) R. Weidner, N. Zeller, B. Deubzer, V. Frey, *DE 3837397 A1*. Wacker, Burghausen **1990**. (b) U. Dittmar, B.J. Hendan, U. Flörke, H.C. Marsmann, *J. Organomet. Chem.* **1995**, *489*, 185-194.

[173] (a) J.F. Brown, L.H. Vogt, P.I. Prescott, *J. Am. Chem. Soc.* **1964**, *86*, 1120-1125. (b) A.J. Barry, W.H. Daudt, J.J. Domicone, J.W. Gilkey, *J. Am. Chem. Soc.* **1955**, *77*, 4248-4252.

[174] (a) Extended version of Bruker Winfit. D. Massiot, H. Thiele, A. Germanus, *Bruker Report* **1994**, *140*, 43-46. (b) D. Massiot, F. Fayon, M. Capron, I. King, S. Le Calvé, B. Alonso, J.-O. Durand, B. Bujoli, Z. Gan,

G. Hoatson, *Magn. Reson. Chem.* **2002**, *40*, 70-76.

[175] Sigma-Aldrich Chemie GmbH, Taufkirchen **2002**.

[176] D.L. Ou, A.B. Seddon, *J. Non-Cryst. Solids* **1997**, *210*, 187-203.

[177] *Materials Studio® Version 2.2*, Accelrys Inc. **2002**.

[178] (a) H. Sun, D. Rigby, *Spectrochim. Acta Part A* **1997**, *53*, 1301-1323. (b) H. Sun, *J. Phys. Chem. B* **1998**, *102*, 7338-7364.

[179] R. Houbertz, U. Memmert, R.J. Behm, *Appl. Phys. Lett.* **1993**, *62*, 2516.

[180] M. Grundner, H. Jacob, *Appl. Phys. A* **1986**, *39*, 73.

[181] M.D. Lechner, K. Gehrke, E.H. Nordmeier, *Makromolekulare Chemie: ein Lehrbuch für Chemiker, Physiker, Materialwissenschaftler und Verfahrenstechniker*. Mit Beiträgen von U. Guhr, S. Jovanovic, R. Heering. Birkhäuser, Basel **1993**.

[182] P.A. Wheeler, M. Brungs, G.R. Atkins, *J. Sol-Gel Sci. Technol.* **2003**, *27*, 321-326.

[183] R. Houbertz, private communication.

[184] (a) P. Etienne, J. Phalippou, R. Sempere, *J. Mater. Sci.* **1998**, *33*, 3999-4005. (b) T.A.C. Flipsen, R. Derks, H. van der Vegt, R. Stenekes, A.J. Pennings, G. Hadziioannou, *J. Polym. Sci., Part B: Polym. Phys.* **1997**, *35*, 1311-1331. (c) J.D. Mackenzie, Q. Huang, T. Iwamoto, *J. Sol-Gel Sci. Technol.* **1996**, *7*, 151-161.

[185] M. Popall, private communication.

[186] H.E. Gottlieb, V. Kotljar, A. Nudelman, *J. Org. Chem.* **1997**, *62*, 7512-7515.

[187] SDBSWeb: *http://aist.go.jp/RIODB/SDBS/* **2001-2003**.

[188] G. Rizzo, P. Barilà, S. Galvagno, G. Neri, A. Arena, S. Patanè, G. Saitta, *J. Sol-Gel Sci. Technol.* **2003**, *26*, 1017-1021.

8 ACKNOWLEDGMENTS – HERZLICHEN DANK!

An erster Stelle möchte ich meinen Eltern danken, ohne deren moralische und auch finanzielle Unterstützung vieles nicht möglich gewesen wäre.

Ich danke Herrn Prof. Dr. Gerd Müller für die Betreuung und sein Interesse am Gelingen dieser Arbeit sowie seine wertvollen Anregungen. Herrn Dr. Michael Popall danke ich für die hochinteressante Themenstellung, sein großes persönliches Engagement und seine stete Diskussionsbereitschaft.

Für das überaus angenehme und motivierende Arbeitsumfeld danke ich der Riege der Wissenschaftler um Dr. Ruth Houbertz-Krauß im Kompetenzfeld „Hybridpolymere für Mikrosysteme“, Gerhard Domann, Dr. Lothar Fröhlich und Dr. Jochen Schulz. Zusammen mit meinen Mitstreitern im Doktorandenamt Sébastien Cochet und Stéphane Jacob waren sie jederzeit mit Rat und Tat zur Stelle, wenn es darum ging, neue Wege auszuloten oder Lösungen für die unterschiedlichsten Problemstellungen auszubrüten.

Heidi Martin und besonders Geli Schmitt danke ich sehr für die Einweihung in die Geheimnisse der Reinraumtechnologie und die geduldige Anfertigung vieler Dünnfilmproben mit Materialien von geringer natürlicher Häufigkeit. Danke an Jang Ung („Bob-Jang“) Park für die Durchführung von Messungen mit dem Prismenkoppler. Für viele kleine und große Tipps, praktische Unterstützung und eine Prima Atmosphäre danke ich Annette Scheraus, Birke Olsowski und Carola Cronauer („ABC-Alarm“) sowie Dr. Jürgen Kappel und Konrad Olma. Kurt Henkel und Rainer Jahn seien gedankt für thermische und SAXS-Analysen.

Für die hervorragende Zusammenarbeit am NMR des ISC möchte ich Dr. Carsten Gellermann meinen Dank aussprechen. Die Durchführung von Festkörper-NMR-Analysen erfolgten durch Dr. Rüdiger Bertermann am Institut für Anorganische Chemie der Universität Würzburg sowie durch Dr. Florence Babonneau und Dr. Christel Gervais am centre national de la recherche scientifique (CNRS) in Paris. Auch hierfür vielen Dank und merci! Dr. Peter Dannberg vom Fraunhofer-Institut für Angewandte Optik und Feinmechanik in Jena hat mit Messungen der optischen Dämpfung von Hybridpolymerschichten sehr zur Abrundung der Arbeit beigetragen – herzlichen Dank!

Stellvertretend für weitere hilfreiche Diskussionspartner, die ihre Erfahrungen und ihr Wissen mit mir teilten, seien Anna Klukowska, Karine Gigant und Stefan Holzner genannt. „Special Thanks“ an Seb und G. für die Realisation unmöglich simulierbarer Wirt-Gast-Beziehungen!

LEBENSLAUF – CURRICULUM VITAE

Persönliche Daten

Name:	Frank Kahlenberg
Geburtsdaten:	geb. am 12.10.1973 in Brilon
Nationalität:	deutsch
Familienstand:	ledig

Ausbildung

08.84 – 06.93	Gymnasium Petrinum Brilon: Abschluss „Allgemeine Hochschulreife“
11.93 – 07.99	Studium der Chemie an der Bayerischen Julius-Maximilians-Universität Würzburg: Abschluss „Diplom-Chemiker Univ.“
02.05.1996	Vordiplom
09.97 – 12.97	Auslandsaufenthalt am University College Dublin, Irland
15.07.1999	Diplomprüfung im Studiengang Chemie
08.98 – 07.99	Diplomarbeit „Polykondensation ausgewählter Perfluorarylalkoxysilane“, durchgeführt am Fraunhofer-Institut für Silicatforschung, Würzburg
seit 08.99	Doktorarbeit „Structure-Property Correlations in Fluoroaryl Functionalized Inorganic-Organic Hybrid Polymers for Telecom Applications“, durchgeführt am Fraunhofer-Institut für Silicatforschung, Würzburg

Berufstätigkeit

seit 08.99	Wissenschaftlicher Mitarbeiter am Fraunhofer-Institut für Silicatforschung, Würzburg